The hydrodynamic and coagulation characteristics of a re-engineered mechanical heart valve in an ovine model

Christiaan Johannes Jordaan

Thesis submitted in fulfilment of the requirements of the degree

PHILOSOPHIAE DOCTOR IN CARDIOTHORACIC SURGERY

(Ph.D.)

Department of Cardiothoracic Surgery
Faculty of Health Sciences
University of the Free State
Bloemfontein, South Africa

Promoter: Prof. FE Smit; Ph.D.

Co-Promoter: Prof. PM Dohmen; Ph.D.

Co-Promoter: Dr L Botes; D.Tech.

January 2017

"I DO NOT KNOW WHAT I MAY APPEAR TO THE WORLD, BUT TO MYSELF I SEEM TO HAVE BEEN ONLY LIKE A BOY PLAYING ON THE SEA-SHORE, AND DIVERTING MYSELF IN NOW AND THEN FINDING A SMOOTHER PEBBLE OR A PRETTIER SHELL THAN ORDINARY, WHILST THE GREAT OCEAN OF TRUTH LAY ALL UNDISCOVERED BEFORE ME…"

Sir Isaac Newton (1643 – 1727)

Declaration of independent work

I, Christiaan Johannes Jordaan, do hereby declare that this dissertation:

The hydrodynamic and coagulation characteristics of a re-engineered mechanical heart valve in an ovine model

submitted to the University of the Free State for the degree ***Philosophiae Doctor*** is my own independent work and that it has not been submitted to any institution by me or any other person in fulfillment of the requirements for the attainment of any qualification.

Principal Investigator:

Signed: _____ Date: _____

Dr. Christiaan Johannes Jordaan

Table of contents

CHAPTER 3: METHODOLOGY

CHAPTER 4: RESULTS

CHAPTER 5: DISCUSSION

Acknowledgements

At the onset, I would like to express my sincere gratitude towards my advisor Prof. Francis Smit, for his support and guidance during my tenure at Universitas Hospital, University of the Free State, Bloemfontein. He played a vital role in my post graduate training as a cardio-thoracic surgeon and was the driving force behind this Ph.D. thesis. I am extremely grateful for the opportunities that were presented to me, the meaningful experiences and the invaluable knowledge gained, all of which will remain with me throughout my professional career.

In addition, I would like to convey my heartfelt appreciation to Prof. Robert Frater for his interminable support, the time he selflessly invested as well as his generous financial contribution to, not only this study, but the department as a whole. Without his belief in and commitment to the department and its fledgling research programme, the department would not be able to boast a state of the art research facility that currently enjoys international recognition.

To endeavour a study of this magnitude on one's own would have been impossible. I would like to thank the entire team that was involved in this study. My utmost appreciation goes to Dr Lezelle Botes for her guidance and patience, always understanding the weight of the clinical burden placed on a part-time researcher and for helping to balance the clinical and experimental workload. I am indebted to Mr Dreyer Bester and Mr Hans Van den Heever for their vast effort in the animal laboratory. Animal research is demanding and this research would not have been possible without a dedicated team possessing their high level of expertise. Not to mention the invaluable contribution of Kyle Davis, the engineer involved with the pulse duplication and CFD, for making sense of all of the data fields that were generated and the effort that went into the analysis and finally; putting it into a format that is comprehensible for non-engineers.

In conclusion and most notably, I extend a singular token of my sincere appreciation and admiration to my wife, Do-Jo Jordaan, for her unwavering support and encouragement; not only during the course of this Ph.D. but also throughout my life. Without her I would not be the person I am today and for that I am eternally grateful.

Statement of compliance

The study was conducted in accordance with the International Conference on Harmonisation guidelines for Good Clinical Practice (ICH E6), the Code of Federal Regulations on the Protection of Human Subjects (45 CFR Part 46), and the World Medical Association Declaration of Helsinki (64th WMA General Assembly, Fortaleza, Brazil, October 2013). All personnel involved in the conduct of this study have completed Good Clinical Practice (GCP) training or will be under direct supervision of such an accredited researcher.

All animal experiments and surgical procedures were performed in compliance with the Guide for the Care and Use of Laboratory Animals as published by the US National Institutes of Health (NIH Publication 85-23, revised 1996).

List of abbreviations

2D	Two dimensional
3D	Three dimensional
ACT	Activated clotting time
ADAMTS-13	A disintegrin and metalloproteinase with a thrombospondin type 1 motif, number 13
ADP	Adenosine diphosphatase
AIDS	Acquired immunodeficiency syndrome
Alb	Albumin
ALE	Arbitrary Langrarian-Eulerian formulation
AHA	American Heart Association
ALP	Alanine transaminase
ALP	Alkaline phosphatase
ARV	Anti-retroviral therapy
AS	Aortic valve stenosis
AST	Aspartate aminotransferase
AT	Acceleration time
ATP	Adenosine triphosphatase
ATS	Advancing the standard valve
AVR	Aortic valve replacement
Bili	Bilirubin
BMI	Body mass index
bpm	Beats per minute
^{o}C	Degrees Celsius
Ca^{++}	Calcium
CAD	Computer aided design
CCD	Charge coupled device
CO	Cardiac output
CFD	Computational fluid dynamics
CI	Confidence interval
cm	Centimeter
Comp	Compliment
Creat	Creatinine
CPB	Cardio pulmonary bypass
CRPM	Centre for Rapid Prototyping and Manufacturing
CRP	C - Reactive protein
CUT	Central University of Technology

CVP	Central venous pressure
D-DPIV	Defocussing digital particle image velocimetry
DMLS	Direct metal laser sintering
dP/dt	Change in pressure over change in time
DVI	Doppler velocity index
DVT	Deep vein thrombosis
DVR	Double valve replacement
EOA	Effective orifice area
ESR	Erythrocyte sedimentation rate
FDA	Food and Drug Administration
FEM	Finite element method
FSI	Fluid-structure interaction
FV	Factor 5
FVM	Finite volume method
FVII	Factor 7
FVIII	Factor 8
FIX	Factor 9
FX	Factor 10
FXIII	Factor 13
GARY	German Aortic Valve Registry
GBH	Graphite-Benzalkonium-Heparin
GELIA	German experience with low intensity Anti-coagulation
GGT	Gamma glutamyl rransferase
g/l	Grams per liter
GOA	Geometric orifice area
GPIa	Glycoprotein 1a
GPIb	Glycoprotein 1b
GPIIb/IIIa	Glycoprotein 2 b 3 a
GPVI	Glycoprotein 6
GPCR	G-protein coupled receptors
H&E	Haematoxylin and eosin stains
Hb	Haemoglobin
HIV	Human immunodeficiency virus
IgA	Immunoglobulin A
IgE	Immunoglobulin E
IgG	Immunoglobulin G
IgM	Immunoglobulin M
INR	International normalised ratio
K^+	Potassium
LDH	Lactic acid dehydrogenase
L/min	Liters per minute

LTI carbon	Low temperature isotropic carbon
LVOT	Left ventricular outflow tract
MAP	Mean arterial pressure
mg/l	Milligrams per liter
NHLS	National Health Laboratory Service
MHV	Mechanical heart valve
mJ	Millijoule
ml	Milliliter
ml/s	Milliliter per second
mm	Millimeter
mm/h	Millimeters per hour
mmHg	Millimeters mercury
Mmol	Millimole
Mmol/l	Millimole per liter
MN	Minnesota
MPA	Main pulmonary artery
MRI	Magnetic resonance imaging
ms^{-1}	Meters per second
m.sec	Milliseconds
MVR	Mitral valve replacement
Na^{+}	Sodium
NHLS	National Health Laboratory Service
OR	Odds ratio
P	Pressure
Pa	Pascal
PE	Phosphatidyl ethanolamine
PET	Polyethylene terephthalate
Pl	Platelet
PIV	Particle image velocimetry
Pr	Protein
PROACT	Prospective randomised On-X anti-coagulation clinical trial
PS	Phosphatidyl serine
Pt1/2	Pressure half time
PT	Prothrombin time
PTFE	Polytetrafluoroethylene
PTT	Partial thromboplastin time
pt/y	Patient year
PU	Polyurethane
PV	Prosthetic valve
Q_{rms}	Root mean square forward volumetric flow rate
RA	Right atrium

RE-ALIGN	Randomised, phase II study to evaluate the safety and pharmacokinetics of oral dabigatran etexilate in patients after heart valve replacement
RF	Regurgitant fraction
RNS	Reynolds normal stress
RPI	Reticulocyte producing index
RV	Right ventricle
RVOT	Right ventricle outflow tract
RVOT-VTI	Right ventricle outflow tract velocity time integral
s^{-1}	Per second
sec	Second
SJM	St Jude Medical
SOP	Standard operating procedures
SV	Stroke volume
t	Time
TAT	Thrombin-antithrombin III
TEE	Trans-oesophageal echocardiograph
TF	Tissue factor
Ti	Titanium
TIA	Transient ischaemic attack
Tx	Texas
U/l	Units per liter
UFS	University of the Free State
UCT	University of Cape Town
Ur	Urea
µm	Micrometer
USA	United States of America
v	Velocity
VC	Vena contracta
V_{LVOT}	Velocity in the LVOT
V_{PV}	Velocity In the prosthetic valve
VTI	Velocity time integral
vWF	Von Willebrand factor
WBC	White blood cell count

Definitions

Cardio pulmonary bypass (CPB)	A technique that temporarily replaces the function of the heart and lungs during surgery, maintaining the circulation of blood and the oxygen content of the body (Stoney, 2009).
Computational fluid dynamics (CFD)	A branch of fluid mechanics that uses numerical procedures and algorithms to solve and analyse partial differential equations that involve fluid flows. Computers are used to perform the calculations required to simulate the interaction of liquids and gases with surfaces defined by boundary conditions (Yoganathan *et al.,* 2005).
Doppler velocity index (DVI)	Is a dimensionless ratio of the proximal velocity in the left ventricular outflow tract (LVOT) to that of flow velocity through the prosthesis (PV): $DVI=V_{LVOT}/V_{PV.}$ This parameter is used to evaluate valve obstruction, particularly when the cross-sectional area of the LVOT cannot be obtained (Pibarot *et al.,* 2009).
Effective orifice Area (EOA)	The aortic valve effective orifice area (EOA) is the minimal cross-sectional area of the flow jet downstream of a native or prosthetic heart valve. The EOA is the standard parameter used for the clinical assessment of valvular stenosis severity. It is determined either from Doppler echocardiography by using the continuity equation or from catheterisation by applying the Gorlin formula (Hakki *et al*., 1981).
Finite element analysis (FEM)	A numerical method for solving partial differential equations. It can be used for predicting how a structure reacts or deforms as a result of real-world forces, vibration, heat energy transfer, fluid flow, and other physical effects. Finite element analysis shows whether a product will break, wear out, or work the way it was designed (Babuška *et al.,* 2004).
Glycar valve	The modified UCT valve in this dissertation will be referred to as the Glycar valve. This term replaces the terms: Modified UCT valve Frater valve Goosen/UCT valve Poppet valve
Lagrangian equation	The Lagrange differential equation is the fundamental equation of calculus of variations. In classical mechanics, it is equivalent to Newton's laws of motion, but it has the advantage that it takes the same form in any system of generalised coordinates, and it is better suited to generalisations (Arfken, 1985).

Navier-Stokes equation	Navier-Stokes equations describe the motion of viscous fluid substances. These balance equations arise from applying Newton's second law to fluid motion, together with the assumption that the stress in the fluid is the sum of a diffusing viscous term (proportional to the gradient of velocity) and a pressure term, hence describing viscous flow (Holdeman *et al.,* 2010).
Non-Newtonian fluid	In a Newtonian fluid, the relation between the shear stress and the shear rate is linear, passing through the origin, the constant of proportionality being the coefficient of viscosity. In a non-Newtonian fluid, the relation between the shear stress and the shear rate is nonlinear and can even be time-dependent (time dependent viscosity). Therefore, a constant coefficient of viscosity cannot be defined (Tropea *et al.,* 2007).
Power law index	Known as the Oswald de Waele law. It is applicable to a fluid in which the shear stress at any point is proportional to the rate of the shear at that point raised to a power (Chanderan *et al.,* 2006).
Pressure drop	In this dissertation it will refer to the averaged pressure difference across a heart valve during the forward flow phase from an engineering perspective. The term will be used during CFD and pulse duplication analysis.
Pressure gradient	In this dissertation it will refer to the pressure difference generated across a heart valve during the forward flow phase from a clinical perspective. The term will be used in the *in vivo* and clinical situation.
Pulse duplication	The pulse duplicator system assesses the performance of cardiovascular devices and prosthetic heart valves under simulated cardiac conditions. It simulates physiological or other complex flow variations while allowing the user to vary the peripheral resistance and compliance of the system (Kuettinga *et al*., 2014).
Pyrolytic carbon	A material similar to graphite. It is a crystalline form of carbon, a semimetal, a native element mineral, and one of the allotropes of carbon. It is the most stable form of carbon under standard conditions (Bokros *et al.,* 2003).
Q_{rms}	Square root of the integral of the volume flow rate waveform squared during the positive differential pressure interval of the forward flow phase used to calculate effective orifice area (Kuettinga *et al*., 2014).
Regurgitant fraction (RF)	Total regurgitant flow expressed as a percentage of the stroke volume [(closing volume + leakage volume)/stroke volume]. The volume of fluid that flows through and around the valve in a reverse direction during one cycle (Annarel *et al.,* 2011).

Reynolds number	In fluid mechanics, the Reynolds number is a dimensionless quantity that is used to predict flow patterns in different fluid flow situations. Laminar flow occurs at low Reynolds numbers, where viscous forces are dominant, and is characterised by smooth, constant fluid motion; turbulent flow occurs at high Reynolds numbers (greater than 1000) and is dominated by inertial forces, which tend to produce chaotic eddies, vortices and other flow instabilities (Chanderan, 2011).
Tribology	Tribology is the study of science and engineering of interacting surfaces in relative motion. It includes the study and application of the principles of friction, lubrication and wear. Tribology is a branch of mechanical engineering and materials science (Fillon *et al.,* 2016)
Vena contracta	Vena contracta is the point in a fluid stream where the diameter of the stream is the least and fluid velocity is at its maximum, such as in the case of a stream emerging from a nozzle or orifice (Falkovich, 2011).

List of figures

Page

CHAPTER 1: Executive summary

CHAPTER 2: Literature review

CHAPTER 3: Methodology

CHAPTER 4: Results

CHAPTER 5: Discussion

List of tables

.

Executive summary

Introduction

A valve with haemodynamic properties mimicking a natural heart valve and having the durability that will exceed the life expectancy of the recipient patient without requiring lifelong anti-coagulation, would be considered by most as the Holy Grail of prosthetic heart valve design. Although mechanical heart valves have a superior durability compared to biological valves, the thrombogenicity of mechanical heart valves necessitates lifelong anti-coagulation therapy, balancing bleeding risk with thrombosis and emboli.

The explantation of two UCT valves that had remained in pristine condition decades after implantation and the reviewing of historical data after implantation in children without anti-coagulation in the 1960s, led to the idea of re-engineering a poppet valve to possibly be used without anti-coagulation. This idea was revisited during the development of the Glycar Valve.

Objective

During the planning phase of this study three main objectives were considered:

1. To understand the principles of heart valve functioning with the resulting influence on thrombosis; to apply these principles while designing a mechanical heart valve that will be easy and affordable to produce and that can safely be used without anti-coagulation. This included an in-depth literature review of heart valve design, fluid-structure interaction within the valve as well as valvular thrombosis.
2. To use computational fluid dynamics followed by pulse duplication testing in the *in vitro* evaluation of a prototype mechanical heart valve (the Glycar valve) and to compare the findings to the commercially available Carbomedics bi-leaflet valve.
3. To study the Glycar valve *in vivo* in the ovine model, evaluating overall function and specifically, to assess the thrombogenicity of the valve without the use of anti-coagulant or anti-platelet therapy, in comparison to the Carbomedics bi-leaflet valve.

Methods

An extensive review of mechanical valve design, coagulation and available mechanical valve research and development methodology was performed .

Thereafter several modifications were made to the original UCT valve in order to create the Glycar valve. The flow across the valve during systole was streamlined, reducing areas of flow acceleration across the valve and the poppet surface, reducing the viscous shear rate. The diastolic flow profile was changed and areas of stagnation were eliminated around the valve leaflets. Regurgitation jets were eliminated, which negated the problems associated with the 'washing jets' seen in bi-leaflet valves.

A two-part CFD analysis (dynamic and non-dynamic) was performed on the Glycar valve to understand the flow patterns generated within the Glycar valve and across the valve components.

Pulse duplication analysis was performed on the Glycar valve and the valvular performance during five simulated physiological conditions were compared to four different commercially available heart valves in the aortic position.

In the *in vivo* study the bio-interaction of the Glycar valve was tested in the ovine model in the absence of anti-coagulation in comparison with a bi-leaflet valve. Two groups of five Glycar valves and one Carbomedics bi-leaflet valve were implanted in the pulmonary valve position in juvenile sheep. Group 1 was followed for six months and Group 2 for twelve months after implantation.

Results

The Glycar valve was centred on a CAD design, which was based on flow-dynamic principles.

CFD confirmed acceptable flow-patterns - both during systole and diastole - with a greater than expected EOA (1.39 cm^2) and a low transvalvular gradient (1.5 mmHg). Systolic flow patterns showed a low incidence of flow separation and recirculation, minimal areas of stasis and turbulence, reduced vortex formation and a surface shear stress that does not exceed the platelet activation threshold.

The Glycar valve had comparative hydrodynamic properties and characteristics compared to the Carbomedics bi-leaflet valve in a simulated pulsatile environment. Pulse duplication comparison of the Glycar valve to commercially available mechanical and biological valves demonstrated similar pressure drops, Q_{rms}, energy losses and EOA's. However, at higher cardiac outputs (>8 L/min) the poppet valve developed significant regurgitation.

The current Glycar valve design in the pulmonary position in the ovine model proved to be reliable and thrombo-resistant in the absence of anti-coagulation in the short term as well as in the long term follow-up. None of the valves, control valves included, showed any macroscopic or microscopic thrombi. Biochemistry and hematology did not demonstrate hemolysis, activation

of coagulation or platelet activity. Histology showed no thrombi on the sewing cuff, housing, poppet or struts. None of the sheep had embolic events and no pulmonary embolic events or sequelae could be identified. Cardiac echocardiography confirmed normal prosthetic function in all valves except those with infective endocarditis.

Conclusion

The Glycar valve proved to be a suitable alternative to the traditional mechanical bi-leaflet valve design. The improvements made to the Glycar valve showed acceptable results in both the CFD analysis and pulse duplication testing, exceeding the minimum standards required by ISO 5840:2015 certification.

In the ovine model the Glycar valve demonstrated acceptable haemodynamics and no trombo-embolic events were recorded in the absence of anti-coagulation or anti-platelet drugs.

Future recommendations

- This prosthesis should be tested in a more aggressive coagulation model at systemic pressures or in the more thrombogenic tricuspid valve position.
- Improvement in the poppet design is required to address the regurgitation experienced at flows exceeding 8 L/min.
- Fatique testing of the final valve design.

CHAPTER 1
Introduction

1.1 Introduction

In 1997 a patient was referred to the department of Cardio-thoracic surgery at the University of the Free State in Bloemfontein, South Africa, for an aortic valve replacement. The patient presented with a high gradient across an aortic valve prosthesis. The patient had undergone an aortic valve replacement performed by Prof. Chris Barnard in Cape Town during the sixties and had not been using anti-coagulation therapy for years. At explantation it was found that the patient had a UCT valve and on closer inspection the valve was found to be in a good condition with some visible wear on the poppet due to the cloth covering on the housing. The base of the poppet belly showed some wear due to contact friction with the retaining strut. The poppet, housing, struts and sewing cuff were free of any visible thrombi. In addition, it was found that the gradient was due to patient-prosthesis mismatch and not valve dysfunction. The fact that the patient had not been using anti-coagulation sparked renewed interest in the UCT valve. This led to the reverse engineering of the valve with modifications to the design based on current valve design concepts.

Despite improvements in valve design over the past fifty years, valve replacement does not provide a cure for the recipient. Instead, the native valve is exchanged for prosthetic valve disease, marred with either prosthesis failure (biologic prosthesis) or anti-coagulation maintenance challenges. Anti-coagulation remains the Achilles heel of mechanical valvular replacement surgery. To avoid the detrimental and often fatal complications associated with valve thrombosis and thrombo-emboli, the use of Warfarin (Coumadin) is indicated (Nishimura *et al.,* 2014). Warfarin has to be monitored closely using the international normalised ratio (INR) (Jamieson *et al.,* 2004) as the therapeutic window is small and deviating from the target levels exposes a patient to risk of bleeding or thrombosis (Kaneko *et al.,* 2013, Ansell *et al.,* 2008). Due to the Warfarin induced coagulopathy, restrictions are placed on the daily lives of patients, contributing to lifestyle limitations on especially the younger patient (Akhthar *et al.,* 2009).

Ideally, mechanical heart valves should mimic the haemodynamic performance of a native heart valve and be durable enough to outlast the patient‘s life expectancy. The valve should also not need any anti-coagulation or anti-platelet management. Although the material used in most modern heart valves is inert and has minimal blood interaction, thrombosis still occurs (Klusak *et al.,* 2015). In the last four decades, significant advances have been observed in the development of bio-compatible materials used in blood interfacing mechanical implants

(Chambers *et al.,* 2014) but the thrombosis risk of the valves remains a significant risk. It would seem from historical data and own experience from the explanted valve, that the poppet valve design performed well in the absence of anti-coagulation. As a result, the need to revisit the poppet valve design and to evaluate the hydrodynamic and coagulation properties of a modification of the valve for possible commercial development was recognised. The valve would be an excellent alternative when valvular durability in the absence of anti-coagulation or anti-platelet therapy is required.

1.2 Aim

The aim of this study was to:

- perform an extensive review of mechanical heart valve research and development,
- re-engineer the UCT valve according to the latest principles of valve design,
- evaluate the flow-dynamics of the valve *in vitro* according to standard benchmark modeling and testing and
- test the bio-interaction of the valve *in vivo* in the ovine model.

1.3 Objectives

The objectives of this study was:

- to re-visit a historical poppet design and to re-design the valve - the Glycar valve - according to modern valve design principles,
- to review applicable literature on mechanical valve design, applicable coagulation considerations, bench testing techniques and the use of animal model testing,
- to explore the possibility of producing a mechanical heart valve that does not require anti-coagulation,
- to perform a computational fluid dynamic study to evaluate the properties of the Glycar valve and to determine the optimal valve design/configuration,
- to test the Glycar valve *in vitro* using pulse duplication to evaluate the Glycar valve's mechanical and fluid interaction properties in comparison to commercially available heart valves,
- to test the short term (six-month) and the long term (twelve-month) outcome of the valve in the pulmonary position without the use of anti-coagulation *in vivo,* in juvenile sheep.

CHAPTER 2
Literature review

2.1 Burden of heart valve disease

The lives of millions of people across the world suffering from heart valve disease were changed forever in the 1960s with the introduction of the mechanical heart valve by Harken *et al.* (1960) and by the first homograft cardiac valve implantation by Ross *et al.* (1962). Since then, changes in technology have improved the haemodynamic and physiologic parameters, and the durability of both the mechanical and bio-prosthetic heart valves (Birkmeyer *et al.,* 2000). Despite the fact that heart valve repair surgery has made great advances in recent years as our understanding of valve function and cardiac physiology have improved, valvular replacement surgery still plays a vital role in the management of heart valve pathology (Pibarot *et al*., 2009).

Heart valves are divided into two main groups: mechanical and bio-prosthetic. Mechanical prosthesis have the advantage of long term durability however, patients receiving a mechanical valve require life-long anti-coagulation within tightly controlled margins (Kaneko *et al.,* 2013). Bio-prosthetic valves made from bovine pericardium or a porcine valve, do not have the durability of mechanical prosthesis but have the advantage of not requiring anti-coagulation (Huth *et al*., 2001, Jamieson *et al.,* 1998).

An estimated 90 000 heart valves are implanted yearly in the United States alone (Pibarot *et al.,* 2009) with 275 000 (Sacks *et al*., 2001) to 370 000 (Butany *et al*., 2005) valve replacements worldwide. By 2050 a predicted 850 000 replacements will be performed yearly worldwide (Yacoub and Takkenberg. 2005). A vast majority of these replacements take place in the developed world and mostly in the elderly (figure 2.1) (Grunkemeier *et al.,* 2000). Western Europe, the United States of America (USA), Canada, Australia and New Zealand have witnessed an average increase of thirty years in the life expectancy of their populations (Christensen *et al.,* 2009). Age related degenerative calcific aortic stenosis (AS) is also the most common form of valvular heart disease in the western world (Thaden *et al.,* 2014*).* Clinically significant AS is age-dependent with an incidence of 0.2% in subjects aged 18–44 and 2.8% in those over 75. The incidence in those aged 80–89 has been reported as being as high as 9.8% (Rayner *et al.,* 2014). Therefore, with increasing life expectancy trends, the incidence of severe AS has risen dramatically and will continue to do so (Barreto-Filho *et al.,* 2013), leading to more patients needing valvular replacement surgery in the near future.

The need for valve replacement is also increasing each year and in Germany for example the number of aortic valve implants increased from 974 in 1978 to 9644 in 1999 (Kalmar *et al*., 2000). Of the implanted valves in the German Aortic Valve Registry (GARY), 90% were bioprosthetic

valves and over 60% TAVI valves (Mohr *et al.,* 2014 and Beckmann *et al*., 2012), due to the ageing of the population with age related increase in AS, as seen in Figure 2.1. Surgical aortic valve replacement rates have increased by nineteen procedures per 100,000 person-years between 1999 and 2011 in the USA (Barreto-Filho *et al.,* 2013). Prosthetic valve recipients in a first world population are predominantly in the age group of 60 –69 years, while the incidence in a developing country such as South Africa is broadly disseminated over an age-spectrum of 20-70 years (Zilla *et al.,* 2008).

Unfortunately, the majority of potential recipients of prosthetic heart valves are in the developing world where resources are scarce and access to cardiology and subsequent surgery is limited or unavailable (Unger *et al*., 2002). The incidence of rheumatic fever is greater in this younger population (McLaren *et al.,* 1975) with early onset heart valve pathology. A study performed by Zilla *et al*. (2008) in Cape Town, South Africa showed the discrepancy in age distribution of cardiac valve recipients between the first world and the developing world. Figure 2.1 illustrates this discrepancy in the age distribution, and therefore highlights the need for mechanical prosthetic valve use in the young population and the need for lifelong anti-coagulation.

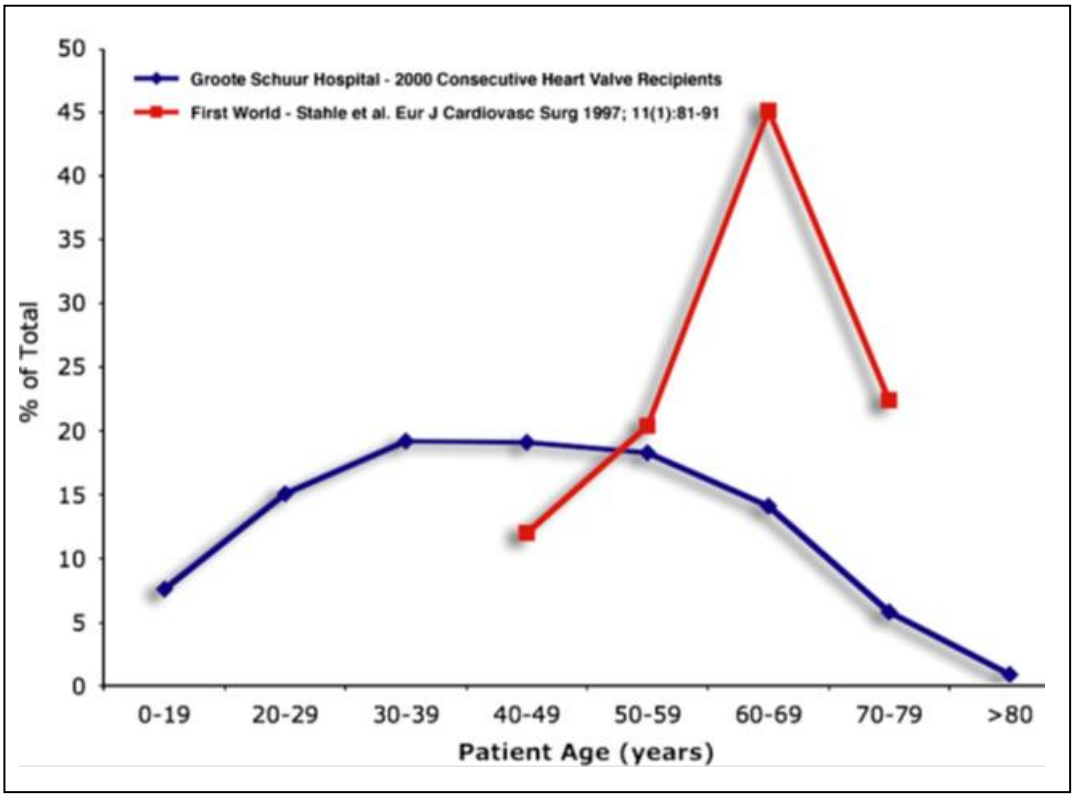

FIGURE 2.1: **Age distribution of patients undergoing heart valve replacement.** Valve replacements in the first world (red line) and in a developing world (blue line) are represented in the figure. The blue line represents 2000 consecutive heart valve replacements at the Groote Schuur Hospital (University of Cape Town) of whom a significant proportion of patients are younger than 20 years. (Adapted from Zilla *et al*., 2008).

The performance, degeneration and complications such as calcification, associated with biological/tissue valves (Jamieson *et al.,* 1998), preclude the use of biological prosthetic valves in the young, although biological valves have superior haemodynamic and clotting performance.

The often fatal complications associated with long term mechanical valve exposure accumulate over patient-years (Mc Anulty *et al.,* 2008). The incidence of mechanical valve associated complications is escalated due to a lack of compliance with anti-coagulation treatment due to educational and infrastructure shortcomings (Antunes *et al*., 1988; Kinsley *et al*., 1986 and Taljaard and Doubell, 2003).

The risk of thrombo-embolic events is higher with mechanical valves than bio-prosthetic valves (Akhthar *et al.,* 2009), higher with mitral than with aortic prosthetic valves, and higher in the early post-operative phase (<3 months) (Vahanian *et al*., 2007 and Jamieson *et al*., 2004). The presence of concomitant risk factors compounds the incidence of thrombosis and include (Heras *et al*., 1995):

- atrial fibrillation,
- left ventricular dysfunction,
- left atrial dilatation,
- previous thrombo-embolism and
- hypercoagulable conditions.

The incidence of obstructive prosthetic valve thrombosis varies between 0.3% to 1.3% patient-years (Horstkotte *et al.,* 1995, Mc Anulty *et al.,* 2008). Thrombo-embolic complications, including systemic emboli, are more frequent and occur at a rate of 0.7% to 6.0% patient-years (Roudaut *et al., 2007)*. Non-obstructive valvular thrombosis is a relatively frequent finding in the post-operative period, with a reported incidence as high as 10% in a transoesophageal echocardiography study performed by Roudaut *et al.* (2007).

According to a series of surgical interventions for valvular thrombosis, the first post-operative year is marked by a 24% incidence of thrombosis, an incidence of 15% between the second to fourth year and decrease to 6% per annum thereafter (Deviri *et al.,* 1991).

The management of anti-coagulation during pregnancy poses a significant burden (Bonow *et al*., 2006 and Elkayam *et al*., 2005). Anti-coagulation management in pregnancy requires a comprehensive evaluation of risk versus benefit. Pregnancy is a hypercoagulable state complicating INR control (Caceres-Loriga *et al.,* 2006). Warfarin is probably safe in the first six weeks of gestation, but the risk of embryopathy is high when Warfarin is taken between six and twelve weeks of gestation (Nishimura *et al.,* 2014; Kaneko *et al.,* 2013 and Bates *et al,* 2012). The patient is therefore required to receive heparin during this interval, followed by Warfarin up to the 36th week, followed with heparin therapy until delivery (Caceres-Loriga *et al., 2015*).

An overview of mechanical valve related complications for a number of commercial valves implanted in the mitral position is provided in table 2.1

Table 2.1: **Comparison of valve related complications in the mitral valve position** (Adapted from Nair *et al.,* 2003)

Valve model	Valve type	Incidence (% / patient-years)					
		Thrombosis	Embolism	Bleeding	Infective endocarditis	Paravalvular leaks	Total
Bjork-Shiley	Tilting disc	0.6	1.7	1.2	0.1	0.7	4.3
Medtronic-Hall	Tilting disc	1.1	3.1	0.5	N/A	0.7	5.4
Chitara	Tilting disc	106.0	2.4	0.4	0.5	0	4.9
St. Jude Medical	Bi-leaflet	0.0	3.4	1.6	0.3	N/A	5.3
Carbomedics	Bi-leaflet	0.4	0.9	0.9	0.5	0.9	5.1

N/A = Not available

The treatment regime in the African setting places an enormous burden on an already overtaxed health system and exposes the patient to complications due to mismanagement of anti-coagulation because of low patient literacy, poor socio-economic circumstances and governmental financial constraints (Zilla *et al.,* 2008). The use of bio-prosthetic valves in the patient of child bearing age is attractive as no anti-coagulation is required and the risk of thrombo-embolism is eliminated (Elkayam *et al*., 1998). Patients between the ages of 16 and 39 at the time of surgery, with either Hancock (Hancock Jaffe Laboratories, Irvine, California) or Carpentier-Edwards porcine bio-prosthesis (Edwards Life sciences, Irvine, California) demonstrated a high incidence of structural valve disease, which became significant as early as two to three years after surgery and was as high as 50% at 10 years and 90% at 15 years, necessitating early re-operation (Jamieson *et al.,* 1998).

The risk of structural valve disease was seven-fold greater (North *et al*., 1999) in the mitral than the aortic or tricuspid position. Women of childbearing age who receive bio-prosthetic valves are likely to need re-operation early on and therefore the risk associated with a second surgery has to be considered when a prosthesis is being selected. The early peri-operative mortality for re-operation to replace the dysfunctional bio-prosthesis ranges between 3.8% and 8.7% (Jamieson *et al*., 1998 and Badduke *et al*., 1991).

2.2 Mechanical cardiac valve development

2.2.1 History of valve design and fluid interaction

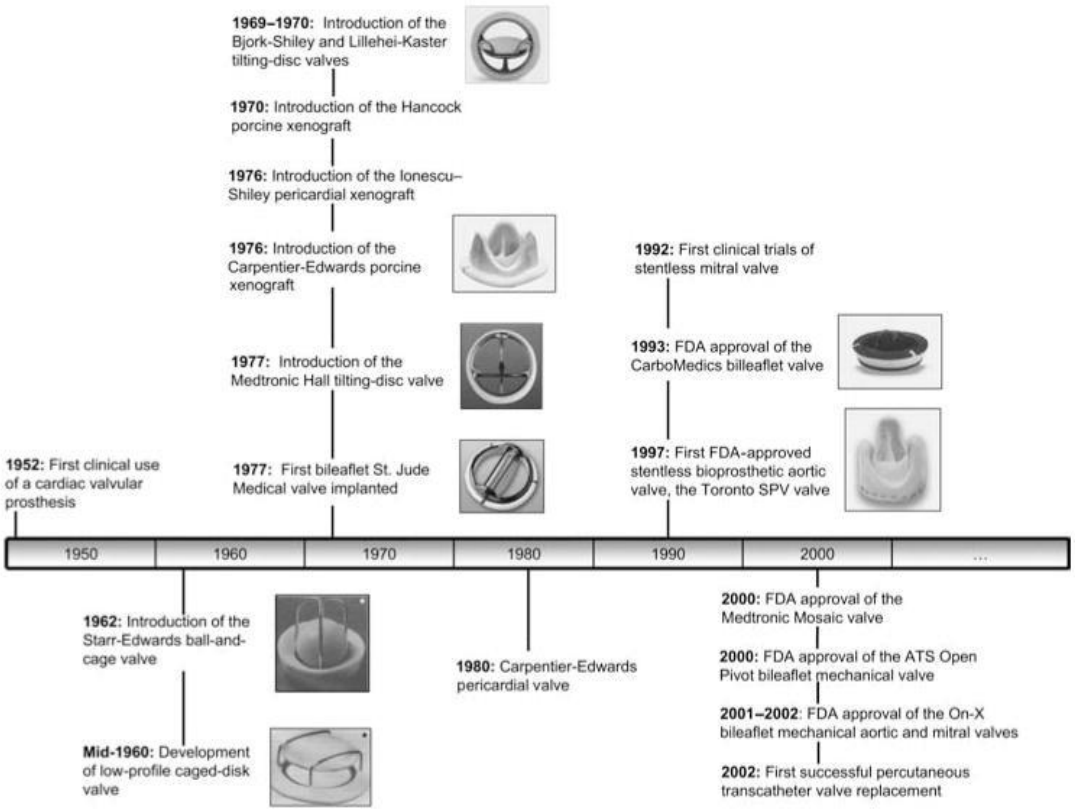

FIGURE 2.2: **The evolutionary timeline in the development of heart valves** (Adapted from Dasi *et al.,* 2009).

The first heart valve replacement was performed by Dr C Hufnagel in 1951 (Vincent *et al.*, 2003). The valve was implanted in the descending thoracic aorta in a patient with aortic valve disease. A valve placed in this location would provide no benefit to a patient with aortic stenosis and only minimal benefit to patients with aortic insufficiency. However, this heralded the age of mechanical valve research.

Seven years after the first open heart procedure was performed by Dr Gibbon (the pioneer behind the heart lung machine), Dr D Harken performed the first successful mechanical heart valve replacement. He implanted a cage-ball valve in the sub-coronary position in a patient with aortic stenosis. Following his sucsess, research in valve design was pursued with vigour and more than seventy different prosthetic heart valves (Figure 2.2) have been implanted into millions of patients (Dasi *et al.,* 2009).

i. The ball-and-cage heart valve

a. History

The first heart valve available was designed by Dr Charles Hufnagel in 1951 (DeWall *et al.,* 2000). This valve had a methyl methacrylate (perspex) outer chamber surrounding a methacrylate ball (Figure 2.3). The valve was implanted in over 200 patients in the descending aorta during a brief aortic crossclamp and was used without anti-coagulation. Some of these valves were recovered thirty years after implantation with no obvious wear (Vincent *et al*. 2003). Due to the bulky design it could not be used as a valve substitute but it introduced the field of bio-interaction and flow-dynamics in a non-Newtonian fluid.

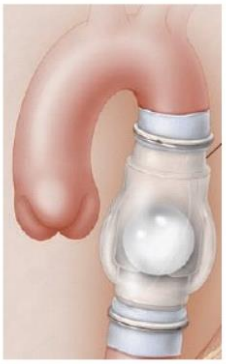

FIGURE 2.3. **Hufnagel valve in the descending aorta.** (Adapted from http://www.slideshare.net/PulkitPal/heart-valves-38655465)

The Harken ball valve and the widely used Starr-Edwards ball valve (Figure 2.4) were both introduced in 1960 and used successfully commercially (Dasi *et al.,* 2009). Designed by Miles Edwards, a hydraulics engineer and Dr Albert Starr, a cardiothoracic surgeon, the Starr-Edwards valve was the most widely used valve in the sixties and more than 200 000 valves were implanted (Godje *et al*., 1997). Over the years the design has undergone several modifications but the basic design has remained the same.

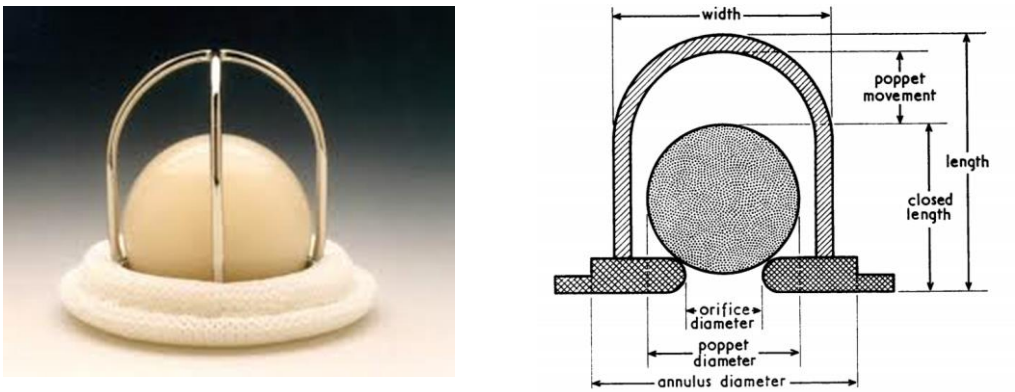

FIGURE 2.4: **The first generation heart valve: Starr Edwards Model 6100** (Adapted from https://www.flickr.com/photos/sacdrbob/7430185090).

The valve consists of a barium impregnated silastic ball confined within two stellite alloy U-shaped arches that form a cage over the ball and a sewing ring of teflon or polypropylene fixed to a stellite alloy frame (Figure 2.4) (Dasi *et al*., 2009).

During the forward flow phase, otherwise referred to as antegrade flow, the ball moves forward into the cage and blood passes circumferentially around the ball, between the sewing ring and the trailing edge of the ball between the struts. During backward flow, the ball then moves back to seat snugly against the sewing ring preventing regurgitant flow (Grunkemeier *et al*., 2000).

b. Haemodynamic flow profile of the ball cage design

Owing to their inferior haemodynamic characteristics and the bulky design, caged-ball valves are not implanted anymore (Godje *et al.,* 1997). The valve design has two major drawbacks. Firstly, it has a high-profile configuration as the smaller valves are more obstructive in nature and cannot be implanted in small left ventricles for mitral valve replacements and secondly, the occluder induces turbulence during antegrade flow (Figure 2.5 and 2.6) (Chandaran *et al.,* 1985). The result is a reduced effective orifice area (EOA), increased turbulent shear stress, large areas of stasis and thus, increased thrombogenicity (Starr *et al.*, 1969).

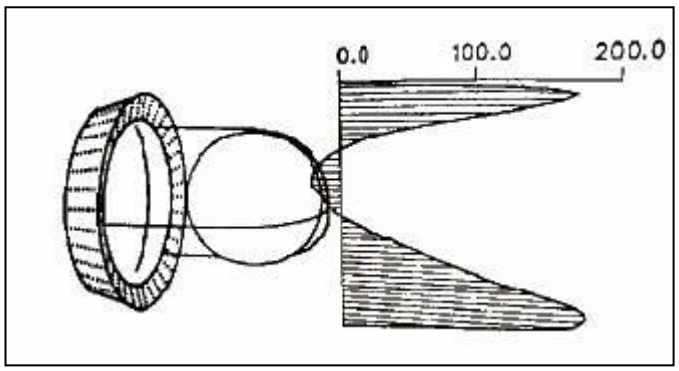

FIGURE 2.5: **The haemodynamic profile of the Starr-Edwards valve.** The primary draw back of the cage-ball design is a flow profile (graph denotes flow velocity in cm/s) that is disrupted towards the centre due to the presence of the ball. (Adapted from www.bme240.eng.uci.edu/ students /07s/ vnguyenhoai/mechanical.html)

During antegrade flow, the flow emerging from the valve forms a circumferential jet that separates from the ball, hits the wall of the aorta and then flows along the aorta (Figure 2.6). Chanderan *et al.* (1985) reported on the flow profile of the Starr-Edwards valve. They reported a maximum velocity as high as 2.20 ms^{-1} near the annulus, which decreases to 1.80 ms^{-1} 30 mm downstream of the valve. Figliola *et al*. (1977) found that downstream of the apex of the ball, a wake develops and a region of low-velocity re-circulating flow is present throughout the forward flow phase. A region of high velocity gradients exists at the edge of the forward flow jet as well as in the recirculation region resulting in an area of high shear stress.

A maximum turbulent viscous shear stress of up to 1850 dyne/cm^2 is measured in this region (Chandaran *et al.,* 1985 and Murphy *et al.,* 1983). Turbulent shear stresses reach a high of 3500 dyne/cm^2 in the annular region between the flow channel wall and the ball. These high shear levels are well above the established thresholds to activate platelets (Wurzinger *et al.,* 1985). The activated platelets eventually get trapped in the recirculation region, where platelet-to-platelet contact is enhanced (Antunes *et al.,* 1988). This is where thrombus formation may occur and is confirmed by clinical results that revealed the presence of thrombi at the apex of the cage seen at explantation of thrombosed valves (Chandaran *et al.,* 1985).

During the back flow phase (Figure 2.6), the ball moves back to seat into the housing. A small gap may form between the ball and the housing permitting mild regurgitation. This regurgitant flow may be beneficial by dislodging micro thrombi that might have formed on the housing or the sewing cuff (Dasi *et al.,* 2009). However, regions of elevated shear may exist at the edges of the leakage jets, encouraging platelet activation (Chanderan *et al.,* 2006).

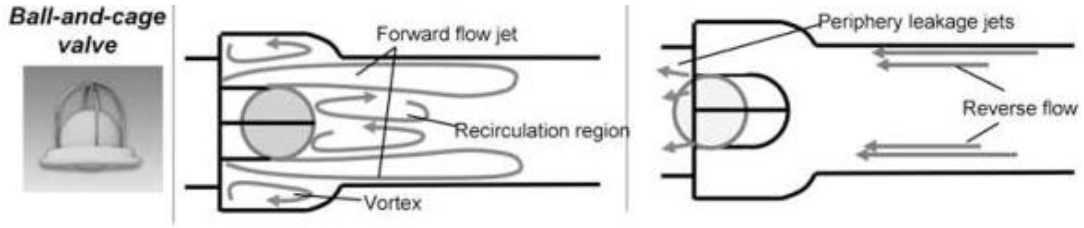

FIGURE 2.6: **Blood flow contours through a ball-and-cage valve**. Notice the large low pressure area with recirculation distal to the ball and areas of turbulent flow. (Adapted from Chanderan *et al.,* 2006)

Harker and Slichter (1970), showed that patients with first-generation mechanical valves such as the ball-and-cage valve had a shortened platelet half-life due to an increased incidence of platelet destruction and activation. The authors concluded that direct mechanical trauma due to continuous impact with the valve superstructure and the shear forces induced by turbulent flow, were two possible mechanisms accounting for this destruction. They also found that continuous sub-lethal haemolysis lead to alterations in red cell membrane morphology and reduced membrane flexibility.

The valve was also not suitable in the mitral position in patients with a small left ventricle or in the aortic position in those with a small aortic annulus and those requiring a valve-aortic composite graft (Chanderan *et al.,* 2006).

ii. The non-tilting disc valve

a. History

The Kay-Shiley disc valve (Figure 2.7) was designed by Dr Jerome Kay, professor of cardiac surgery at the University of Southern California Medical Centre, and the valve engineer, Mr Donald Shiley in 1965 (Dasi *et al.,* 2009). The valve was a mitral prosthesis based on the ball-cage design. It had a stellite alloy housing with a restraining cage of two U-shaped wire struts, and the ball was replaced with a flat silicone elastomer disc (Vincent *et al.,* 2003).

The durability of the valve was markedly improved when the silicone disc was replaced with a delran disc. Approximately 12 000 Kay-Shiley valves were implanted worldwide in the mitral and tricuspid position (Lillehei *et al.,* 1989). However, due to poor haemodynamic performance, high thrombogenicity, material dysfunction causing strut fractures, disc embolisation and disk impingement, the use of this valve fell out of favour early (Lillehei *et al.,* 1989).

The Cooley-Cutter aortic prosthesis was designed by Dr Denton Cooley in collaboration with Cutter laboratories and introduced in 1971 (Saddoughi *et al*., 2014). The device used 2 sets of titanium struts to contain a biconic occluder composed of pyrolytic carbon. A total of 3275 patients (1786 in the aortic position and 1475 in the mitral) received the valve over a 10-year period, with very good clinical results (Cooley *et al*., 1973).

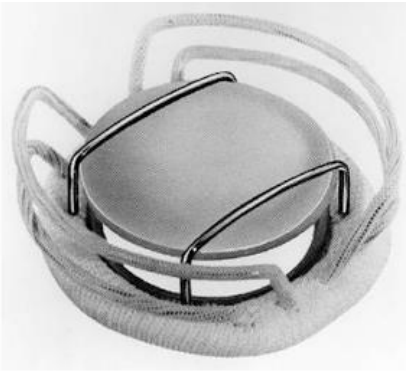

FIGURE 2.7: **The non-tilting disk valve** (Adapted from https://sites.google.com/site/heartvalveproject).

b. Haemodynamic flow profile of the non-tilting disk valves

The disc caused high velocity, turbulent jets adjacent to the cage and the occluder, similar to those observed with the ball-and-cage valves (Jones and Eidbo, 1989). However, the jets and the turbulence were greater in magnitude. Chanderan *et al.* (2006) evaluated the flow-dynamics of this valve and found that the high velocity jets decayed in such a way that the flows became nearly laminar and had low velocities approximately 2 cm distal to the valve housing.

The portions of the peripheral circumferential jets adjacent to the valve housing were small, demonstrating flow widths of no more than 5 mm. Dasi *et al.* (2009) described a large region of vortex eddy formation producing flow reversals, with velocities as high as 0.50 ms^{-1} distal to the disc. These regions had diameters approaching 2 cm distal to the occluder and extended as far as 2 cm toward the left ventricular apex. Additionally, there were small areas of stagnation with no detectable velocities immediately distal to the disc explaining the high thrombogenicity of the valve.

iii. The tilting disc valve

a. History

A big innovation in valve design occurred in 1963 with the introduction of the tilting disc valve by Lillehei, Cruz and Kaster (Magovern *et al*., 1989). The aim of this valve was to mimic the natural flow patterns of blood in the aorta and to minimise the obstructive nature of the occluder as found in the ball-cage designs. A typical tilting disk valve comprised of a circular sewing ring and an eccentrically hinged or pivoting pyrolyte carbon disk occluder (Dasi *et al.,* 2009). The disk opens to show two unequal orifices; a major and a minor orifice (Figure 2.8) allowing for antegrade blood flow. During retrograde flow, pressure against the leading portion of the tilted disk results in closure by rotating on the hinge or pivot (Chanderan *et al.,* 2006 and Gott *et al.,* 1964). The tilting motion provides improved central laminar flow while it prevents back flow and also reduced mechanical damage to blood cells (Chanderan *et al.,* 2006). Although it was a great advancement with a decreased risk of thrombosis and infection, damage to blood cells still occurred (Lillehei et al., 1989).

FIGURE 2.8: **The Bjork-Shiley tilting disk valve** (Adapted from www.pages.drexel.edu/~nag38/History.html)

The first tilting disc design was riddled with complications and problems and the design was modified by Bjork and Shiley (Magovern *et al.,* 1989). They moved the pivot point away from the midline and the valve hinge was replaced with two U-shaped wire struts welded to the housing as the disc retainer and the polymer disk were replaced with a pyrolyte carbon disc (Figure 2.8). The Bjork-Shiley valve was extremely successful worldwide, with nearly 300 000 aortic and mitral prosthesis implanted between 1969 and 1986 (Lindblum *et al.,* 1989).

FIGURE 2.9: **The Medtronic-Hall valve**. (Adapted from www.pages.drexel.edu/~nag38/History.html)

Further improvements had to be made as strut failure due to metal fatigue, was a complication commonly observed (Grunkemeier *et al.,* 2000). The Omniscience and Omnicarbon valve designs removed the problematic wire struts and replaced them with small earlike guards welded to the sewing cuff (Pinney *et al*., 2004), but this valve design was discontinued due to leaflet escape with embolisation (Kornberg *et al.,* 1999).

The Medtronic-Hall valve (Figure 2.9), introduced clinically in 1977 (Butchart *et al.,* 2001) is the most commonly implanted tilting disk valve and is second only to the St Jude bi-leaflet valve as the most frequently implanted mechanical prosthesis (Antunes *et al.,* 1988). The pyrolytic carbon disk has a small central orifice through which a strut passes, enclosed within a titanium housing (Dasi *et al*., 2009).

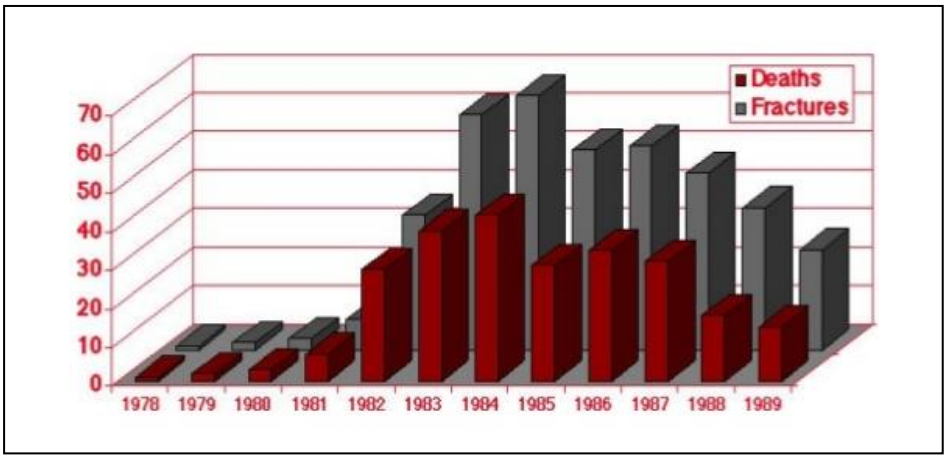

FIGURE 2.10**: Mortality graph of the Bjork-Shiley Convexo-concave tilting disk valve**. The grey bars refer to strut failures due to metal fatigue and fracturing with the red bars indicating deaths as a result. (Adapted from Butchard *et al*., 2001).

The Bjork-Shiley convexo-concave tilting disc valve was another modification to the tilting disk design. In an effort to provide a larger flow through the orifice on the backside of the open disc, a concave pyrolyte disc was used and the inlet and outlet struts were modified (Lillehei *et al.,* 1989). The disc could now slide forward and down about 2 mm, achieving the desired enlargement of the lesser valve orifice. Although it improved the flow characteristics it caused

excessive closing stress on the hinge mechanism and the valve was plagued with strut fractures and valve failures (Butchart *et al.,* 2001 and Harrison *et al.,* 2013). Figure 2.10 shows the fate of the valve design.

At an average of five years after implantation the valves experienced metal fatigue and subsequent strut fractures with disc embolisation, leading to severe acute insufficiency and in many patients this was fatal (Butchart *et al.,* 2001). In the aortic position the sudden loss of the valve leaflet reduced coronary perfusion acutely and in the mitral position acute pulmonary oedema. Although the haemodynamic characteristics were very good compared to other tilting disc valves, the valve was discontinued and due to litigation most of these valves have been explanted prophylactically.

b. Haemodynamic flow profile of tilting disk valves

Monoleaflet valves have a single tilting disk, placed off-centre within the valve housing with an opening angle ranging from 75^{o} to 90^{o} depending on the valve design (Butchard *et al.,* 2001). During antegrade blood flow the disc tilts into the open position to form a major and a minor orifice. The major orifice has a large forward flow jet (Figure 2.6 and Figure 2.12), whereas a smaller jet of lesser velocity flows from the minor orifice (Chanderan *et al.,* 2006). These two jets of different velocities induce a recirculation in the wake of the disc and a recirculating flow pattern in the sinus region (Chandaran *et al.,* 2006).

High turbulent shear stresses are confined to narrow areas at the edges of the major orifice jet (Figure 2.11 and 2.12) (Manning *et al.,* 2008). Maximum turbulent shear stresses measured at peak systole are in the order of 1500 dyne/cm^2 (Chandaran *et al.,* 1983). High turbulent shear stresses are more dispersed in the minor orifice than those in the major orifice region (Jones and Eidbo, 1989).

During the closed phase, the tilting disc moves back and seats on the valve housing to occlude the valve orifice. A small gap may be present at the periphery of the disc, permitting a small amount of flow regurgitation or leakage flow (Dasi *et al.,* 2009). The Medtronic-Hall valve has a central retaining strut protruding through the disc (Figure 2.11 and 2.12). This mechanism requires the presence of a hole in the centre of the tilting disk, allowing for a high velocity jet through the hole during the closed phase. The shear stress and turbulence experienced during the leakage phase is associated with elevated shear stress on the edge of the jets leading to platelet activation (Butchard *et al.,* 2001).

Chanderan *et al.* (2006) performed detailed flow pattern analyses on tilting disk valves and found that jets through the minor orifice were delayed compared with the jets through the major orifice (Figure 2.11). The authors describe how these jets decelerate and the flow becomes laminar and nonturbulent during mid-diastole with velocities reaching 5.60 cm/s.

Vortex shedding from the jet boundary layers were visualised as velocity reversals in the left ventricular outflow tract. Vortex eddies, producing flow reversals with velocities of -20 to -30 cm/s (Figure 2.12) occur just distal to the disc (Akutsu *et al.,* 1999). However, these areas of flow reversal are smaller than those occurring with the ball-and-cage valves (Jones and Eidbo, 1989).

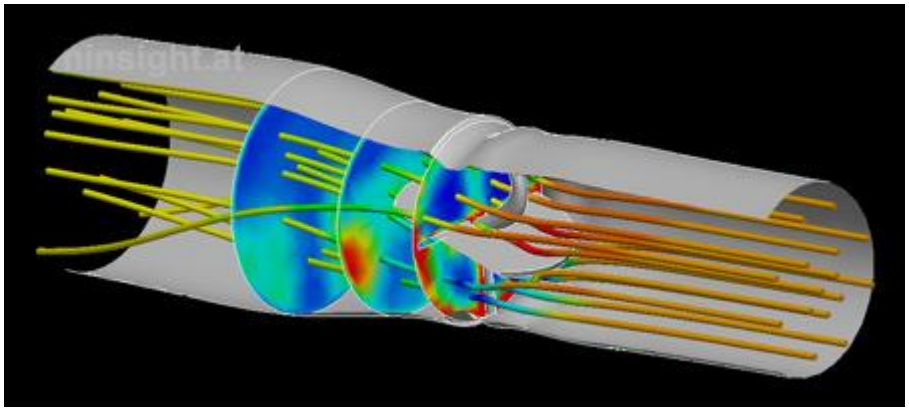

FIGURE 2.11: **CFD simulation of the tilting disk valve**. The image shows flow during the systolic phase with the valve fully opened at 75°. Streamlines are coloured by the local pressure. Section planes show the turbulent dissipation and shear stress. (Adapted from www.ninsight.at/bioSamplesHeartValve.shtml)

The Medtronic-Hall valve disk has a maximum opening angle of 75^{o} for the aortic valve and 70^{o} for the mitral prosthesis (Butchard *et al.,* 2001). Due to the fact that the disk does not open 90^{o} it generates resistance to forward flow (Figure 2.11, 2.12 and 2.13) (Manning *et al.,* 2008), causing small eddies of stagnant flow proximal and around the valve disk, increasing the thrombosis risk (Lillehei *et al.,* 1989).

The design of most mechanical heart valves include areas that allow for deliberate leakage or retrograde flow upon valve closure (Manning *et al.,* 2008). The intention of this reverse flow is to 'wash' critical areas in the valve such as the hinge mechanism and the areas between the housing and the valve leaflet to limit and prevent stagnation and recirculation.

Yoganathan *et al.* (1986) evaluated the leakage flow phase of the tilting disk valve in detail. They found that under pulsatile flow conditions the peak reverse velocity through the Medtronic-Hall valve was 0.28 m/s, with a peak turbulent shear stress of 680 dyne/cm^{2}, which is above the platelet activation threshold, explaining the increased thrombogenic risk of the valve. These findings are supported by fluid dynamic studies performed by Manning *et al.* (2008).

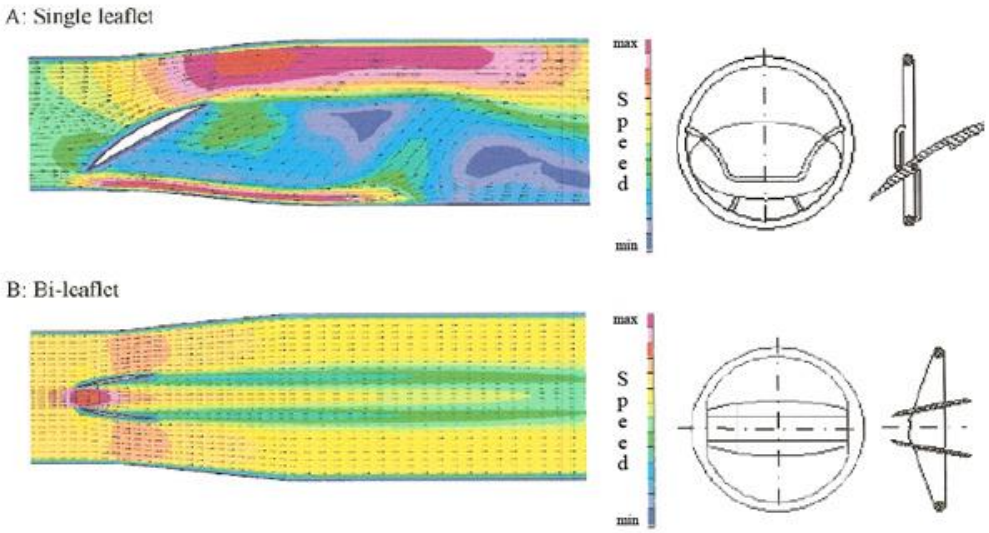

FIGURE 2.12: **Comparative flow velocity patterns through a tilting disk and bi-leaflet valve**. (A) Represents the velocity distribution through a tilting disk valve and (B) bi-leaflet valve. The blue areas indicate the presence of stagnant and turbulent flow with recirculation. These areas are responsible for the less desirable influence on thrombosis formation of the tilting disk valves when compared to the bi-leaflet valves. The red areas represent high flow velocity with increased shear stress. (Adapted from Manning *et al* 2008)

Baldwin *et al.* (1991) found that when a Bjork-Shiley valve was placed into a left ventricular assist device the highest shear stress near the aortic valve was found to be 9900 dyne/cm^2 and the corresponding peak velocity in the leakage jet 2.8 ms^{-1} during diastole. Near the mitral valve the highest turbulent shear stress was 9000 dyne/cm^2 with a peak leak velocity of 4.4 ms^{-1}. These findings were confirmed by Meyer *et al.* (1997) and Yoganathan *et al.* (2005). Meyer *et al.* (1997) reported on measurements in the regurgitant flow region proximal to a Bjork-Shiley valve in the mitral position and recorded maximal flow velocities of 3.7 ms^{-1} and peak turbulent shear stresses of 10 000 dyne/cm^{2,}.

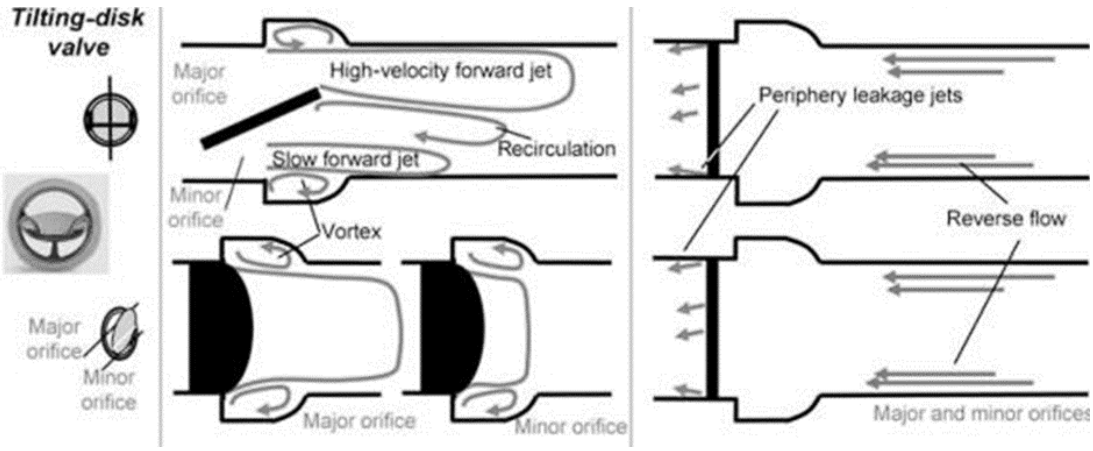

FIGURE 2.13: **Flow fields in a tilting disk valve during forward flow (left) and during the leakage flow phase (right)** (Adapted from Chanderan *et al.,* 2006).

iv. The bi-leaflet valve

a. History

FIGURE 2.14: **Examples of commercially available bi-leaflet valves** (Adapted from Kheradvar *et al.,* 2014).

The need for a low profile valve with improved fluid dynamic performance led to the introduction of the bi-leaflet valve in 1979 and largely replaced the mono-leaflet valve (Dasi *et al.,* 2009). These valves consist of two semi-circular leaflets that pivot on hinges in a supporting ring (Figure 2.14). The pyrolytic carbon leaflets swing open completely, parallel to the direction of blood flow resulting in the closest reproduction of central flow achieved in the heart (Dumont *et al.,* 2007). The pyrolyte carbon leaflets and the carbon housing exhibit high strength and has excellent biocompatibility. For this reason the bi-leaflet valve remains the most popular valve design available and to date a total of four million implantations have been performed since its introduction in 1979 (Kheradvar *et al.,* 2014 and Dasi *et al.,* 2009).

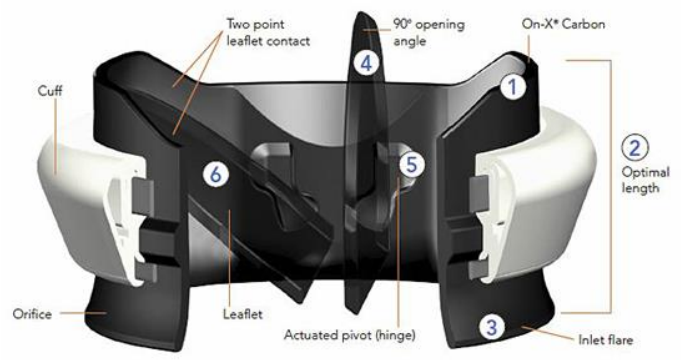

FIGURE 2.15: **The anatomy of the On-X bi-leaflet valve.** The two pyrolytic carbon semi-circular leaflets (4 and 6) are housed between pivot points (5) inside a carbon housing (1). A titanium locking ring holds the sewing ring in position on the housing, but still allows for rotation of the valve after implantation. (Adapted from www.onxlti.com/medical-professionals/on-x-prosthetic-heart-valve-design-and-features/)

i. The St Jude medical bi-leaflet valve

The St Jude Medical (SJM) bi-leaflet valve (Figure 2.14) was designed in 1979 and is the most widely used heart valve with more than one million valves implanted (Ellis *et al.,* 2000). The entire valve, the leaflets and the housing, is made from a graphite core with a pyrolytic carbon covering and impregnated with tungsten for radio-opacity (Dasi *et al.,* 2009). Each semi-circular leaflet has an extension region at the base that pivots/hinges on a recess in the housing (Yun *et al.,* 2014). The leaflet hinge mechanism requires no supporting struts, and therefore reduces the orifice obstruction caused by the leaflets and supporting mechanisms, providing a favourable flow profile with lower transvalvular gradients (Dumont *et al.,* 2007). With antegrade flow the leaflets open to a maximum of 85^{o} resulting in a central rectangular orifice and two large lateral semi-circular orifices, resulting in central near laminar flow (Butany *et al., 2005)*. With sufficient back pressure the leaflets rotate on their hinges to close at an angle of 25^{o} to the plane of the supporting ring.

ii. The Carbomedics bi-leaflet valve

Since the introduction of SJM bi-leaflet valve, several attempts have been made to improve upon that bi-leaflet valve design. In 1993 the Sorin Group (Austin, Texas, USA) introduced the Carbomedics bi-leaflet prosthesis (Figure 2.16) (Dasi *et al.,* 2009). According to Grunkemeier *et al.* (2000) several changes were made to this design. The opening angle of the leaflets is 78^{o},which encourages synchronous closure. The shapes of the hinge region were changed to have sharper features than the hinge region of the SJM valve. It has a solid pyrolytic carbon housing and has flat leaflets with a pyrolytic carbon coating over a tungsten loaded graphite substrate. The prosthesis has excellent radio-opacity with a radio-opaque titanium stiffening ring and increased tungsten content in the leaflet substrate (Chanderan *et al.,* 2006). The pivot mechanism is within the housing and is not protected by pivot guards, struts, or orifice projections, thus allowing for leaflet motion by rotation within the recessed hinge (Yun *et al.,* 2014).

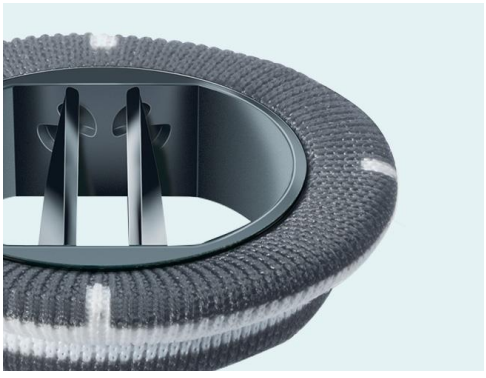

FIGURE 2.16: **The Carbomedics valve showing the hinge mechanism**. Leaflets rotate in the two semi-circular leaflet hinge depressions. Both the leaflets and the housing is covered with pyrolytic carbon and the dacron sewing cuff is impregnated with silver nitrate to reduce the incidence of Infective endocarditis. (Adapted from www.surgicaltechnology.com/15-149-CS-Page3-.html)

iii. The ATS open pivot bi-leaflet valve

The ATS (Advancing The Standard) Open Pivot valve from Medtronic (Minneapolis, USA) was introduced in 2000 (ATS, 2000). The ATS prosthesis differs from other bi-leaflet models in that there are no cavities in the valve ring in which stasis or eddy currents may develop (Emery *et al.,* 2003). The traditional recessed pivot mechanism is inverted to a protruding hinge design, exposing the pivot to the bulk forward flow (Dumont *et al*., 2007). According to Emery *et al.* (2003) the valve leaflets hinge on convex pivot guides on the pyrolytic carbon orifice ring (Figure 2.17). This allows for a low profile valve with no cavities in the region of the pivot area. The pivot guides are fully exposed to blood so there is continual washing of the leaflets and hinge. The sewing cuff is mounted on a titanium ring allowing rotation during implantation and radio-opacity of the leaflets is ensured by adding 20% tungsten to the leaflets.

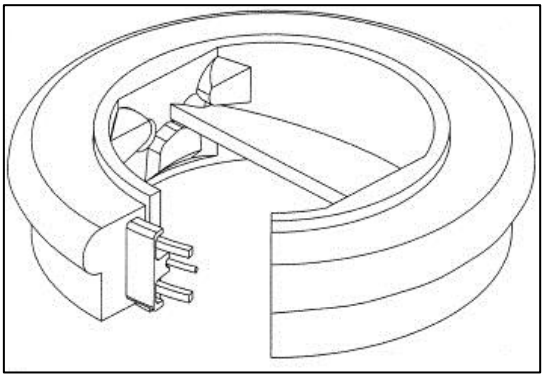

FIGURE 2.17: **A close-up view of the hinge mechanism of the ATS valve**. Note the protruding hinge design in which the valve leaflets freely float. (Adapted from Emery *et al.,* 2003).

iv. The On-X bi-lealfet valve

The On-X valve, marketed by the Medical Carbon Research Institute (Austin, Texas, USA), is the most recent mechanical valve design introduced in the USA (Dasi *et al.,* 2009, Bokros *et al.,* 2003 and Williams *et al.,* 2006). Puskas *et al.* (2014) describes the valve as a bi-leaflet prosthesis with a pure, non-silicone carbide alloyed pyrolytic carbon housing, with flat valvular leaflets made of a tungsten loaded graphite substrate with a pyrolytic carbon coating. The prosthesis design provides a curved housing in flow geometry (Figure 2.15) with an orifice diameter-to-housing height ratio to minimise the vena contracta and facilitate laminar blood flow through the valve phenomenon (Vena contracta is the point in a fluid stream where the diameter of the stream is the least and fluid velocity is at its maximum, such as in the case of a stream emerging from a nozzle or orifice (Falkovich, 2011). The leaflet motion is by translation and rotation within the housing. The opening angle is 90º to the housing, but usually opens to an unstopped position of 85º. The leaflets travel an arc of 50º and close at an angle of 40º. The leaflets have a two-point landing mechanism during valve closure, thereby reducing cellular damage (Figure 2.15) (Palatianos *et al.,* 2007).

b. Haemodynamic flow profile of bi-leaflet valves

During the open position the two leaflets rotate to a maximum angle of between 75º to 90º (Puskas *et al.,* 2014 and Aluri and Chanderan, 2001). Yun *et al.* (2014) studying the flow-dynamics of bi-leaflets, state that the leaflets divide the valve orifice into three distinct regions of blood flow: two lateral orifices and a central orifice (Figure 2.18 and 2.19). This explains the triple jet structure seen with the major part of the forward flow emerging from the two lateral orifices. Measurements along the centre plane of the valve 8 mm distal to the valve annulus show that the peak velocity in the lateral orifices is 2.2 ms^{-1}, which is higher than the velocity in the central orifice (2 ms^{-1}).

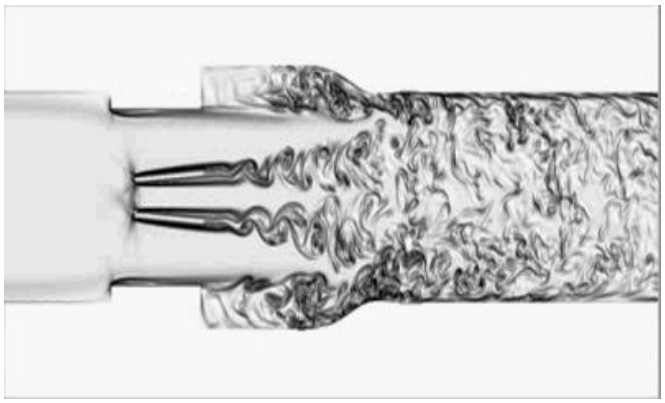

FIGURE 2.18: **Flow pattern across a bi-leaflet valve**. (Adapted from Chanderan *et al.*, 2006)

Figure 2.18 and 2.21 clearly illustrate the flow pattern associated with bi-leaflet valves downstream of the valve at peak forward flow. Chandaran *et al.* (2006) described these high turbulent shear stresses present at areas of high-velocity gradients and at areas immediately distal to the valve leaflets. The flow becomes disturbed as it travels downstream of the valve. The illustration depicts the chaotic vorticity contours occurring downstream to the valve, also referred to as vortex shedding..

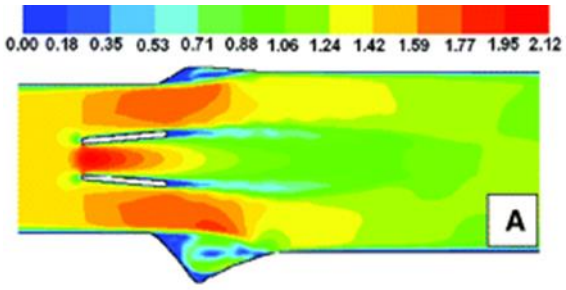

FIGURE 2.19: **Numerical simulation of flow across a bi-leaflet valve** (Adapted from Yun *et al.*, 2014).

Chanderan *et al.* (2006) describes how, during peak forward flow, alternately rotating counter vortices in the wake of the leaflets are created (Figure 2.21) and disappear during the deceleration phase and are replaced by a highly chaotic flow field. The peak turbulent shear stresses measured along the centreline plane at peak systole are in the order of

1500 dyne/cm^2 (Figure 2.21 and 2.23) downstream of the valve (Yun *et al., 2014)* and peak shear stress in the narrow central orifice is in the order of 35 kPa (Dumont *et al.,* 2007). Figure 2.19 shows the flow velocity distribution in a bi-leaflet mechanical valve at a cardiac output of 5 L/min. Yun *et al.* (2014) investigated the flow velocity across a bi-leaflet and found that within the central orifice the flow is higher than the flow in the lateral orifices. Accordingly, the peak gradient across the central orifice is 19 mmHg, which is higher than the actual peak trans-prosthetic gradient of 10 mmHg.

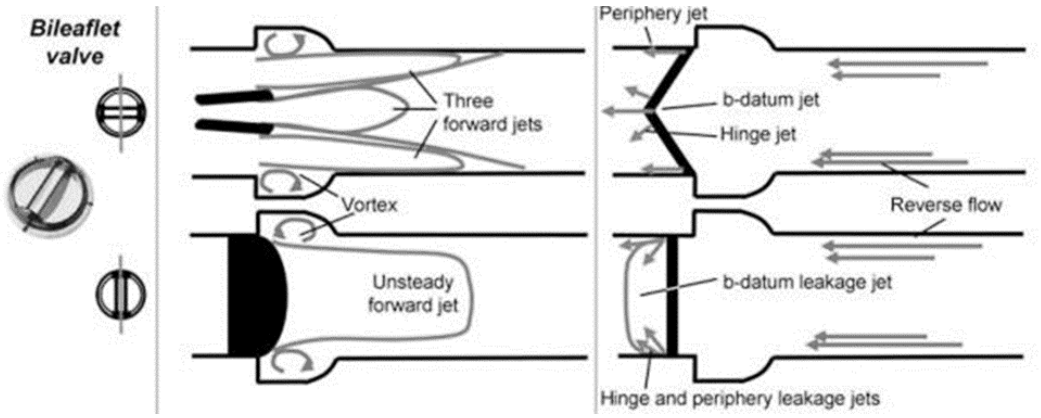

FIGURE 2.20: **Flow fields across a bi-leaflet valve**. On the left is the flow pattern during forward flow and on the right the flow pattern during the back flow phase. Note the three areas permitting regurgitant flow; the periphery, hinge and b-datum jets. (Adapted from Chanderan *et al.,* 2006)

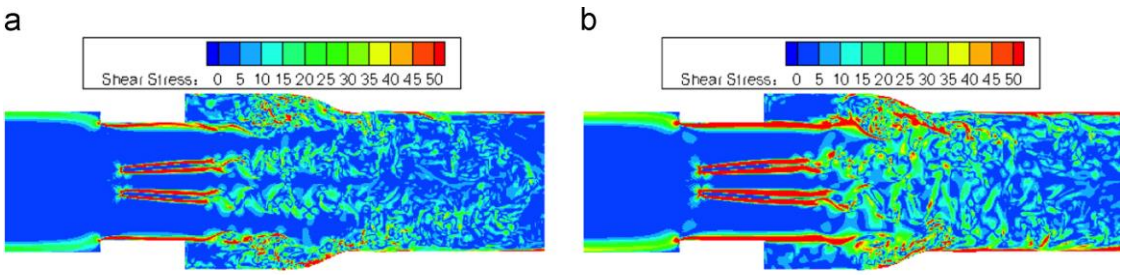

FIGURE 2. 21: **Shear stress fields of a bi-leaflet valve**. (a) Cardiac output of 5 L/min (b) Cardiac output of 8 L/min (Adapted from Yun *et al.,* 2014)

Yun *et al.* (2014) plotted the shear stress experienced within the bi-leaflet valve at peak flow in increasing cardiac outputs (CO). Figure 2.21 shows the shear stress fields generated as the CO is increased. The comparison shows moderate shear stresses in the leaflet wake vortices at resting CO (Figure 2.21a). As the CO increases (Figure 2.21b) so does the shear stresses, particularly immediately downstream of the valve. The Peak Reynolds number for the inlet velocity was 17% higher compared to resting CO resulting in a chaotic downstream flow pattern.

An important design feature of bi-leaflet mechanical heart valves includes a back or leakage flow (Figure 2.20 and 2.22) through the valve to prevent stasis in three distinct areas (Shu *et al.,* 2003):

- the b-datum gap (the central line where the two leaflets are in contact)
- at the periphery of the valve, between the leaflets and the housing
- the gap present in the hinge mechanism (where most of the leakage occurs)

Once the valve is in the closed position, the high pressure difference across the valve causes high velocity jets emerging from the hinge (Leo *et al.,* 2003 and Murphy *et al.,* 2010) and can be as high as 2,7 ms^{-1} (ATS valve) to 3 ms^{-1} (SJM valve) (Xenos *et al.,* 2010). These narrow jets were originally designed to 'wash' the hinges of the valve (Dumont *et al.,* 2007), preventing areas of flow stasis and thus, micro-thrombus formation. However, the magnitude of this retrograde flow has been shown to be detrimental to blood cells and the shear stress generated in the three areas of leakage flow, invoked thrombosis (Yun *et al.,* 2014, Dumont *et al.,* 2007).

FIGURE 2.22: **Particle dispersion patterns during the closed or leakage phase of an SJM bi-leaflet** valve (Adapted from Dumont *et al.,* 2007).

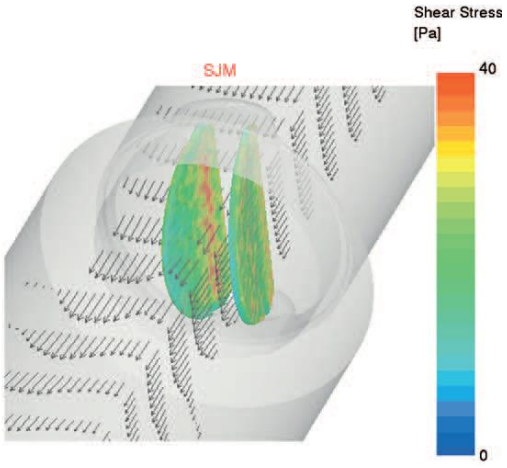

FIGURE 2.23: **The flow field and wall shear stress during peak forward flow in the SJM valve**. Note the inner surface of the leaflets in the central orifice reaching the 35 Pa threshold for platelet activation. (Adapted from Dumont *et al.,* 2007)

Mechanical valves will always be obstructive in nature, due to the dynamic fluid interaction with the valve components (Aluri *et al.,* 2001 and Vincent *et al.,* 2003). Although the design principles may be the same, small alterations in the basic design of bi-leaflets may have a large influence on the overall function. Table 2.2 compares the haemodynamic performance of the most common valves available today. A 19 mm valve is used in each group. The mean gradient generated across the valve, the EOA, geometric orifice area (GOA) and the ideal BSA indicated for each valve is compared. Because of the unique design features of the On-X valve near laminar transvalvular flow is promoted, reducing the gradient across the valve and increases the EOA (Puskas *et al.,* 2014, Palatianos *et al.,* 2007 and Williams *et al.,* 2006).

TABLE 2.2: **Haemodynamic comparison between mechanical and bio-prosthetic heart valves**. The Perimount valve is a stented bio-prosthetic valve and the Freestyle valve (Medtronic) is a stentless valve. These valves are compared in terms of EOA, GOA and the maximum BSA indicated for each valve. (Adapted from www.onxlti.com/medical-professionals/on-x-prosthetic-heart-valve-design-and-features/)

19 mm Annulus	Gradient (mmHg)	EOA (cm^2)	GOA (cm^2)	BSA (m^2)
On-X Valve	8.3	1.5	2.0	1.76
SJM Regent	9.7	1.6	1.96	1.88
ATS	20.2	1.2	1.25	1.41
Medtronic Advantage	16.0	1.0	n/a	1.18
Medtronic Freestyle	12.0	1.1	n/a	1.29
Edwards Perimount	22.0	0.82	n/a	0.96

EOA = Effective orifice area; GOA = Geometric orifice area; BSA = Body surface area (based on 0.85 EOA index); mmHg = millimeter mercury; cm^2 = centimeter square; m^2 = meter square; SJM = St Jude medical; ATS = Advancing the Standard; n/a = not available

v. The tri-leaflet valve

a. History

FIGURE 2.24: **A tri-leaflet mechanical heart valve**. (a) The tri-leaflet valve seen from above in the fully open position. (b) Side view of the valve with leaflets in the open position. (c) Disassembled valve showing the pyrolyte components. (Chanderan *et al.*, 2006)

Although the tri-leaflet valve design has been available for the past ten years (Rudolph *et al.,* 2013), it has not been used clinically. Gallegos *et al.,* (2006) reported that the valve has three pyrolytic carbon leaflets in a pyrolytic housing. The hinges are frictionless and wear is virtually zero. The haemodynamic properties of a native valve are closely resembled as the valve leaflets open laterally away from the central blood flow and provide flow characteristics achieving nearly identical to that of the native aortic valve flows.

Goldhaber *et al*. (2006) describes how, due to the airfoil shaped valve leaflets and a unique pivoting mechanism, the leaflets close before flow reverses, resulting in a minimal regurgitant fraction. The early leaflet closure avoids the sudden rapid closure seen in bi-leaflets minimising cellular damage due to the water hammer effect. The leaflets therefore close gently during flow deceleration and there is no audible ‘click’. Since no leaflets are within the majority of the jet area, the valve is not obstructive and has a greater EOA in comparison to a similar sized bi-leaflet valve. In summary, the authors found:

- similar flow structures and opening and closing kinematics as in tissue valves,
- no pathological micro bubbles (cavitation) at closure,
- no pathological fluid forces and turbulences; unlike current mechanical valves,
- no permanent stagnation areas could be detected by CFD,
- no high velocity back flow ‘washing’ jets during diastole, reducing shear stress induced platelet activation,
- DPIV studies show well-defined core flow with small wakes behind the leaflet and washout of the sinuses of Valsalva during valve closure and opening and
- no wear and structural failure during durability testing (400 million cycles equivalent to 11 years).

Furthermore, there is a central flow of 98.0% of the total flow and because of this central unobstructed flow there is an 83.6% surface free flow with a lower pressure drop compared to bi-leaflet designs (Chanderan *et al.,* 2006). This three-leaflet configuration minimises flow separation. The position and the design of the pivot have minimum effects on blood flow and because the valve operates physiologically like a native human heart valve (opens and closes like a tissue valve) it does not produce high velocity back flow jets. The valve therefore do not elicit a haemostatic response and may thus function without anti-coagulation and even anti platelet therapy (Gallegos *et al.,* 2006). Animal trials have been conducted without anti-coagulation and the initial results are promising.

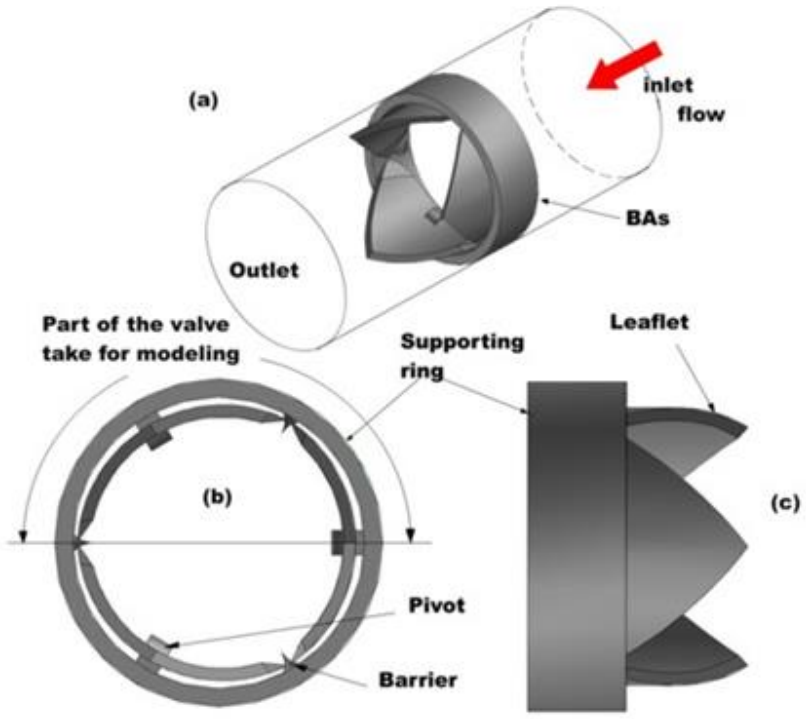

FIGURE 2.25: **A cylindrical tri-leaflet valve design**. (a) Represents the valve orientation in the outflow tract of the aorta. Upper view (b) and lateral view (c) with the leaflets in the maximum opening (Adapted from Gallegos *et al.,* 2006).

Haemodynamic flow profile of tri-leaflet valves

The tri-leaflet design has been shown to reduce outflow tract obstruction, myocardial hypertrophy and increased blood compatibility (Chanderan *et al.,* 2006). Dasi *et al.* (2009) studied the flow-dynamics of this valve. The authors reported that CFD results showed that only 0.7% of the blood volume moving through the tri-leaflet valve was exposed to shear rates high enough to cause platelet activation (Figure 2.26). During peak forward flow a jetlike flow emerged from the open leaflets, which is characterised by a vena contracta immediately downstream of the valve, followed by an expansion region. Chanderan *et al.* (2006) reported on the flow properties of the valve.

Velocities as high as 3.7 ms^{-1} have been reported downstream of the valve during peak flow. Slower velocities, in the order of 1.75 and 1.7 ms^{-1}, were reported during the acceleration and deceleration phase, respectively. Yoganathan *et al.* (2006) found that the forward flow jet was surrounded by counter-rotating recirculation regions. High turbulent shear stresses occurred at the edge of the jet. Mean and maximum turbulent shear stresses of up to 2000 and 4500 $dyne/cm^2$ respectively, have been measured at peak systole.

In summary, these valve functions exceptionally with a haemodynamic profile mimicking native aortic flow during systole with diastolic flows not high enough to initiate coagulation. The early soft closure of the leaflets minimise cellular damage. Animal trials have been promising and therefore the recommendation is that this valve could be safely used without anti-coagulation therapy. No recommendation has however been made regarding anti-platelet therapy.

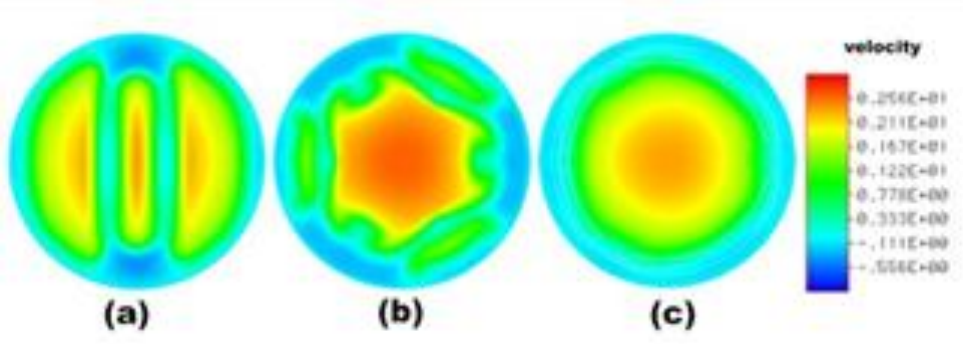

FIGURE 2.26: **Comparison of cross sectional flow velocities in three different valves**. (a) Represents a bi-leaflet. The peak flow velocity generated in this valve is 0,354 ms^{-1}. (b) Represents the tri-leaflet valve with a velocity of 0,329 ms^{-1} and (c) represents a native aortic valve with a flow velocity of 0.329 ms^{-1}. (Adapted from Chanderan *et al.,* 2006)

vi. THE UCT VALVE

a. History

In 1963, at the dawn of cardiac surgery, Mr. Carl Goosen (chief cardiopulmonary bypass technician at UCT) and Prof. Christiaan Barnard at the University of Cape Town (UCT) designed a mechanical prosthetic valve based on the Starr-Edwards valve, which they subsequently implanted into humans without conducting animal trials (Schrire *et al.,* 1970; Frater, 1969 and Barnard *et al.,* 1963).

FIGURE 2.27: **The first generation heart valve**. The Starr-Edwards Model 6100 valve, 1963 (Adapted from https://www.flickr.com/photos/sacdrbob/7430185090).

Due to the poor haemodynamics and the thrombogenic risk of the Starr-Edwards valve Prof. Barnard and his team set out to improve the ball-and-cage design by improving on the flow characteristics of the valve (Godje *et al.,* 1997). The stellite alloy cage was removed and replaced with two stainless steel (316L alloy) restraining struts/arms fixed to a stainless steel valve housing. The struts were placed proximal and distal to the blood flow and ended in a ring which acted as a restraining guide for the poppet during the cardiac cycle.

The ball was modified by adding a rod proximal and distal to the poppet and these rods were seated in the guiding rings. Laminar flow distal to the rounded occluder was encouraged by the distal conal configuration as seen in Figure 2.28 (Schrire *et al.,* 1970 and Frater, 1969). The shape was more streamlined and according to the author, reduced distal turbulent flow as well as cavitation and reduced viscous shear stress across the valve (Schrire *et al.,* 1970).

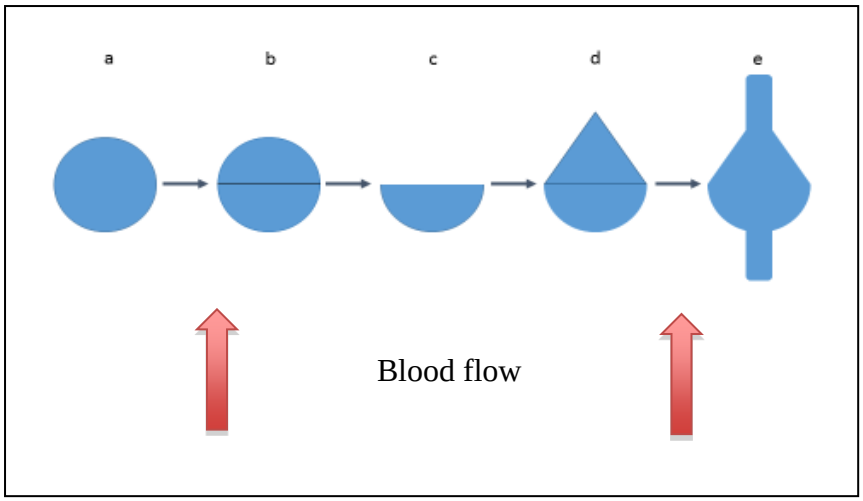

FIGURE 2.28: **The design of the UCT valve poppet**. Turbulent flow develops distal to the ball in the Starr-Edwards valve. To improve on the laminar flow, the top half of the ball is removed (b and c) and replaced with a conal shape (d), tapering into a rod (e). This rod is duplicated proximal to maintain alignment of the poppet in the valve housing.

In the closed position, the conical shape of the occluder forms a smooth slope down onto the housing, directing retrograde blood flow into the sinuses of the aorta, eliminating areas of stasis around the housing, the poppet and the sewing cuff.

Due to the conal shape of the poppet a laminar flow pattern distal to the poppet was created, improving flow characteristics. In theory, this would lead to less activation of the coagulation cascade and reduced platelet activity. The INR threshold was reduced and later on Warfarin therapy was discontinued altogether (Frater, 1969).

In a study published in 1970 by Prof. Christiaan Barnard (Schrire and Barnard, 1970) 149 UCT valves were implanted in 122 patients and followed up for up to seven years post-operatively. A further thirty UCT valves were implanted, but were excluded in this report because a six-month follow-up was not available at the time of publication. All the patients were placed on either Warfarin or Phenindione post-operatively. Midway into the study the UCT valve was modified again as Prof. Barnard postulated that thrombo-embolic events were associated with the bare metal housing. A dacron-velour cloth covering was added to the housing of the valve to reduce platelet adhesion and thrombosis. The last sixty-three patients included in the study received the dacron covered valve and in these patients Warfarin therapy was discontinued three months after implantation as there was no evidence of thrombi or emboli. The valves in the mitral position were however associated with a thrombogenic risk but in the aortic valve position, regardless of cloth cover, there was a very low thrombogenic risk. In the aortic valve position no complications were recorded during the follow-up interval, supporting the theory that the UCT valve could be used without Warfarin therapy.

Prof. RWM Frater, (Einstein institute, New York, USA) replaced aortic valves in fourty-five patients with the UCT valve in 1969 and followed up on the patients for a total of eighty-two patient-years (Frater, 1969). During this interval none of the patients received anti-coagulation

therapy; the rationale being that the flow across the valve would not activate coagulation. Six early post-operative deaths were recorded in this series. Two patients died of post-operative myocardial infarction, one patient from a ruptured aorta and three patients due to post-operative left ventricular failure. Two late deaths were recorded. The first patient died due to acute coronary thrombosis. A thrombus was thought to have originated from the suture ring of the valve, embolising into the left anterior descending artery. The second patient died four years after receiving the UCT valve when he was re-operated to correct valvular dehiscence. However, the explanted valve in this patient showed no signs of wear, pitting, or fat infiltration of the silicone poppet. The cloth covering was adequately covered with neo-intima. Although the poppet showed yellow discolouration, no wear was found on the occluder and the thin metal struts were free of thrombus. No complications such as emboli, strokes, cardiac failure or valvular dysfunction were recorded in the remaining patients during the follow-up interval and the author concluded that the UCT valve could be used in the aortic valve position without anti-coagulation.

Pipilis *et al.* (2007) reported on a case study of an explanted UCT valve in Athens, Greece. A sixty year old patient had received a UCT valve in the aortic position thirty-seven years earlier in Cape Town. She presented with a high gradient across the UCT valve and she had concommittant mitral valve stenosis. The UCT valve was replaced, but the valve was found to be in perfect condition and with no thrombus, even after being in the patient for thirty-seven years. The high gradient was blamed on patient prosthesis mismatch.

Production and commercialisation of the UCT valve was halted due to the emergence of the second generation tilting disk valves. These valves had superior flow and fluid dynamics compared to the Starr-Edwards valve with an approximation to central flow and had an improved coagulation profile. However, no direct comparative hydrodynamic studies were performed on the UCT valve.

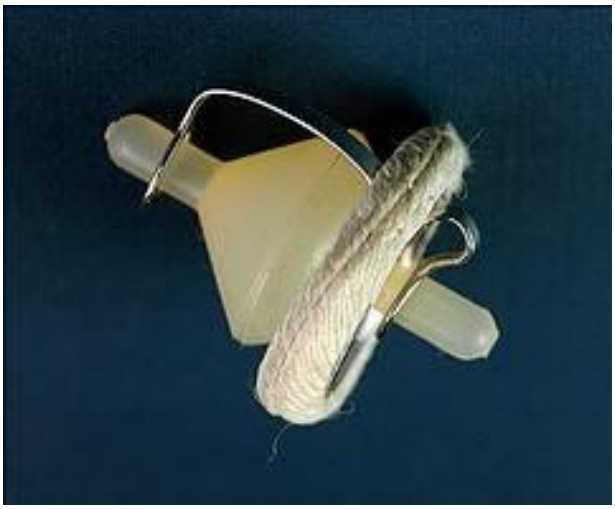

FIGURE 2.29: **The UCT valve, Mark 1** (Adapted from https://www.flickr.com/photos/68899531@N02/sets)

2.2.2 Evolution in valve material science

i. Introduction

Only a very few engineering materials are suitable in the manufacturing of mechanical heart valves (Mohammadi and Mequanint, 2011 and DeWall *et al.,* 2000). Artificial heart valves have to be durable in order to sustain about 3.2 billion cycles in a patient's lifetime (about 100,000 cycles per day). The valves are subjected to a cyclical pressure of about 120 mmHg (~200 g/cm^2) in a very corrosive fluid of a high viscosity (Daebritz *et al.,* 2004). The material used is therefore exposed constantly to this environment and the failure rate of the material will depend on the maximum stress level experienced. The choice of materials is closely related to structural factors, as fatigue and wear resistance depend not only on its configuration and loading but also on its material properties and compositions (Boloori-Zadeh *et al.,* 2013, Vincent *et al.,* 2003). Table 2.3 outlines the various materials used for the components of heart valves.

Table 2.3: **Biomaterials used in mechanical heart valves** (Adapted from Mohammadi and Mequanint, 2011)

Component	Material used
Cage, housing or hinge design	Titanium alloys – Ti6A14V
	Cobalt based alloys (Stellite-21, Haynes-25)
	Pyrolytic carbons (LTI carbon)
	Stainless steel
Leaflet, disc, or ball	Pyrolytic carbons (LTI carbon)
	Silicone rubbers
	Polyurethane
	Polyacetate (Derlin)
	Polyolefins
Sewing ring	Polypropylene
	Polytetrafluoroethylene (Teflon)
	Polyethylene terephthalate–PET (Dacron)
	Silicone rubber

LTI = Low temperature isotropic carbon, PET = Polyethylene terephthalate, Ti = titanium

The early valve frames were made from either stainless steel or titanium due to the inherent strength, durability and bio-compatibility of the metal (Boloori-Zadeh *et al.,* 2013). The Starr-Edwards valve for example, was made from stellite 21 alloy, a cobalt-chromium based alloy (Mohammadi and Mequanint, 2011) and the UCT valve frame from 316L stainless steel (Schrire *et al.,* 1970 and Frater, 1969).

The Starr-Edwards valve was plagued by thrombo-embolic events (Chanderan *et al.,* 2006). In an effort to reduce the valvular thrombogenicity the cage of the Starr-Edwards Mark 2 valve was covered with a dacron-velour cloth (Schrire *et al.,* 1970). According to the author the cloth did reduce thrombus incidence but the cloth was abrasive causing erosion of the ball. The

combination of erosion and friction caused cloth dehiscence, which led to entrapment of the ball in the cage and valve dysfunction.

The eroded ball also developed small irregularities in which thrombi formed, causing transient ischaemic neurological events (personal communication with Prof. RWM Frater). The UCT valve is another valve that was covered in dacron to reduce the thrombogenicity of the valve. It was soon realised that the influence of flow patterns across the valves had a greater impact on valve thrombogenicity and the cloth covering was discontinued as the stainless steel and stellite alloy proved to have an acceptable low thrombosis risk (Akins, 1999).

ii. Polymeric materials

Reporting on the use of synthetic polymers in cardiac surgery Boloori-Zadeh *et al.,* (2013) stated that polymers such as silicone rubber, polyolefin, polytetrafluoroethylene (PTFE) and polyurethane (PU) have been used in different heart valve designs with mixed success. The authors stated that with vacuum forming or solution casting techniques, synthetic valves can be made at a fraction of the price of mechanical valves and at a shorter manufacturing time.

Human implantation of flexible polymeric aortic valve prosthesis was carried out in the late 1950s, but persistent problems such as thrombo-embolism and degeneration of the material precluded further use (Daebritz *et al.,* 2004). Although PU proved to have a superior biocompatibility, durability, tensile strength and thrombogenic resistance compared to some of the other polymers it still failed due to its susceptibility to calcification (Yoganathan *et al*., 1986).

According to Golomb and Wagner (1991), the calcification rate is affected by local stress concentrations and calcium-binding serum protein absorption by the material. The presence of surface defects and surface adhered organic or cellular debris contributes to the calcification susceptibility. The authors concluded that by increasing the thickness of the membrane/leaflet, the porosity decreased with less calcification, but the added weight to the leaflet increased the inertial velocity with higher regurgitant leakage.

Daebritz *et al.* (2004) found that leaflet calcification accelerated as a result of the increased diffusion of Ca^{++} through surface pores, rather than surface voids serving as preferred sites for mineralisation. They reported that material degradation occurs due to a combination of oxidative reactions and the high dynamic stresses borne by the material.

Silicone rubber was used with success in the ball of the first generation Starr-Edwards valves (Boloori-Zadeh *et al.,* 2013 and Akins, 1991). Initially the valves failed due to serum lipids infiltrating the silicone, leading to changes in the ball geometry, which often resulted in valve dysfunction with regurgitation, stenosis or embolisation. This problem was overcome with heat

curing of the silicone (Boloori-Zadeh *et al.,* 2014). Overall silicone had an acceptable bio-compatibility and was used with success in the UCT valve (Schrire *et al.,* 1970).

Delrin (Polyacetal) was also a candidate material for the ball in the Starr-Edwards valve (Vincent *et al.,* 2003). Unfortunately, most of these materials are prone to structural dysfunction and was deemed obsolete when pyrolyte carbon was introduced (Yoganathan *et al.,* 2006).

iii. Pyrolytic carbon

The introduction of pyrolyte carbon in 1969 by Dr Jack Bokros was a landmark in heart valve design and material (Bokros *et al.,* 1969). Bokros's pyrolytic carbon, originally developed for the encapsulation of nuclear fuel rods, would become the principal biomaterial for virtually all new mechanical valves (Grunkemeier *et al.,* 2000).

Pyrolytic carbon is an isotropic turbostratic form of carbon, which has a similar structure to that of graphite (Schimmelpfenning *et al.,* 2012). Gonzalez *et al.* (2003) describes how in graphite the molecules are covalently bonded in stacked planar hexagonal arrays (Figure 2.30). The authors explain that in pyrolyte carbon, the stacking sequence is distorted, resulting in wrinkles and distortions within the layer, resulting in the superior ductility and durability. It also results in electrical conductivity and is useful in allowing it to become electrostatically charged, repelling blood cells.

According to Zeng *et al.* (2016) the crystalline structure of pyrolyte has a distorted lattice structure with random associated carbon atoms (Figure 2.30), unlike graphite. Pyrolyte carbon is produced by pyrolysis of a hydrocarbon gas at 1200^{o}C creating crystallisation on a high-density graphite surface (Schimmelpfenning *et al.,* 2012). To increase the strength and wear resistance silicon (up to 8% by weight) is co-deposited to form a silicone carbide. Pyrolyte has been shown to have exceptional properties enhancing its bio-compatibility with a low thrombogenicity, at a low production cost and ease of manufacturing (Vincent *et al.,* 2003). It has excellent stability and strength, wear and fatigue resistance and is therefore the material of choice in all heart valve designs (Grunkemeier *et al.,* 2000).

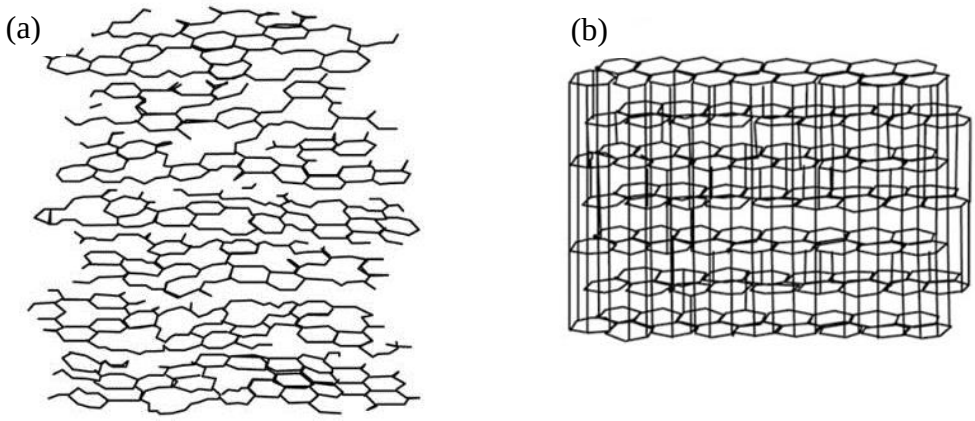

FIGURE 2.30: **Atomic structure of (a) pyrolyte carbon (turbostratic structure) compared to the structure of (b) graphite** (Adapted from Schimmelpfenning *et al.,* 2012).

Pyrolytic components still fail and release carbon particles into blood due to scratches at the valve hinge area, which may cause blood contamination (Zang *et al.,* 2009). At the same time, although pyrolyte carbon has better bio-compatibility than many other materials currently employed for medical purposes, patients who receive mechanical heart valves still need to take anti-coagulation drugs for the rest of their lives (Baudet *et al.,* 1995).

As an alternative, tissue valves eliminate the use of anti-coagulants, but the lifespan of tissue valves is usually less than fifteen years and the patients may need to undergo multiple thoracic surgeries (Ozaki *et al.,* 2004).

Ronald Daggett, Professor of Polymer Engineering at the University of Wisconsin, developed the Gott-Daggett bi-leaflet valve with a heparinised carbon coating (Gott *et* al., 1964 and Gott *et al.,* 1999). To reduce the bio-interaction of the valve leaflets, they were coated with a graphite-benzalkonium-heparin (GBH) coating (Gott *et al.,* 1963).

Doctor Bokros explored the possibility of binding this heparin coating to his pyrolytic carbon, but it was found that the highly polished pyrolytic carbon would not bond with GBH. The *in vivo* tests however, showed that the pyrolyte was the most thromboresistant, non-heparinised material available, outperforming the GBH material (Grunkemeier *et al.,* 2000) as pyrolyte carbon is one of the most blood compatible of all the man made materials known (Gonzalez *et al.,* 2003).

On-X carbon is a purified form of isotropic pyrolytic carbon (Chambers *et al.,* 2014 and Chan *et al.,* 2010) and does not require silicon carbide alloying to ensure wear resistance (Gonzalez *et al.,* 2003). By removing the silicon inherent to pyrolyte carbon, the bio-compatibility is improved without compromising the wear resistance (Williams *et al.,* 2006). The carbon has a smoother surface and can be polished to a high gloss, reducing cellular interaction and increasing

thromboresistance (Figure 2.31) (Vincent *et al.,* 2003). On-X carbon is 50% stronger than conventional pyrolyte (Gonzalez *et al.,* 2003).

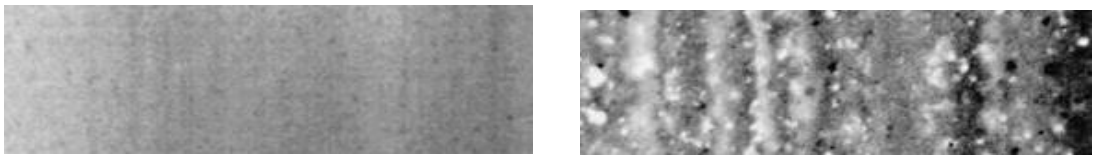

FIGURE 2.31: **Electron microscopy of pyrolyte carbon.** On the left is the On-X pyrolite in which the silicon has been removed. Note the smoother surface in comparison to traditional silicon embedded pyrolyte carbon on the right. (Adapted from www.onxlti.com)

iv. Stainless steel

According to Wong *et al.* (2007) the first stainless steel alloys used in implants were the 18-8 steel alloy (type 300 in the modern classification) that consists of approximately 18% chromium and 8% nickel, which is stronger and more corrosion resistant than vanadium.

Molybdenum was added later (18-8 sMo alloy) to improve on the corrosion resistance of stainless steel (Cieslik *et al.,* 2012). This alloy became known as type 316 stainless steel. The carbon content was also reduced from 0,08 to 0,03% and the chromium from 18% to 11% giving it excellent corrosion resistance and it is this alloy (316L) that is the most widely used in human implants (Wong *et al.,* 2007). It is this alloy that is used in severe environments and in industrial applications (Vincent *et al.,* 2003) and the Glycar valve used in this study is manufactured by using this alloy.

v. Future developments

The integration of **ultrananocrystaline diamond** with pyrolyte carbon in heart valve leaflets was explored by Hongjun Zeng and his team at Advanced Diamond Technologies, Illinois, USA. (Zeng *et al.,* 2016). The aim was to improve on the bio-compatibility of pyrolyte carbon and thereby reducing the anti-coagulation requirements of the patient. They found that the material had exceptional chemical inertness, increased bio-compatibility, excellent mechanical durability and tribological properties due to its diamond nature and unmatched smoothness.

Zeng *et al.* (2016) reported that this process of covering the pyrolyte was very difficult to achieve. During the diamond coating process, graphitisation and film delamination of the pyrolyte was caused. At the same time the graphite became porous and the diamond adhesion poor.

Zeng *et al.* (2016) have overcome these challenges by introducing an interlayer with stress matching and carbide bonding between the film and the pyrolyte substrate by using a thin layer of tungsten applied by atomic layer deposition. Figure 2.32 shows the superior bio-compatibility of the material compared to other materials used in heart valves, including pyrolyte carbon. Unfortunately the manufacturing process is very complex, time consuming and expensive, and may therefore not be commercially viable.

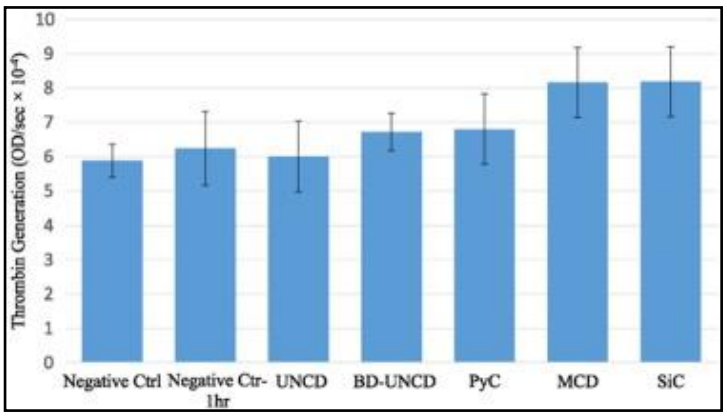

FIGURE 2.32: **Thrombin generation of fresh human platelets after one hour exposure to different heart valve materials.** Negative control, Negative Control after one hour, (UNCD), Ultra nanocrystaline Diamond, (BD-UNCD) Boron doped, (PyC) Pyrolyte carbon, (MCD) Microcrystaline diamond, (SiC) Silicon carbide. (Adapted from Zeng *et al.,* 2016)

Gonzalez *et al.* 2003 produced **alumina (Al_2O_3)** which is a bio-ceramic. The authors reported on its properties. They stated that it is a traditional ceramic that has a higher tensile strength than steel, is more heat and corrosion resistant than metal alloys and polymers, less dense than metals and their alloys, and the raw materials are plentiful and inexpensive. It has a low thrombogenic potential and it owes its bio-inertness to a thin layer of titanium on the outer surface. The hardness of alumina is second to diamond and is therefore extremely resistant to wear. The authors concluded that applications in the hinge area of a valve will reduce possible leaflet or housing damage after prolonged use. It is also highly resistant to cavitation erosion. Unfortunately alumina is extremely hard and machining it is difficult and costly. The superiority to pyrolyte has not yet been proven.

Mohammadi *et al.* (2009) designed a nanocomposite material consisting of a combination of **polyvinyl alcohol hydrogel** as the matrix and bacterial cellulose nanofibres as the reinforcing fibres. The result is a material that has properties comparable to those of tissue found in native cardiac valve leaflets. It allows for a flexible biomaterial that has mechanical and haemodynamic properties and compares well with porcine valve tissue. Although the material is promising, it unfortunately is not durable enough for long term use.

2.3 Coagulation and thrombo-embolism

2.3.1 Principles of coagulation

i. Coagulation factors

An in depth discussion of coagulation falls outside the scope of this dissertation however there will be a focused review of the most important aspects of the chain-of-events relevant to thrombosis in heart valves.

Haemostasis is from the Greek language and means: *aimóstasis*: *aíma* "blood" + *stasis* "standing still" (Smith, 2009). It is a vital protective mechanism with a sequence of responses that stops bleeding and is responsible for preventing blood loss by sealing sites of injury in the vascular bed. When blood vessels are damaged or ruptured, the haemostatic response must be quick, localised to the region of damage, and carefully controlled in order to be effective. Three main mechanisms coinside to reduce blood loss: initial vascular spasm leading to platelet plug formation and lastly blood clotting (coagulation).

According to Smith (2009) central to the management of coagulation is the endothelial layer found on the inner surface of blood vessels. This layer is far from inert. It is equipped with a number of mechanisms to attenuate thrombus formation. Endothelial cells prevent platelet activation by the production and local release of prostacyclin and nitrox oxide, both of which induce vasodilation. In the resting state surface neutral phospholipids (primarily phosphatidylcholine, sphingomyelin and sphingolipids) are found on the external surface of the endothelial membrane and is responsible for the anti-coagulant properties found in the resting state (Yamaji-Hasegawa and Tsujimoto, 2006). Phosphatidyl serine (PS) and phosphatidyl ethanolamine (PE), both pro-coagulant receptors, are located on the inner surface of the same membrane. When the endothelial cell is stressed, during injury for example, both the PS and PE are transported to the external surface creating a pro-coagulant surface (Levi *et al.,* 2002). The coagulation proteins factor VII, FIX, FX, prothrombin, protein C, S and Z (containing glutamic acid residues), bind to these two surface proteins ensuring a concentration of clotting factors at the site of injury (Zwaal *et al.,* 2005).

In addition to the resting membrane that does not support coagulation; non-activated endothelial cells express a number of other proteins preventing propagation of thrombus past the site of injury. These include thrombomodulin (Sagripanti *et al*., 2000), heparan sulphated proteoglycans and tissue factor pathway inhibitor (Levi *et al.,* 2002). As these molecules play no role in MHV thrombosis, a discussion of these molecules will not be provided.

ii. Platelets

For the purpose of this study, it is important to note that platelets play the most important role in coagulation. According to Schouten *et al.* (2008) platelets are the smallest of the cells in circulating blood, averaging only 2.0 to 5.0 µ*m* in diameter and 0.5 µ*m* in thickness and are derived from megakaryocytes. They have a mean cell volume of six to ten femtoliters and a seven- to ten-day life span. Between 150,000 and 400,000 platelets are present in each microliter of blood. Platelets are disc-shaped and have many granules that store an impressive array of chemicals.

Smith (2009) reported that the intracellular granules contain clotting factors, ADP (adenosine diphosphate), ATP (adenosine triphosphate), Ca^{++}, and serotonin. Also present are enzymes that produce thromboxane A2 (a prostaglandin) and a fibrin-stabilising factor (F XIII). Platelets contain platelet-derived growth factor, responsible for the proliferation of vascular endothelial cells, vascular smooth muscle fibers, and fibroblasts to help repair damaged blood vessel walls.

Versteeg *et al.* (2013) describes that platelet plug formation consists of three main steps: adhesion, activation and aggregation (Figure 2.33). Circulating Von Willebrand factor (vWF) in the blood stream binds to exposed collagen after vascular injury (Mackman *et al.,* 2007). Platelets in the resting state adhere to exposed vWF by binding to the glycoprotein 1b (GPIb) receptor in the platelet membrane (Smith, 2009). Platelets can also bind directly to exposed collagen through the GPIa receptor, both of which anchor the platelet to the site of injury.

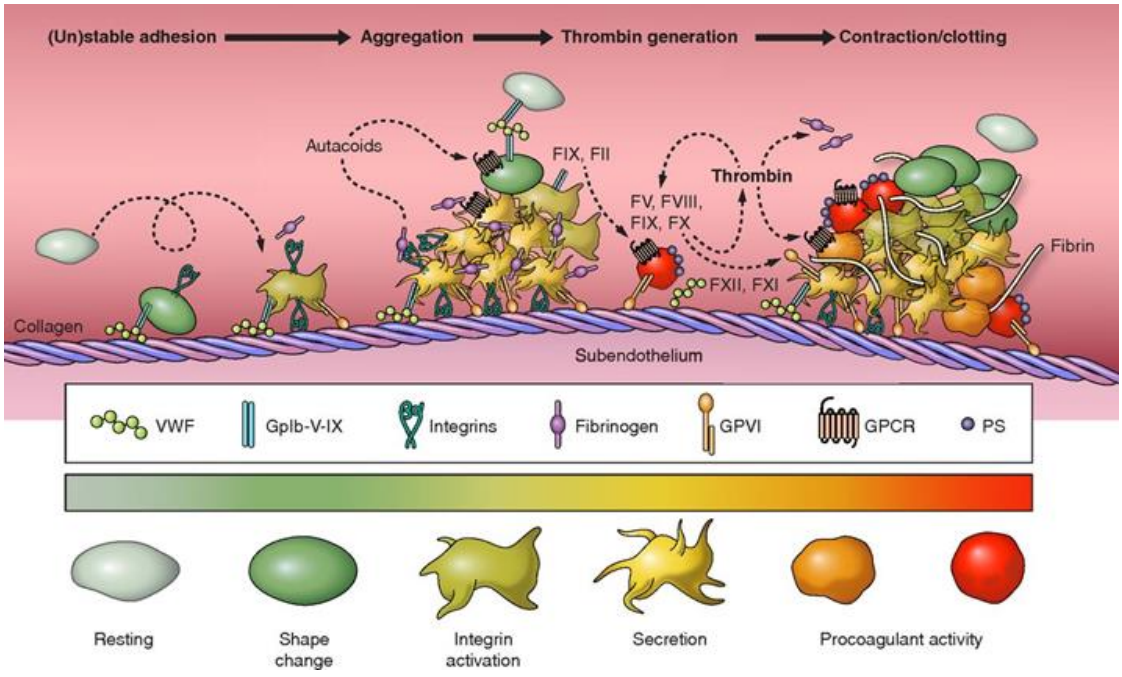

FIGURE 2.33: **The role of platelets in coagulation**. FII = Factor 2; FV = Factor 5; FVIII = Factor 8; FIX = Factor 9; FX = Factor 10; FXI = Factor 11; FXII = Factor 12: GPIb = Glycoprotein 1b; GPVI = Glycoprotein 6; GPCR = G protein coupled receptors; PS = Phosphatidyl serine; vWF = Von Willebrand Factor (Adapted from Versteeg *et al.,* 2013)

Furie and Furie (2007) reported on the process of platelet **adhesion**. Extreme conformational changes take place in the platelet, enlarging the surface area of the platelet and the metabolism within the platelet spikes. The platelet releases its intra-cellular granules into the environment or site of injury. ADP, released by the platelet, acts as a chemoattractant and strong activator of platelets binding to the surface ADP receptors (Bhatt, 2008). This initiates platelet **aggregation** at an exponential rate. Platelet derived thromboxane A2 is produced, which causes vasoconstriction and platelet aggregation. Through a positive feedback the platelet auto enhances itself to increase thromboxane A2 and thrombin production (Smith, 2009).

As soon as the platelets have aggregated and undergone its conformational changes, the coagulation cascade is initiated. This has three distinct phases, the initiation phase followed by amplification and propagation.

a. Initiation of coagulation

Colman *et al.,* (2006) describes the initiation phase as follows. The aggregated platelets produce a small amount of thrombin through the extrinsic pathway, using tissue factor (TF) supplied by the TF-bearing cells (endothelial cells, monocytes, tumor cells, etcetera). F VII binds to TF to form a TF-FVII complex. After binding FV and Ca^{++} this complex cleaves and activates FX which in turn produces a limited amount of thrombin (F II) which will be available for the next phase (amplification).

b. Amplification

Once a small amount of thrombin has been generated on the surface of the TF-bearing cell, the thrombin diffuses away to the platelets in the vicinity of the injury. Binding of thrombin to platelet surface receptors causes extreme conformational changes in the platelet and secretion of intracellular granules (Colman *et al.,* 2006).

c. Propagation

A limited number of platelets are activated in the amplification phase resulting in the release of their granule content and in the recruitment of additional platelets to the site of injury. F IX binds F VIII on the platelet surface and then rapidly begin to produce activated FX which in turn binds to FV (Smith, 2009). This complex cleaves prothrombin to produce thrombin in what is known as a thrombin burst (Furie and Furie, 2007). Thrombin cleaves fibrinogen to produce fibrin, which spontaneously polymerises to an insoluble form (Bhatt, 2008). When binding to the activated platelets by adhering to the GPIIb-IIIa receptors, a stable clot is formed. FXIII modifies the polymerised fibrin to form cross links between the fibrin strands. This cross linking increases the stability and elasticity of the clot and prevents fibrinolysis by plasmin (Colman *et al.,* 2006).

2.3.2 Thrombo-embolism and clotting in mechanical heart valves

i. Introduction

Harken and Slichter (1970) showed that patients with first-generation mechanical valves such as the ball-and-cage and the second generation valves (tilting disc) had a shortened platelet half-life due to increased incidence of platelet destruction and activation. Brown *et al*. (1975) found that when platelets were exposed to shear stresses in excess of 50 dyne/cm^2, the platelets released a significantly greater amount of ADP and tend to aggregate faster than platelets exposed to lower shear stresses. This study showed that shear stress could induce platelet aggregation and thus cause thrombosis.

Thrombus forms on all endovascular surfaces or cardiovascular devices anywhere in the circulation. This is a pathological consequence of activated haemostatic mechanisms under variable flow conditions (Caceres-Lopez *et al.,* 2006 and Taljaard and Doubell, 2003). The thrombotic process is usually rapid and localised and involves a complex interaction between surfaces exposed to blood, platelets and pro-coagulation clotting factors (Huang *et al.,* 2006).

When blood is exposed to heart valves, thrombogenesis is initiated and the following sequence of events is triggered (Dasi *et al.,* 2009):

1. The thrombogenic surface is exposed to blood
2. Platelet adherence to the surface with aggregation and release of platelet cellular proteins
3. Generation of thrombin and thus fibrin formation
4. Thrombus size is limited due to plasmin activity with fibrinolysis

Artificial surfaces rapidly acquire a layer of absorbed plasma proteins when exposed to blood and is mainly composed of albumin, fibrin and globulin fractions (Roudaut *et al.,* 2007 and Schneider *et al.,* 2007). The degree of absorption depends directly on the material used as well as the fluid motion which may affect the pattern of protein deposition, which may be non-uniform. Albumin for example, dissolves from silica surfaces but absorption of albumin to polyethylene may be irreversible, triggering or initiating clotting factor adherence to the surface (Schneider *et al*., 2007). Pyrolyte carbon has a very low absorption potential contributing to its exceptional bio-compatibility (Chambers *et al.,* 2014).

The suture zone and sewing cuff undergoes healing with scar tissue and/or endothelialisation. This creates a bio-compatible surface by covering potential areas that may lead to thrombus formation (Roudaut *et al.,* 2007). This process may take up to six weeks to be completed and for this reason Warfarin is indicated after a tissue valve is implanted (Akhthar *et al.,* 2009).

Haemodynamic factors influencing thrombosis include both haemodynamic characteristics of the prosthesis as well as the overall cardiac haemodynamic status of the patient. Although the

profile of new generation mechanical bi-leaflet valves is largely superior to that of earlier generation prosthesis (associated with a lower occurrence of thrombo-embolic complications), localised regions of turbulent flow can still develop and lead to stasis and thrombus formation (Ma *et al.,* 2015).

The location of the prosthesis also plays an important role in thrombogenicity. Obstruction of a tricuspid mechanical prosthesis is twenty times more frequent than a left-sided mechanical valve (Lengyel, 2008 and Caceres-Lopez *et al.,* 2006). For the same reason, mitral valves are two to three times more frequently associated with thrombo-embolic events than an aortic prosthesis (Ma *et al.,* 2015).

Conditions of low flow or reduced cardiac output and atrial fibrillation in combination with a prosthetic valve (Huang *et al.,* 2013) increases thrombogenecity. Thrombosis is also higher in the early (<3 months) post-operative phase (Vahanian *et al*., 2007 and Jamieson *et al*., 2004). The presence of concomitant risk factors such as left ventricular dysfunction, left atrial dilatation, a history of previous thrombo-embolism and- hypercoagulable conditions compound the incidence of thrombosis (Heras *et al*., 1995).

ii. Cellular components of blood

Alemu and Bluestein (2007) reported that red blood cells have flexible membranes and employ a “tank treading” motion that enable them to sustain higher shear stresses than platelets before haemolysis occurs. In comparison to red blood cells, platelets have relatively rigid membranes and therefore experience higher membrane strains.

Dasi *et al.* (2007) reports that haemolysis requires a shear stress in excess of 1500 dyne/cm^2 with an exposure time of 102 milliseconds, while platelets will activate at this exposure time but at a much lower shear stress of 100 dyne/cm^2. This is seen in regurgitant eddies in mechanical heart valves where the measured turbulent stresses are in the range of platelet activation (Huang *et al.,* 2006). Platelets are also small, causing them to respond negatively to viscous shearing experienced in the valve mechanism leading to activation (Caceres-Loriga *et al.,* 2015).

iii. Shear stress

Blood circulating in vessels are exposed to shear stress caused by the force necessary to produce flow (Cáceres-Lóriga *et al.,* 2006 and Bluestein, 2004). The difference in velocity between the layers situated at varying distances from the vessel wall determines the shear rate, which is directly proportional to the shear force and inversely proportional to the viscosity of blood (Ikeda *et al.,* 1991). Recently, turbulent stress, which is a substitute measure of the shear stress experienced by blood cells and platelets during turbulent flow have been used to assess the potential for valves to cause thrombi (Kang *et al.,* 2016).

Brown *et al*. (1975) showed that platelets exposed to viscous shear stress in excess of 50 dyne/cm^2 released ADP and aggregated faster than platelets exposed to lower shear stresses. They were the first to illustrate the relationship between viscous shear stress and platelet aggregation. Kang *et al.* (2016) stated that turbulent stress levels from 10 to 100 Pa are considered high enough to trigger platelet activation. The threshold, also known as the Hellums criteria, state that platelets will activate if the product of shear stress and its time duration is above 3.5 Pa or 35 dyne/cm^2 (Hellums *et al.,* 1994). The threshold for haemolysis is much higher; in excess of 800 Pa.

Shear stress induced aggregation produces two distinct phases. The first phase occurs at a peak shear stress of 12 dyne/cm^2 and is of a small amplitude. This does not produce clinical thrombosis as it is lower than the shear stress experienced normally in the smaller arteries, which measures on average 15 dyne/cm^2. The second phase, two to four times greater in magnitude, occurs maximally at 80 dyne/cm^2 and results in pathology irrespective of the provoking cause (Ikeda *et al.,* 1991).

The mechanisms facilitating platelet-to-platelet contact under varying shear stress are different. Fibrinogen interaction with GPIIb-IIIa platelet surface receptors occurs at a low shear stress, while vWF interaction with both GPIb and GPIIb-IIIa, but independent of fibrinogen, is necessary at high shear flows (Ikeda *et al*., 1988). Aggregation of platelets peak at 81 dyne/cm^2. Under these conditions, platelet-to-platelet contact can only be maintained by vWF binding to both GPIb and GPIIb-IIIa.

Platelet aggregation at low shear flows do not correspond to pathological thrombosis and this explains the absence of stable platelet aggregates in the normal circulation, where the average shear stress in the arteriolar walls is 15 dyne/cm^2 (Yoganathan *et al.,* 2005).

Yoganathan *et al.* (1986), using 2D LDV conducted the first detailed investigation of the pulsatile forward flow fields of the SJM and Medtronic-Hall valve. They reported maximum turbulent shear stress downstream of the leaflets ranging from 1200 dyne/cm^2 for the SJM to 2000 dyne/cm ^{2} for the Medtronic-Hall valve.

iv. Shear stress and fibrinogen

According to Schneider *et al.* (2007), shear stress influences the structure and function of GPIIb-IIIa and fibrinogen. In the absence of an external stimulus shear stress in excess of 50 dyne/cm^2 causes binding of fibrinogen to unstimulated platelets with inactivated GPIIb-IIIa receptors. Shear stress below 30 dyne/cm^2 prevents the interaction of platelets with valve material and also prevents the release of intracellular granular components, maintaining a resting inert state.

Thromboxane A2 is released once platelets are activated through the thrombin or ADP receptor mechanisms (Smith, 2009). The release acts as a chemo-attractant causing platelet aggregation and also provides a positive feedback mechanism with exponential platelet activation as well as auto induction of the releasing platelet. Thromboxane A2 synthesis is also induced with a shear stress in excess of 54 dyne/cm^2, interacting with dormant platelets resulting in activation. This however, is not a leading cause of shear induced thrombosis, but contributes greatly to the thrombotic process in valves (O'Brian, 1990).

v. Von Willebrand factor (vWF)

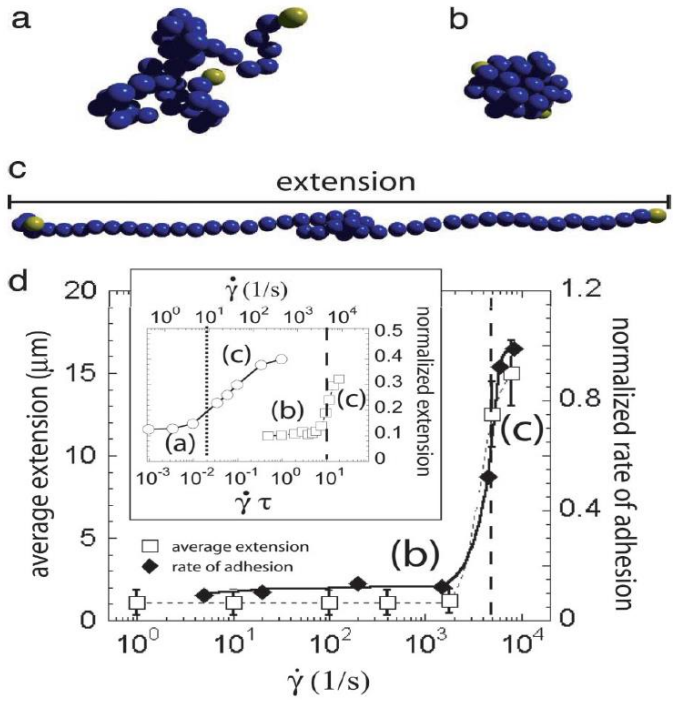

FIGURE 2.34: **The relationship between vWF and shear stress.** Due to shear stresses vWF unfolds and becomes active initiating platelet adhesion and the activation of coagulation. During low shear (a) vWF is coiled and inactive and corresponds to a low shear force in the graph above. As the shear increases (b) the vWF uncoils and attaches to surfaces. At high shear the vWF is elongated with pro-coagulant properties, binding to surfaces and anchoring platelets. Threshold shear (γ) (Adapted from Schneider *et al*., 2007)

vWF is a large multimeric protein found in blood plasma. vWF mediates the adhesion of platelets to sub-endothelial connective tissue and is the key protein in arterial vessels and the microcirculation for thrombosis in the event of an injury (Rugeri, 2007). To avoid pathological platelet aggregation the vWF macromolecule (inactive form) is regulated in size and is mediated by the metalloprotease ADAMTS-13. Proteolysis, which cleaves the large multimeric molecule leads to subsequent activation and adhesion to surfaces and exposed collagen (Jilma-Stohlawetz *et al.,* 2015).

Under increased shear stress ADAMTS-13 activity is enhanced, cleaving the A2 domain in the vWF macro molecule and the vWF molecule unfolds (Schneider *et al*., 2007), binding to collagen or foreign surfaces. Platelets adhere to the exposed vWF by binding with its GP 1b surface receptor. Figure 2.32 shows the unfolding of vWF due to stress flow induced cleavage at a threshold shear (γ) of 10^3 (50 dyne/cm^2) (Kang *et al.,* 2016 and Schneider *et al.,* 2007).

In a low shear environment the vWF molecule maintains its coiled structure and remains dormant. As the shear stress increases the ADAMTS-13 activity is enhanced and once the shear

threshold is bridged the vWF molecule is cleaved, becomes active, and adheres to surfaces with initiation of thrombosis (Kang *et al.,* 2006).

vi. Summary

TF is released when cell rupture occurs with blood trauma playing a central role. High stresses during the leakage flow phase in aortic valves and forward flow in mitral valves lead to blood damage releasing both TF and the platelet activating ADP. Plasma factor VII binds to TF, setting off a chain reaction, which activates F X and F V to form a complex producing thrombin, which in turn activates platelets (activation phase of coagulation) and F VIII. In parallel, platelet activation is triggered when shear stresses reach a level higher than 60–80 dyne/cm^2, followed by vWF binding to the platelet receptor GPIb and platelet activation. GPIIb–IIIa facilitates platelet–platelet adhesion by binding insoluble polymerised fibrin strands forming a stable clot.

Last, but not least, contact activation begins when F XII binds to the non-endothelialised artificial surfaces of prostheses. This in turn activates prekallikrein and high molecular weight kininogen initiating the intrinsic pathway of coagulation. Although ‘back-wash’ designs have aimed at reducing thrombus formation in the hinge area, it may be one of the most important sites for the activation of the entire cellular and coagulation cascade (Chapter 2.3.3).

vii. Future directions in coagulation experimentation

The past five years have seen an increased number of experiments focused on quantifying shear-induced coagulation properties of heart valves. Several novel *ex vivo* and *in vitro* methods have allowed for the measurement of the thrombo-embolic potential of different heart valve and hinge designs (Fallon *et al.,* 2008). In these experiments, fresh citrated blood is used as the working fluid in a physiological flow loop containing the test heart valve. Upon gradual recalcification, the coagulation properties of the blood are restored, with platelet activation and thrombin formation occurring in a valve-dependent manner.

Platelet-specific assays, haemolysis assays and thrombin–antithrombin assays enable accurate quantification of the procoagulant potential of any cardiovascular device, including heart valves (Bluestein *et al.,* 2006). Results have shown significant differences in the thrombo-embolic potential for various valves, with the Medtronic Parallel having the worst level, consistent with the recall of this valve during clinical trials associated with high incident of thrombus formation.

According to Bluestein *et al.* (2006) and Dasi *et al.* (2009) experiments show that subtle differences in hinge geometries can impact the net thrombo-embolic potential of valves. Such biological experiments are crucial to fully understand the effect of non-physiological flow on blood damage and, once combined with computational methods, constitute the essential approach for valve design optimisation. By combining numerical simulation of flow-dynamics and the coagulation as well as cellular bio-interaction models, a predictive computerised model will be available prior to costly and time consuming *in vitro* and *in vivo* trials. Failures such as the Duromedics valve and Medtronic Parallel valve will be avoided and will therefore increase patient safety.

2.3.3 Valve design and thrombosis

The triad of Virchow dictates that three interacting factors influence haemostasis in the body (Cáceres-Lóriga and Morais, 2015):

- The thrombo-resistance of surface membranes in contact with blood
- The coagulability of blood and
- Smooth non-turbulent flow of blood

According to the authors deviation in any one or more of these factors may lead to thrombosis and mechanical heart valves clearly violate all three principles. Surfaces are not endothelialised and are thus inherently thrombogenic in nature. The flows experienced through and around the mechanical valves are often marked by turbulence and flow eddies. Each one of these factors can induce thrombosis because of local areas of hypercoagulability.

Durrleman *et al.* (2004) reported that over a lifetime of a mechanical heart valve, platelets will be repeatedly exposed to valvular elevated viscous shear stresses. Platelets have a life span of about ten days on average and will pass through the valve every thirty to ninety seconds, corresponding to 9 600 to 29 000 valve passages during the platelet's lifetime. Figures 2.35, 2.37 and 2.38 illustrate the interaction between the valve leaflets during the forward and reverse flow phases with platelets. During the entire cycle platelets are in contact or interact with the components of the valve (Dumont *et al.,* 2007).

Platelets are activated due to shear stresses generated as a result of flow acceleration around the valve and clotting factors are activated and deposited on valvular surfaces (Dasi et al., 2009). Eventually the cumulative effect of this seemingly small percentage of platelets that get fully activated, even during a single passage through the valve, may eventually initiate thrombo-embolic events. It is therefore vital that every aspect in the valve design be thoroughly investigated as a small insignificant effect/interaction may lead to thrombosis.

i. Flow patterns and regurgitant flow

Since valvular materials used are not thrombo-resistant, prevention of thrombosis has been achieved by using materials known for its bio-compatibility such as pyrolyte carbon (Nishimwa *et al.,* 2014). The generation of flow patterns to enhance so-called 'washing' jets around the valvular components to reduce stasis and to eliminate accumulation of micro deposits of thrombi have been employed in most valve designs (Klusak *et al.,* 2015 and Cáceres-Lóriga and Morais, 2015). Blood chemistry is altered using Warfarin with/without Aspirin regimens to minimise the activation of the clotting cascade.

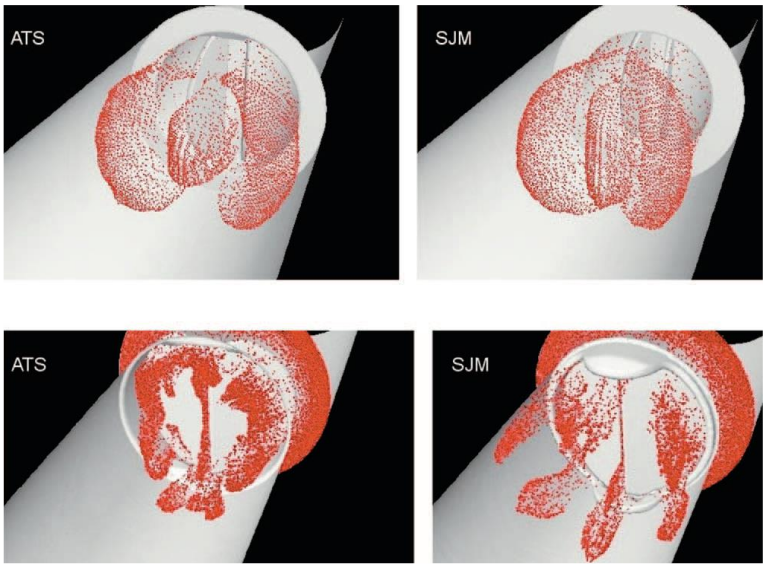

FIGURE 2.35: **The dispersion pattern of platelets in two bi-leaflet valves**. The top panel represents forward flow through an ATS valve on the left and an SJM on the right. The bottom panel represents the back/leakage flow through the valves. (Adapted from Dumont *et al.,* 2007)

Thrombosis and the activation of the clotting cascade are therefore inherent to all mechanical heart valves (Cáceres-Lóriga and Morais, 2015 and Bluestein, 2004). During the forward flow phase the only obstruction to blood flow is the leaflets. With the leaflets in the open position, blood is exposed to foreign surfaces with hydrodynamic interaction. Shear stresses are generated due to flow acceleration in and around the valve as well as the occurrence of turbulence and recirculation (Herberson *et al.,* 2011, Krishnan *et al.,* 2006).

The leaflet faces are constantly 'washed' by blood as the valve opens and closes and in the closed position there is stasis around all the components of the valve (Figure 2.36) (Fallon *et al.,* 2005). The success of a mechanical prosthesis therefore depends on the absence of persistent flow stasis that may lead to thrombosis. Flow stasis may however occur at the leaflet pivot depending on the design and location (Shu *et al.,* 2003). Most pivot points found in mechanical heart valves have a butterfly recess in which the valve pivot. Contact between the valve leaflet and the recess is a dynamic mechanism that constantly changes throughout the cardiac cycle.

Dasi *et al.* (2009) pointed out that inherent to the design of bi-leaflet mechanical heart valves a certain degree of leakage flow is allowed during the closed position to avoid stagnation zones and recirculation of flow and prolonged residence times of blood borne particles and cells. This is known as the 'washing jets'. The authors stated that areas of turbulence and high shear stress zones that can initiate platelet activation should be avoided in the valve design. Two areas where high shear stress are generated are the b-datum gap, which is the central line where the two valve leaflets meet in the closed position, and at the periphery of the valve leaflets next to the housing (Huang *et al.,* 2013). The high pressure difference across the closed valve causes fast-moving leakage flow that eventually emerges as narrow jets (Heberson *et al.,* 2011). Figure 2.36

illustrates the flow field and wall stress experienced during the closed position in the SJM and the ATS valve in the aortic position. Note the higher shear stress experienced by the SJM valve around the edges of the leaflets, which is 30% higher than in an ATS valve, above the platelet activation threshold. The b-datum gap clearly contributes to the shear stress experienced by the platelets during the platelet transit time.

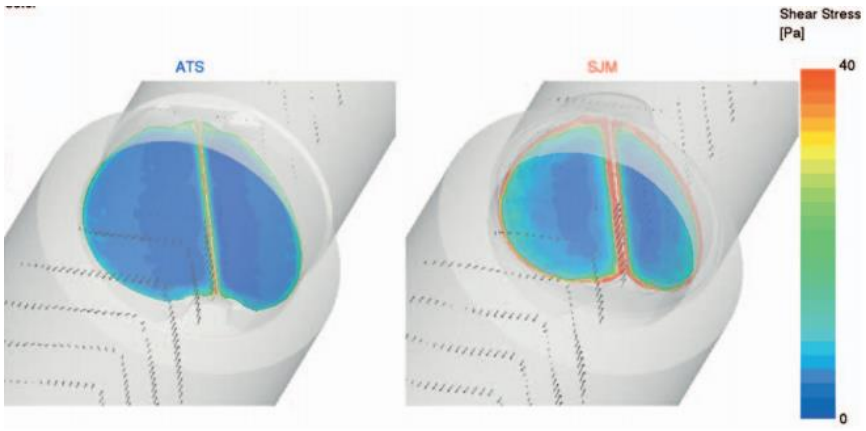

FIGURE 2.36: **The flow field and wall stress of two bi-leaflet valves.** Deceleration of flow during the closing phase of two bi-leaflet valves is depicted with the ATS valve on the left and the SJM on the right. (Adapted from Dumont *et al.,* 2007). ATS = Advancing the standard; Pa = Pascal; SJM = St Jude medical

Figure 2.37 shows an aortic valve prosthesis in the closed position with red blood cells and platelets leaking back into the left ventricle. While flowing through the valve prosthesis these cells are subjected to unnatural flows and stresses, causing cellular damage with rupture of red blood cells and platelet activation, the first step towards initiation of the coagulation response (Dasi *et al.,* 2009).

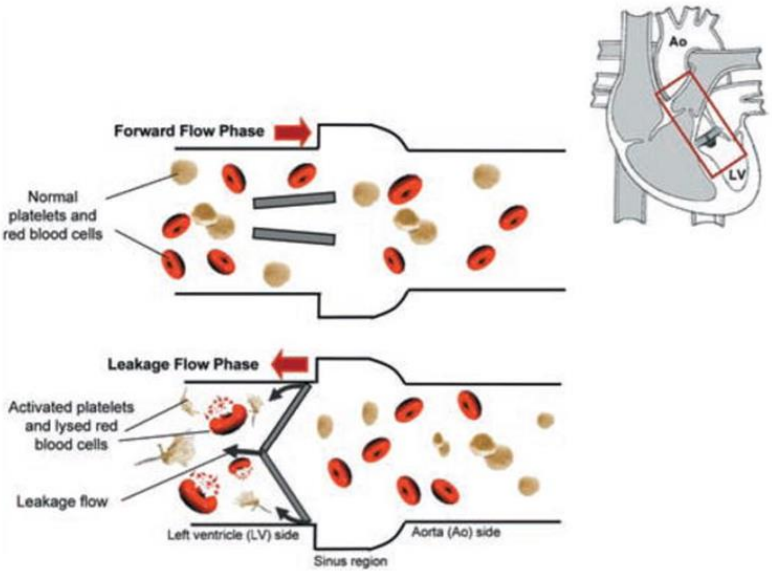

FIGURE 2.37: **A bi-leaflet mechanical heart valve in the aortic position during the leakage flow phase.** Blood cell damage occurs due to the high shear environment experienced within the leakage gaps (not to scale). Top panel: forward flow phase; bottom panel: leakage flow phase. Grey arrows indicate leakage flow; red arrows indicate bulk blood flow direction; Ao = aorta; LV = left ventricle. (Adapted from Dasi *et al.,* 2009)

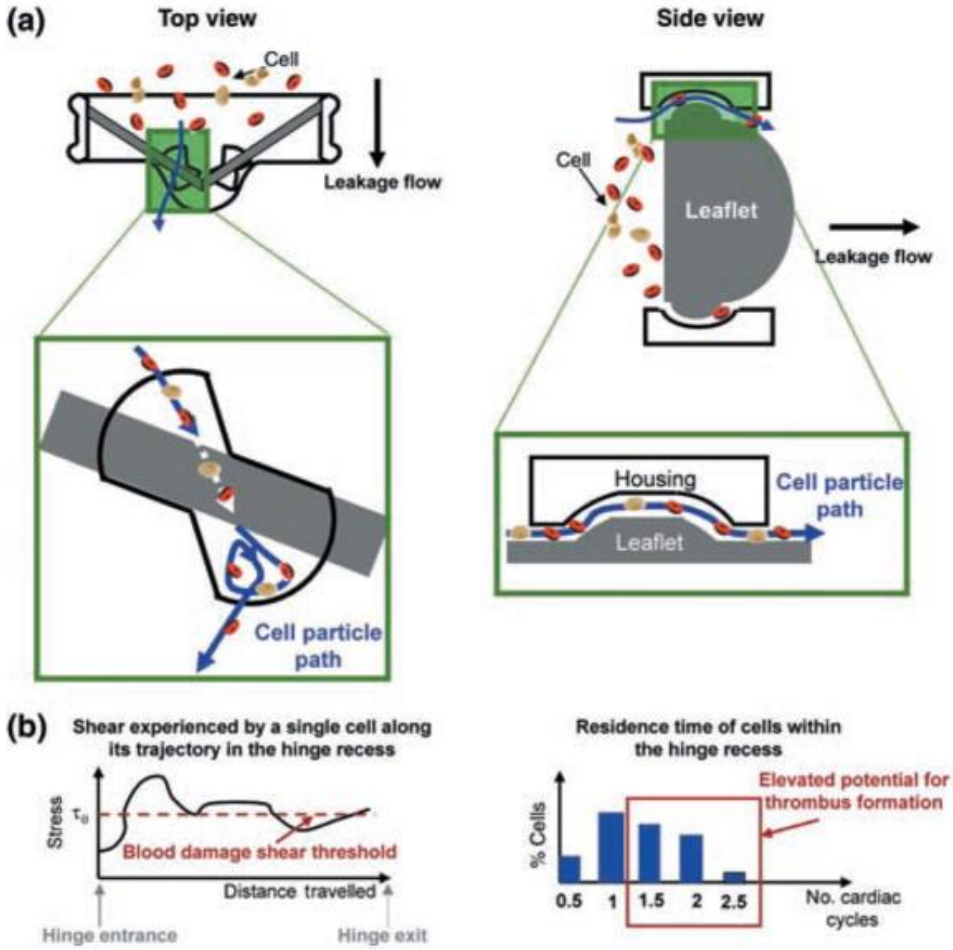

FIGURE 2.38: **Blood flow in the hinge recesses of a bi-leaflet valve**. (a) The cell particle pathway inside the hinge recess seen from the side (left) and the particle pathway around the leaflet in the recess (right). (b) The shear stress experienced by cells along its trajectory in the hinge recess on the left with cellular contact time with the valve surface on the right. (Adapted from Dasi *et al.,* 2009)

Klusak *et al.,* (2015) identified the hinge area as one of the leading contributing factors to the injury of platelets and other blood borne particles. Studying the reversal leakage jet in the hinge of a bi-leaflet valve flow-field at high spatial and temporal resolution using particle image velocimetry (PIV), the authors found high velocity jets at the hinge outflow with a time average velocity up to 5.7 ms^{-1}, higher than previously reported. The mean viscous shear stress was up to 60 Pa. Strong unsteady flows were also observed in the leakage jet. The peak instantaneous shear stress was as high as 120 Pa.

These high resolution measurements identified the hinge jet as a region of very high fluctuating shear stress, explaining the incidence of thrombosis. In Figure 2.38, Dasi *et al*. (2009) clearly shows the cellular particle pathway within the hinge area during the reverse flow phase. The shear stress experienced by the cells along their trajectory in the hinge is well above the threshold for platelet activation and the occurrence of blood damage. The prolonged residence time within the hinge increases the potential for thrombus formation.

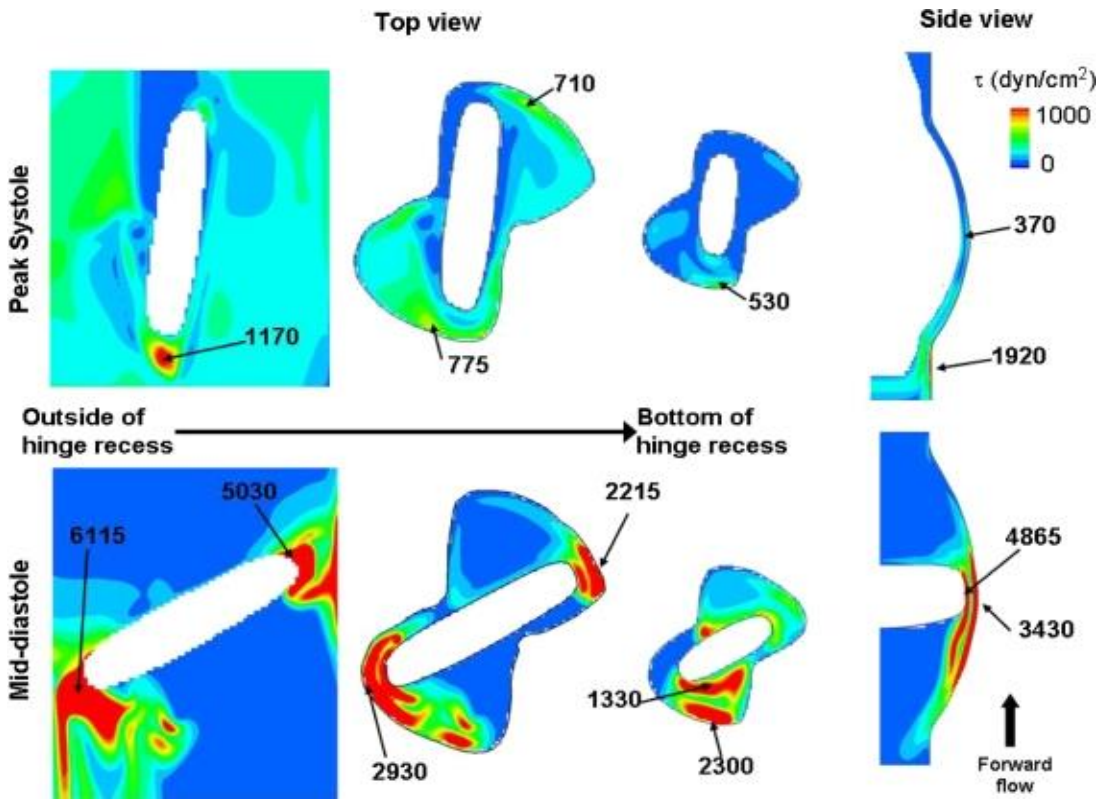

FIGURE 2.39**: Shear stress distribution within the hinge of a bi-lealfet valve.** Shear stress level contours are shown along three planes: (1) outside of the recess, near the leaflet edge surface, (2) at the flat level, and (3) at 390 μm within the hinge recess. Also included is a cross-sectional view through the center plane of the hinge. The local maxima, with their approximate location, are given. (Adapted from Simon *et al.,* 2010)

In a 3D time accurate simulation Simon *et al.* (2010) modelled the flow through the hinge recesses of an SJM valve under aortic physiological conditions. Figure 2.39 presents the principal shear stress contour maps at peak systole and mid-diastole within the valve hinge. The shear stress level distribution is similar throughout the forward flow phase, but it is at peak systole that the maximal shear occurs. At this particular instance of the cardiac cycle, a region of high shear stresses (with a peak of 1920 dyne/cm^2) is present near the flat level, outside and immediately upstream of the recess.

The region underneath the open leaflet, upstream of the hinge, is also characterised by elevated shear stresses (up to 1170 dyne/cm^2). The hinge recess itself, on the other hand, is associated with lower shear stress values and its shear stress distribution is characterised by higher levels in the ventricular side compared to the aortic side. A local maximum of 775 dyne/cm^2 is recorded along the wall of the ventricular corner close to the flat level. The maximum shear stress within the hinge recess is located near the tip of the leaflet ear with a peak of 370 dyne/cm^2.

It is during the leakage phase that the maximum shear stress levels are seen. During this phase, very large shear stresses are observed where the flow squeezes between the closed leaflet and the valve housing and forms two strong leakage jets on either sides of the leaflet ear. The shear stress levels reach up to 5030 dyne/cm^2 in the lateral jet and 6115 dyne/cm^2 in the adjacent jet

along the leaflet surface. Values of up to 2930 and 2215 dyne/cm^2 are seen at the flat level along the adjacent and lateral recess walls, respectively. Elevated levels of shear stress are also present at the center of the hinge, in the gap formed between the bottom of the hinge recess and the leaflet ear surface. In this region, the maximum shear stress is seen near the tip of the leaflet ear with a peak of 4865 dyne/cm^2.

The authors therefore concluded that during the forward flow phase the central region of the hinge, underneath the leaflet ear, and the near-wall region of the adjacent hinge corner both appeared as potential zones of thrombus formation. This is due to the fact that slow flow reversal and recirculation may enhance cell-to-cell contact and favour platelet aggregation. During diastole on the other hand, the strong leakage flow pattern through the hinge and peripheral gaps prevents flow stasis. However, these fast flowing jets yield elevated viscous shear stresses, with a peak value up to 6115 dyne/cm^2, well above the platelet activation threshold and therefore the diastolic flow is more detrimental to the blood elements than the forward flow phase.

ii. The valve hinge

A hinge mechanism is essential for a mechanical valve to function normally. The hinge design can affect the durability, functionality and potential thrombogenicity of the valve (Klusak *et al.,* 2015 and Murphy *et al.,* 2010). Small alterations in the design may lead to unacceptably high thrombosis risk, as was experienced in the Medtronic Parallel valve (Ellis and Yoganathan, 2014). The valve had a highly convoluted flow in the hinge, which was dominated by unsteadiness, vertical structures and multiple areas of stagnation, especially in the inflow pockets (Dasi *et al*., 2009 and Bluestein, 2004). Use of this valve was stopped early due to a high rate of thrombogenic events. The case clearly indicated how a change in hinge design may translate into a difference in the thrombogenic potential of otherwise very similar bi-leaflet mechanical valves. Typical hinge mechanisms found in modern mechanical valves are of the depressed type with rotation of the leaflet in the housing, for example SJM and Carbomedics valves (Figure 2.38). The ATS valve on the other hand has an elevated open hinge design (Figure 2.40 and 2.41), which theoretically causes less detachment of flow with reduced recirculation and stagnation, therefore reducing the thrombogenicity of the valve (Dumont *et al.,* 2007)

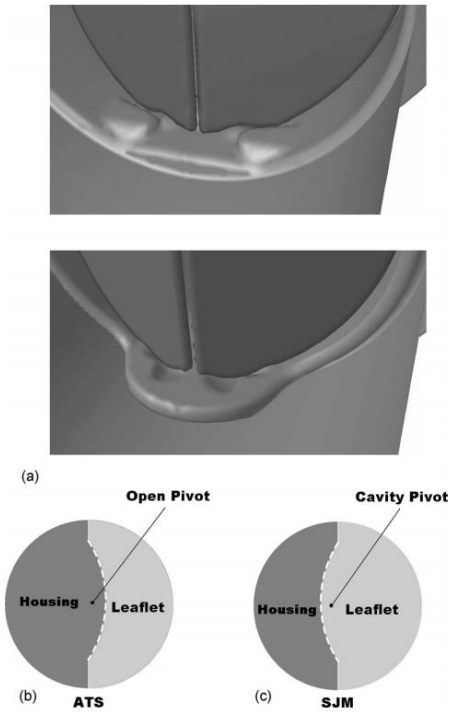

FIGURE 2.40: **Comparison of valve hinge mechanisms between the ATS and SJM valves.** (a) The valve hinge mechanism of the ATS open pivot valve (top) compared to the SJM depressed hinge (bottom). (b) The geometry of the hinge in the housing of the ATS valve compared to the (c) SJM valve (Adapted from Dumont *et al.,* 2007).

The shape of the hinge mechanism influences the levels of turbulence and unsteadiness of blood flow during the back flow phase or leakage jet (Jun *et al.,* 2014 and Simon *et al.,* 2010). Ellis and

Yoganathan (2014) describe how the leakage jet flows through these abrupt changes in the geometry of the hinge (Figure 2.38 and 2.39) where jet detachment may occur. They describe how the jet then impact directly against the corner of the inflow ramp and how both the detachment of flow and impact could lead to the formation of stagnation sites and possible regions of turbulence. By streamlining the hinge recess in the ATS valve (Figure 2.41) the geometry change is more gradual, leading to a leakage jet flowing through the hinge, following the contour of the inside of the surface, resulting in fewer regions of flow separation and turbulence.

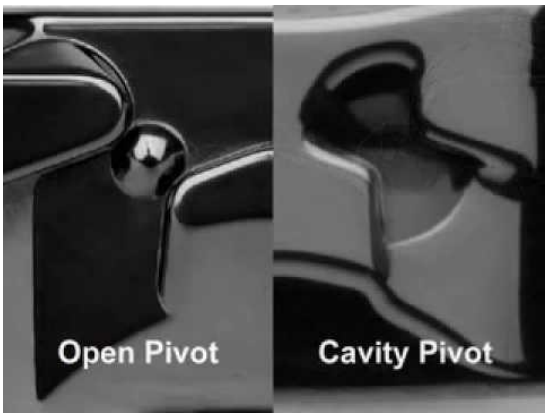

FIGURE 2.41: **Comparison between the ATS open pivot hinge and the SJM hinge**. The elevated pivot hinge of the ATS valve is seen on the left with the SJM valve cavity pivot on the right. (Adapted from Murphy *et al.,* 2010).

The extent of this retrograde flow has been shown to be detrimental to blood cells. (Murphy *et al.,* 2010 and Ellis *et al.,* 1996). Figure 2.39 shows the flow fields during the forward and leakage flow phases within the hinge region of the SJM valve (Simon *et al.,* 2010). In the hinge there are areas of stagnant flow and recirculation and these areas are the primary locations where clots begin to form by increasing cell-to-cell contact time. In valves such as the Medtronic Parallel valve the flow pattern within the hinge mechanism led to severe clot formation during clinical trials (Dasi *et al.,* 2009).

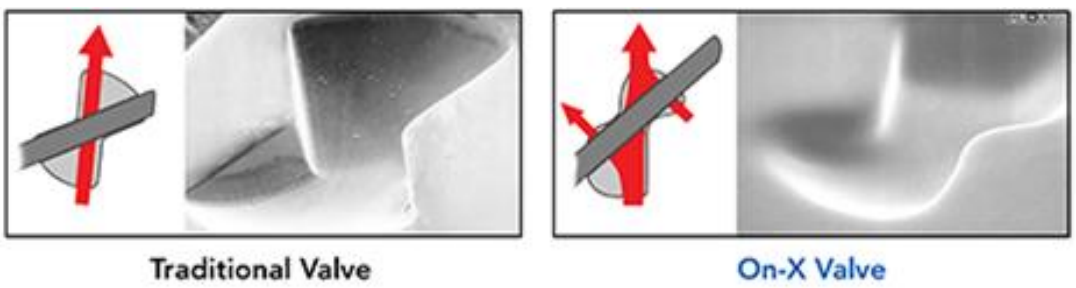

FIGURE 2.42: **Comparison between the hinge of a traditional valve and the On-X valve**. Back flow over smooth, blended contours is key to the low thrombosis rate of the On-X valve. (Adapted from www.onxlti.com).

The lower thrombosis incidence found in the On-X valve (Figure 2.42) can be ascribed to the “actuated pivot design” and to the smooth blended design of the hinge, which facilitates laminar flow with no flow detachment (Yezbick *et al.,* 2008). The design facilitates increased ‘washing’ through the entire pivot eliminating areas of potential flow stagnation without increasing the shear stress and platelet activation (Puskas *et al.,* 2014 and Chambers *et al.,* 2014).

According to Rudolph *et al.* (2013) the flow patern in the unique hinge of the mechanical tri-leaflet valve and the early closure of the valve leaflets reduced the shear stress in the hinge area, reducing the thrombogenic potential of the valve. The authors concluded that the valve can be used safely without the use of anti-coagulation.

iii. Valve housing

The On-X valve design differs from the traditional designs in that it increases the length-to-diameter ratio, thereby simulating that of a native valve (Figure 2.43). This reduces turbulence and improves laminar flow during forward flow across the valve (Puskas *et al.,* 2014 and Bokros *et al.,* 1992). It also allows for reduced leaflet excursion during the closing phase of the valve leaflets and therefore reduces back flow losses. The housing provides leaflet protection from tissue encroachment from the sewing cuff (Chambers *et al.,* 2013 and Chan *et al.,* 2010). The aerofoil housing profile optimises the organisation of flow across the valve. Turbulent flow is decreased, pressure recovery is favoured and it improves surface continuity with the suture ring (Reul *et al.,* 1993). The same principle was employed during the re-engineering of the GLYCAR valve. The length of the housing was increased and a flared design was utilised to promote near laminar transvalvular flows.

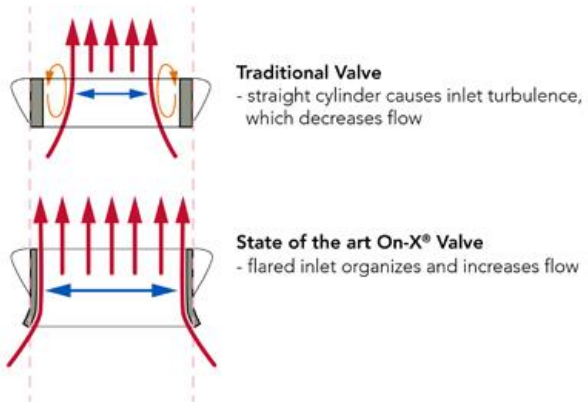

FIGURE 2.43: **Comparison of the valve housing between a traditional valve and the On-X valve**. By increasing the housing length and flaring the inlet, a laminar central flow is achieved in the On-X valve. (Adapted from www.onxlti.com).

iv. Sewing cuff

The sewing cuff and the suture zone of a prosthesis, owe their bio-compatibility to tissue cicatrisation and endothelialisation, thereby forming a layer on the material preventing adhesion of platelets and F XII, resulting in reduced thrombus formation. Although no anti-coagulation is needed for tissue valves, this healing process requires a few weeks to be completed and it is for this reason why anti-coagulation is indicated for tissue valves six weeks after implantation in order to allow for complete healing to take place (Ma *et al*., 2015 and Roudaut *et al.,* 2007).

Surgical studies have underlined the high prevalence of fibrous pannus formation that is also associated with a risk of thrombosis and may be present in 45–75% of valves (Barbetseas *et al.,* 1998 and Horstkotte *et al*., 1995). Caused by an excessive cicatricial response, pannus development is usually observed in proximity to the suture site and can be located on both sides of the prosthesis, with variable degrees of obstruction and leaflet motion interference.

v. Inlet flared orifice

According to Bokros *et al.* (1998) the On-X valve is the first prosthetic heart valve to successfully incorporate a flared inlet design (Figure 2.43). It is a well-known fluid dynamic principle for producing smooth and organised flow across a surface during increased forward flow and therefore reduces turbulence (Puskas *et al.,* 2014). The flare creates an environment conducive to laminar flow and increases the volume of flow, comparable to that of a larger orifice. Because the inlet flare extends through the annulus, it is not compromised by encroaching annular tissue and thus maintains the favourable annular shape for a lifetime of consistently optimal flow (Chan *et al.,* 2010). The Glycar valve is designed with a housing that flares outward along the flow of blood across the valve. It directs laminar flow laterally around the poppet thereby promoting distal laminar blood flow.

vi. Opening angle

Valve leaflets project into the flow of blood and are therefore always obstructive in nature (Murphy *et al.,* 2010). According to Sotiropoulos *et al.* (2016) all cardiac valves share the same principle of vortex shedding. The created eddies around the valve edges during forward flow are influenced by the opening angle of the valve leaflets and are pronounced in valves in which the angle is less than 90^{o}. A drop in pressure distal to the free edges of the leaflets is experienced and directly influences platelet adhesion and/or activation. By increasing the opening angle of the leaflets the exposed surface to forward flow and therefore the hydrodynamic interaction with blood is reduced (Puskas *et al.,* 2014). The On-X valve for example has an opening angle of 90^{o} however, although this angle is not achieved *in vivo* the leaflets are free to follow the flow and usually open between 78^{o}– 85^{o} (Bokros *et al.,* 2003).

vii. Valve leaflet closure

Several recent studies strongly suggest that the fluid dynamics during the closing phase, particularly in the mitral position, may be dominant in the development of thrombus in the vicinity of the mechanical heart valves (Sotiropoulos et al., 2016, Klusak et al., 2015 and Ellis and Yoganathan, 2014). Thrombus deposition in mechanical valves is often found in the peripheral region of bi-leaflet MHV in the vicinity of the leaflet edge and the valve housing as well as in the hinge region.

Manning *et al.* (2008) found that the leaflet impact produced by the closing mechanical leaflet onto its rigid housing yields the highest fluid stresses observed during the cardiac cycle. They measured mean velocities as high as 2.4 ms^{-1} during the initial valve impact. Yoganathan (1995) measured the velocities at the leaflet tip during closure and found that this resulted in sustained shear rates in the range of 1500–3500 dyne/cm^2, with peak values in the order of 11,000–23,000 dyne/cm^2.

By using velocity maps and three dimensional unsteady flow analysis past valve leaflets, Manning *et al.* (2008) gave a detailed flow-dynamic analysis showing regurgitation zones near the valve tip and through the central orifice of a bi-leaflet valve. Klusak *et al.* (2015) demonstrated how entrained flow from the transvalvular jets and flow shed off the leaflet tip during closure of bi-leaflet valves, combined to generate a dominant vortex posterior to both leaflets after each valve closing cycle.

Hebertson *et al.* (2011) showed that the strength of the peripheral vortex peaked within 2 m.sec of the initial impact of the leaflet with the housing and rapidly degenerated thereafter. In contrast, the vortex near the central orifice continued to grow during the rebound phase of the valve. The rebound phenomenon of the leaflets play a secondary role in sustaining closure induced vortices with subsequent cellular damage (Mohammadi, 2009).

Relatively high velocities are generated in the valve clearance area between the valve leaflet edge and the housing with resulting high wall shear stresses at the leaflet edge during the impact-rebound duration (Murphy *et al.,* 2010). The result is the presence of large negative pressure transients at the leaflet edge at the instant of valve closure with the initiation of cavitation bubbles (Lee *et al.,* 2007). CFD analysis during the last few degrees of closure of mechanical heart valves demonstrated the presence of these negative pressure transients on the inflow side of valve leaflets and their subsequent enhancement during the valve rebound phase (Chandran *et al*., 2004).

Shi *et al.* (2003) has determined that the total time required for a leaflet to come to rest in the closing phase in a bi-leaflet to be about 108–115 m.sec after three impacts with the valve housing, with the first impact taking place at 33–42 m.sec. However, for the opening phase, as Shi *et al*. (2003) reported, the opening phase without fluttering takes 44 m.sec. The time that is

required for the leaflet to come to a complete rest is a function of the material properties of the leaflet and the housing. Subramanian *et al.* (2000) using PIV, determined that the maximum leaflet tip closing velocity is 1.4 ms^{-1} for a 25 mm diameter bi-leaflet valve (flow conditions of 3.5 L/min, heart rate of 72 bpm and systolic duration of 300 m.sec).

The maximum velocity of the leaflet tip in a 25 mm diameter mechanical bi-leaflet aortic valve using a laser sweeping technique was measured by Whu *et al.* (1994). They reported a maximum velocity of 1.9, 2.5 and 2.6 ms^{-1} at 70, 90 and 120 bpm with a flow rate of 5.0, 6.0 and 7.5 L/min, respectively. The maximum leaflet tip velocity that was calculated upon first impact was in the range of 3.5–4.4 ms^{-1}. The tip velocity of the leaflet falls off rapidly after the first impact and comes to rest after the third impact. In addition to the leaflet tip velocity, the velocity of the fluid in the vicinity of the leaflet is also calculated. It can be seen that relative to the leaflet tip velocity, the velocity of the fluid in the vicinity of the leaflet is always higher (Yoganathan *et al.,* 2004); contributing to vortex formation, leaflet pitting, platelet activation and valvular material wear (Heberson *et al.,* 2011).

A study performed by Fallon *et al.* (2005) investigating the influence of the hinge gap within valvular orifices on thrombin activation, found that a gap of 200 to 400 μm induced significant thrombin-antithrombin III (TAT) generation. They also found that slit orifices greater than 800 μm produced no TAT generation and therefore no platelet activation.

In an effort to reduce impact-rebound cellular damage, the On-X valve has a patented two-point “soft landing” leaflet design (Bokros *et al.,* 2003). This design distributes and minimises closing impact and reduces the closing impact velocity with 40% (Pibarot *et al.,* 2009). This reduces cellular damage by bringing the two points of contact closer to the pivots. The two point landing distributes the closing impulse, glancing the impact rather than causing direct impact and finally minimising the potential for cavitation (Puskas *et al.,* 2014).

Murphy and Yoganathan (2010) showed that by adding vortex generator arrays to the downstream leaflet surfaces of bi-leaflet valves, passive flow control over the leaflet edge is enforced. The authors found that the turbulent stresses were diminished in the b-datum leakage jet flow. Although no difference was seen in the jet spreading, there were lower peak turbulent stresses and significantly lower TAT levels.

viii. Cavitation

Freed *et al*. (1981) observed pitting on the edges of the leaflets of dysfunctional explanted valves. The authors concluded that cavitation may have played a role in causing the pitting and erosion. Klepetko *et al.* (1989) were the first investigators to investigate the damaging effects that blood flow has on valve closure when clinical failures were reported for a small number of Edwards-Duromedics bi-leaflet valves. Pitting and erosion, markers of cavitatory damage, were noted on the free edges of the valve leaflets. Examination of other explanted valves of different valve designs have also revealed pitting of the same nature (Lee *et al.,* 1995).

Cavitation occurs when the operating pressure of a fluid falls below its vapour pressure causing gas bubbles to form and collapse (Mohammadi *et al*., 2009). When these bubbles collapse in the vicinity of a solid surface, the resulting high-speed micro-jet that is formed is one of the major causes of damage to valve surfaces (Woo and Yoganathan, 1986). Cavitation has been observed in MHV through *in vitro* experiments and has been clinically verified with damaged explanted valves (Lim *et al.,* 2003).

The major cause of cavitation takes place at the end of the closing cycle (Bluestein *et al.,* 1994). Fluid contained in the gap between the housing and the approaching leaflet is squeezed out, resulting in a local pressure drop (Eichler and Reul, 2004 and Lim *et al.,* 2003). When cavitation bubbles flow onward into a higher pressure region, the rapid collapse or implosion of these bubbles generates a high-speed micro-jet and shock waves, resulting in a very high local pressure (Lee *et al.,* 2007 and Kini *et al.,* 2000) and the local release of high energy (Paulsen *et al.,* 1999). The cavitation event causes erosion pitting on the leaflet surface and has been shown to be restricted to an area on the valve surface next to the edge of the valve where the squeeze flow occurs (Graft *et al.,* 1994).

The shock wave and the pressure difference are also responsible for platelet activation and the combination of pitting and active platelets may lead to accelerated thrombosis (Krishnan *et al.,* 2006). Cavitation bubble implosion also causes the release of TF (Anderson *et al.,* 2006), initiating the coagulation cascade. The bi-leaflet Edwards–Duromedics valve is an example of a valve where the design caused excessive cavitation with resulting mechanical failure due to fatigue-crack growth and an unacceptable high *in vivo* valve thrombosis (Mohammadi, 2009).

There seems to be consensus that elevated valve closing velocity and deceleration, which are related to elevated dP/dt (where P is the pressure in the left ventricle and t is the time), play a role in cavitation because they lead to a reduction in local pressure through a ‘water hammer’ mechanism. Several experimental studies (Lee *et al.,* 1996; Shu *et al*., 1994; Graf *et al.,* 1994 and Graf *et al*., 1991) have attempted to correlate cavitation to a maximum dP/dt. However, recent studies have shown that the dP/dt loading calculated only during the closure time is a more meaningful quantity for predicting cavitation with a value in excess of 1500 dynes (Krishnan *et al.,* 2006 and Chandran *et al.,* 1998). This is high enough to generate high frequency pressure

oscillations (Paulsen *et al., 1999)*. Table 2.4 compares the threshold dP/dt loading state for the different valve designs. Note the very low threshold for the Duromedics valve and the Jomed tilting disk valve, both of which failed due to excessive thrombosis. Interestingly, the Bjork-Shiley and the failed Chitra (A bi-leaflet valve designed and made in India and introduced in 1990) had the highest threshold rates (Nair *et al.,* 2003).

Table 2.4: **Threshold loading rate for the initiation of cavitation for mechanical heart valves**. (Adapted from Nair *et al.,* 2003).

Valve model	Design type and occluder material	Threshold loading rate dP/dt (mmHg)
Medtronic Hall	Tilting disc Pyrolytic carbon on graphite	300
Bjork-Shiley Standard	Tilting disc Pyrolytic carbon on graphite	1500
Jomed implantate	Tilting disc Carbon/delrin composite	200
Edwards Duromedics	Bi-leaflet Pyrolytic carbon on graphite	200
Carbomedics	Bi-leaflet Pyrolytic carbon on graphite	750
Chitara	Tilting disc Pyrolytic carbon	>3000

mmHg = millimeter mercury, dP/dt = Change in pressure over change in time.

Another mechanism that contributes to cavitation is the generation of high squeeze flow velocity that is characterised by large pressure drops (Figure 2.44). During valve closure, maximum velocities of up to 2.5 ms^{-1} have been experimentally documented (Chandran *et al.*, 1998) as the flow is squeezed into a narrow passage while being subjected to the high closing velocity of the valve itself (Bluestein *et al*., 1994 and Lee *et al., 1996*).

Cavitation in squeezed flows was studied experimentally (Lim *et al.,* 2003 and Lee *et al.,* 1996) and proved as a contributing factor for cavitation. Bluestein *et al.* (1994) supported this finding with a simulated numerical model. The flow in the clearance between the valve leaflet and the housing was also studied numerically by Lee and Chandran (1995). The authors found that the sudden stopping and subsequent rebound motion of the valve leaflets, coupled with tension waves generated immediately after the instant of valve closure, resulted in a sharp local pressure drop and contributed to cavitation and vortex formation. These findings have been validated by Lim *et al*. (2003) and Kini *et al*. (2000).

Due to the higher thrombosis incidence in tilting disk valves, this phenomenon was studied by Manning *et al.* (2008) in tilting disk mechanical valves during leaflet closure. In this study the author showed that the mean and axial velocities reached as high as 20 ms^{-1} with a peak wall shear rate of up to 80 000 s^{-1}. An atrial vortex developed on the major orifice side of the valve

and was shed off the tip of the valve, leading to significant cavitation. Although the cavitation was not high enough to cause pitting on the leaflet surface, it induced thrombosis.

Lee *et al.* (2006) showed cavitation occurring in bi-leaflets as well as tilting disk valves. In figure 2.45 two valves are represented: the Medtronic-Hall tilting disk at the top and the Carbomedics bi-leaflet valve at the bottom, showing cavitation occuring at (a) 70 bpm and at (b) 100 bpm. The valve stop area in the tilting disk valve, in which cavitation bubbles were visible, was three times larger than the valve stop area in the bi-leaflet valve. In addition, the valve-closing velocity of the tilting disk valve was 1.2–1.5 times that of the bi-leaflet valve.

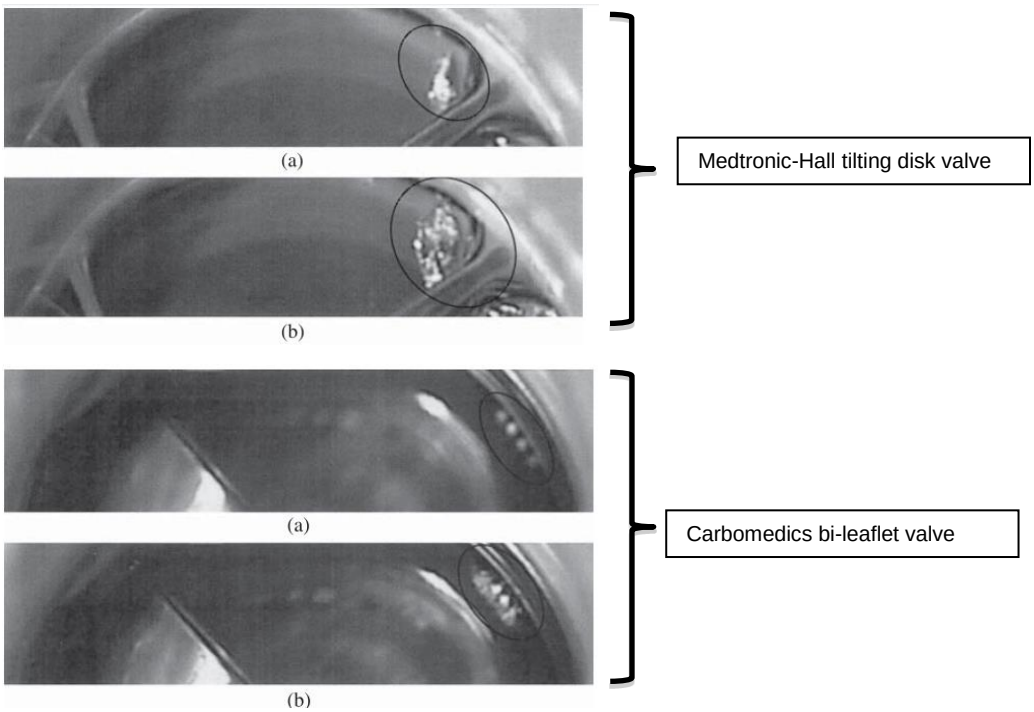

FIGURE 2.44: **Cavitation bubbles occurring in mechanical heart valves**. Two valves are represented, the Medtronic-Hall tilting disk at the top and the Carbomedics bi-leaflet valve at the bottom. Cavitation occurs at (a) 70 beats and at (b) 100 beats per minute (Adapted from Lee *et al.*, 2006).

ix. Vortex shedding

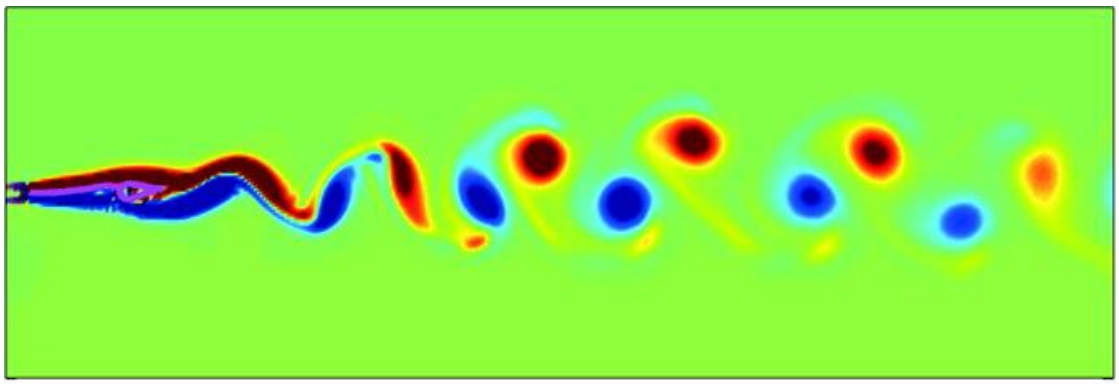

FIGURE 2.45: **Velocity plot showing flow around a leaflet with vortex shedding trailing the leaflet**. The warm colors are regions of positive vortex flow with the cool colors depicting negative vortex flow. (Adapted from Bluestein *et al.,* 2000)

In fluid dynamics, vortex shedding is an oscillating flow that takes place when a fluid such as blood, flows past a bluff (as opposed to streamlined) body at certain velocities (Sotiropoulos *et al.,* 2016). During this flow, vortices are created at the back of the body and detach periodically from either side of the body (Gross *et al.,* 1988). The fluid flows past the object and creates alternating low-pressure vortices on the downstream side of the object (Figure 2.45)

In the wake of a valve leaflet during the deceleration phase, there is an intricate pattern of interacting shed vortices (Bluestein *et al.,* 1999 and Bluestein *et al.,* 2000). Particle paths showed that platelets that were exposed to the highest flow stresses around the leaflets were entrapped within the shed vortices. In the aortic position, a Karman-like vortex pattern appears downstream of the SJM at the end of the ejection phase (Gross *et al.,* 1988). Platelets may be activated as the shear stress in this region reaches the threshold for platelet activation. Aggregation may occur and free emboli may form, increasing the risk of systemic micro-emboli (Herberson *et al.,* 2011).

Large vortical flow have been observed experimentally (Manning *et al.,* 2008) and computationally (Cheng *et al.,* 2004) immediately after valve closure and leaflet rebound. Some of the platelets that are activated during valve closure may be trapped in these vortical flows for a significant period of time and have a tendency to aggregate and attach to the valve structures in this region resulting in the initiation of thrombus formation (Ellis and Yoganathan, 2014).

x. Valve orientation

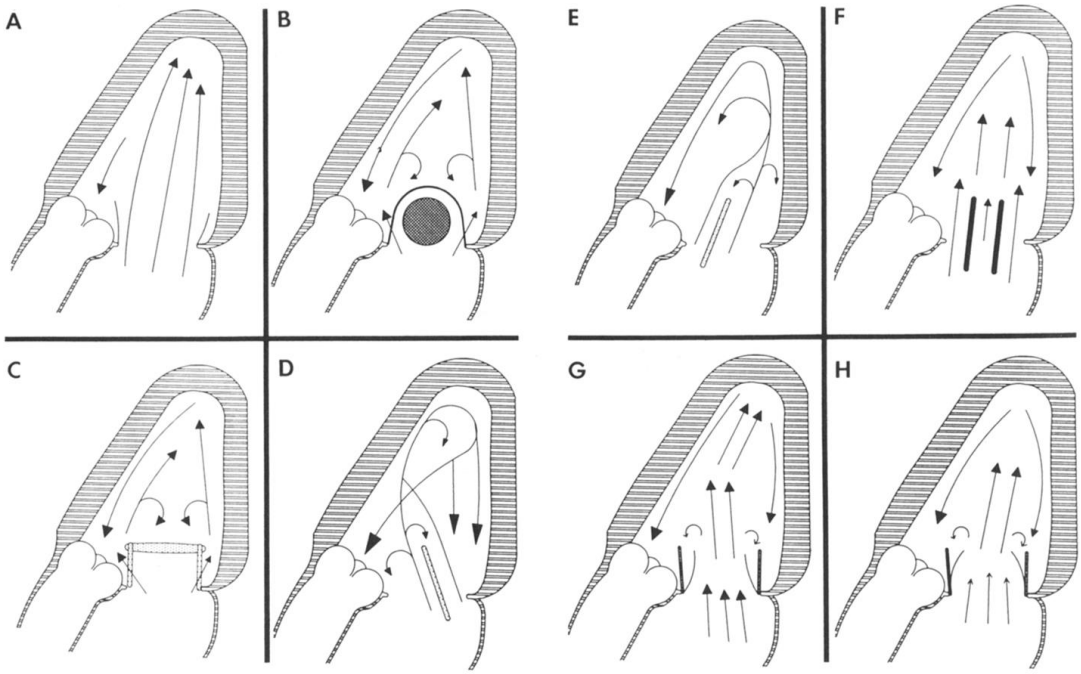

FIGURE 2.46: **Comparison of flow patterns during the forward phase in the left ventricle of eight different mitral valve prosthesis**. Note how the flow patterns are influenced by the valve orientation. (a) Native valve, (b) Starr-Edwards valve, (c) Non tilting disk, (d) Tilting disk orientation 1, (e) Tilting disk orientation 2, (f) Bi-leaflet valve, (g and h) Tri-leaflet porcine bio-prosthetic valve (Adapted from Jones *et al.,* 1989).

According to Chandran *et al.* (1989), the geometry of valve prosthesis as well as the orientation of the valves may significantly affect the flow development, including vortex formation, regions of stasis and disturbed flow in the left ventricular cavity. The wake of the valve is influenced by orientation, whether this includes tilting of the valve or simply rotation.

Aoyagi *et al*. (1991) reported that the frequency of mechanical haemolysis associated with the use of the SJM valve was relatively high. They concluded that valve orientation seemed to be one of the primary causes of haemolysis. Because of this finding, their group at Kurume Medical School adapted the anti-anatomical orientation during mitral valve replacement when using bi-leaflet mechanical valves.

Baudet *et al.* (1985) also reported, based on their five year experience, that bi-leaflet prosthesis requires an anti-anatomical orientation to provide optimal haemodynamics and subsequently to reduce turbulence in the downstream areas. This has been validated using echocardiographic studies (Akutsu and Higuchi, 2000; Jones *et al., 1989* and Deveau *et al.,* 1983) and is common worldwide practice today.

a. Tilting disc valve orientation

The effect of valve rotation within the heart has been extensively evaluated by Chanderan *et al.,* (1989). The author reported that the flow downstream of a bi-leaflet MHV is characterised by the formation and interaction of three jets during the systolic part of the cardiac cycle and their interaction in an asymmetric area with sudden expansion into the ventricle. The blood flow across the mitral valve can be divided into three distinct phases: an early acceleration flow, mid peak flow, and late deceleration flow, which are all influenced by the orientation of mechanical valves.

Manning *et al.* (2008) and Chanderan *et al.* (1989) investigated the effect of valvular orientation in the mitral position of a tilting disk valve. They concluded experimentally that when the major orifice of a tilting disc valve was oriented toward the aortic valve (**anterior orientation**), flow from the major orifice during the acceleration phase tends to flow toward the ventricle wall at the aortic valve side due to the shallow opening angle at the initial opening phase (Figure 2.46d). As the flow accelerated further into the ventricle, it collided with the ventricular wall and moved both up and down along the wall on the aortic valve side. Because of the small opening angle during the acceleration and peak flow phase, flow tended to deflect sideways and this may lead to decreased flow through the minor orifice resulting in stagnant flow (Jones *et al.,* 1989). This has been an area prone to thrombus initiation and/or adhesion.

The two-directional flow after collision tends to form two small circulations within the ventricle, one in the counter-clockwise direction, located close to the aortic valve and one in the clockwise direction, located close to the centre of the ventricle (Aoyagi *et al*., 1991 and Baudet *et al.,* 1985). When the flow reaches the peak phase, these counter-rotating flows become more stable. The decelerating phase is characterised by the sudden reduction of all velocities and stresses (Manning *et al.,* 2008).

Manning *et al.,* (2008) and Chanderan *et al.,* (1989) reported that in the **posterior anti-anatomical orientation** (rotated 180^{o}), flow through the mitral valve is directed downwards (Figure 2.47e). There is significant turbulence immediately after passing the mitral valve with a mean maximal velocity of 1.5 ms^{-1} in contrast to a mean maximal velocity of 1.1 ms $^{-1}$ in the anatomical position (findings supported by Machler *et al.,* 2007). As the flow accelerates, it continues very strongly downward along the ventricular septum at the mitral valve side, and is observed to be more organised, forming a clear velocity pattern with higher velocities of flow towards the apex (Jones *et al.,* 1989). This means that disturbances and laminar flow velocity/flow is directed towards the left ventricular apex. This trend continues until peak flow is reached. As the flow reaches the peak phase, the flow pattern inside the ventricle is a very clear, large, single circulation. The decelerating phase is characterised by the sudden reduction of all velocities and stresses. The posterior orientation does not provide physiological flow patterns.

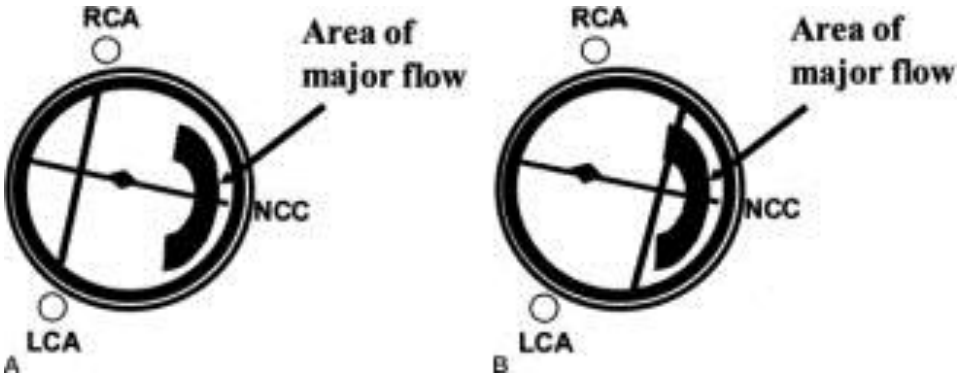

FIGURE 2.47: **Optimal (A) and worst (B) orientation of the tilting disc valve in the aortic valve position.** *RCA*, Right coronary artery; *NCC*, noncoronary cusp; *LCA*, left coronary artery. (Adapted from Kleine *et al*., 2002)

In a study performed by Kleine *et al.* (2002) evaluating the role of valve orientation in the aortic position on coronary flow (figure 2.47), the author was able to show that coronary blood flow was significantly influenced by MHV implantation and the orientation of the prosthesis. The authors were able to show that in the haemodynamically best orientation (Figure 2.47A), the major orifice faces the noncoronary cusp of the aortic valve, the region of major flow during ejection in systole. Rotation of 180° leads to the haemodynamically worst orientation (Figure 2.47B) with the disk placed in the major flow field increasing flow resistance.

The flow in the aorta is influenced by the angled outflow tract of the left ventricle, the sinuses of Valsalva and the natural angle of the aortic arch. *In vivo* studies reflect this complex anatomy, resulting in asymmetric and eccentric flow in the aortic root with the highest flow velocities along the noncoronary cusp (Figure 2.47 and 2.48) (Nygaard *et al*., 1992). After aortic valve replacement, left anterior descending flow increased significantly to 58.2 ± 10.6 mL/min. Highest flow rates at normal CO were found in the optimum orientation, especially for the Medtronic valves (Medtronic-Hall, 64 ± 8.7 mL/min; Medtronic Advantage, 64.6 ± 11.6 mL/min; SJM, 48.3 ± 10.3 mL/min), whereas the worst position demonstrated significantly lower left anterior descending flow, with no differences among valves (Medtronic Hall, 37.5 ± 1.3 mL/min; St Jude Medical, 35.7 ± 10.7 mL/min; Medtronic Advantage, 39.8 ± 10.0 mL/min).

The disk valve showed minimum Reynold's normal stress values (RNS) with orientation of the large orifice to the right posterior aortic wall (Figure 2.46), which is the area of highest velocities during ejection and with this orientation, near normal aortic flow is simulated. Increased turbulence was observed with any other position (Kleine *et al*., 2000 and Jin *et al.,* 1999). Minimum RNS values were measured with one orifice facing the right posterior wall of the aorta. Kleine *et al*. (2000) concluded that with optimum orientation (major orifice facing the right posterior aortic wall) the tilting disk valve matched the aortic flow pattern to near-normal physiology.

b. Bi-leaflet valve orientation

Jun *et al*. (2014) were able to show that during early acceleration flow across a bi-leaflet valve in the mitral position, flow through the valve was mainly downwards and partly directed sideways. The result was a diverse flow field due to the slope of the two half-disc leaflets. The dominant flow direction was towards the aortic side of the ventricle wall, however, the velocity vectors in general are shorter, indicating a lower velocity. As the flow accelerates, the flow becomes more organised, forming a clear velocity pattern with the flow towards the aortic side of the ventricle wall. Flow also crosses diagonally at the centre of the ventricle.

Jones *et al.* (1989) and Yoganathan *et al*. (1986) was able to illustrate experimentally that due to the initial directional flow generated by the two half-discs, the flow tended to form two circulatory flows, one located close to the aortic valve and the other located close to the apex of the ventricle, where the flow becomes unclear. This trend gradually weakens, but continues until peak flow is reached. Once the flow reaches its peak value, the velocity pattern becomes a large, circulatory flow pattern with slight directional instability. The decelerating flow phase is categorised by diminishing velocity vectors, as indicated by the shorter velocity vectors.

When the valve is rotated 90º to the **anti-anatomical orientation**, a similar general trend is seen, in that it tends to form a single circulatory flow at the end. At the onset of opening, flow through the mitral valve is predominantly downwards (Akutso *et al.,* 1999 and Yoganathan *et al*., 1986). Flow in the sideways direction, as observed in the anatomical orientation is present, although the affected area is now facing away from the observed plane. Subsequently, as the flow accelerates, it is observed to be more organised and quickly forms a clear circulatory velocity pattern. This trend continues until peak flow is reached. At the peak flow phase, the velocity pattern is a clear, large, circulatory flow pattern.

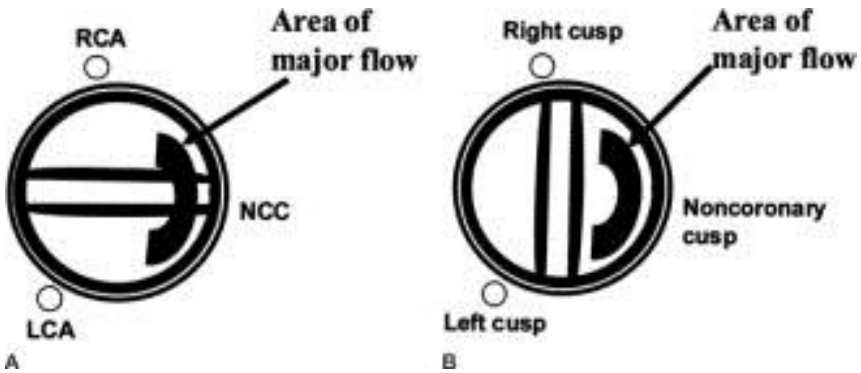

Figure 2.48: **Optimal (A) and worst (B) orientation of a bi-leaflet valve.** Optimal haemodynamics are achieved with one orifice facing the right cusp. The area of major flow is distributed equally to the 3 openings. Rotation of 90° leads to the worst orientation. *RCA*, Right coronary artery; *NCC*, noncoronary cusp; *LCA*, left coronary artery. (Adapted from Kleine *et al.,* 2002).

Akutso *et al.* (2000) and Reul *et al.* (1993) were able to show how, at the beginning of the accelerating phase, the valve opens briefly to a full 85^{o}. However, this opening angle, does not remain for very long. The opening angle is soon somewhat reduced and seems to keep this angle for the rest of the acceleration and peak flow period. This implies that the outer two orifices have the possibility to have lower pressure than the central orifice, thus a higher velocity in that region. The central orifice however, may have very low velocity. This circulatory flow offered by the anti-anatomical orientation provides a smoother flow field and generates less turbulence during the cardiac cycle.

A study performed by Kleine *et al.* (1998) and later confirmed by Kleine *et al*. (2000) and Jin *et al.* (1999) evaluating the effect of valve orientation in the aortic position found that turbulence downstream of bi-leaflet valves demonstrated a significant change with rotation and the flow patterns of the bi-leaflet valve were optimal when the hinge was facing the noncoronary cusp.

In summary: higher vorticity, turbulence and vortex intensity levels are evident in the anatomical orientation when compared to those of the anti-anatomical orientation in bi-leaflet valves, producing higher shear rates and enhanced platelet activity and increased haemolysis (Kleine *et al.,* 2002 and Reul *et al., 1*993).

2.3.4 The challenges of Warfarin therapy

i. Introduction

To avoid the detrimental and often fatal complications associated with valve thrombosis, including thrombo-emboli, the use of Warfarin is indicated (Garcia *et al*., 2005). Warfarin is a 4-hydroxycoumarin-containing molecule that decreases blood coagulation by inhibiting vitamin K epoxide reductase (Vit K E.R.). Vit K E.R. is an enzyme that recycles oxidised vitamin K1 to its reduced form after it has participated in the carboxylation of several blood coagulation proteins; mainly PT and F VII (Ansell *et al*., 2008).

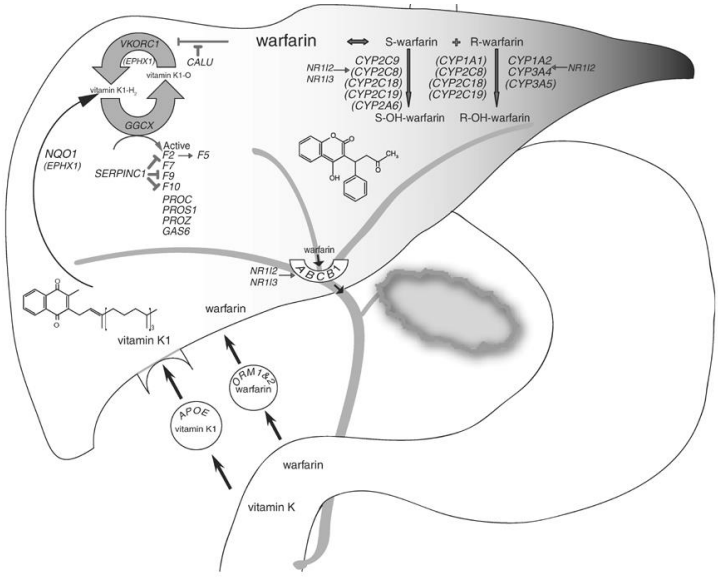

FIGURE 2.49: **The Warfarin and vitamin K pathway in the liver**. (Adapted from www.nature.com/tpj/journal/v7/n2/images/6500417f1.jpg)

Although Warfarin minimises the risk of thrombosis, it never completely eliminates it (Kaneko *et al*., 2013). There is also a risk of haemorrhage associated with Warfarin, which may be life threatening. Therefore INR control is critical to avoid or at least reduce the risk of developing either set of complications (Ma *et al.,* 2015). The optimal level of anti-coagulation therapy has not yet been sufficiently determined, and most of the current recommendations are based on clinical results with an earlier generation of mechanical prosthesis, which were associated with a relatively high incidence of thrombo-embolism (Puskas *et al*., 2014; Nishimura *et al.,* 2014 and Pruefer *et al*., 2001).

Warfarin has a narrow therapeutic window, slow onset and offset of action, and an unpredictable response demanding frequent monitoring of the INR, dose adjustment and awareness of interactions with food and with other drugs (Nishimura *et al.,* 2014).

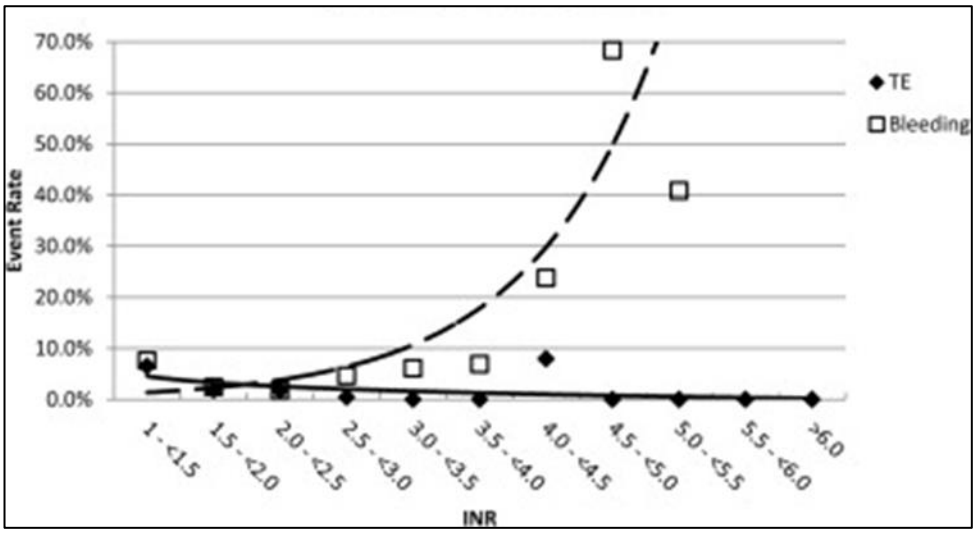

FIGURE 2.50: **Relationship between the international normalised ratio (INR) at the event and event rates**. TE= Thrombo-embolism. (Adapted from Puskas *et al.,* 2014).

The responsible clinician must also manage the logistics of patient education, ongoing support and regular drug administration. Warfarin control is challenging even in the first world. Warfarin contributed to 33% of hospital admissions related to adverse drug events in individuals older than 65 years in the USA (Budnitz *et al*., 2011). Figure 2.50 shows the relationship between INR and event rate of thrombo-embolism and the risk of bleeding complications. The figure illustrates that once the threshold INR of 4.0 is crossed, the risk of bleeding increases exponentially. Even with an optimal INR control, thrombotic events still occur.

TABLE 2.5: **Anti-coagulation related complications in patients following prosthetic heart valve replacements on Warfarin therapy**. (Adapted from Akhtar *et al.,* 2009)

Variable	N (%) (n=507)	Cumulative %/patient-years
Thrombo-embolic events	23 (4.5%)	1.13
Valve thrombosis	9 (1.8%)	0.44
CNS complications	14 (2.7%)	0.69
CVA	9 (1.8%)	0.44
TIA	5 (1.0%)	0.25
Bleeding events	41 (7.9%)	2.04
- minor	8 (1.6%)	0.39
- moderate	20 (3.9%)	0.99
Severe	5 (1.0%)	0.34
Haemorrhagic CVA	8 (1.6%)	0.39

CNS=Central nervous system, CVA= Cerebro-vascular accident, TIA= Transient ischaemic attack

Table 2.5 summarises a study performed by Akhtar *et al.,* (2009). The event rate for all thrombotic events was 1.13% per patient year with optimal Warfarin therapy in all patients and a total cumulative percentage complication rate of 6.9% per patient year. The risk of anti-coagulant related haemorrhage in patients using Warfarin varies between 0.6% to 4.9% per patient year, depending on the valve type and INR target (Grunkemeier *et al.,* 2000). The rate for major thrombo-embolism is 0.34% per patient year (Xiaogang *et al*., 2003) to 0.37% per patient year (Koertke *et al*., 2007).

Warfarin also carries a risk during child bearing, which necessitates conversion to an alternative anti-coagulant. According to Bates *et al,* (2012) Warfarin therapy during pregnancy is associated with a substantial increase in foetal anomalies. Because Warfarin crosses the placenta it can cause foetal bleeding and teratogenicity, with the latter occurring mainly during the first trimester (Yurdakök, 2012). It is thus associated with an increased incidence of miscarriages (approximately 30%), premature births (approximately 45%), and low birth weight (approximately 50%).

ii. Patient demographics

In the African population rapid and predictable therapeutic anti-coagulation is difficult because dose requirements vary substantially. There is a genetic predisposition to increased hepatic clearance leading to large dose variability in this population as was shown by Perera *et al*., (2013) in the African-American population in the USA.

The incidence of valvular pathology needing replacement surgery in a developing country such as South Africa is broadly disseminated over an age-spectrum from 20 to 70 years with a peak incidence at 30 years (Zilla *et al.,* 2008 and Unger *et al*., 2002*)*. This in part due to the high prevalence of rheumatic fever (McLaren *et al.,* 1975) with early onset heart valve pathology. Zilla *et al*. (2008) in Cape Town, South Africa showed the discrepancy in age distribution of cardiac valve recipients between the first world and the developing world and is reflected in Figure 2.1. This study highlights the need for mechanical prosthetic use in the young population and the need for lifelong anti-coagulation.

According to the *South African national human immunodeficiency virus (HIV) prevalence, incidence and behavior survey, 2012*, the incidence of people living with HIV in South Africa is 12.2% (higher than in 2008) with the peak age of 25 in women and 36 in men (www.hsrc.ac.za). The prevalent increase of approximately 1.2 million between 2008 and 2012 is likely a result of new HIV infections that occurred over the past four years. Another probable cause for the increase is a reduction in mortality among those living with HIV and AIDS, due to the large-scale roll-out of anti-retroviral therapy (ARV) (Bor *et al.*, 2013). Warfarin is susceptible to drug-to-drug interactions with ARV drugs and the required maintenance dose is significantly higher in patients receiving ARV (Esterly *et al.,* 2013).

The European Society of Cardiology (Gohlke-Barwolf *et al*., 1995) recommends an INR of 3.0–3.5 for second generation valves in the mitral position and an INR of 2.5–3.0 for second generation valves in the aortic position. The American College of Cardiology and the American Heart Association guidelines of 2006 (AHA guidelines, 2006) recommend an INR of 2.0–3.0 for aortic valve replacement with bi-leaflet mechanical or Medtronic-Hall prosthesis in patients with no risk factors. With risk factors an INR of 2.5–3.5 is indicated. After aortic valve replacement with other MHV, or after mitral valve replacement, an INR of 2.5–3.5 is also recommended (Nishimura *et al.,* 2014). With an increase of 1 unit of INR greater than 2.5, the risk of death from cerebral bleeding, as well as from other causes, was approximately doubled (Oden and Fahlen, 2002).

Unfortunately, the literature is unclear as to precicely which INR targets to be the ideal and conflicting evidence in the real world actually prompts an increase in the INR level (Kaneko *et al.,* 2013). A retrospective study of 16 081 patients with mechanical heart valves in the Netherlands at four regional anti-coagulation clinics (target INR 3.6 to 4.8), found a sharp rise in the incidence of embolic events when the INR fell to less than 2.5. The authors also found that the risk of bleeding increased, as well as an increase in mortality due to the prevalence and severity of severe insults when the INR rose to 5.0 (Cannegieter *et al*., 1995).

The INR level is also determined by the prosthesis type (Ma *et al.,* 2015 and Butchard *et al.,* 2005). Low risk valves include Medtronic-Hall, SJM, Carbomedics and bio-prosthetic valves. For low risk valves an INR of 2.5 will suffice while medium risk valves and high risk valves demand an INR of 3.0 and 3.5 to 4.0, respectively. The Bjork-Shiley valve is an example of a medium riks valve. The Lillehei Kaster, Omniscience and the Starr–Edwards valves fall into the high risk valve category.

The trend is to lower the INR in the new generation valves as flow-dynamics have improved and the shear activation of platelets across the valves have been reduced (Puskas *et al.,* 2014). Guidelines regarding INR requirements have been lowering the INR target as valve designs improved. Changes in prosthesis design from the ball valve and tilting disc valve to the bi-leaflet valve and changes in the blood contact surface material from titanium, silicone, delrin and dacron to carbon, have not been able to remove the disadvantage of lifelong anti-coagulation (Akins, 1991). Standard oral anti-coagulation therapy with a high target INR of 3.0–4.0 is indicated in patients with the first generation of heart valves such as the Starr-Edwards valve (Huth *et al*., 2001) with the newer generation valves needing an INR of 2.5–3.5.

Even in the first world the control and maintenance of adequate INR levels remain a challenge. In Germany, where INR is often strictly controlled by a physician, only 43% of INR measurements (INR target 3.0–4.5) were within target range (Pruefer *et al*., 2001). Patients, who undertook self-management of their anti-coagulation with home testing, achieved an INR within the target range up to 83% of the time.

The early self-controlled anti-coagulation trial (ESCAT) demonstrated that self-management of oral anti-coagulants improves the percentage of INR values within the target range, reduces thrombo-embolic events and improves long-term survival, compared to the management of oral anti-coagulant by a general practitioner (Koertke *et al*., 2007). The ESCAT II study is a large prospective interventional trial that evaluated oral anti-coagulant related complications in patients with mechanical heart valve prosthesis. The effects of low-dose INR self-management were compared with conventional dose INR self-management. It was subsequently found that the INR target range could be reduced from 2.5–4.5 to 1.8–2.8 in patients with aortic valve replacement and from 2.5–3.5 in patients with MVR or DVR, without increasing the risk of thrombo-embolic events (Koertke *et al*., 2005).

During a study performed by Yamac *et al.* (1999) on the SJM, the INR threshold was lowered and a fixed Warfarin dose was used regardless of INR. The study included 2 585 patients (mean age 40.3 ± 13.5 years) living in a rural environment. Of the patients receiving heart valves, 865 underwent aortic valve replacement, 1 231 mitral valve replacement and 489 double valve replacement. Warfarin was combined with anti-aggregation therapy which included dipyridamole 3 x 75 mg/day plus aspirin 100 mg/day. During follow-up, there were eighty-eight anti-coagulant haemorrhages (1.2% per patient-year), eleven para valvular leaks (0.2% per patient-year), fifty-two thrombo-embolisms (0.7% per patient-year), sixty mechanical valve thrombosis (0.8% per patient-year) and seventy-eight reoperations (1.1% per patient-year). Complications occurred in one hundred and one patients after AVR, one hundred and twenty five after MVR, and sixty-three after DVR (4.2%, 3.7% and 4.6% per patient-year, respectively). They concluded that the implantation of the SJM mechanical heart valve prosthesis, combined with fixed dose (2.5 mg/day) Warfarin and dipyridamole/aspirin, provided comparable results to similar patients using higher Warfarin doses.

These findings are supported by various other studies including the GELIA 4 (German experience with low intensity anti-coagulation) study. Performed in Germany in 2001, it is the largest multi-centre study investigating the optimal dose of Warfarin as well as comparing high, medium and low dose Warfarin with the use of the SJM valve (Pruefer *et al*., 2001). Bleeding occurred in 1.5-2.5% per patient-year regardless of the dose of Warfarin however, the frequency of severe bleeding was reduced from 0.75% to 0.25% with a decrease in the Warfarin dose, whilst at the same time showing no increase in thrombo-embolic events.

A study performed in Denmark on 3075 patients spanning a period of five years (1996 to 2012) using a patient self-management program, reported lower all-cause mortality when compared to conventional management (adjusted hazard ratio of 0.49, 95% confidence interval: 0.34 to 0.71). The hazard ratios for thrombo-embolism and major bleeding were 0.91 (95% confidence interval: 0.66 to 1.24) and 0.83 (95% confidence interval: 0.56 to 1.22) (Christensen *et al.,* 2016).

iii. Valve design and Warfarin use

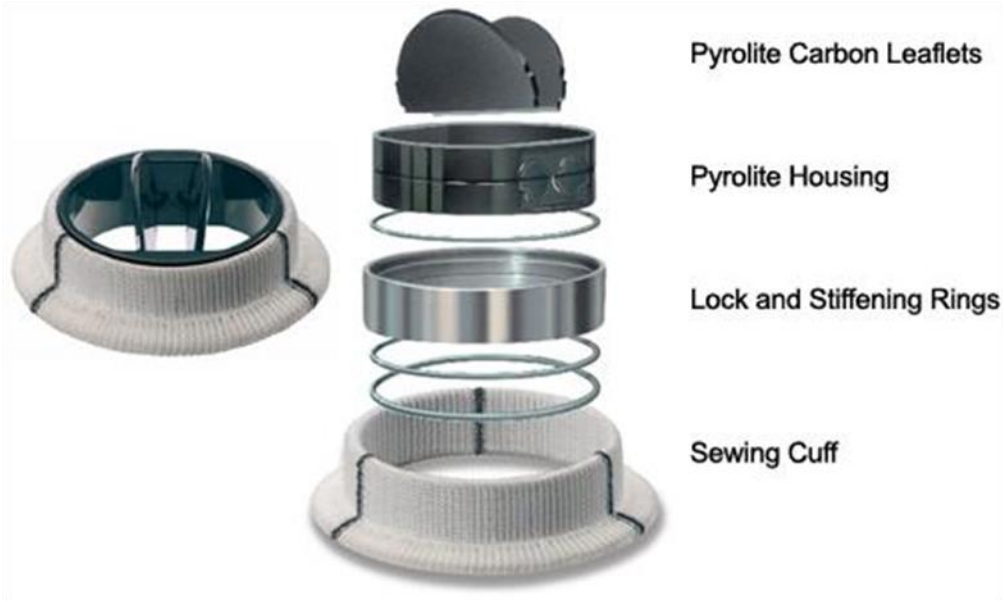

FIGURE 2.51**: The components of a bi-leaflet, prosthetic heart valve**. (Adapted from: http://www.ctsnet.org/products/Sorin-group/Carbomedics)

As it stands today, all heart valves that are available commercially, are of a similar bi-leaflet design (Figure 2.51) comprising of similar components. Bi-leaflet valves consist of two semilunar disks attached to a rigid valve ring by small hinges and the components are made of pyrolytic carbon.

As mechanical cardiac valve design have improved, so has the requirement for INR control and as a result, the required INR has been reduced for each generation of heart valves (Kaneko *et al*., 2013). The flow characteristics of a heart valve influence the activation of both the coagulation cascade and blood platelets. Incorporating current understanding of flow and fluid dynamics as well as an understanding of the characteristics of ideal valve design, theoretical valves can thus be perceived (Puskas *et al.,* 2014). The On-X valve (Medical Carbon Research Institute, Austin, Texas, USA) is such a valve (Figure 2.15), where the flow characteristics of blood is manipulated within the design of the valve thereby improving the thrombogenic potential of the valve and reducing the Warfarin dose needed (Chambers *et al.,* 2014 and Chan *et al.,* 2010).

The pure isotropic pyrolytic carbon in the On-X valve causes a smoother surface reducing cellular interaction and in combination with the flared inlet design (reduces inlet turbulence) and an elongated orifice (organises flow and reduces exit losses), laminar blood flow is created (Figure 2.52(Chambers *et al.,* 2014).). Fluid dynamics is improved and damage to blood cells is reduced (Puskas *et al.,* 2014 and Hwang *et al*., 1998). The two-point “soft landing” leaflet design (Bokros *et al.,* 2003) distributes and minimises closing impact as well as reduces the

closing impact velocity with 40% (Pibarot *et al.,* 2009). Cellular damage is reduced by bringing the two points of contact closer to the pivots and distributing the closing impulse by glancing the impact, rather than causing direct impact, which minimises the potential for cavitation (Puskas *et al.,* 2014).

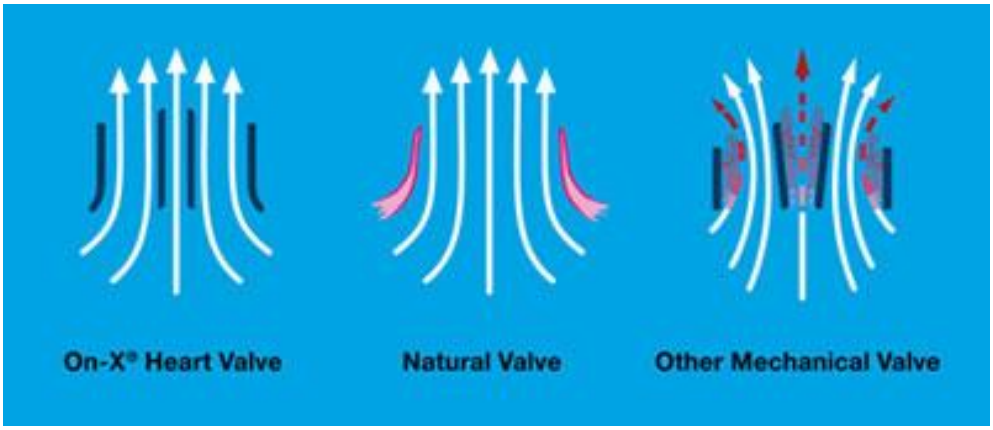

FIGURE 2.52**: Comparative flow patterns in the On-X Valve**. (Adapted from www.onxlti.com).

Long-term outcomes on this valve have been reported to have a low thrombosis rate, as low as 0% in some papers (Chambers *et al*., 2013 and Palatianos *et al*., 2007). The carbon technology and transvalvular flow patterns make this valve a low thrombogenicity valve and thrombo-embolism is uncommon even in a population of which 40% have inadequate anti-coagulation (Williams and Van Riet, 2006).

The Prospective Randomised On-X Anti-coagulation Clinical Trial (PROACT) study was performed on high-risk profile patients all having had AVR procedures at thirty-six centres across the United States (Puskas *et al.,* 2012). Patients were randomised to either low dose Warfarin (INR 1.5–2.0) or to standard dose Warfarin (INR 2.0–3.0) for three months following mechanical AVR using the On-X valve. All patients received 81 mg of aspirin daily. The patients in low dose Warfarin had mean INR of 1.89 and the standard group, a mean of 2.50. The low dose group had significantly lower major and minor bleeding event rates and there were no significant differences between the two groups in terms of stroke, transient ischemic attack (TIA), or total neurological events. There was no significant difference in all-cause mortality between the low dose and standard dose groups. This report is expected to increase the use of new generation mechanical valves requiring a lower INR target. The FDA has approved an INR of 1.8 in On-X valves in the aortic position in lower risk patients however, in the higher risk patient aspirin (100 mg daily) has to be combined with Warfarin, also with an INR of 1.8 to 2.0 (Puskas *et al.,* 2014).

The AHA guidelines and recommendations for standard oral anti-coagulation therapy remains unchanged with a high target INR of 3.0–4.0 in patients with the first generation valves and an INR of between 2.5–3.5 for the newer generation valves (Nishimura *et al.,* 2014).

iv. Anti-platelet therapy

A meta-analysis Cochrane review (2013) stated that by adding antiplatelet therapy, either dipyridamole or low-dose aspirin (100 mg daily), to Warfarin decreased the risk of systemic embolism or death among patients with prosthetic heart valves (Massel and Little, 2013). Thirteen studies with a total of 4122 patients were included in this meta-analysis. The INR was safely reduced and patients were placed on fixed dose Warfarin (2.5 mg daily). The risk of major bleeding increased when target INR levels of 2.5 and greater were maintained. Compared with anti-coagulation alone, the addition of an anti-platelet agent reduced the risk of thrombo-embolic events [odds ratio (OR) 0.43, 95% confidence interval 0.32 to 0.59; $p < 0.00001$] and total mortality [OR 0.57, 95% CI 0.42 to 0.78; $p = 0.0004$]. The meta-analysis also showed that the effectiveness and safety of low-dose aspirin appeared to be similar to higher-dose aspirin.

In the only prospective randomised study performed, Aramedi *et al.,* (2005) compared compared the efficacy and safety of triflusal (an antiplatelet agent, it is a derivative from aspirin that inhibits cyclo-oxygenase but not completely) versus acenocoumarol for primary prevention of thromboembolism in the early postoperative period after implantation of a bioprosthesis. In this prospective, multicentric, randomized, open pilot trial, patients were assigned to treatment with triflusal (600mg/d) or acenocoumarol (target INR 2.0–3.0). The primary end-point was a composite of the rate of thromboembolism, severe hemorrhage and valve-related mortality. The author found that there were no significant differences in efficacy between both groups during the critical 3 months post implantation of the valve, however, triflusal showed a significantly lower incidence of bleeding episodes and a safer profile. The author also concluded that the use of anti-coagulation after aortic valve replacement in patients without co morbidities was no longer justified.

For patients with bio-prosthesis, Warfarin therapy is generally recommended during the first three months after implantation based on the rationale that endothelialisation of the valve sewing cuff may take several weeks to complete (Vahanian *et al*., 2007 and Bonow *et al*., 2006). However, several investigators (Jamieson *et al*., 2007 and Gherli *et al*., 2004) have questioned the relevance of this recommendation in patients with no thrombo-embolic risk factors, and according to a recent survey, 30% of centres use only aspirin during the first three months in these patients (Colli *et al*., 2008). After three months, Warfarin therapy is indicated in patients with a bio-prosthetic only if they have greater than one risk factor for thrombo-embolism. Using only aspirin to prevent thrombosis in bio-prosthetic aortic valves has been proven to be safe in the absence of compounding co-morbidities, such as atrial fibrillation and low cardiac output (Colli *et al*., 2007).

v. New generation anti-coagulants

Recently, new generations of anti-coagulation drugs have been approved by the FDA for the management and prevention of deep venous thrombosis (DVT) and pulmonary embolism (Van

Ryn *et al*., 2010). These drugs elicit their effect by either direct inhibition of thrombin (Dabigatran) or by binding to and deactivating of FX (Fundaparinux and Rivaroxiban) (Kaneko and Aranki, 2013). They offer an alternative to Warfarin in the prevention of strokes in patients with atrial fibrillation and in the prevention and management of DVT.

The advantages of these new generation drugs over Warfarin are (Forsberg *et al.,* 2014):

- half-life of twelve hours,
- no need for INR monitoring, indeed minimal monitoring is needed,
- fixed dosing is possible,
- less drug to drug interaction than with Warfarin and
- rapid clinical onset with a predictable dose response.

In an early feasibility study (Mc Kellar *et al*., 2011) a swine model was used to evaluate the safety of Dabigatran for thrombo-prophylaxis. Dibigatran showed similar efficacy to enoxaparin without adverse effects. However, in the RE-ALIGN trial, a large randomised control study in the Phase II trials, the safety and pharmacokinetics of oral Dabigatran etexilate in patients after heart valve replacement was evaluated (Eikelboom *et al*., 2013). The trial was terminated prematurely after enrolling 252 patients because of an excess of thrombo-embolic and bleeding events among patients in the Dabigatran group. Following this report, the FDA announced a statement to contraindicate the use of Dabigatran for mechanical heart valves (FDA, Safety Labelling Changes Approved by the FDA Centre for Drug Evaluation and Research; November, 2012).

This study was supported by the results published by Forsberg and De Sancho (2014). They reinforced the guidelines recommending against the use of Dabigatran in mechanical valve anti-coagulation due to higher thrombotic and bleeding events.

Currently, Dabigatran is contraindicated and should not be used as sole therapy in patients with mechanical valves.

vi. Summary

In the African context (and developing world) there is a growing population with large numbers of patients presenting with rheumatic fever and associated valvular pathology at an early age. Even in the developed world Warfarin therapy is challenging where access to medical expertise and pathology services for INR monitoring is readily available and this in a well-educated population. With the new generation valves the INR requirement has been lowered, reducing the risks of Warfarin substantially and rendering frequent INR measurements unnecessary as fixed dosing can be used. However, the prevalence of HIV in this young population is increasing in a poor socio-economic, uneducated environment with more patients on ARV therapy, making Warfarin dosing and management challenging. Therefore, there is a need for a durable valve that will negate the use of Warfarin.

2.4 The evaluation of mechanical heart valves for commercial use

2.4.1 Introduction

The *in vitro* testing of an MHV is a key element in the evaluation of the performance of the valve (Kuettinga *et al.,* 2014). The ISO 5840:2005 and FDA standards stipulate the specifics for the testing equipment and testing conditions, providing strict parameters to assess valve function.

2.4.2 Computational fluid dynamics (CFD)

i. Introduction

In the process of designing an MHV, the fluid dynamics of the valve has to be taken into consideration as it determines the durability of the valve and the thrombogenicity of the design prior to *in vivo* implantation. Imanparast *et al.* (2016) described how advanced computational tools will eventually give the engineer the ability to design a new MHV and assess the performance of the prototype in a virtual environment, utilising computerised models. As soon as they are developed and validated, these numerical tools will revolutionise current valve design and testing practices. These tools will be capable of predicting flow fields within the valve at a level of detail not currently possible by experiments alone. It will also be able to fully predict both the systolic and diastolic flow patterns within the valvular mechanisms, leading to substantial time and cost savings during the research and development phase. Each new prototype could be tested numerically prior to extensive and time-consuming *in vitro* and *in vivo* testing, thus accelerating the process of valve optimisation.

CFD is used to assess the valve design and the flow patterns occurring across valve components in a simulated numerical model, thereby predicting both the functional lifespan and the thrombosis risk of the valve design (Yoganathan *et al*., 2005). Software such as CFD-FloEFD (CFD software used in this study) solves the Navier-Stokes equations by iterate methods (Gross *et al.,* 1996*)*. This is however a theoretical and mathematical model, predicting the fluid-structural interaction (FSI) between blood and the valve components during a cardiac cycle.

Unfortunately CFD has its limitations due to the complexity of the mathematical model in a dynamic non-conformational environment. Not only is the blood flow unsteady at relatively high Reynolds numbers, but it also occurs within a complex geometry of the atrium and the ventricle (Chandaran *et al.,* 2006). The elasticity of the cardiac chambers and the vessel walls as well as the motion of the valve leaflets are complications that need to be taken into consideration mathematically and this is difficult to achieve (Yoganathan *et al.,* 2005 and Tangsley *et al.,* 1988).

CFD simulations provide a detailed description of the unsteady flow field across the surfaces exposed to the blood flow, including regions that are difficult to access experimentally, such as the hinge areas (Arefin and Morsi, 2014). Unfortunately the numerical simulation of the full

problem is beyond the routine capabilities of existing computational resources (Kamenski *et al.,* 2015, Seo *et al.,* 2014).

With the increase in computing power and the advances in parallel processing it is now possible to simulate the flow within MHV in a dynamic three-dimensional (3D) model during the entire cardiac cycle (Kamensky et al., 2015). The development of sophisticated CFD algorithms has also increased the accuracy of these 3D simulations (Arefin and Morsi, 2014) however, these simulations are complex, difficult to perform accurately and the computing resources required to perform the simulations are vast. Therefore, CFD models are routinely simplified. Some of the simplifications commonly employed include:

- two-dimensional (2D) simulations (Chandaran *et al.,* 2006),
- steady flow computations (Seo *et al.,* 2014),
- simplifications of the configuration (Seo *et al.,* 2014) and
- assuming fixed rather than moving valve components (King *et al.,* 1996).

In an effort to reduce computational resources, 2D calculations are used instead of 3D simulations. The required computational resources and simulation time are thereby considerably reduced however, 3D effects such as cross flows and spiral vortices that can only be appreciated when CFD is viewed in its entirety are excluded (Lei *et al.,* 1992). It does however include the main flow features such as the strong shear layers near the edges of the valve, the shedding of large-scale vortices downstream of the valve and the simultaneous creation of vortices during the deceleration phase of the physiological flow (Cheng *et al.,* 2004).

ii. Principles of computational fluid dynamics

According to Chanderan (2011) the dynamic simulation of mechanical heart valves can be divided into two main categories:

1. The first is the FEM (finite element method) structural analysis method in which the focus is the deformation pattern on the valve leaflets and the stress distribution on the surface of the valve. The author states that in these analyses the pressure exerted on the valves by the fluid at the appropriate surface of the leaflet is specified numerically within uniform boundary conditions within the valve structure. The simulation does however not involve the solution of the blood flow-dynamics past the valve prosthesis. The postulation that the pressure on the valve is a uniform pressure boundary condition ignores any variation in the pressure load as well as the effect of flow induced shear stresses on the valve leaflets resulting from 3D flow around the valve.

2. The second category of the dynamic simulations involves a detailed FSI analysis, which involves the dynamic interaction between the structural analysis of the valve apparatus and the fluid dynamic analysis of blood flow past the valve.

Prosthetic valves are geometrically complex and the shape and motion of their valve leaflets evolve dynamically in response to changing flow conditions. The pulsatile nature of the flow pattern generated during the cardiac cycle and the non-Newtonian fluid-surface interaction give rise to a very complex and highly unsteady borderline turbulent flow (Dasi *et al.,* 2009). Klusak *et al.* (2015) describes how the high Reynolds number flows (greater than 1000) experienced in MHV, especially in the aortic position is characterised by:

- regions of stagnation,
- high pressure areas before the valve,
- low pressure area with flow separation within the valve and
- flow recirculation and vortex shedding after the valve.

These complexities of FSI in a dynamic geometrically complex environment pose an enormous challenge in evaluating MHV's. The ideal will be to have a numerical method capable of quantitatively and accurately predicting the haemodynamics of a MHV and the FSI under physiological conditions prior to implantation. One of the challenges posed in performing a 3D, unsteady, full fluid-structure simulation is that of the moving fluid mesh domain. Kheradvar *et al.* (2015) solved this problem by implementing numerical solution techniques that can move the fluid mesh in an optimal way in order to maintain quality. Jasak and Tukovic (2010) performed topology changes on the valve surface using dynamic localised remeshing when the grid quality degraded in certain regions within the valve.

In 2007, the first fully validated, 3D resolved, large-scale flow field within a bi-leaflet valve was computed by Dasi *et al*. (2007). The authors used techniques that required the integrated use of complex FSI to model both the structural deformation and fluid interaction, by incorporating FEM with fluid flow using the finite volume method (FVM).

Research is currently moving to a multiscale approach where both the large-scale fluid mechanics (the bulk valvular flow field) and the small-scale fluid mechanics (such as the flow through the hinge region) can be resolved simultaneously (Mihalef *et al.,* 2011). It is likely that within the next five years it will be possible to capture the entire range of fluid mechanics on a multiscale level up to the cellular level in order to predict the mechanical loads on each individual blood cell that passes through the valve (Choi *et al*. 2014).

Kheradvar *et al.* (2015) proposed that it could be done by "coupling a 3D large-scale flow solver with a highly resolved small-scale solver deployed only in selected regions within the valve structure". In their model, the large-scale solver determines the equations for mass and momentum balance for both the fluid phase and solid phase at a large scale (several hundred blood cells in length). The small-scale solver uses a no continuum formulation of blood to resolve the effects of gaps in the fluid properties owing to the suspension of blood cells and platelets. Ding *et al.* (2006) proposes using the Lattice-Boltzmann formulation as the small-scale solver to

provide a means to assess fluid forces on individual blood cells and to obtain new insight into the interaction of blood and blood cells with the valve.

CFD rely on the discretisation of a body into finite elements and calculations are performed over each finite element. The solution for each of these elements is added to arrive at a solution for the entire body. Figure 2.53 below illustrates the differences between the Lattice-Boltzmann (a particle based formulation) and that of a typical mesh based formulation that solve the Navier-Stokes equations. The Navier-Stokes method has been employed routinely and have been validated in modelling blood flow across MHV in several recent studies (Borazjani et al., 2013 and Seo and Mittal, 2013).

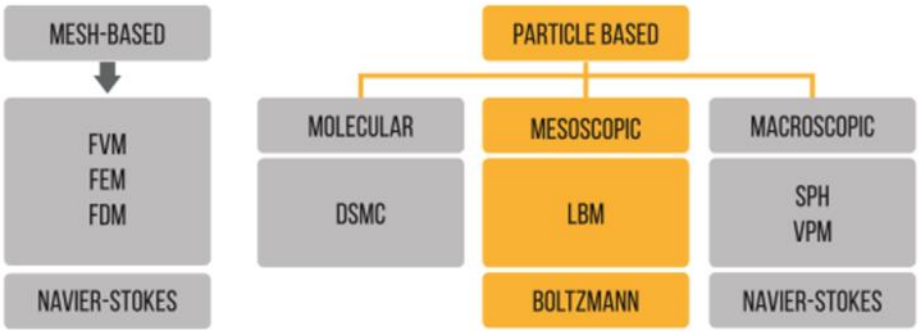

FIGURE 2.53: **The discretisation approach in fluid structure interaction.** FVM = Finite volume method; FEM = Finite element method; FDM = Finite difference method; LBM = Latice-Boltman method; DMSC = Direct Simulation Monte Carlo; SPH = Smooth particle hydrodynamics; VPM = Vortex particle method (Adapted from www.xflowcfd.com/technology/view/cfd)

The mesh based methods include the FEM, FVM and FDM (finite difference method) and are based on the Navier-Stokes equations. FVM equates the Cartesian mesh grid volumes (See Figure 3.5) by using the centre of each node block as a reference point and calculates the difference in the points in the adjacent blocks. With FEM the node points at the edges of the node blocks are used, and an integration function is then employed to get values within each node block. A partial differential equation employed by tying a weighted function to the differential is used to equate the shape function. As soon as all the node blocks are the same throughout (width and height are equal) the FVM becomes the FDM and becomes second order accurate. FEM is therefore employed to calculate structure interaction and FVM and FDM to measure fluid flow.

As mentioned earlier, previous studies have shown that high shear stress experienced within the valve encourages platelet activation and haemolysis and regions of low flow promote stagnation and thrombus formation. It is therefore important to analyse the flow fields through the valve at a cellular level by performing a Lagrangian analysis. It is the most widely used method in engineering for simulating FSI and is based on arbitrary Langrarian-Eulerian (ALE) formulations. Kheradvar *et al.* (2015) propose these ALE methods to solve FSI problems as they are extensions of conventional FEM that treat governing equations of conservation of

momentum along with coupling conditions and using disjoint, dynamically updated meshes for the fluid and structure regions. These methods are then able to provide sharp resolutions of velocities and stresses at the FSI and will be able to facilitate the construction of graded meshes that will be able to efficiently resolve fluid boundary layers. Eventually the simulation accuracy will be comparable with the experimental *in vivo* findings.

Dasi *et al.* (2009) reported on the flow environment experienced by blood cells as they transit through the valve. This FSI is what ultimately determines the rate of red blood cell lysis, platelet activation and deposition and the overall potential for thrombo-embolic complications. It is therefore necessary to recognise the exposure times to shear stresses or residence times within recirculation regions in order to predict the likelihood that a particular MHV may be prone to clinical complications.

According to Imanparast *et al.* (2016) Lagrangian-tracking methods can be used as a numerical approach to assess the transit of platelets and red blood cells through artificial heart valves. The trajectories of individual cells can be computed through direct numerical integration, based on the velocity fields computed by a highly resolved computational solver. The stresses experienced by these cells as they travel through critical areas in the valve, such as the hinge area, can be evaluated and can provide insights into platelet activation and haemolysis as well as transit times. The Lagrangian analysis can be used to assess the potential for cellular damage experienced within valve prototypes in the critical regions in an effective and economical manner. Therefore, a Lagrangian approach combined with a fully validated, accurate and efficient numerical solver, would eventually provide the necessary tool to identify the potential role of specific flow structures in inducing haemolysis, platelet activation and thrombosis.

The ideal model will be to form an integrated computerised numerical simulation incorporating complex flow-dynamics in an MHV with coagulation models. The numerical methods capable of quantitatively accurately predicting the haemodynamics of a prosthetic valve experience under physiological conditions have not been perfected yet. However, great progress has been made and the next ten years will validate most of the newer methods.

iii. Advances in computational fluid dynamics

The development of the ideal CFD model has resulted in some leading advances in computational fluid dynamics and will subsequently be discussed in brief. The 3D Navier-Stokes equations were solved by Shim and Chang (1994) using FEM to simulate laminar flow through a half open valve. Building on their success Kiris *et al.* (1997) employed a "finite volume, artificially compressibility method using overset grids to solve the Reynolds averaged Navier-Stokes equations with an algebraic mixing-length turbulence model".

This was followed by Ge *et al.* (2003) who carried out direct numerical simulations for a typical MHV in the open position without adopting simplifying geometry assumptions on fine grids. The authors illustrated the highly 3D structure of the flow through the valve and demonstrated the need for a highly resolved fully 3D simulation if CFD was to accurately predict the flow in MHV.

Chen and Chanderan (2003) reported on a simulation involving FSI to evaluate mechanical valves during closure. They employed 2D and 3D CFD to investigate the cavitation potential during the closing phase of a mechanical mitral valve using grids with 2048 nodes in 2D and 56,200 nodes in 3D. This process had limitations that Lai *et al*. (2002) sought to overcome using a grid of 9830 nodes in 2D, coupled with an ALE solver. They also investigated the effect of leaflet tip geometry on the pressure in the vicinity of the valve during closure. However, Rosenfeld *et al*. (2002) found that even in 2D, resolving the fine details of the flow near the leaflet required 80,000 nodes for grid-independent solutions.

To study the aortic root in 3D a model was developed by Nicosia *et al*. (2003) by using coupled fluid structure FEM. The authors could simulate the opening and closing of the aortic valve leaflets in the aortic root under physiological conditions in a completely unsteady analysis.

Dumont *et al.* (2007) were the first to perform a numerical study of bi-leaflet valves, combining FSI and 3D modelling successfully in order to compare haemodynamics with a validated algorithm. The authors could comparatively study the thrombogenic potential of MHV by computing the stress accumulated by platelets flowing through the valves.

Evaluating a prosthetic valve in the mitral position, because of the dynamic nature of the valve environment, makes CFD analysis difficult and unreliable. Therefore, some researchers have proposed simple generic geometries during simulations or have simplified the boundary conditions in their models (e.g., Arefin and Morsi, 2014; Seo *et al.,* 2014; Zheng *et al.,* 2014; Zheng *et al.,* 2012 and Cheng *et al.,* 2004). By combining CFD and medical imaging techniques, more realistic results have been obtained from LV models. One approach is to use the geometry parameters from medical imaging and impose a simplified deformation pattern based on electrical excitation to the computational field (Borazjani *et al.,* 2013 and Seo and Mittal, 2013). Brosjani *et al*. (2013) developed an "overset-curvilinear immersed boundary method in a general non-inertial frame of reference" to simulate a wide range of challenging biological flow problems

for the evaluation of MHV. The immersed boundary method avoids the grid generation difficulties associated with ALE methods but it yields a relatively low accuracy at fluid–solid interfaces. A complete 3D simulation therefore requires a high spatial resolution that necessitates the use of high performance computing resources (Kheradvar *et al.,* 2011).

A more advanced approach is to utilise either an ultrasound 2D generated cardiac simulation (Dahl *et al.,* 2012) or MRI derived data for a more realistic 3D cardiac model simulation (Mihalef *et al.,* 2011). By employing MRI data, Choi *et al.* (2014) were able to develop an immersed boundary method CFD to evaluate and study the flow structure interaction of bi-leaflet valves in the mitral position, which provided unique insights and data that are difficult to obtain from *in vivo* studies. The LV fluid dynamics and the function of its valves were studied by Imanparast et al. (2016). The author provided a simplified valve model with a simulated LV flow using 3D CFD, based on geometrical and deformational information obtained from MRI. Their model proved to be more accurate in predicting complex flows and patterns.

Kamensky *et al.* (2015) reported on their technique in which a geometrically flexible technique for computational FSI was developed based on the ALE. The technique was developed to simulate the function of a tri-leaflet mechanical valve during a complete cardiac cycle. Due to the complex motion of the valve leaflets, the fluid domain undergoes large deformations, including changes in topology. The method “directly analysed a spline-based surface representation of the structure by immersing it into a non-boundary-fitted discretisation of the surrounding fluid domain” and introduced the term “immerse-geometric analysis”. Applying this technique, the problem of large pressure differences generated across heart valves in a cylinder is overcome. The downside of the immersed boundary methods is that they do not accurately represent the shear stresses near the vascular wall since the flows near the wall are estimated.

iv. Particle image velocimetry

A new era of flow analysis was introduced with the use of digital particle image velocimetry (Digital-PIV). D-PIV is the equivalent of conventional laser speckle velocimetry and PIV techniques.

According to Hasler *et al.* (2016) PIV is an optical measurement flow and a flow visualisation technique through which the instantaneous velocity of seeded tracer particles is measured in fluids. The fluid is seeded with tracer particles that follow the flow-dynamics represented by the Stokes number. During the illumination of two short laser flashes in the measurement area, a double-exposure of the flow field is captured. The velocity vector of each frame is then extracted by performing mathematical correlation analysis on a cluster of particles within each region between the two frames. The motion of the particles is then used to calculate the speed and direction (the velocity field) of the flow being studied for example, the flow within an MHV. The area within the flow field in which the investigative measurements are taken is defined by the position and physical dimension of a fan of laser light.

Grigioni *et al.* (2004) employed laser techniques and digital-PIV to investigate the fluid dynamics of prosthetic valves. Digital PIV in its various forms, such as high speed PIV has substantially improved our understanding of fluid flows through valves. PIV is 2D based but Brucker *et al.* (1997) introduced stereo PIV based algorithms to study flows past MHV in two perpendicular planes simultaneously.

Another breakthrough was the development of defocussing digital particle image velocimetry (D-DPIV) by Pereira *et al.* (2000). In D-DPIV particle depth and velocity are determined by quantifying the natural blurring of the particles as they move out of the focal plane. The D-DPIV technique uses three cameras and identifies the image shift produced by the apertures to measure the depth of the particle from each camera. More recently, multiplanar PIV has been introduced to measure flows in 3D. Falahatpisheh *et al.* (2014) described a method where 2D two-component velocity fields were acquired on multiple perpendicular planes and reconstructed the images into a 3D velocity field through Kriging interpolation.

Although a lot of effort has been made in the development of the ideal computerised model, the search is far from over. As computing power increases and the understanding of 3D fluid-body interaction in a non-Newtonian fluid environment evolves, new simulation methods will be incorporated into the equations and algorithm of CFD thereby improving the predictive power of CFD.

2.4.3 Pulse duplication

Although findings from *in vitro* valve testing results cannot be expected to be identical to the *in vivo* performance of the valve, the results do provide a comparative model. Patient factors are removed and it allows for isolated valvular examination and evaluation under similar simulated cardiac conditions (Walker and Yoganathan, 1992). Therefore, hydrodynamic testing is an evaluation of MHV performance conducted under dynamic conditions in a controlled environment (Wheatley *et al.,* 2000, Fisher *et al.,* 1986).

According to the ISO 5840:2015 guidelines (Appendix E, section 9b) the *in vitro* evaluation of an aortic MHV only requires simulation of the systemic circulation, including the left atrium, LV and large arteries. The large arteries provide no resistance to flow and are considered as compliance elements. The drop in pressure across the smaller arteries is high and these arteries therefore contribute to the resistance. Blood is then routed back to the left atrium, which acts as the reservoir for the system. As a result, the systemic circulation can be represented by a reservoir (left atrium), a pump (LV), compliance elements (aorta) and a resistance element (peripheral resistance) (figure 2.54). A system comprising these elements and that is capable of reproducing the physiological flow characteristics, is referred to as a “pulse duplicator” (Fisher *et al.,* 1986).

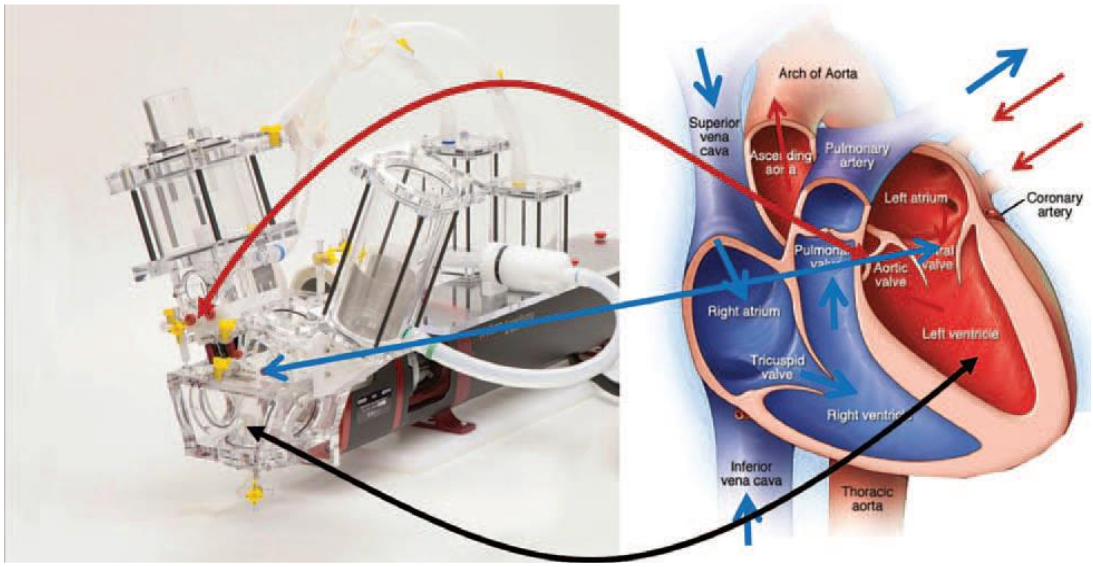

FIGURE 2.54: **The ViVitro system with a schematic representation of the heart.** (Adapted from www.vivitrolabs.com)

ISO 5840:2015 requires a pulse duplicator to have a valve chamber with the relevant dimensions to replicate the haemodynamic characteristics across the valve. The system must be capable of producing pressure and flow waveforms that simulate a range of physiological parameters, from a resting state to exercise. Pressure and flow measurements are the primary determinants of valve performance and the hydrodynamic performance is evaluated with respect to the following

parameters:

- stroke volume: the volume of fluid flowing through a valve in the forward direction during a cardiac cycle,
- regurgitation: the volume of fluid that flows through a valve in the reverse direction during one cycle. It is the sum of the closure volume and the leakage volume and is expressed as a percentage of the stroke volume,
- cardiac output: the mean flow through a valve per minute and
- mean systolic pressure difference: the average value of the pressure difference across the valve during the systolic or forward flow phase (ventricle pressure – aortic pressure).

The pulse duplication environment consists of simulated pulsatile cardiac flow in which the following control parameters are manipulated:

- heart rate,
- mean aortic pressure gradient,
- cardiac output,
- stroke volume and
- afterload.

Physiological and other complex flow variations can be simulated while the peripheral resistance and compliance of the system are manipulated. In accordance with the ISO 5480:2015 guidelines for the hydrodynamic assessment of heart valves (Appendix E, section 9b). the following hydrodynamic parameters should be calculated for any condition (Kuettinga *et al*., 2014):

- effective orifice area (EOA),
- Q_{rms} (forward flow),
- transvalvular pressure gradient,
- regurgitant volumes and
- trans-valvular energy losses.

The *in vitro* test results have to meet or exceed the minimum performance requirements provided in Table 2.6, which are given as a function of valve size, valve annulus diameter, and valve position (ISO 5840:2015). The minimum performance requirements correspond to the following pulsatile-flow conditions: bpm of 70 cycles/min, a simulated CO of 5.0 L/min, a mean aortic pressure of 100 mm Hg and a systolic duration of 35%.

TABLE 2.6: **Minimal performance requirements for pulse duplication evaluation (ISO 5840:2015).**

Position	Aorta							Mitral			
Valve size (TAD, mm)	19	21	23	25	27	29	31	25	27	29	31
EOA (cm^2)	>0.70	>0.85	>1.00	>1.20	>1.40	>1.60	>1.80	>1.20	>1.40	>1.60	>1.80
Regurgitant fraction (%)	<10	<10	<10	<10	<10	<10	<10	<10	<10	<10	<10

EOA = Effective orifice area in square centimeters; TAD = test valve annulus diameter; mm = millimeter

2.4.4 Animal experimentation

i. Introduction

Animal studies evaluating MHV have to comply with either the ISO 5480:2015 or FDA guidelines. The ISO 5480:2015 guideline was used in this study and an abbreviated version is attached as part of appendix E (See section 9b for *in vivo* trials). Following hereafter is a summary of the most important aspects regarding the *in vivo* evaluation of mechanical heart prosthesis from the ISO 5480:2015 guidelines. According to the ISO 5840:2015 guidelines the pre-clinical *in vivo* evaluation must:

1. Reflect the haemodynamic performance of the MHV as assessed *in vitro*
2. Provide an assessment of the surgical handling characteristics of the MHV and its accessories
3. Provide data to assess the biological reaction to the MHV. Consideration should be given, but not be limited to the following items, as relevant to the specific MHV under evaluation:
    - healing characteristics (pannus formation, tissue overgrowth),
    - haemolysis,
    - thrombus formation,
    - embolization,
    - foreign body reaction (inflammation, rejection),
    - calcification (flexible valves),
    - acoustic characteristics (rigid valves), if manufacturer claims are made on this issue,
    - structural deterioration and/or non-structural dysfunction and
    - cavitation.
4. Use a test heart valve substitute of clinical quality
5. Investigate MHV in all the positions for which it is intended (aortic and mitral)
6. Use the same surgical techniques for the implantation of both the test and the control MHV (for example, suture technique and orientation)
7. Be performed by appropriately experienced and knowledgeable test laboratories

Complications occurring after MHV implantation can be ascribed to the implanted valve as well as the environment it is implanted into, or the interaction between the two. Therefore, complications arising during or after valve implantation must be carefully analysed and interpreted in order to be able to accurately attribute the complication to the valve or the animal or a combination of the two.

The ISO8540:2015 guidelines state that implant animals must be of the same species and preferably of the same gender as well as of a similar age. The test MHV has to be assessed in a long term setting in all anatomical positions for which the valve is clinically intended. Animals suffering from heart valve substitute endocarditis may be excluded from the group of study animals, but the endocarditis event must be reported.

The guidelines state that the number of animals used for implantation of test and control heart valve substitutes must be fully justified for each test, based on the risk analysis. For long term studies, the duration of the observation period of the animals must be specified according to the parameter(s) under investigation. The observation period has to be appropriately justified in each study protocol, but be no less than ninety days. In each long term animal test case where a heart valve substitute has been implanted, a macroscopic and histological post-mortem examination shall be performed. Thus, the data shall include information from all animals that have been entered into the study. If serial blood analysis is performed, sampling shall be made pre-operatively, then one week post-operatively, then at appropriate intervals during the observation period as well as at termination.

The assessment shall provide at least the following:

1. Any macroscopically detectable pathological consequences (including but not limited to: thromboembolic phenomena, pannus formation, inflammatory reactions) around the heart valve substitute and/or in the major organs;
2. Any macro- or microscopically detectable structural alterations in the heart valve substitute (for example cavitation, macroscopic damage, material degeneration, deformation and calcification);
3. Histologic assessment of any thrombo-embolic material, inflammatory reactions and/or degenerative processes.

ii. Test report

The test facility has to compile an extensive test report, which has to include a summary assessment of the data generated during the course of the investigation. The test report must also include the complete study protocol. All the data generated from the preclinical *in vivo* evaluation must be incorporated into the comprehensive test report.

The test report must include the following:

1. Identification of each of the valves used for implantation (product, serial number and other appropriate valve identification);
2. Detailed description of the animal model used; the rationale and justification for its use. The pretest health assessment, including any medication given, of each animal must include documentation of the gender and age of the animal at implantation;
3. Description of the operative procedure, including suture technique, test valve substitute orientation, valve position and operative complications;

4. Description of the pre-operative and post-operative course of each animal including, clinical observations, medication and clinical condition leading to the prescription of each drug. If anti-coagulation therapy is used, monitoring data for this treatment - that is the international normalised ratio (INR) - must be included;
5. Any significant deviations from the protocol or amendments to the protocol;
6. Names of the investigators and their institutions along with information about the implanting surgeons and the laboratory experience with heart valve implantation and animal handling;
7. Interpretation of data and a recommendation relative to the clinical safety and performance of the heart valve substitute under investigation.

iii. The Ovine test model

Embarking on animal valve testing, the ovine model is thought to be an acceptable model for the *in vivo* evaluation of MHV and complies with the ISO 5840:2015 guidelines. According to Meuris *et al.* (2005) the ovine model is a good model for heart valve testing due to:

- the availability of the Dorper sheep
- the heightened coagulation response to foreign surfaces
- the favourable anatomy allowing for easy heart valve surgery
- their tolerance for cardiac surgery

For the *in vivo* evaluation of prosthetic heart valves and the evaluation of thrombosis resulting from mechanical prosthetic heart valves the sheep model is preferred (Yin et al., 2006 and Meuris et al., 2005). The sheep model also provides an ideal model for echocardiographic evaluation of cardiac valves and serves as an excellent calcification model (Meuris et al., 2005 and Ozaki et al., 2004).

In recent years, many research groups have demonstrated that the sheep model is ideal for the evaluation of prosthetic heart valves because of the ease of cardiac surgery and performance of endocardiographic studies (Meuris *et al.,* 2005; Tran *et al.,* 2000 and Wheatley *et al.,* 2000). Anaesthetic doses for sheep are similar to those for humans, and general anaesthesia is well tolerated without any respiratory complications after extubation (Wheatley *et al.,* 2000). Sheep also have a blood coagulation profile similar to that of humans (Tillman *et al.,* 1981 and Pelagalli, 2003), which was an important consideration with regard to the sheep platelet activity measurements. The resilience of the Dorper sheep to surgery is well documented and the post-operative care is minimal. Highly specialised holding facilities are unnecessary and their nutritional needs are easily met.

2.3 Summary of the literature review

i. Important principles of the history

Even though great advances have been made during the last four decades, the basic design of the mechanical heart valve has not changed. The material used in most, if not all of the 'modern' MHV replacements, is pyrolytic carbon and has been around since 1966. Efforts to improve on the materials used have been fruitless and even the older materials such as silicone and stainless steel have stood the test of time and is not inferior to the pyrolytic carbon.

The claims from companies such as On-X that they have improved on the carbon substrate to reduce thrombogenicity may be unsubstantiated as the entire valve design of the On-X valve has also changed. This may have an even greater impact on thrombosis than the materials used. Therefore, the valve design plays a more important role due to flow interaction with the surfaces exposed to the cellular components of blood. As the valve designs changed so did the flow characteristics and therefore the thrombogenic postential. A steady decline in Warfarin dosing requirement has been observed and thus lower anti-coagulation induced complications. Unfortunately, anti-coagulation is still a requirement currently and valves such as the tri-leaflet valve may be one step away from Warfarin therapy.

.

ii. Highlights of design, flow and coagulation

Valve design has a great impact on the valve performance and the thrombogenicity of the valve. The systolic flow across mechanical heart valves have been improved by principles gained from aeronautical and aerospace research as well as fluid dynamic advancements. These have led to modifications in valve designs which resulted in reduced fluid structure interaction and improved flow-dynamics. Near perfect laminar systolic flow is created and turbulence has largely been eliminated in the bi-leaflet valve design, reducing viscous shear stress induced platelet activation. By adhering to aerofoil principles the systolic flows have been perfected. However, thrombosis remains a major risk in MHV replacements.

The retrograde flow that is allowed across a valve during diastole (AVR) to prevent stasis within the valve mechanism (the hinges of the valve, the b-datum line and the gap created between the valve housing and the valve leaflets) have been identified as probably the most important cause of valvular thrombosis. The viscous shear stresses experienced in the valve hinge during this back flow phase is far greater than the threshold activation value for the activation of platelets and the cavitation created at high pressures damage cells and activate platelets. Therefore, inherent to the design of a bi-leaflet valve the washing jets have enhanced thrombosis and platelet activation in return for the reduction in stasis.

Stasis should not be a problem as the entire valve surface facing the aorta during diastole is in contact with stagnant blood, but this does not lead to thrombosus development. Therefore, by applying the principles of Virchow, the change in blood flow (flow acceleration through narrow gaps) and the secondary damage to the blood cells caused by these high velocity jets increase thrombosis.

The closing velocity of the valve leaflets causes a waterhammer effect, slamming onto the valve housing. This, in turn also causes cellular damage, not only resulting in haemolysis but also the initiation of thrombosis. With reference to the discussions in this paper as well as the literature review, the production of a valve that will negate most of the factors that are leading causes of thrombosis and all being well, will not need anti-coagulation, is possible.

iii. Literature review applied to the Glycar valve

The Glycar valve , a re-engineerd UCT valve, was developed as a prototype using principles set out in this literature review.. As was seen with the tri-leaflet mechanical valve, as soon as the systolic flows are laminar and the diastolic flow accelerations are eliminated, the thrombosis risk drops to the point where discontinuation of anti-coagulation can be considered. The shape of the poppet in the Glycar valve allows for laminar flow during systole. As the poppet seats flush against the housing during diastolic no 'washing jets' are created. Due to the closure mechanism of the sillcone poppet, the poppet seats softly onto the housing and absorbs impact energy. The waterhammer effect is eliminated and therefore no cellular damage and cavitation are observed. The materials used in the Glycar valve are biologically inert and as a result no blood interaction will take place.

In conclusion, the Glycar valve abides to the principles of blood flow and fluid structure interaction as discussed. The main causes of valvular thrombosis have been addressed and the valve modified accordingly. The next task will be to subject the prototype Glycar aortic valve to standard bench-mark testing as required by the ISO and FDA guidelines to evaluate the hydrodynamic properties of the valve, followed by *in vivo* testing to evaluate the coagulation potential of the valve.

CHAPTER 3

Methodology

3.1 Study location

Computer aided design (CAD) of the modified Glycar assembly was compiled by Mr G Jansen using 3D CAD software (Dassault Systèmes Solidworks Corp., Vélizy, France) at Southern Medical SA Pty Ltd, Pretoria, South Africa (ZA). (www.southmed.co.za).

The CFD analysis of the Glycar valve was performed in conjunction with Mr K du Plessis (senior engineering consultant), ESTEQ engineering, Pretoria, ZA. (www.esteq.co.za).

Stainless steel prototypes of the housing assemblies were manufactured by JHPE Pty Ltd (Jan Hugo Precision Engineering), Pretoria, ZA. (www.jhprecision.co.za).

The possibility of manufacturing the Glycar housing from titanium using direct metal laser sintering (3D printing) was explored. Glycar titanium valve assembly prototypes (designated: Ti6Al4V) were created using the EOSINT M280 system (Electro Optical Systems, Munich, Germany) at the Centre for rapid prototyping and manufacturing (CRPM), Central University of Technology (CUT), Bloemfontein, ZA. The engineer involved was Mr Gerrie Booysen, senior engineering consultant at CRPM. (www.cut.ac.za/crpm/).

Tensile strength testing on the prototype Glycar titanium housing was performed by Mr Johan Els at CRPM, CUT, Bloemfontein, ZA. (www.cut.ac.za/crpm/).

The initial pulse duplication on the Glycar valve was performed in conjunction with Mr Andrew Wasserman (senior engineering consultant) ESTEQ engineering, Pretoria, ZA to assess the valve design. The comprehensive pulse duplication analysis on the Glycar valve and the reference valves were performed in Bloemfontein using the ViVitro pulse duplicator (ViVitro Labs. Inc., British Columbia, Canada) at the department of Cardiothoracic surgery, Faculty of Health Sciences, University of the Free State (UFS), Bloemfontein, ZA. Mr Kyle Davis (engineer) and Mrs Liezl Thompson (perfusionist) were involved in the data acquisition and interpretation. (http://www.ufs.ac.za/health/departments-and-divisions/cardiothoracic-surgery-home)

The *in vivo* study was performed at the Centre for large animal experimentation, University of the Free State, Bloemfontein, ZA.

Intraoperative echocardiography was performed by Dr Edwin Turton from the department Anaesthetics, Faculty of health sciences, UFS, Bloemfontein, ZA.

Haematology, biochemistry and histology were performed by the National Health Laboratory service (NHLS), Bloemfontein, ZA.

Statistical analysis was performed by Mrs Sharon Rossouw, biostatistician at the department of Cardiothoracic surgery, UFS, Bloemfontein, ZA.

3.2 Study layout

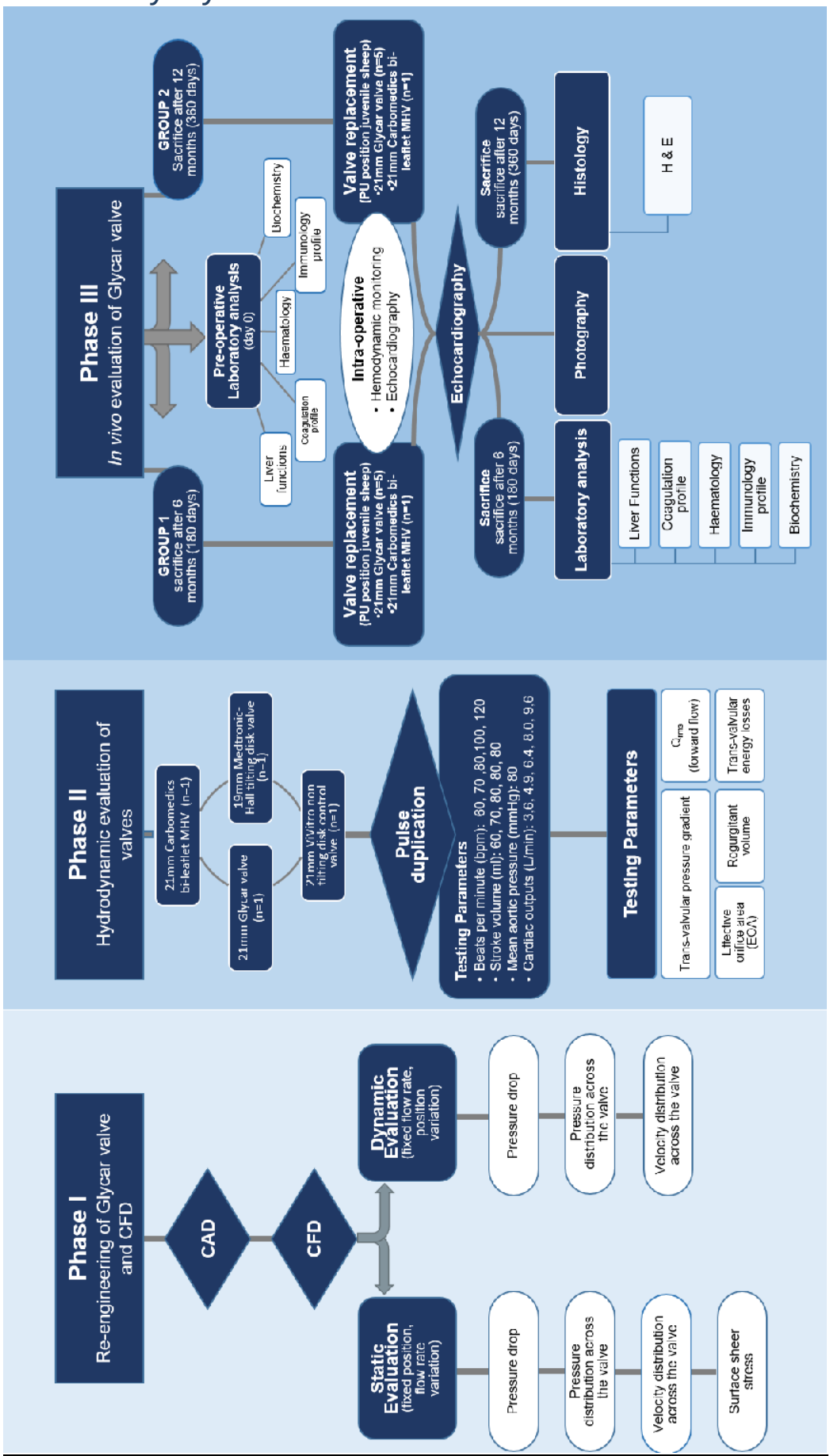

FIGURE 3.1: **Outline of the three phases in this study**

3.3 Study outline

3.3.1 Phase I: Re-engineering of the Glycar valve and CFD

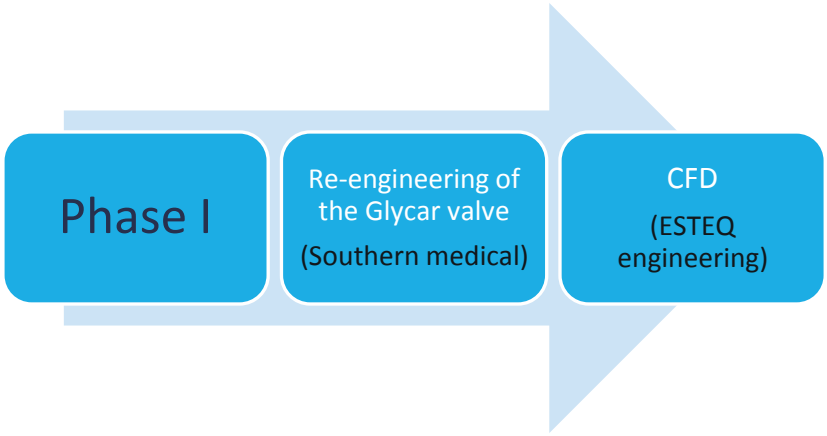

FIGURE 3.2: **Outline of phase I**

i. Re-engineering of the Glycar valve

The valve parameters of the original UCT valve recovered in Bloemfontein during explantation were assessed and modifications to the design were made according to the flow-dynamic principles (see section 2.2.3). A digital graphic rendering was made using 3D CAD software (Dassault Systèmes Solidworks Corp., Vélizy, France) at Southern Medical SA Pty Ltd, Pretoria, ZA. All the modifications were included in the design.

The prototype Glycar housing assembly and poppet were manufactured by JHPE (Jan Hugo Precision Engineering) Pty Ltd, Pretoria, South Africa, from a solid block of 316L stainless steel. The possibility of manufacturing the Glycar valve from titanium using DMLS (3D printing) was explored and tensile strength testing was performed on the titanium housing assembly. Although it was not part of this thesis the initial tensile strength testing results of the titanium prototype are presented in Appendix E.

ii. Computational fluid dynamic evaluation (CFD)

a. Analysis protocol

A CFD analysis was performed on the Glycar valve at ESTEQ, Pretoria, ZA, using FloEFD (Mentor Graphics Corporation, Wilsonville, Oregon, USA). FloEFD is a full-featured 3D CFD analysis solution built into major mechanical-CAD systems such as SolidWorks. The CAD assembly model of the Glycar prototype valve, supplied by Southern Medical Pty Ltd, Pretoria, ZA, was programmed into the simulation and the analysis performed.

The CFD analysis was separated into two parts, depending on the poppet position in the aortic valve position and the different phases of the systolic cycle were simulated:

- Firstly, the poppet was evaluated in the fully opened position (peak systole), varying the volumetric flow rates (static evaluation).
- Secondly, the poppet was evaluated by varying the poppet's location (dynamic evaluation) at a constant flow rate (simulating the systolic phase).

The following factors were determined:

- the pressure drop across the valve,
- the maximum flow velocity across the valve,
- the pressure distribution on the valve surface,
- the viscous shear stress on the valve surface and
- the velocity distribution contours across the valve.

General parameters and assumptions made as part of the analysis include:

- A surrounding atmospheric pressure of 101.325 kPa.,
- The fluid construct used was a blood based substitute, which is a non-Newtonian fluid.
- Internal flow was considered.
- The inlet temperature was 37°C, corresponding to the average human temperature.
- Steady-state conditions were analysed.
- Surface roughness was not taken into account as it is expected that roughness will have a relatively insignificant influence on the final results.

b. Valve geometry

The CAD generated of the Glycar valve assembly for the CFD analysis was supplied by Southern Medical. The valve geometry was then modified for the purpose of the CFD analysis and included the addition of an inlet and outlet section on the original valve assembly geometry supplied. The supplied geometry, with the cross-section of the artery, is shown in Figure 3.3.

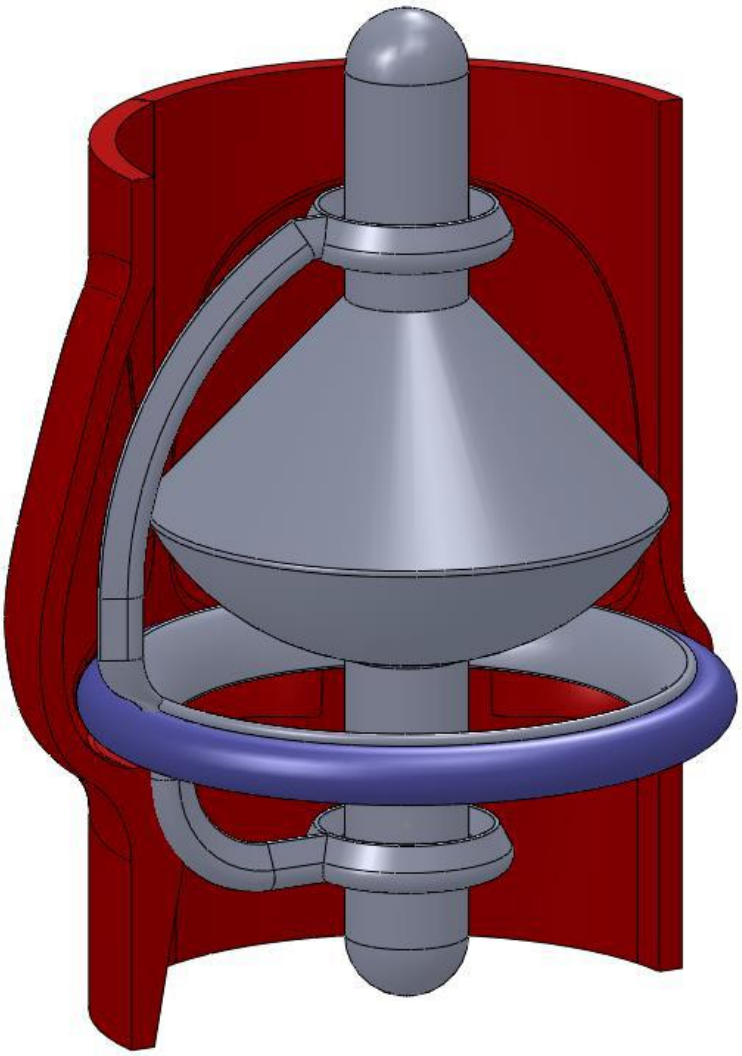

FIGURE 3.3: **Isometric view of the artificial heart valve geometry**

The computational area around the valve was analysed and the inlet and outlet “artery” section lengths were increased until they had no effect on the flow over the valve, that is flow recirculation at the outlet. The purpose of this was to find the smallest possible area in order to increase the mesh density around the critical components of the heart valve. The final geometry is illustrated in figure 3.4 with the inlet on the left and the outlet on the right. The diameter of the “artery” was approximately 22 mm.

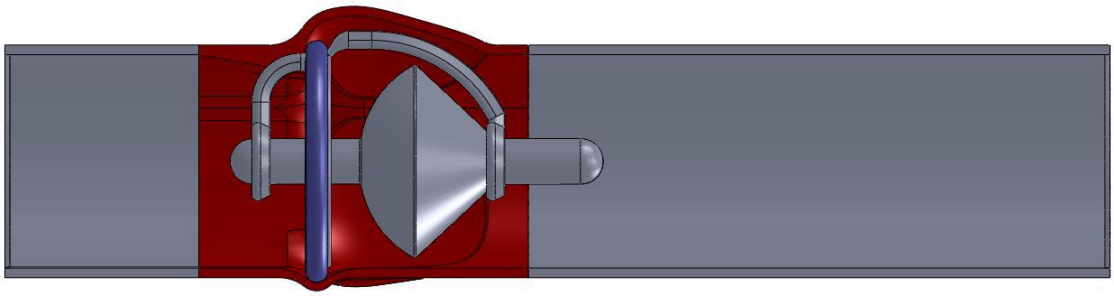

FIGURE 3.4: **Side view of the Glycar valve and the extent of the computational domain**

c. Computational grid

A cut-cell Cartesian mesh was used to discretise the computational domain. To illustrate this type of grid, the images of the fully opened position of the poppet are presented in figures 3.5 and 3.6. Once the domain size had been finalised, a base mesh was created throughout the domain, with two mesh refinement regions added to refine the base mesh in the areas of most importance. The first refinement was to capture the flow up and downstream of the valve and the second refinement was to capture the areas close to the valve. The cell length in the area of the first refinement is half that of the base mesh and the cell sizes in the second mesh refinement region are half that of the first refinement. These two regions are depicted in figure 3.6.

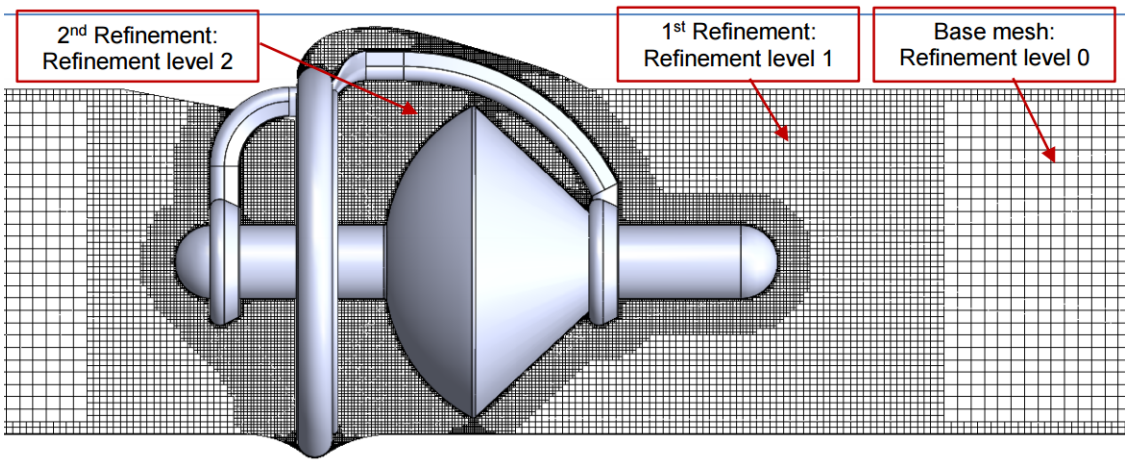

FIGURE 3.5: **Initial mesh refinement regions around the Glycar valve**

The finalisation of the mesh was done by refining the computational cells around the critical components such as the poppet and the frame. Narrow channels were also refined to ensure an adequate number of cells in these areas. Figure 3.6 illustrates one of the areas with the additional refinements on the valve geometry and in between any narrow channels. The final mesh contained a total of approximately 3,600,000 cells throughout the domain.

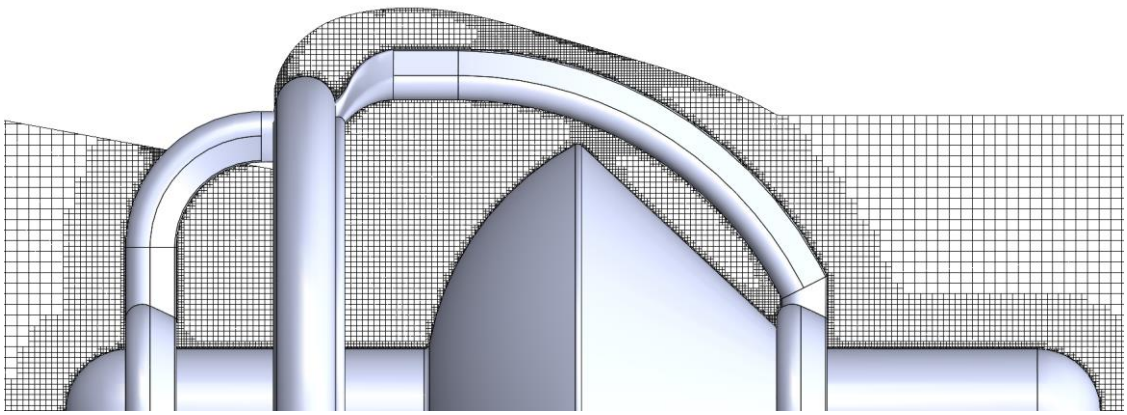

FIGURE 3.6: **Zoomed view of the final mesh with additional mesh refinements**

d. Boundary conditions and configuration

i. Part 1: Static evaluation (peak systole)

Part one of the analysis was performed with the poppet in the fully open position simulating peak systole, varying only the volumetric flow rates. The analysis is thus a static evaluation of the Glycar valve. The purpose of the different configurations was to simulate the range of flow rates to which the heart valve may be exposed. The boundary conditions and the different flow configurations of the first part of the analysis are summarised below in table 3.1. The configurations refer to the volumetric flow rate across the valve and these values are representative of an average male person (1.75 m, 80 kg). In addition, the static pressure (absolute pressure) set on the outlet is the blood pressure (gauge pressure) plus the atmospheric pressure. The pressure was not varied as this does not have an effect on the pressure drop and the flow patterns if the inlet volume flow rate is specified.

TABLE 3.1: **Boundary conditions and configurations for the first part of the CFD analysis**

Configuration	Volume flow rate		Static pressure	
	m^3/s	L/min	Pa	mmHg
1	0.0000275	1.65	117325	120
2	0.0000550	3.30	117325	120
3	0.0000825	4.95	117325	120
4	0.0001100	6.60	117325	120
5	0.0001375	8.25	117325	120

m^3/s = Cubic meters per second; L/min = liters per minute; Pa = Pascal; mmHg = millimeter mercury

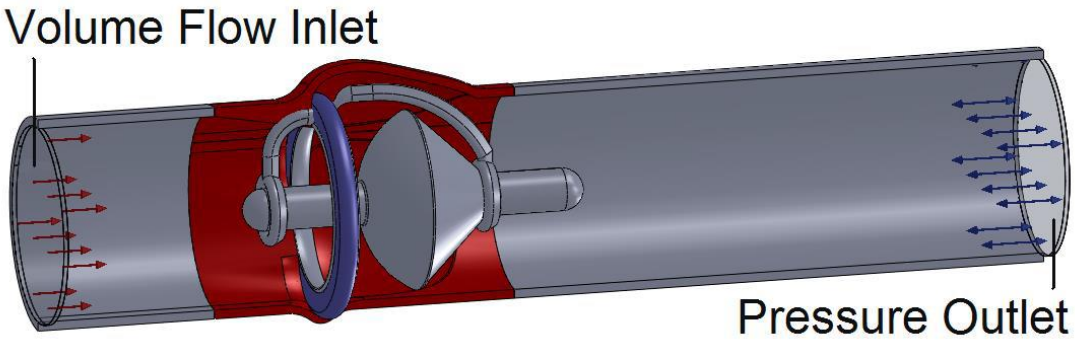

FIGURE 3.7: **Boundary conditions for the static evaluation**

ii. Part 2: Dynamic evaluation (systolic phase)

During the dynamic evaluation of the Glycar valve the poppet was evaluated by varying the poppet's location (simulating stages in the systolic phase) at a constant dynamic flow rate. Figure 3.8 illustrates the dimension used to configure the second part of the analysis. The volume flow rate used in this analysis was 0.0000825 m^3/s or 4.95 L/min and the pressure set on the outlet was 117325 Pa or 120 mmHg. The position of the poppet was determined by the distance between the poppet and the top of the housing. Figure 3.8 shows how the distance (X) is determined. Position 1 corresponded to a poppet to housing distance of 4 mm, position 2: 5 mm, position 3: 6 mm; position 4: 7 mm and position 5: 8mm (fully open position).

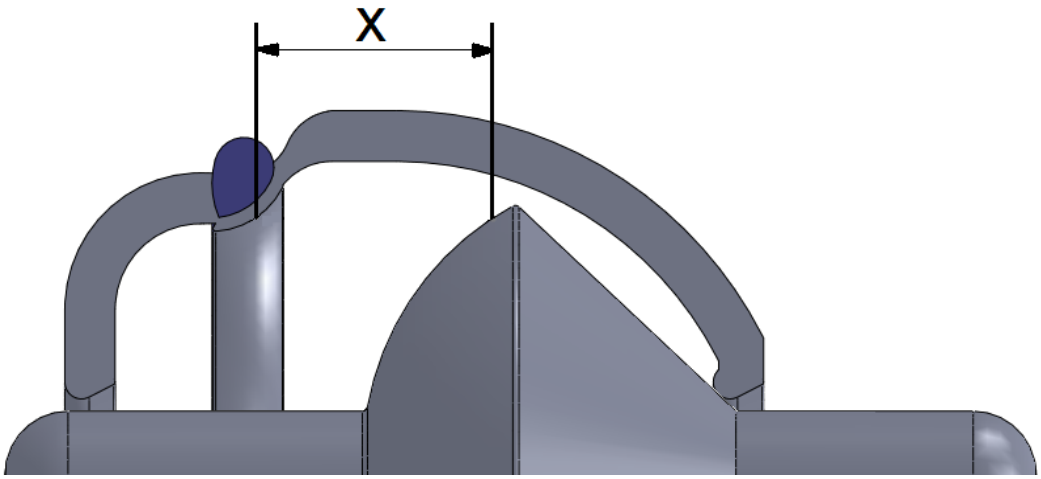

FIGURE 3.8: **Dimension of poppet position for the second part of the CFD analysis.** X denotes the distance variance between the poppet and the housing during systole.

e. Material properties

The properties of the blood used in the analysis are summarised in table 3.2. Blood is regarded as a non-Newtonian fluid, therefore the shear stress (τ) is not directly proportional to the velocity gradient or shear strain rate [$(\partial u)/\partial y$] through the viscosity (μ). Instead, blood as a non-Newtonian fluid follows a power-law function of the velocity gradient or shear strain rate since the effective viscosity is a function of the shear strain rate itself:

$$\mu_{eff} = f(\partial u/\partial y)$$

Consider the distinction explained below:
For a Newtonian fluid:

$$\tau = \mu\ (\partial u/\partial y)$$

Where μ is the dynamic viscosity [Pa.s] and $(\partial u/\partial y)$ is the shear strain rate.
For a non-Newtonian fluid:

$$\tau = K(\partial u/\ \partial y)^{n}$$

where K and n are constants described in table 3.2 below and the effective viscosity:

$$\mu_{eff} = (\partial u/\partial y)^{-1}$$

TABLE 3.2. **Properties of blood**

Viscosity	Power-Law model
Consistency coefficient, K (Pa.s)	0.01220
Power law index, n	0.79910
Minimum dynamic viscosity (Pa.s)	0.00304
Maximum dynamic viscosity (Pa.s)	0.01220
Density (kg/m^3)	1003.00

Pa.s = Pascal second; n = flow behaviour index (dimensionless); kg/m^3 = kilogram per cubic meter

f. Measurements

i. Part 1: Static evaluation (peak systole)

The following measurements and calculations are determined during the CFD analysis for the static poppet configuration. By applying the FloEFD software the following data on the Glycar valve was calculated/determined:

1. the pressure drop across the Glycar valve, calculated for each of the configurations during the static evaluation (parameters in table 3.1 applies),
2. the maximum flow velocity in meter per second across the valve for the same configurations as in I,
3. the pressure distribution across the valve and the pressure contours on the valve surface,
4. the viscous shear stress on the surface and the edges of the valve, the poppet and the housing. The areas on and around the valve surfaces where the peak shear viscous stress exceeds 20 Pa are identified and shown on a shear stress surface plot of the valve,
5. the velocity distribution contours, in order to identify areas of flow separation, stagnation, recirculation and turbulence,
6. a combination of the velocity cut plots and the surface viscous shear stress to determine the relationship between flow velocity and surface shear stress.

ii. Part 2: Dynamic evaluation (systolic phase)

The following measurements and calculations were determined during the dynamic CFD analysis of the Glycar valve. Five configurations were analysed at a constant flow rate, varying only the poppet's location. Position 1 corresponded to a poppet to housing distance of 4 mm, position 2: 5 mm, position 3: 6 mm; position 4: 7 mm and position 5: 8 mm. By applying the FloEFD software the following data on the Glycar valve was calculated/determined:

1. the minimum and maximum static pressures and the pressure drops for each of the poppet positions,
2. the maximum flow velocity for each of the poppet positions,
3. the pressure distribution on the poppet surface for each of the poppet positions,
4. the velocity contours during the systolic phase with the poppet in different positions,
5. the position of the poppet with the lowest transvalvular flow velocity across the valve.

3.3.2 Phase II study: Hydrodynamic evaluation of the Glycar valve

i. Introduction

The hydrodynamic evaluation of the Glycar valve and the comparison between the Glycar valve and commercially available heart valves as well as the ViVitro control valve was performed during this phase of the study. Pulse duplication was performed using the ViVitro pulse duplicator (ViVitro Labs Inc., British Columbia, Canada). Due to the bulky design of the Glycar valve it is not intended for use in the mitral valve position therefore all the simulations were performed in the aortic valve position only.

*This part of the study was performed in collaboration with Mrs L Thompson-Jooste as part of her Master of Health Sciences in Clinical Technology, at the Central University of the Freestate, Bloemfontein; submission date 2017. The title of the thesis: "**Comparison of heart flow dynamic assesment between echocardiography and pulse duplication**". The focus of her dissertation was to compare the pulse duplication findings between the tested valves to the echocardiography derived findings. The pulse duplication data acquired for the valves were used in this dissertation to assess the overall comparative functioning of the Glycar valve. Data between the Glycar valve and the Carbomedics bi-leaflet valve were subsequently analysed and is relevant to this thesis.*

A comparative hydrodynamic *in vitro* evaluation (pulse duplication) was performed on the re-engineered Glycar valve and the results were compared to the pulse duplication results from the following valves:

- 21 mm Carbomedics bi-leaflet valve (Sorin medical)
- 21 mm Perimount tissue valve (Edwards Life sciences Corp.)
- 19 mm Medtronic-Hall tilting disc valve (Medtronic medical)
  (Only a 19 mm tilting disc valve could be procured as the valves are not produced any more)
- 21 mm ViVitro non tilting disc valve (ViVitro Labs Inc.)

The parameters that were analysed during the simulation:

- The total forward flow volume (Q_{rms})
- The EOA
- The transvalvular pressure drop
- The regurgitant fraction (RF)
- The transvalvular energy losses

The valves were tested under five different physiological conditions and is summarised in table 3.3. Once the data had been obtained a comparative analysis between the Glycar valve and the Carbomedics bi-leaflet was performed. As these were the valves used in the *in vivo* evaluation a detailed analysis was warranted.

Table 3.3: Testing conditions used during pulse duplication

Measurement point	Mean Aortic pressure (mmHg)	Beats per minute	Stroke volume (ml)	Cardiac output (L/min)
1. Resting state	80	60	60	3.6
2. Minimal effort	80	70	70	4.9
3. Moderate effort	80	80	80	6.4
4. Exercise	80	100	80	8.0
5. High intencity sustained effort	80	120	80	9.6

mmHg = millimeter mercury; ml = milliliter; L/min = liter per minute

ii. The pulse duplicator

The ViVitro pulse duplicator (ViVitro Labs Inc., British Columbia, Canada) (figure 3.10) combined with the ViVitest Data Acquisition System (ViVitro Labs Inc.) were used during the evaluation of the test valves. This system is validated and meets ISO 5840:2015 requirements for the evaluation of cardiovascular implants. The system comprises of (figure 3.9):

- a left ventricle,
- aortic valve,
- silicone aorta,
- aortic flow sensor,
- impedance chamber,
- resistance chamber,
- compliance chamber and
- mitral valve.

A pump using a linear actuator to control the ventricular pressure was used. The valve test chambers in this setup simulated the geometry of the left ventricle and aorta in an attempt to simulate realistic physiological flow (ISO 5840:2015). The test method was performed according to the standard operating procedures as published by ViVitro (manual).

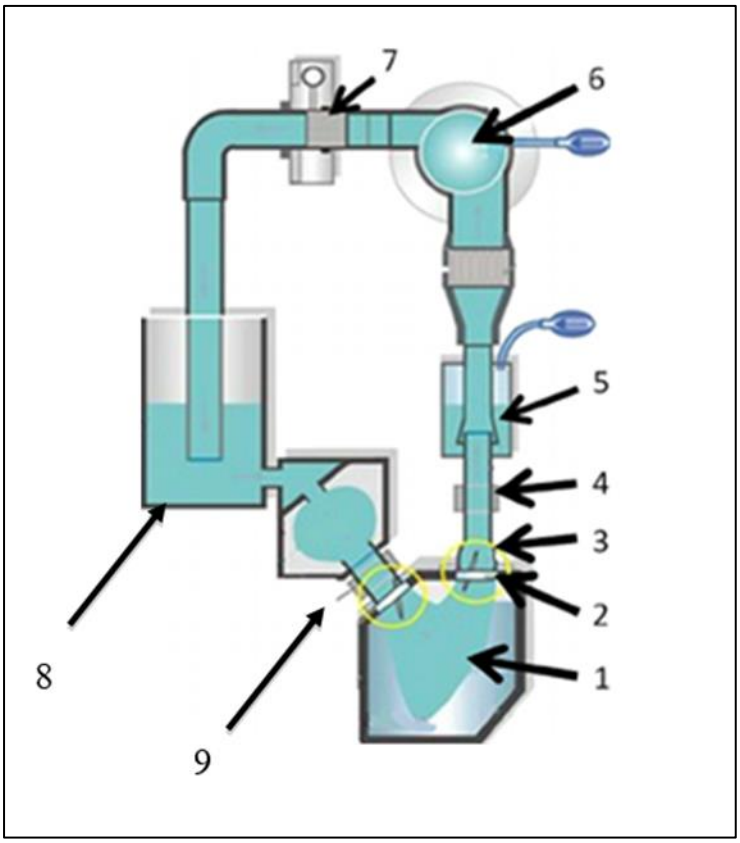

FIGURE 3.9: **Schematic depiction of the pulse duplicator assembly.** (1) Ventricle, (2) aortic valve position, (3) silicone aorta, (4) aortic flow sensor, (5) impedance chamber, (6) impedance, (7) resistance, (8) compliance chamber, (9) mitral valve position (Adapted from https://www.researchgate.net/Figure/259981007)

FIGURE 3.10: **The ViVitro pulse duplicator** (Adapted from www.vivitrolabs.com)

iii. Summary of testing method

All five of the heart valves were evaluated in the aortic position. ViVitro medical supplies a control valve which is a non-tilting disk valve that was used during the calibration of the system and was used as a reference valve during all of the simulations. The pressure drops obtained during the analysis of the ViVitro valve were compared to the manufacturer's reference values for quality assurance.

The mean pressure gradients were measured using pressure transducers placed in the ventricle chamber and at the outflow tract distal to the aortic valve. Additional data that were collected included the volumetric flow rate across the valve, closing volume and leakage volume during the deceleration phase.

A compression retainer and sealing ring were used to house the test valve and to eliminate regurgitation due to possible para-valvular leaks. A 45% by weight aqueous glycerine solution was added to the saline solution to create a viscosity of 3.5 centipoise (cps) as a blood analogue (ISO 5840:2015), heated to a physiological temperature of 37^{o}C.

Measurement parameters used in this test are summarised in table 3.3 and were utilised to simulate five characteristic physiological flow conditions for each of the five valves. The mean systolic pressure difference was maintained at 80 mmHg and the stroke volume, pump beats (beats per minute) and cardiac output were varied.

The pressure transducers were calibrated statically and the calibration factors were stored in the data acquisition system. The ViVitro pulse duplicator was calibrated by a ViVitro technician prior to use. The pump was then used to calibrate the electromagnetic flow meter by oscillating a column of fluid in the aortic chamber and verifying the electromagnetic flow meter results with that of the pump. The zero position of the flow and pressure signals were set immediately prior to the measurements being taken to minimise drift.

The pump velocity waveform, stroke volume and rate were set by adjusting the programmable waveform generator (table 3.3) and the mean aortic pressure set to 80 mmHg by adjusting the afterload. As soon as the flow conditions were stable, the acquisition programme was run and data captured for 10 cycles per test condition.

The pulse duplicator takes 256 measurements (referred to as samples) per cycle measured over 10 cardiac cycles (referred to as cycles only). Measurements began at the start of systole or during the forward pump phase.

Pressures were measured throughout the cycle at set points as outlined in ISO 5840:2015 and included the atrial pressure, ventricle pressure and aortic pressure, all in mmHg. The following were recorded simultaneously and calculated based on flow and pressure data acquired with the ViVitest Data Acquisition System:

- Q_{rms}
- EOA
- Pressure drop
- RF
- Transvalvular energy losses

The flow/pressure/volume graphs as represented in figure 3.10 were generated.

iv. Calculating the total forward flow volume (Q_{rms})

The average waveform was calculated for each signal in the test series for each of the valves. After acquiring the physiological parameters the Q_{rms} was determined according to the ISO 5840 guidelines. The Q_{rms} and pressure difference was measured during the interval shown in figure 3.11. The time interval starts as soon as the ventricular pressure crosses the aortic pressure line (t_1) during the upstroke and ends when the ventricular pressure crosses the aortic pressure line at the down stroke (t_2). The Q_{rms} is calculated by squaring the volumetric flow rate measurements and using trapezoidal numerical integration to calculate the integral during the interval where the ventricular pressure is larger than the aortic pressure. The integral is then divided by the same time interval and the square root is calculated to obtain the Q_{rms}. The equation is defined as (Kuettinga *et al.*, 2014):

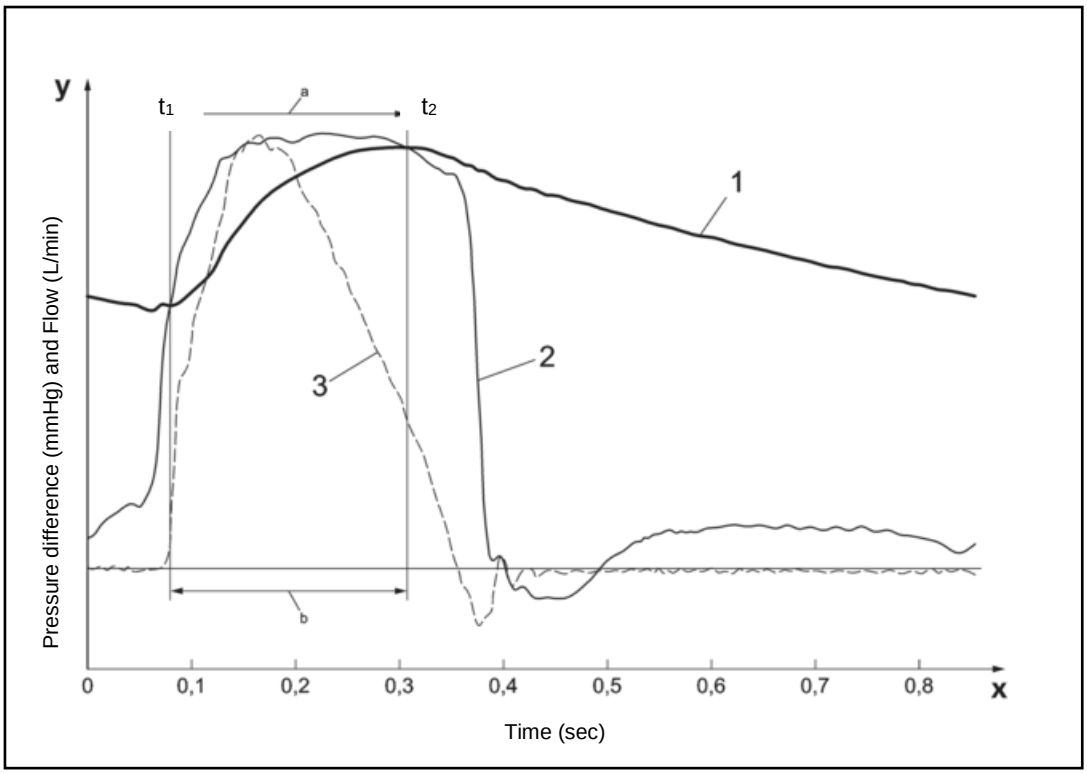

FIGURE 3.11: **Schematic representation of the positive pressure period of an aortic forward flow interval**. Line 1 represents the aortic pressure, line 2 the pressure generated in the left ventricle and line 3 the aortic flow rate (Adapted from Kuettinga *et al.*, 2014 and ISO 5840:2015).

$$Q_{rms} = \sqrt{\frac{\int_{t2}^{t1} q_v(t)^2 dt}{t_{2-} t_1}}$$

The equation defines Q_{rms} where:

- Q_{rms} is the root square forward flow during the possitive differential pressure period in ml/s
- $q_v(t)$ is the instantaneous volumetric flow at time t
- t_1 is the time at the start of the positive differential pressure period
- t_2 is the time at the end of the positive differential period

v. Calculating the effective orifice area (EOA)

The EOA was determined using only the volumetric flow rate and pressure difference during the positive pressure interval of the forward flow phase, until the ventricular pressure dropped under the aortic pressure during systole (Figure 3.9) as per ISO definition (Kuettinga *et al*., 2014):

$$EOA = \frac{Qrms}{51.6\sqrt{\Delta p/\rho}}$$

This equation defines EOA [cm^2], where:

- Q_{rms} (ml/s) is the forward flow volume during the positive transvalvular pressure period,
- Δp (mmHg) is the mean pressure difference during the positive transvalvular pressure drop period and
- ρ (g/cm^3) is the fluid density

vi. Calculating the pressure drop (∆p)

To determine the pressure drop across the valve the following were employed (figure 3.12 to 3.14). From the 256 sample values acquired during the cardiac cycle the pressure generated in the ventricle (figure 3.12) and the pressure in the aorta (figure 3.11) were charted and the difference between the two pressure graphs was generated to produce the graph in figure 3.14. Using the graph in figure 3.14, the point at which the trans-aortic pressure (ventricle – aortic pressures) became positive was used as the starting point (point 1 in the graph) and ended as

soon as the pressure dropped below zero (point 2 in the graph). This was employed in all of the twenty-five tests (five valves at five test conditions – table 3.3) in this study. The pressure was then averaged over this interval using trapezoidal numerical integration.

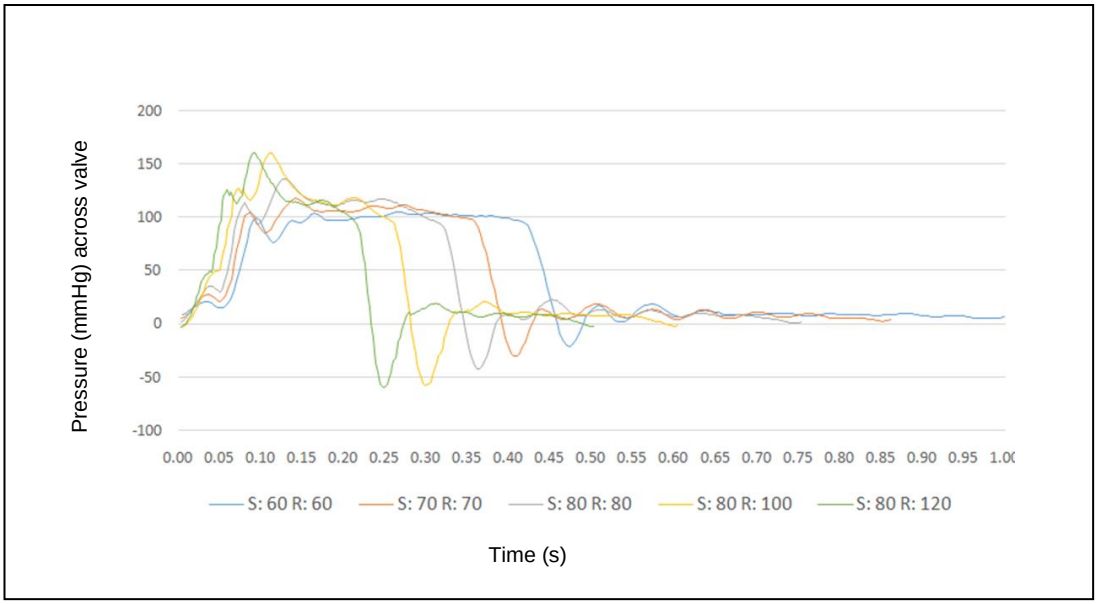

FIGURE 3.12: **The pressure generated across the bi-leaflet valve during a cardiac cycle in the five test conditions**. S = stroke volume in ml; R = rate in bpm

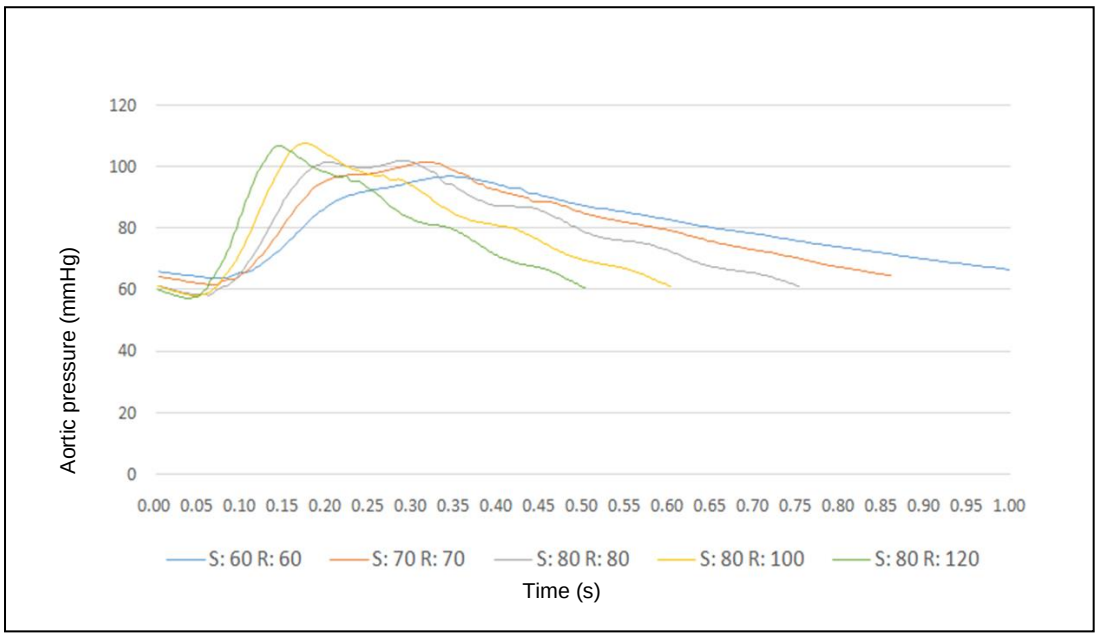

FIGURE 3.13: **The pressure generated on the aortic side of the bi-leaflet valve during the five test conditions.** S = stroke volume in ml; R = rate in bpm

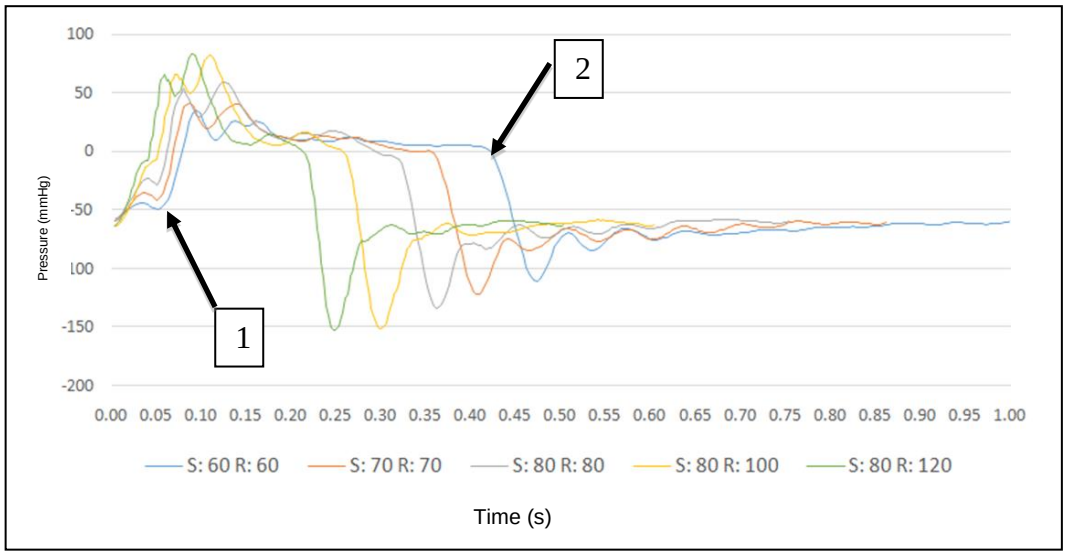

FIGURE 3.14**: The difference between the pressure generated across the valve (figure 3.13) and the pressure generated in the aorta (figure 3.13).** The pressure gradient or drop is determined between points 1 and 2. S = stroke volume in ml; R = rate in bpm

vii. Calculating the regurgitant fraction (RF)

The RF was determined according to the ISO 5840:2015 guidelines, which detail the differentiation between closure and leakage volume. The total regurgitation volume is made up of both the closure and the leakage volume. The volumetric change across the valve is measured over the cardiac cycle and plotted against time on a graph (figure 3.15).

Using this graph the regurgitant fraction is calculated. The closing volume (1) and the leakage volume (2) are determined once the volumetric rate drops below the zero reference point. The amount of regurgitation was analysed in volume and in percentage of the total stroke volume. The closing volumes of the different valves as well as the regurgitation or leakage volumes for each of the set parameters (table 3.3) were then determined.

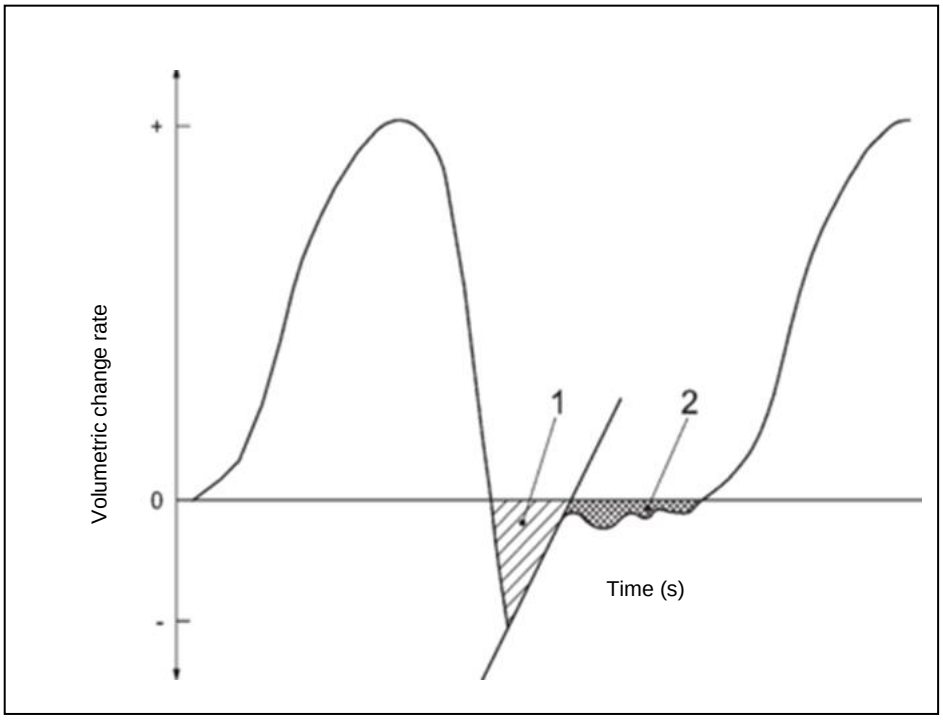

FIGURE 3.15: **The flow wave form and regurgitant volumes for one cardiac cycle**. Using this graph the regurgitant fraction is calculated. The closing volume (1) and the leakage volume (2) is determined once the volumetric rate drops below the zero reference point (Adapted from Kuettinga *et al.,* 2014 and ISO 5840:2015).

viii. Calculating the transvalvular energy losses

The transvalvular energy is an important value to calculate as it can highlight potential inefficiencies in the valve. The energy is typically divided into three types: forward energy loss, closing energy and leakage energy. The energy loss is a function of the flow rate and transvalvular pressure drop and is given by the formulas (Kuettinga *et al*., 2014):

Forward Energy (FE) (mj):

$$FE = \text{Conversion factor} * \int_{F1}^{F2} \Delta P * \text{flow}\left(\frac{ml}{s}\right) * dt$$

Closing Energy (CE) (mj):

$$CE = \text{Conversion factor} * \int_{F2}^{F3} \Delta P * \text{flow}\left(\frac{ml}{s}\right) * dt$$

Leakage Energy (LE) (mj):

$$LE = \text{Conversion factor} * \int_{F3}^{F4} \Delta P * \text{flow}\left(\frac{ml}{s}\right) * dt$$

The equation defines transvalvular energy loss where:

- *dt in the integral implies that the equation ΔP*flow is integrated with respect to time
- F1 – is the point when the flow rate becomes positive at the beginning of systole (not the pressure drop)
- F2 – is the point where the flow rate becomes negative again at the end of systole
- F3 – is the point when the valve closes and leakage flow begins
- F4 – is the point at the end of the cycle/leakage flow
- Δ P is the pressure drop across the valve in mmHg
- Flow dt is the change in time

Energy loss is calculated by integrating the flow times with the transvalvular pressure over a relevant flow interval. A conversion factor/constant 0.1333 is applied to convert the energy from mmHg*ml to millijoule (mJ). When calculating the Q_{rms}, one looks at the region at the time when the pressure drop across the valve (ventricle - aortic) is positive. One then takes the same time period and integrate the flow rate according to the formula for Q_{rms}.

The energy loss is therefore dependant on both the pressure drop and flow rate, where a significant increase in either can result in significant losses. During the cardiac cycle, energy is expended to pump blood throughout the body. Some of this energy is lost by overcoming the resistance of the valve, by overcoming the resistance of the valve occluder during forward flow, by overcoming the inertia of the occluder to close the valve and lastly loss of forward kinetic energy due to regurgitant back flow. By examining the energy loss, the potential long term impact of the stress of the heart can be envisaged.

ix. Comparative analysis between the Carbomedics bi-leaflet valve and the Perimount tissue valve

Once the data for all five valves had been collected and the data comparison and analysis completed, the data for the Carbomedics and the Glycar valves were extracted. As these were the two valves used in the *in vivo* evaluation, they were compared separately. The pressure drop was compared between the two valves, as well as the Q_{rms}, the closing volume and the regurgitation volume.

x. Validating the pulse duplicator data

Performing pulse duplication is notoriously difficult with varying levels of accuracy in the findings. In an effort to validate the findings of this study and to verify the accuracy of the data, two methods were utilised. Firstly, the ViVitro reference valve was used as a control valve and secondly a literature comparison was made by using two studies in which the ViVitro pulse duplication system was used to evaluate prosthetic heart valves.

a. ViVitro reference valve

ViVitro medical supplies a control valve that is used during the calibration of the ViVitro pulse duplication system by a certified ViVitro technician. This is a non-tilting disk valve and is not meant for human implantation. During the evaluation of the prosthetic valves the ViVitro valve was also used as part of the analysis and the pressure drop obtained from the ViVitro valve in the aortic position was compared to the ViVitro reference values (manual).

b. Literature comparison

To guarantee further quality assurance in pulse duplication setup for the development of the Glycar valve, a literature comparison was applied. Nobili *et al.* (2008) tested an SJM Haemodynamic plus 27 mm mechanical bi-leaflet valve and compared the valve with numerical simulations. The valve was tested with an MCS-VSI (ViVitro Systems Inc.) pulse duplicator. The valve was tested at a cardiac output of 4.5 L/min at 72 bpm, equating to a stroke volume (SV) of 62.5 ml at a mean arterial pressure of 100 mmHg. The pressure drop obtained across the valve in the study was used as a reference point. By simulating the test conditions in the Nobili study, the results generated for the Carbomedics bi-leaflet valve's simulation was compared to the findings in the publication. The maximum pressure drop across the valves was compared.

A second literature comparison was performed. Piatti *et al.* (2015) performed a numerical and experimental comparison on a 19 mm tri-leaflet polymeric heart valve. The experimental tests were performed on a ViVitro pulse duplicator at 70 bpm and a CO of 5.6 L/min. The data generated for the Perimount tissue valve (tri-leaflet valve) in the study were compared to the author's findings. The EOA was determined for both valves and a comparison was made to the CO. An EOA vs CO graph was generated for both valves and compared. A third order polynomial trend line was plotted to fit the experimental data of the study's tissue valve measured in the pulse duplicator.

3.4.3 Phase III: The *in vivo* evaluation of the Glycar valve

i. Introduction

Part III of study involved the evaluation of the *in vivo* performance of the Glycar valve in the ovine model. The incidence of thrombosis of the Glycar valve and a commercially available bi-leaflet (Carbomedics) valve was compared, in the absence of anti-coagulation therapy.

Twelve (n=12) juvenile wether Dorper sheep were used and surgery was performed at the age of six months. At six months the sheep weighed between 35 to 40 kg, large enough to allow for the implantation of the 21 mm Glycar valve. The study was divided into two groups depending on the follow-up interval post-operatively. Group one was sacrificed six months (180 days) after implantation and group two sacrificed after one year (365 days). Each group consisted of six Dorper sheep. One received a mechanical Carbomedics bi-leaflet valve as the control valve and the other five Dorper sheep received the Glycar valve. All of the valves were implanted in the pulmonary valve position. Haemodynamic parameters were acquired during surgery, prior to CPB initiation for a baseline. After implantation of the valves, once the CPB had been stopped, haemodynamic stability was reached in the absence of inotropic support. Haemodynamic evaluation of the valves was performed intra-operatively, prior to sacrifice. Echocardiographic evaluation was performed on all of the implanted valves after the surgery and the valves were reassessed prior to sacrifice. Blood analysis was performed during the follow-up interval at regular interludes according to the protocol and involved biochemistry, haematology, immunology and liver enzyme analysis.

At sacrifice the valves were carefully dissected and photographed to evaluate the components of the valve. Histology was performed on the sewing cuff and the areas of healing to determine healing on the sewing cuff as well as possible platelet deposition.

ii. Laboratory analysis

Blood samples were drawn from the external jugular vein at the following intervals:

- Pre-operatively
- Day 0, 1, 7, 14, 30, 90, 180 and 360 (only for group two) post-operatively

All blood analyses were performed by the National Health Laboratory Service (NHLS), University of the Free State, Bloemfontein, according to their standard operating procedures (SOP's). Table 3.4 summarises the investigations carried out.

Table 3.4: **Data collection for blood and laboratory investigations**

Post-operative Days	0	1	7	14	30	90	180	360
Biochemistry								
Urea (mmol/l)								
Creatinine (mmol/l)								
Sodium (mmol/l)								
Potassium (mmol/l)								
Liver functions								
Albumin (g/l)								
AST (U/l)								
ALT (U/l)								
ALP (U/l)								
GGT (U/l)								
LD (U/l)								
Bili (µmol/l)								
Immunology profile								
CRP (mg/l)								
IgG (g/l)								
IgA (g/l)								
IgM (g/l)								
Coagulation profile								
PT (sec)								
PTT (sec)								
INR								
Haematology								
White cells (x 10^9/l)								
Hb (g/dl)								
Haematocrit (l/l)								
Platelets (x10^9/l)								
Neutrophil (x 10^9/l)								
ESR (mm/h)								
RPI								
Haptoglobin (g/l)								

AST= Aspartate aminotransferase; ALT= Alanine transaminase; ALP= Alkaline phosphatase; GGT= Gamma glutamyl transferase; LD= Lactate dehydrogenase; Bili= Bilirubin; CRP= C Reactive Protein; IgG= Immunoglobulin G; IGA= Immunoglobulin A; IGM= Immunoglobulin M; PT= Prothrombin time; PTT= Partial thromboplastin time; INR= International normalised ratio; HB= Haemoglobin; ESR= Erythrocyte sedimentation rate; RPI= Red cell production index; sec= seconds; mm/h= millimeter per hour; mmol/l= millmole per liter; g/l= gram per liter; U/l= units per liter; g/dl= gram per deciliter; mg/l= milligram per liter.

iii. Echocardiographic evaluation

Trans-oesophageal and epicardial echocardiography were performed before the valves were implanted to acquire a baseline reference. The heart sonar was repeated once the valve was successfully implanted and cardiopulmonary bypass stopped. The sheep had to be haemodynamically stable with no inotropic support. All of the sonars were performed by an echocardiography certified anaesthetist using a Philips CX 50 portable general imaging ultrasound machine (Philips, Eindhoven, Netherlands) and a Philips S5-1 broadband sector array transducer.

At the planned sacrifice echocardiography was performed once the thoracic cavity was exposed to allow for unobstructed epicardial echocardiography. Table 3.5 summarises the data that were captured in each. Refer to appendix A for the sonography protocol.

Table 3.5: **Data capture sheet for the *in vivo* echocardiographic evaluation**

Glycar study *in vivo* echocardiographic data	
Sheep number:	
Date:	
Valve type:	
Time period:	☐$_1$ Pre-operation ☐$_2$ Intra-operative valve surgery ☐$_3$ Pre-sacrifice
Left ventricle function:	☐$_1$ Normal ☐$_2$ Mild impairment ☐$_3$ Moderate impairment ☐$_4$ Severe impairment
Right ventricle function:	☐$_1$ Normal ☐$_2$ Mild impairment ☐$_3$ Moderate impairment ☐$_4$ Severe impairment
Pulmonary valve:	
Regurgitation: - central/ eccentric:	
VC:	
Regurgitation Doppler signal density:	
Velocities over valve – V max (ms^{-1}): VTI	
Velocities over valve – V mean (ms^{-1}): VTI	
Gradients over valve – P max (mmHg):	
Gradients over valve – mean (mmHg):	
Velocities in RVOT – V max (ms^{-1}): VTI	
Velocities in RVOT – V mean (ms^{-1}): VTI	
Gradients in RVOT – P max (mmHg):	
Gradients in RVOT – P mean (mmHg):	
EOA:	
Poppet valve: excursion of poppet:	☐$_1$ Normal ☐$_2$ Abnormal
Pannus:	☐$_1$ Absent ☐$_2$ Present ☐$_3$ Impending on valve
Thrombus:	☐$_1$ Absent ☐$_2$ Present ☐$_3$ Impending on valve

ms^{-1}= meter per second; VC= vena contracta; VTI= velocity time integral; mmHg= millimeter mercury; RVOT= right ventricle outflow tract; V max= maximum velocity; V mean= mean velocity; P max= maximum gradient; P mean= mean gradient

The following parameters were mathematically deduced from the acquired data and the recommendations for the evaluation of mechanical heart valves with echocardiography as described by Zoghibi *et al.,* (2009) were applied:

- Peak trans valvular velocity (ms^{-1})
- Gradient across the valve (pressure loss across the valve) (mmHg)
- EOA (cm^2)
- Pressure half time
- Regurgitation

The poppet and valve leaflets were evaluated and the flow pattern across the valves was scrutinised.

iv. Haemodynamic data

Table 3.6 summarises the haemodynamic data parameters that were monitored during valvular implantation. The measurements were taken prior to CPB of the native valve and repeated once the valve was replaced. The same measurements were taken at sacrifice and the values compared to assess the gradient across the valve and to monitor the gradient across the valve after the follow-up interval.

TABLE 3.7: **Data capture sheet for the haemodynamic data.**

Valve type:												
Pressure measurement	Ao sys	Ao diast	Ao mean	CVP sys	CVP diast	CVP mean	RVOT sys	RVOT diast	RVOT mean	MPA sys	MPA diast	MPA mean
Pre-bypass												
Post-bypass												
Pre-sacrifice												

Ao= aorta; sys= systole; diast= diastole; CVP= central venous pressure; RVOT= right ventricular outflow tract; MPA= main pulmonary artery. All values were measured in mmHg.

v. Surgical procedure

All the animals were evaluated by a qualified veterinary surgeon, to determine their fitness for surgery and to rule out any medical problems that might influence surgical outcome of each. All the test animals were starved from the night before surgery, allowing free access to water. Pre-anaesthesia was administered two hours prior to surgery. The sheep were managed in the right decubitus position. The neck and the left thorax were shaved to clear wool from the surgical sites. A 14 French CVP catheter was placed in the left external jugular vein, the relevant blood specimens were drawn (see blood tests) prior to induction. The sheep were then anaesthetised using Thiopentone sodium (Pfizer Pty. Ltd.)(4-5 mg/kg) intravenous induction in combination with Morphine sulphate (0.1 mg/kg) and Atropine (0.01 – 0.03 mg/kg). The sheep were intubated by either the veterinarian or a qualified medical practitioner and then transferred to the cardiac theatre where the surgical team, consisting of an anaesthetist, a cardiothoracic surgeon and a senior perfusionist (all of whom have experience in large animal experimentation) performed the surgery.

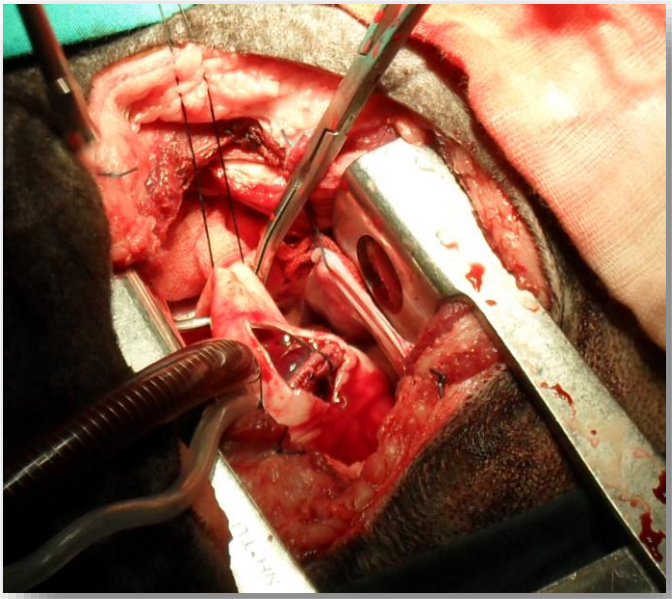

FIGURE 3.16: T**he Glycar valve in the pulmonary position prior to MPA closure**. The guiding strut was positioned anteriorly, following the natural curve of the MPA.

A longitudinal incision of approximately 3 cm was made posterior to the left external jugular vein midway in the neck. The platysma was split and the left jugular vein mobilised and retracted anteriorly. The carotid sheath was identified as well as the vagus nerve running in close proximity of the carotid artery. Taking care not to injure the vagus, the carotid was mobilised and a sling was placed around the artery. Haemodynamic monitoring was achieved by arterial cannulation of the distal carotid artery under direct vision. A baseline pressure was attained before ligation

of the carotid artery. The carotid artery was ligated and a stump pressure was attained. Surgery proceeded when the stump pressure decline was less than 20% of the baseline mean, ensuring cerebral perfusion. Heparin (5mg/kg) was administered prior to ligation of the carotid artery once an activated clotting time of 480 s. was achieved. The proximal carotid artery was cannulated with a DLP arterial canula (Medtronic medical) for cardiopulmonary bypass (CPB) (Dagum *et al*., 1999).

A left thoracotomy was performed and the fourth rib removed. The pericardium was opened anterior/ventral to the phrenic nerve. The main pulmonary artery and its branches were isolated and dissected free. Haemodynamic pressures in the cardiac chambers were acquired as well as in the main pulmonary artery. The right atrium was cannulated and CPB initiated. Normothermia was maintained and no cardioplegia was administered; the surgery was performed on a beating heart.

The main pulmonary artery was opened and the native pulmonary valve leaflets excised. The Glycar valve was sutured into the pulmonary annulus with a continuous 4.0 prolene suture (Ethicon Inc., Somerville, New Jersey, USA). Figure 3.17 denotes the Glycar valve in the pulmonary artery. Note the strut position during implantation. To avoid contact between the strut and the native pulmonary artery a redundant pericardial patch (Glycar S.A., Southern medical, Johannesburg, ZA) was sutured into the pulmonary arteriotomy. The end result can be appreciated in figure 3.17. The heart was de-aired routinely and the pulmonary incision closed.

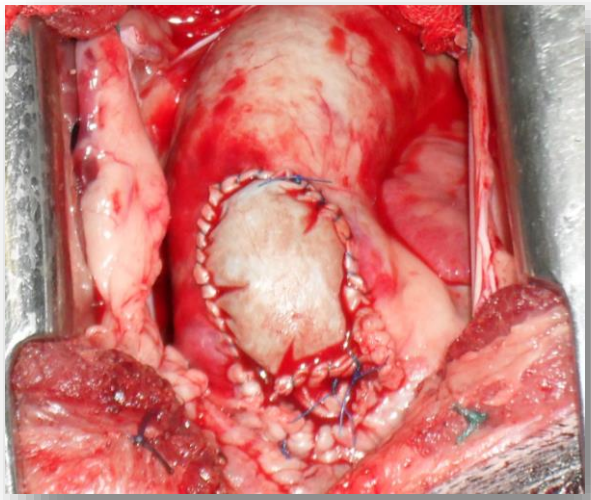

FIGURE 3.17: **The pericardial patch in the native pulmonary artery**. The dome created by the patch prevents contact between the valve strut and the arterial wall, thereby avoiding arterial wall injury and an iatrogenic cause for thrombus formation.

CPB was weaned and stopped, all cannulae removed and all incisions routinely closed using standard surgical techniques. Protamine sulphate (1 mg Protamine for every 1 mg Heparin

administered) was then administered intravenously to counter-act the Heparin sulphate. After zeroing the transducer at the height of the right atrium, a needle was placed into the following chambers and the following haemodynamic values/pressures recorded:

- Right atrial pressure (mmHg)
- RVOT (mmHg)
- MPA pressure (mmHg)
- Pressure difference between MPA and RVOT (mmHg)
- Aorta/arterial pressure (mmHg)

The diastolic, systolic and mean arterial pressures in mmHg and heart rate (bpm) were measured. Epicardial echocardiography was performed (Echo Protocol, Appendix A) prior to wound closure. The intercostal spaces around the wound were infiltrated with Marcaine (0.5%) for pain relief. Cell-saving (XTRA auto transfusion system, Sorin medical, Mirandola, Italy) was performed during all procedures to contain blood loss to the minimum. An underwater drain was inserted to prevent blood from pooling in the thoracic cavity post-operatively and removed once bleeding ceased.

All surgical procedures were performed under strict sterile operative conditions with laminar air flow. Cefazolin (25mg/kg) was administered intravenously during induction, midway through the surgery and during wound closure.

vi. Post-operative care

At completion of the surgery, anaesthetic drugs were halted and the animals kept in the theatre in an ICU environment until they were haemodynamically stable. They were nursed in an upright position in a specialised sling and were extubated two to four hours post-operatively as soon as they were awake and breathing on their own. They were then transferred to a holding facility next to the theatre as soon as it was deemed safe. In the holding facility the patient was placed with a companion sheep overnight to help alleviate stress. By the third day, most of the animals were transferred to the animal unit on the West campus where they were cared for with the rest of the flock, for the remaining six to twelve months.

An opioid analgesic (Morphine 0.1 mg/kg) was administered intra-muscularly twice daily for three days post-operatively in combination with an antibiotic (Depomycin 5 mg daily intra-muscularly). At the West campus holding facility blood was drawn according to protocol (table 3.5) from the left external jugular vein and the patient sheep were evaluated during the venepuncture for any signs of cardiac failure, neurological signs or respiratory problems.

vii. Sacrifice

Prior to sacrifice all the sheep were clinically assessed for any signs of cardiac failure, gross neurological deficits or pulmonary pathology. Thereafter, the sheep were anaesthetised and trans-oesophageal and epicardial echocardiography performed (Appendix A). The sheep in group one were sacrificed six months after the date of implantation and the sheep from group two were sacrificed one year after the date of implantation.

a. Sacrifice anaesthetic protocol

The sheep were fasted for twenty-four hours however, they had free access to water in order to facilitate trans-oesophageal echocardiography and to reduce the risk of aspiration.

The sheep were anaesthetised using Thiopentone (4-5 mg/kg) through intravenous induction, standard intra-operative monitoring was connected and the sheep were intubated. The sheep were managed in the right decubitus position and the neck and left thorax shaved to clear the surgical sites.

A 14 French central venous pressure (CVP) catheter/line was placed in the left external jugular vein and the relevant bloods drawn (see blood investigations), prior to induction. Heparin was administered until an activated clotting time (ACT) of 480 s was reached. After the surgery was completed potassium chloride 4.5 g was administered intravenously as a bolus to induce ventricular fibrillation whereupon the sheep were exsanguinated.

b. Excision surgery protocol

A left lateral thoracotomy was performed over the previous incision wound. The second to fourth ribs were resected and the sternal rib adhesions removed. The sternum was also resected as needed to allow for unobstructed epicardial echocardiography of the heart. The adhesions on the heart were carefully mobilised. Epicardial echocardiography was performed as well as trans-oesophageal echocardiography according to the echo protocol (Appendix A).

Haemodynamic data were obtained: After zeroing the transducer at the height of the right atrium, a needle was placed into the following chambers and the relevant pressures recorded:

- Right atrial pressure (mmHg)
- RVOT pressure (mmHg)
- MPA pressure (mmHg)
- MPA and RVOT pressure difference (mmHg)
- Aortic/arterial pressure (mmHg)

The diastolic, systolic and mean arterial pressures in mmHg and heart rate (bpm) were measured. Heparin 3 mg/kg was given intravenously. The inferior vena cava was transected after a lethal dose of potassium chloride was administered and the subject was exsanguinated.

The pulmonary valve was dissected en-bloc from the heart, taking care not to disturb any clots that may have formed on the valve or sewing ring. The right ventricular side was approached first. The excess ventricular muscle was cautiously removed right up to the sewing cuff area. Any abnormalities were noted and photographs of the pathology were taken. Following, the pulmonary artery was opened on the posterior aspect opposite the pericardial patch.

The valve was inspected for any macroscopic clots in the following areas:

- pericardial patch, proximal and distal to the valve and the sewing ring
- sewing ring and pulmonary annulus junction
- proximal and distal junction between the sewing cuff and the pulmonary artery
- around the housing and the struts
- the guide openings proximal and distal on the valve
- the poppet

The pericardial patch was inspected for any signs of strut contact with the patch or the pulmonary artery. The sewing cuff was inspected for any pannus overgrowth.

Tissue was taken from the lungs, kidneys, spleen and liver to search for and investgate possible thrombo-emboli. Both lungs were removed and inspected for any visible macroscopic abnormalities. Sections of 1 cm were cut into the lungs and inspected for infarctions and emboli. Any suspicious lung lesions were sampled and placed into formalin and evaluated histologically for thrombo-emboli. On completion of the evaluation the sheep were sent for incineration.

viii. Valve photography

The following steps were taken to prepare the surgically removed valve for photography:

- Any excess tissue around the annulus and the pulmonary artery was removed, taking care not to disturb any clots or artefacts that may have formed in and around the valve.
- The valve was gently rinsed in saline, not water, as this will injure and remove platelets from the valve and sewing cuff.
- The valve was carefully placed on the photography table and prepared for photography.
- The following areas of interest were included in the photos:
    - Pericardial patch, proximal and distal to the valve and sewing cuff
    - The sewing ring and annulus junction
    - The proximal and distal junction between the sewing ring and the pulmonary artery
    - The stainless steel housing and the struts
    - The guide openings in the struts
    - The poppet

- The pericardial patch and pulmonary tissue were removed for histology. A section of the sewing cuff was removed to allow for a side view of the sewing cuff and valve housing and this was repeated with the pericardial patch-sewing cuff junction. Photos of these views were also taken.

After photography the valve was placed in formalin for further processing and evaluation. It is important to note that these photos are for visual display only and is used for comparative purposes and visualisation of pathology.

ix. Histological evaluation

The NHLS evaluated the haematoxylin and eosin stains (H&E) according to their SOP's. H&E were performed after surgical excision of the valve (Appendix C).

a. Specimens for histology:

- The pulmonary valve is removed en-bloc from the heart and the tissue carefully removed from the RVOT up to the sewing cuff, taking care not to dislodge any clot or thrombus that may have formed on or around the valve.
- The valve was carefully rinsed with 0.9 % saline solution.
- Any abnormalities on the proximal side of the valve were noted and photographs of this area were taken.
- The pulmonary artery was now dissected and a sliver of the native pulmonary artery and the Glycar patch was taken for analysis.
- A part of the sewing cuff of the Glycar valve bordering the pericardial patch was removed and also placed in formalin.
- Any clot or thrombus was removed from the struts after the valve was photographed according to protocol, and placed in formalin.
- A sliver of tissue containing the junction between the pericardial patch and the sewing cuff and a sliver of tissue containing native pulmonary artery and sewing cuff were taken.
- Cut sections were made through the lungs at 1 cm intervals evaluating the lung for possible pulmonary emboli. Specimens of any suspicious lesions were taken and analysed.

b. The pathologist reported on the following questions posed (figure 3.18):

- Sewing cuff:
  - Were there cellular infiltration of the sewing cuff and if there were, which cells are they?
  - Was the sewing cuff covered with pannus or epithelium?
  - Were there platelets adhered to the cuff?
  - Were there signs of thrombus on the cuff?
  - Were there signs of infective endocarditis?
- Thrombus: Is this only organised clot or are there signs of infection?
- Lung: Any signs of pulmonary embolism?

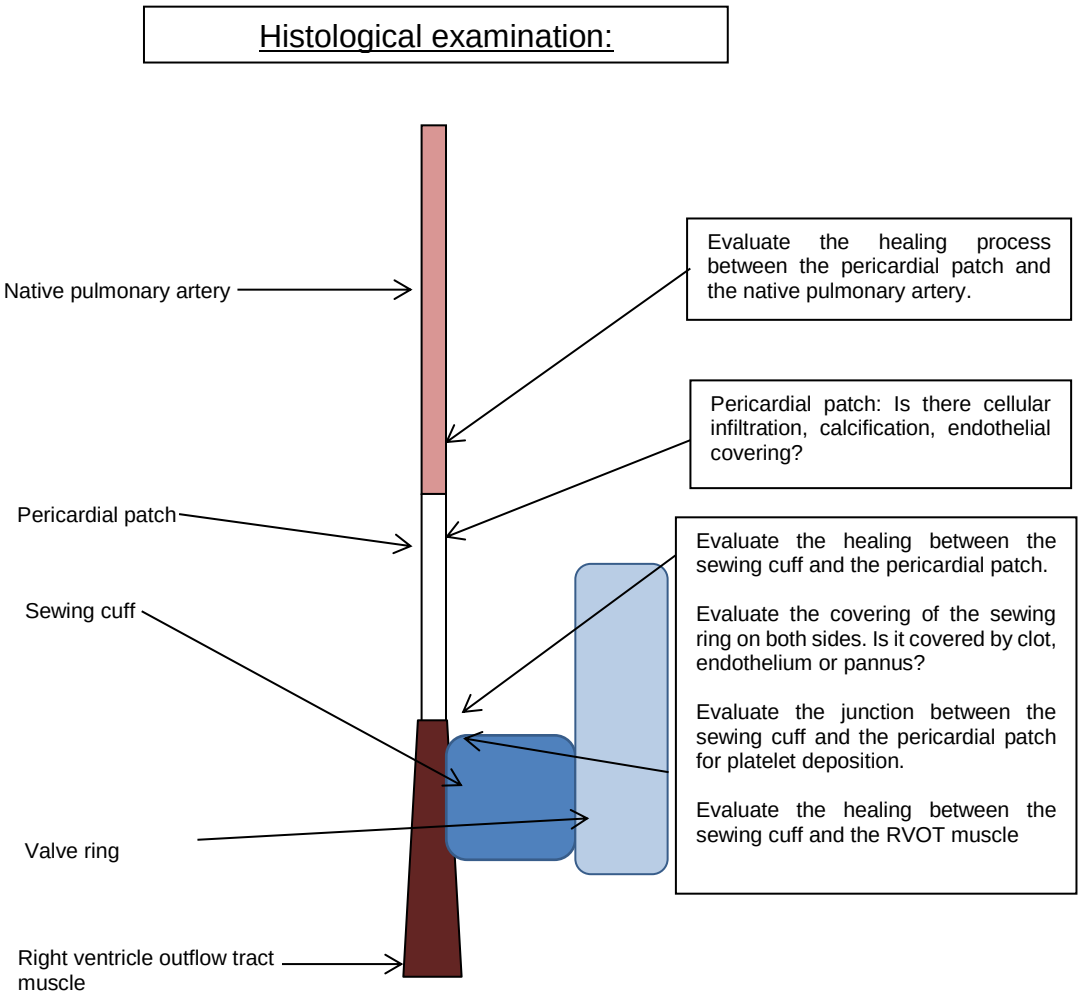

FIGURE 3.18: **The areas of interest during histological examination.**

3.5 Statistical analysis

CFD testing will only be performed on the Glycar valve. The results generated in CFD will be compared to the fluid hydrodynamic findings established during Phase II of the study. Results generated during the CFD simulation will include flow patterns around the different structures/solid body and housing, velocity vectors and pressures. Factors that will be taken into account during the analysis are:

- Geometry of the valve
- Influence of fluid properties on the valve (viscosity, temperature etcetera)
- Boundaries around the poppet
- The effect of the shape of the poppet on the pressure drop
- Shear stress generation in a Newtonian fluid

In phase III of the study the six-month and twelve-month follow-up groups will be analysed separately. The results will be categorised by the type of heart valve implanted into the sheep. Differences between the analysis groups will be evaluated, if possible, using appropriate statistical tests. However, since the control in each group only has one subject, comparisons may not be possible and the data will only be presented descriptively. The same applies to echocardiography, hematology, biochemistry and immunology parameters measured at multiple time points during group one and group two of the study. As the sampling group is too small for any meaningful statistical analysis, the data will be presented as mean values and the outlier values will be highlighted and discussed. The photographic data are only measured at a single time point (at sacrifice).

The statistical analyses will be performed by a statsitician based at the Department of Cardiothoracic Surgery, UFS, Bloemfontein.

3.6 Ethical aspects and good clinical practice

3.6.1 Ethical clearance

Phase III of the study was submitted to the Animal Ethics Committee of the University of the Free State to gain ethical approval before the study commenced. Approval was granted with ETOVS number 08/2012 (appendix F).

3.6.2 Good clinical practice (GCP) / quality assurance

All animal experiments and surgical procedures will be performed in compliance with the Guide for the Care and Use of Laboratory Animals as published by the US National Institutes of Health (NIH Publication 85-23, revised 1996).

All clinical work conducted under this protocol is subjected to the GCP guidelines (The principles of ICH GCP, 2004).

The Declaration of Helsinki's basic principle number 3 states that research should be conducted by scientifically qualified people and under the supervision of adequately qualified people (World Medical Association, 2002). Adequately qualified people will be used to conduct this research.

3.6.3 Safety Variables

The research project will be evaluated by a panel consisting of researchers and clinicians from different disciplines. All the procedures will be performed by a trained medical practitioner and be overseen by the animal laboratory personnel and a private veterinarian. The study will be discontinued prematurely if the researcher, or any of the study supervisors consider any of the events to be unethical.

Should any of the sheep die prior to scheduled sacrifice it will be noted as such and a necropsy will be performed to determine the cause of death. In such an event, haemodynamic studies and trans-oesophageal echocardiography will not be performed. The heart and organs will be removed and examined and the valve examined in detail.

CHAPTER 4

Results

4.1 Phase I: Re-engineering of the Glycar valve and CFD results

4.1.1 Re-engineering of the Glycar valve

A digital rendering of the UCT valve was made using 3D CAD (Dassault Systèmes Solidworks Corp., Vélizy, France) by Southern Medical SA Pty. Ltd. Modifications were made to the original design and the design of the housing assembly can be appreciated in figure 4.1.

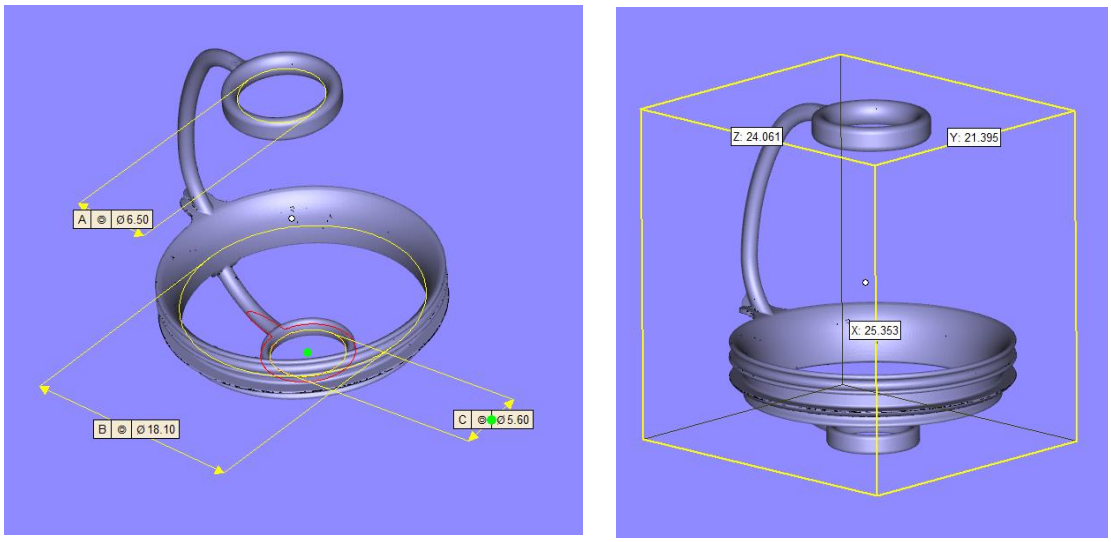

FIGURE 4.1: **CAD renderings of the Glycar valve housing assembly**

4.1.2 Modifications made to the Glycar valve

During the reverse engineering of the Glycar valve several modifications were made to the UCT design. To summarise, the following alterations were made (figure 4.2):

a. The rounding of the leading and trailing edges of the poppet was increased to allow for laminar flow across the poppet rods and to reduce stagnation distal to the distal poppet rod.

b. The angle of the distal conal tapering of the poppet was increased to improve laminar flow across the poppet and to reduce flow separation during forward flow.
c. The sharp edges at the periphery of the poppet at the junction between the cone and the belly were removed and rounded to reduce flow acceleration across the edges of the poppet and to reduce viscous shear stress.
d. The proximal and distal restraining arms were configured into a teardrop shape as were the proximal and distal guiding rings to improve fluid dynamic interaction.
e. The guiding ring diameters were increased to 5.6 mm proximal and 6.5 mm distal. This will allow for a circular motion of the distal poppet rod during valve excursion to dissipate vortex shedding downstream from the poppet.
f. The valve housing height was increased by 1.5 mm. Valves such as the On-X valve design employ the same principles, thereby simulating the height-to-diameter ratio of a native valve. Turbulence is reduced and laminar flow is improved during forward flow.
g. A rounded configuration to the inner surface of the housing was created to simulate aerofoil principles. The aerofoil housing profile optimises the organisation of flow across the valve, turbulent flow is decreased, pressure recovery is favoured and surface continuity with the suture ring is improved. It also provides poppet protection from tissue encroachment from the sewing cuff.
h. The distal diameter of the housing was increased by 2 mm, producing a flared housing design. The flare produces an increased volume of flow, comparable to that of a larger orifice valve due to smooth, organised flow and a reduction in turbulence. Blood flow is directed laterally around the poppet promoting laminar blood flow.
i. In the closed position the poppet seats flush against the housing and the conical shape of the occluder forms a smooth slope down towards the valve housing, directing laminar retrograde blood flow across the conical shape of the conus, over the housing and the sewing cuff into the sinuses of the aorta. Points of stasis around the junction between the poppet and the sewing cuff as well as between the sewing cuff-native tissue interface are eliminated.
j. In the closed position the poppet seats flush against the valve housing, producing no retrograde flow across the valve for example, washing areas such as the b-datum line. No blood cells are subjected to the shear stresses experienced in the hinge areas of bi-leaflets and therefore no platelet activation should occur.
k. The sewing cuff profile was reduced to allow for healing across the sewing cuff and to protect the poppet against encroachment of cicatricial tissue or pannus. Endothelialisation of the sewing cuff is necessary as the layer on the sewing cuff material prevents adhesion of platelets and F XII, reducing thrombus formation. Soft closure of the valve due to the complaint silicone poppet hitting the housing reduces impact trauma.
l. The housing was machined from a solid block of stainless steel, circumventing the problems associated with welding of struts to the housing, thereby eliminating possible areas of metal weakness that may occur due to metal fatigue.

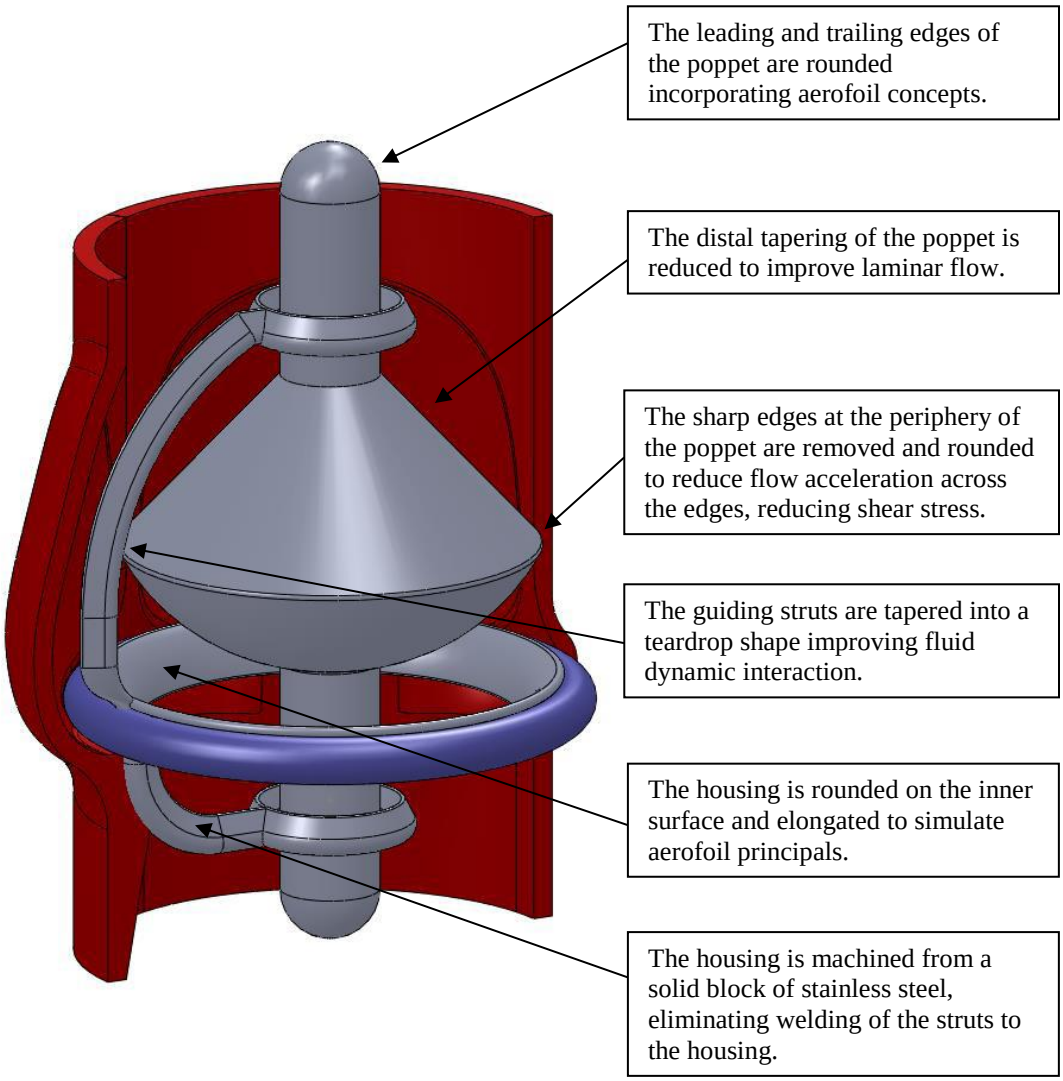

FIGURE 4.2: **Modifications made to the Glycar valve**

4.1.3 CFD analysis results

i. Part 1: Static evaluation (peak systole)

a. Introduction

Five configurations were analysed during the evaluation of the Glycar valve. Different inlet volume flow rates were used. The purpose of the different configurations was to simulate the range of flow rates to which the heart valve may be exposed. The summary of the static pressures and velocities is shown in table 4.1 and table 4.2, respectively.

Table 4.1: **Part 1 - Summary of the minimum and maximum static pressures.**

Configuration	Minimum static pressure		Maximum static pressure	
	Pa	mmHg	Pa	mmHg
1. 1.65 L/min	117.29	120.3	117.36	120.9
2. 3.30 L/min	117.21	119.7	117.45	121.5
3. 4.95 L/min	117.14	119.2	117.58	122.5
4. 6.60 L/min	116.92	117.5	117.77	124.0
5. 8.25 L/min	116.61	115.2	117.98	125.5

Pa = Pascal; mmHg = millimeter mercury; L/min = liter per minute.

Table 4.2: **Part 1 - Summary of the maximum velocity.**

Configuration	Maximum velocity (ms^{-1})
1. 1.65 L/min	0.242
2. 3.30 L/min	0.513
3. 4.95 L/min	0.813
4. 6.60 L/min	1.112
5. 8.25 L/min	1.443

L/min = liter per minute; ms^{-1} = meter per second

b. Summary of the pressure drop

The effects of the change of the inlet volume flow rate on the pressure drop are summarised in figure 4.3. The three graphs represent the total pressure drop contribution, the pressure drop in the artery and the pressure drop of the valve. The contribution due to the valve was calculated by subtracting the pressure drop through the artery without the valve (artery contribution) from the pressure drop with the valve included (total contribution). It can be seen that the pressure drop is proportional to velocity squared and therefore second order polynomial trend curves were added to forecast the pressure drop for higher flow rates.

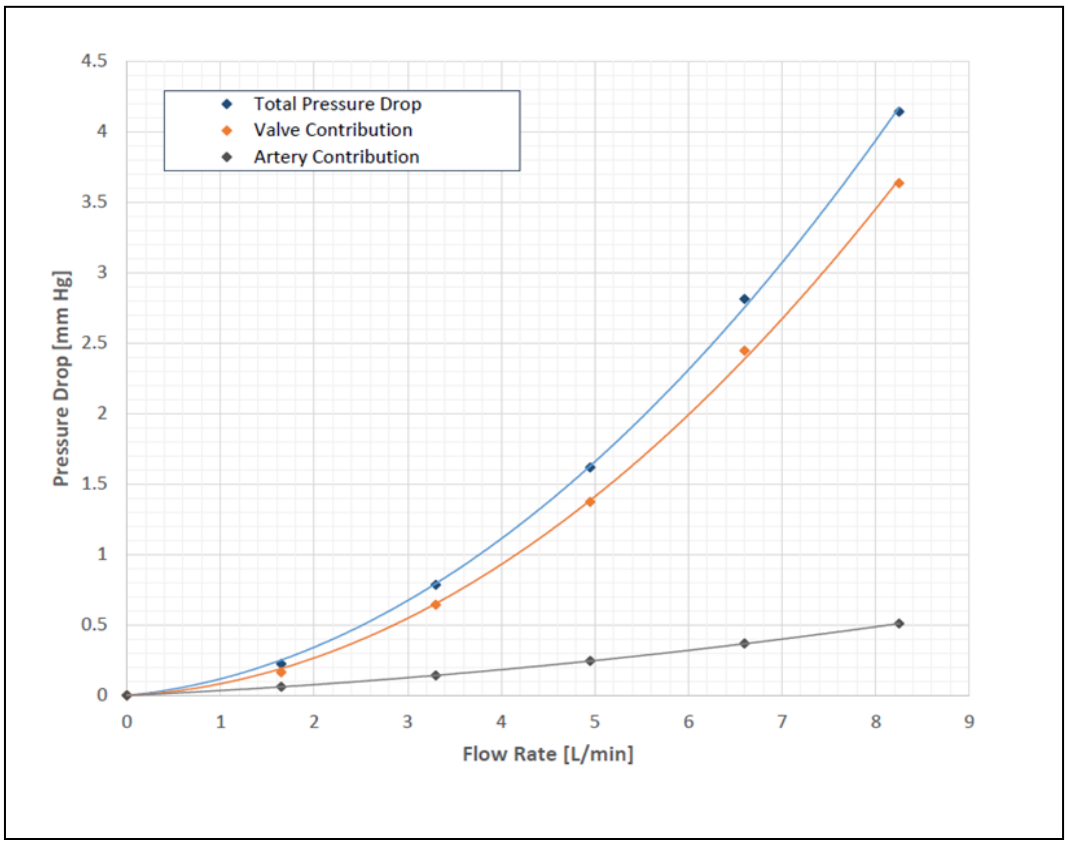

Figure 4.3: **The pressure drop compared to the flow rate of the Glycar valve in the fully opened position.** mmHg = millimeter mercury; L/min = liter per minute

c. Pressure distribution across the valve

Figure 4.4 and figure 4.5 show the pressure contours on the front plane and the surfaces of the poppet and the ring, respectively. It is important to note that the pressures have been scaled between 117.20 and 117.56 kPa corresponding to the minimum and maximum static pressure in the domain, respectively (1kPa = 7.5 mmHg).

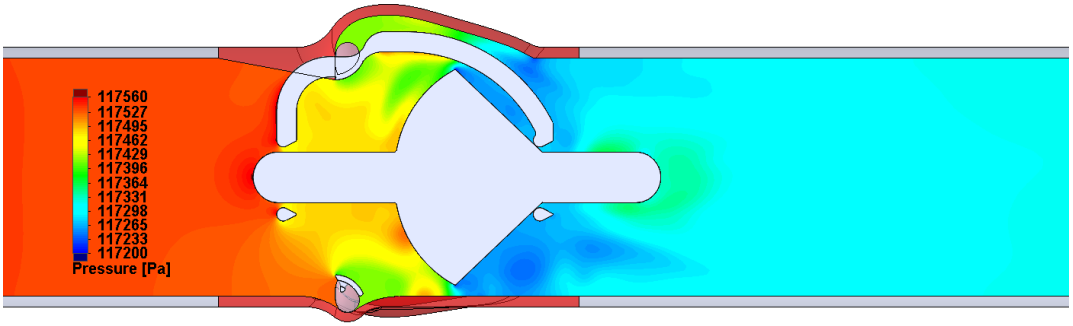

Figure 4.4: **Pressure cut plot of the Glycar valve at 4.95 L/min**

Both the high and the lower pressures acting on the poppet and the ring can be seen in figure 4.5. The high pressure due to stagnation and the low pressure due to flow separation can also be seen in figure 4.5.

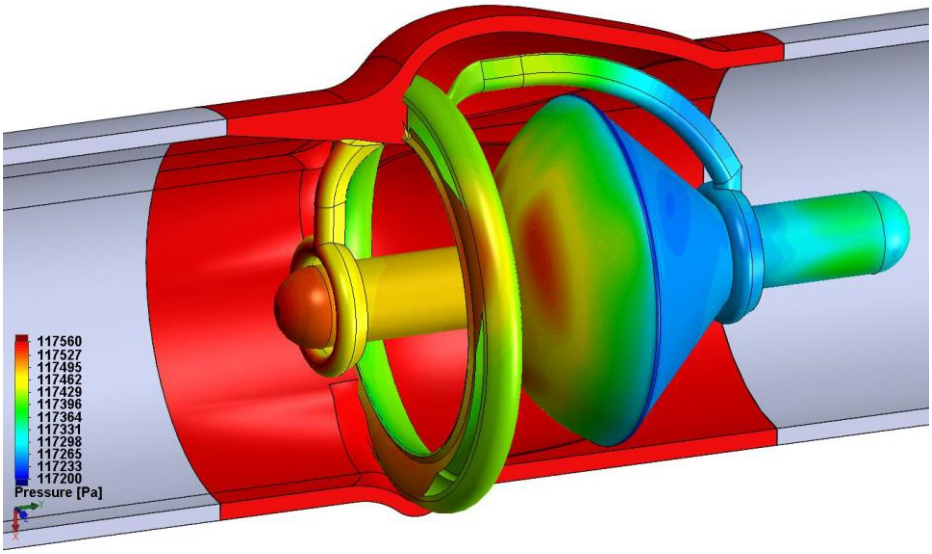

Figure 4.5: **Surface pressure plot on the valve at 4.95 L/min**

d. Velocity distribution across the valve

Figure 4.6 and figure 4.7 show the velocity contours on the front and top plane. Clearly there are a number of regions where the velocity approaches zero. These areas are due to the shape of the geometry causing recirculation. This is explained in more detail following the velocity and vector plots.

It is important to note that the images in figure 4.6 and figure 4.7 have been scaled between 0 and 1.4 ms^{-1} in order to compare between the same cut plots across all configurations, so that one can easily identify any distinct differences between the various configurations. Recall from table 3.1 that the maximum velocity reported for configuration 3 is 0.813 ms^{-1}. The maximum velocity is due to the acceleration through the narrow channel between the poppet and the artery wall, which is more clearly visible in figure 4.8, which has been scaled to the local maximum for configuration 3.

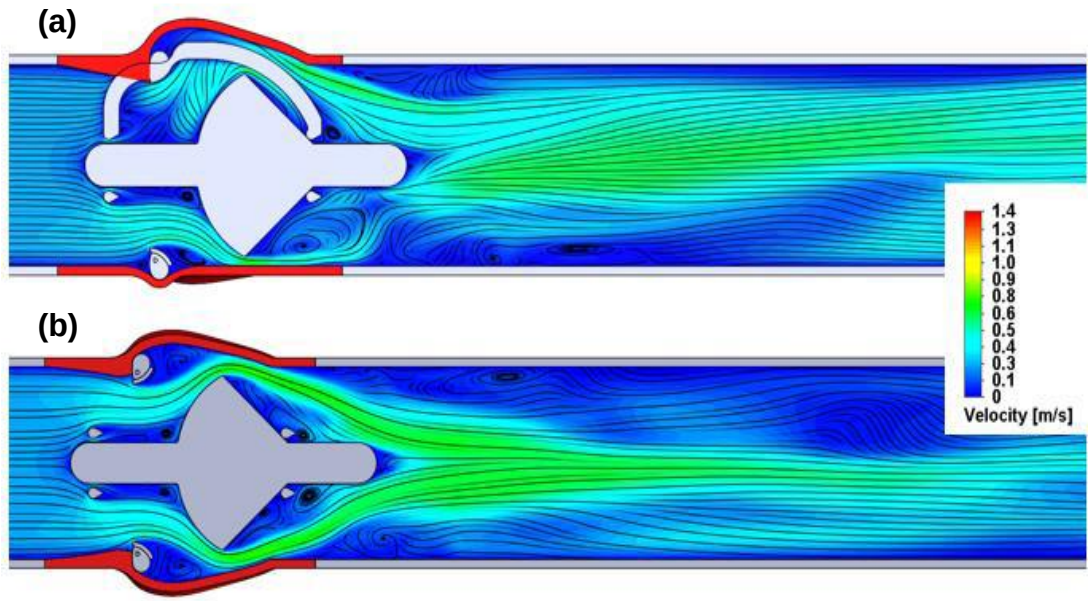

FIGURE 4.6: **Velocity cut plots at a CO of 4.95 L/min. (a) front and (b) top plane**. m/s = meter per second.

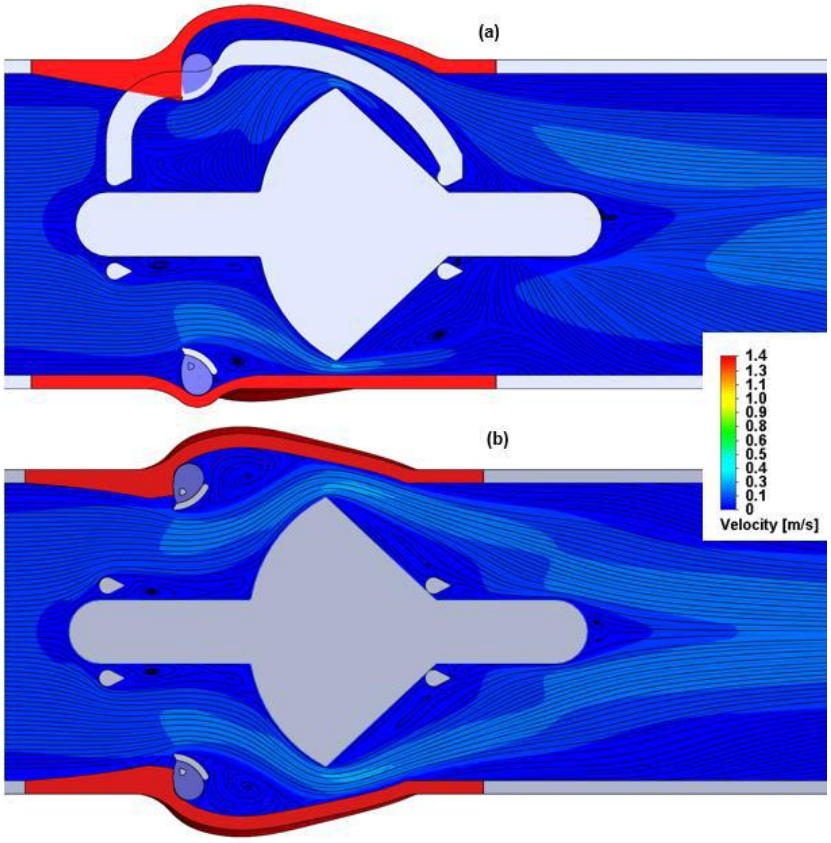

FIGURE 4.7: **Velocity cut plots at 1.65 L/min**. (a) front & (b) top plane.

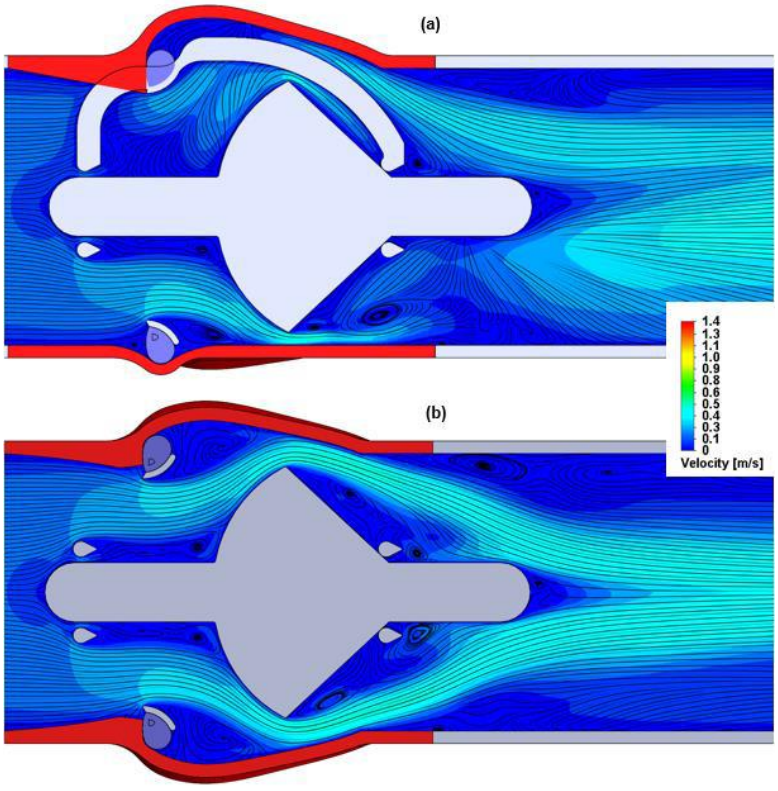

FIGURE 4.8: **Velocity cut plots at 3.3 L/min**. (a) front & (b) top plane.

Figures 4.6, 4.7, 4.8 and 4.9 illustrate a zoomed image of the streamlines and contours of velocity in the region of the valve. It is evident that there are definite areas of re-circulating flow in regions in an adverse pressure gradient (converging region of the poppet) and directly after the ring structure as the flow increases.

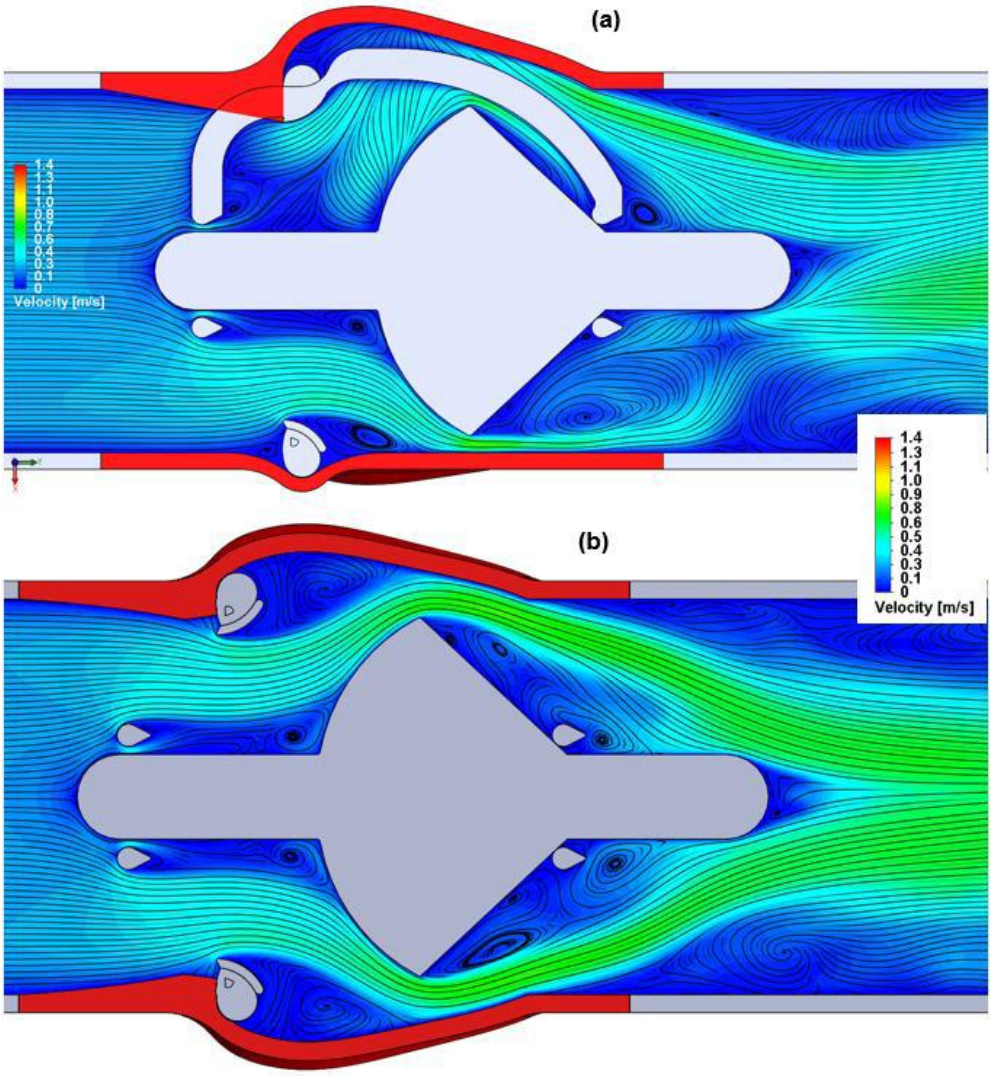

FIGURE 4.9: **Zoomed view of velocity cut plots at a CO of 4.95 L/min.** (a) front and (b) top plane.

Figure 4.10 shows the velocity magnitudes at a cardiac output of 8.25 L/min. The magnitude of the maximum velocity is higher than for a cardiac output of 4.95 L/min (figure 4.6). Since the fluid domain is the same in both figures, the velocity gradients for a cardiac output of 8.25 L/min are higher, indicating a higher shear stress in the fluid.

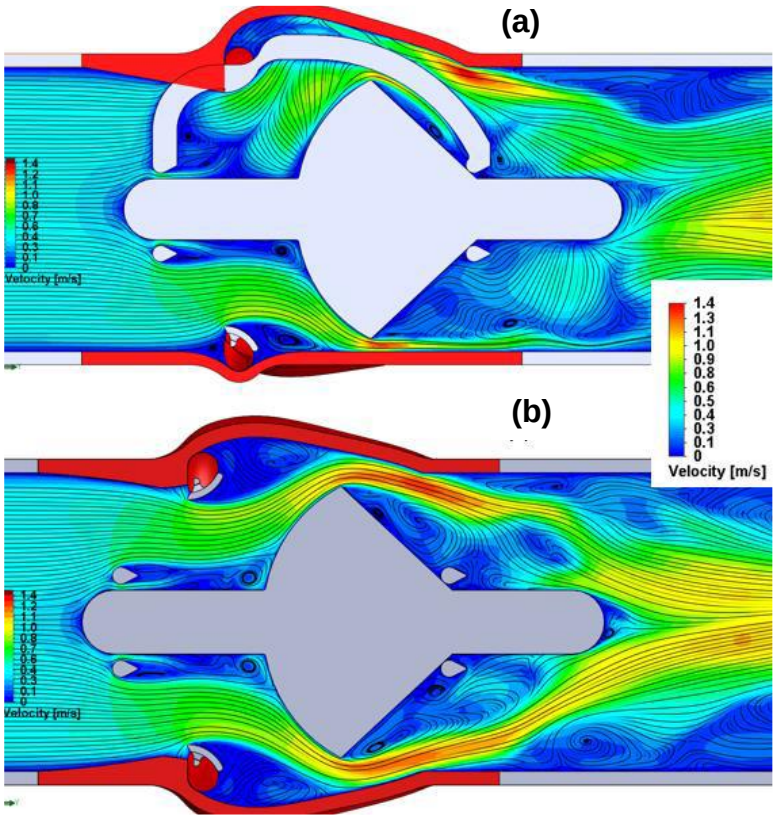

FIGURE 4.10: **The velocity plot at a CO 8.25L/min.** (a) front & (b) top plane.

e. Surface shear stress

Figure 4.11 shows the shear stress plot on the surfaces of the valve geometry at a flow of 4.95 L/min, clearly showing the areas of high shear stress resulting from local flow accelerations past geometric features, causing abrupt changes in the fluid motion. The peak viscous shear stress occurs at the poppet edge and has a magnitude of 20 Pa.

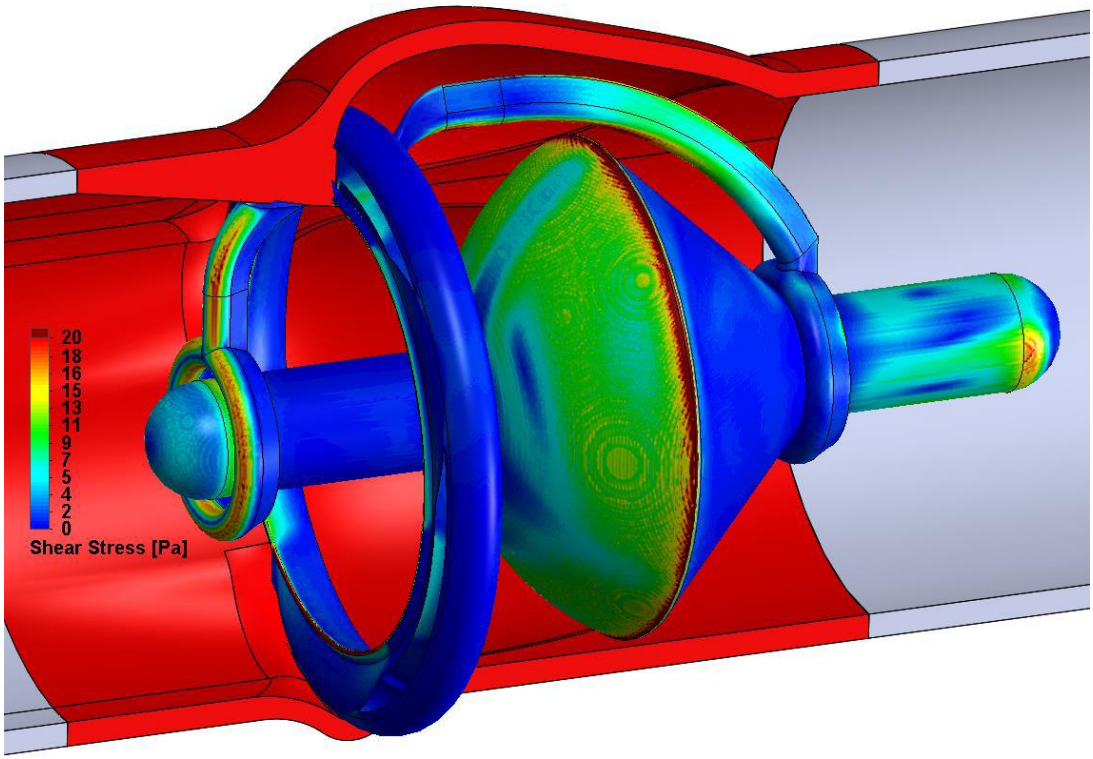

FIGURE 4.11. **Shear stress plot on the Glycar valve at 4.95 L/min.**

Figure 4.12 combines the images from figure 4.6 and figure 4.10 depicting the shear stress on the valve surfaces and the velocity distribution on the front and top cut plots for configuration 3. This image gives one an idea of how the flow develops over the entire valve as well as the areas of high shear stress as a consequence of local acceleration and high velocities associated with certain geometric features. The shear stress for the cardiac output of 8.25 L/min is much higher than for a cardiac output of 4.95 L/min due to the higher velocity gradients. It is also apparent that the outer most edge of the poppet is a major contributor to high shear stresses and maximum velocity that can induce thrombosis and platelet activation.

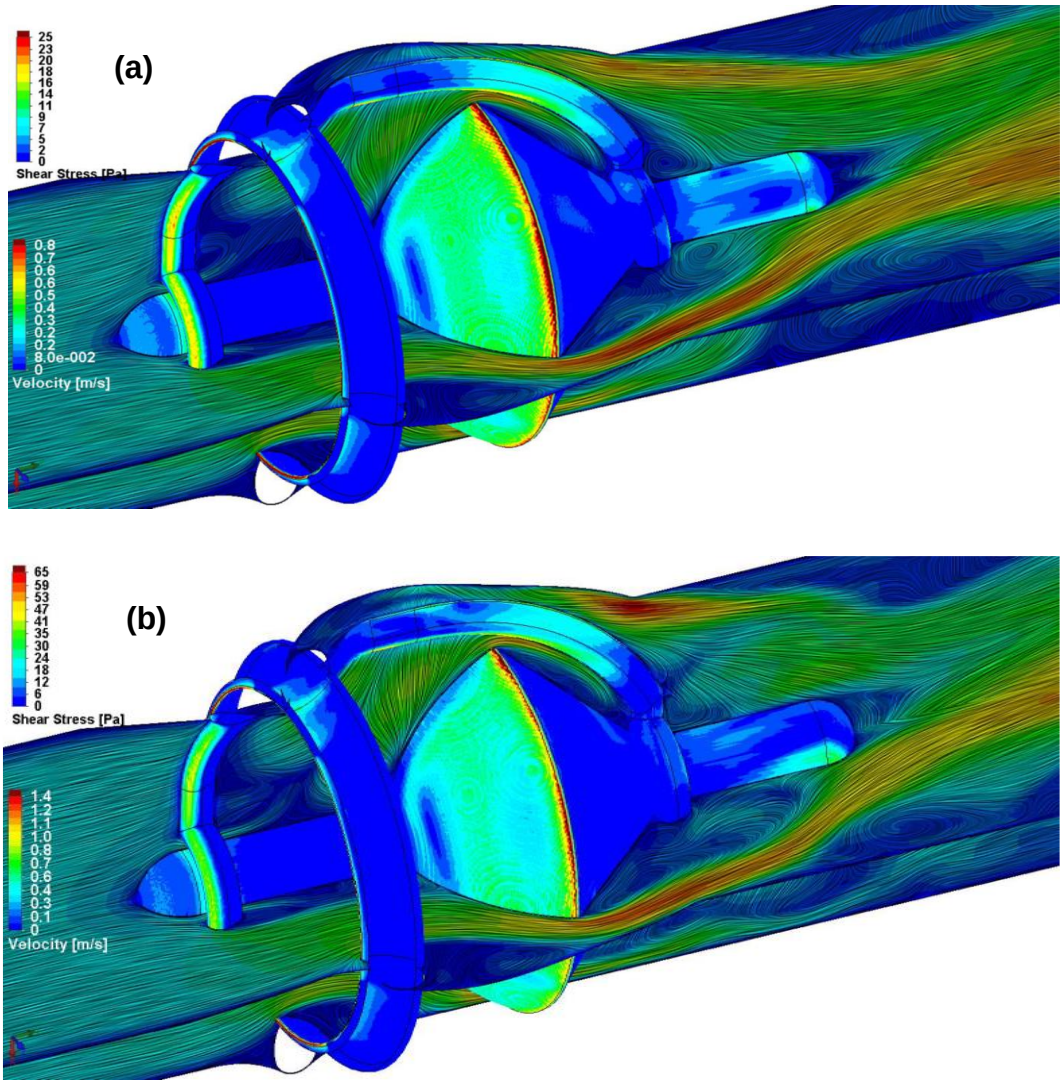

FIGURE 4.12: **Velocity cut plots and valve surface shear stress.** (a) 4.95 L/min and (b) 8.25 L/min.

ii. Part 2: Dynamic evaluation (systolic phase)

a. Introduction

Five configurations were analysed, differing only by the distance illustrated in figure 4.9. The volume flow rate used in this part of the analysis was 0.0000825 m^3/s or 4.95 L/min and the pressure set on the outlet was 117325 Pa or 120 mmHg. The summaries of the minimum and maximum static pressures and the pressure drops are shown in table 4.3 and table 4.4, respectively for each valve position. The maximum velocity recorded for each of the configurations was 0.833 m/s.

Table 4.3: **Part 2 - Summary of the minimum and maximum static pressures.**

Position (mm)	Minimum static pressure		Maximum static pressure	
	Pa	mmHg	Pa	mmHg
4	117057	118.5	117691	123.3
5	117160	119.9	117625	122.9
6	117211	119.7	117567	122.5
7	117144	119.2	117570	122.4
8	117169	119.4	117572	122.5

mm = millimeter; Pa = pascal; mmHg = millimeter mercury.

Table 4.4: **Part 2 - Summary of pressure drop.**

Position (mm)	Pressure drop	
	Pa	mmHg
4	268	2.02
5	226	1.7
6	216	1.63
7	205	1.55
8	207	1.56

mm = millimeter; Pa = pascal; mmHg = millimeter mercury.

b. Summary of the pressure drop

The effects of the change in valve position on the pressure drop are summarised in figure 4.13. The gradient or pressure drop across the valve remained stable at 1.7 mmHg.

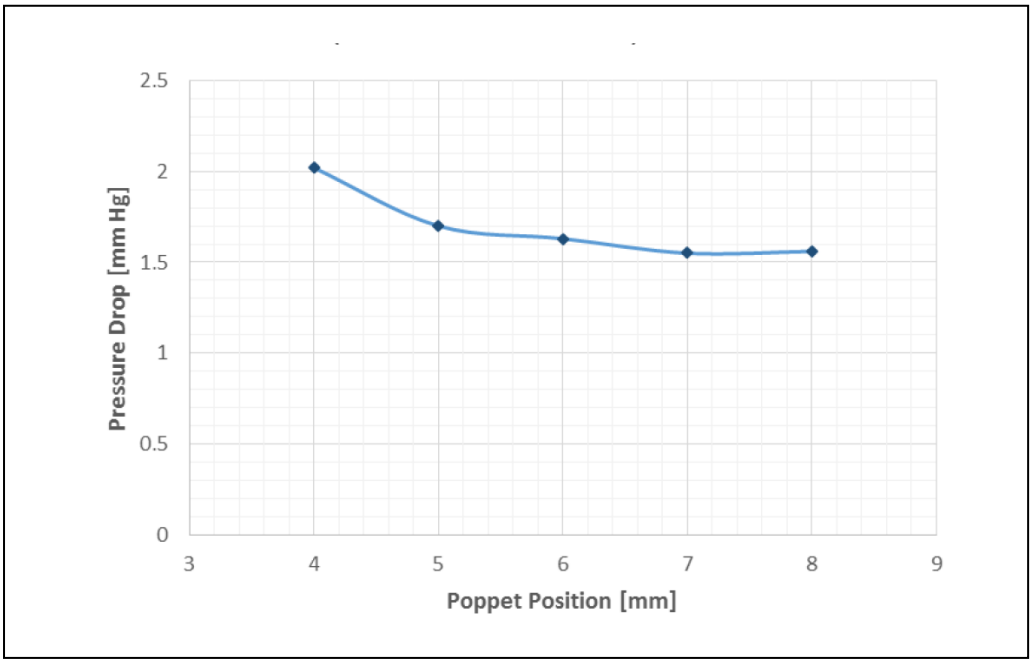

FIGURE 4.13: **Pressure drop at different valve poppet positions**. mm = millimeter; mmHg= millimeter mercury.

c. Pressure distribution across the valve

Figure 4.14 shows the pressure contours on the front plane for the different positions of the poppet, 4 mm configuration (figure 4.14.a) and 8 mm configuration (figure 4.14.e). The pressure drop can clearly be seen for all positions. As the position of the poppet increases, the pressure gradient on the converging flow side decreases, but increases on the diverging side. This is related to the respective flow areas. Therefore to obtain the lowest pressure drop across the valve, the combined blood flow area must be the largest. This occurs at the 7 mm position, which can also be seen in figure 4.13.

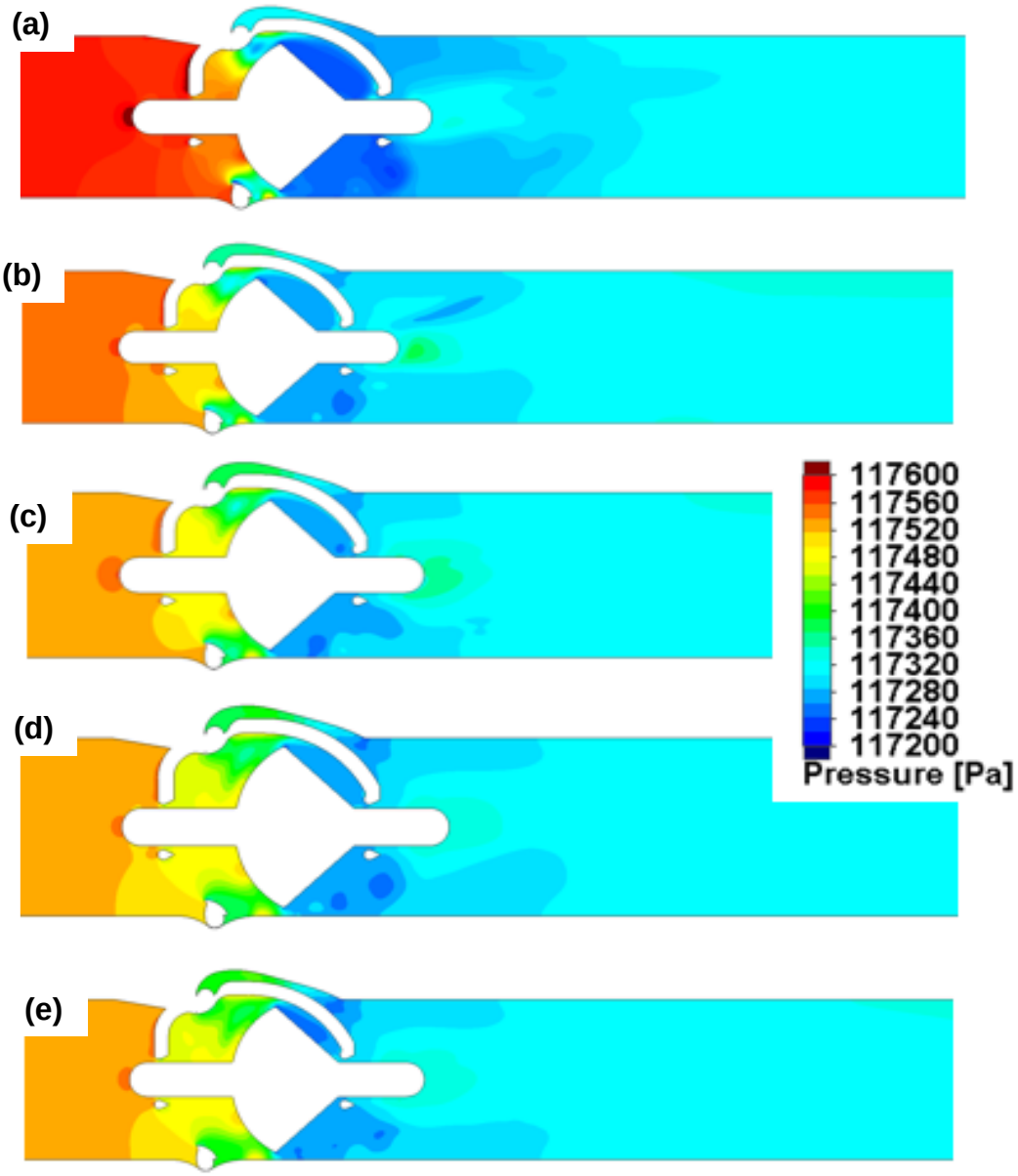

FIGURE 4.14: **Pressure cut plots at the different poppet positions.** (a) 4 mm, (b) 5 mm, (c) 6 mm, (d) 7 mm, (e) 8 mm. Pa = Pascal.

d. Velocity distribution across the valve

Figure 4.15 shows the velocity contours during the systolic phase with the poppet in different positions. The pressure gradients seen in the previous image are due to the flow acceleration as the flow area reduces. It can be seen that the 7 mm position has the lowest overall velocities and therefore correlates with figure 4.13.

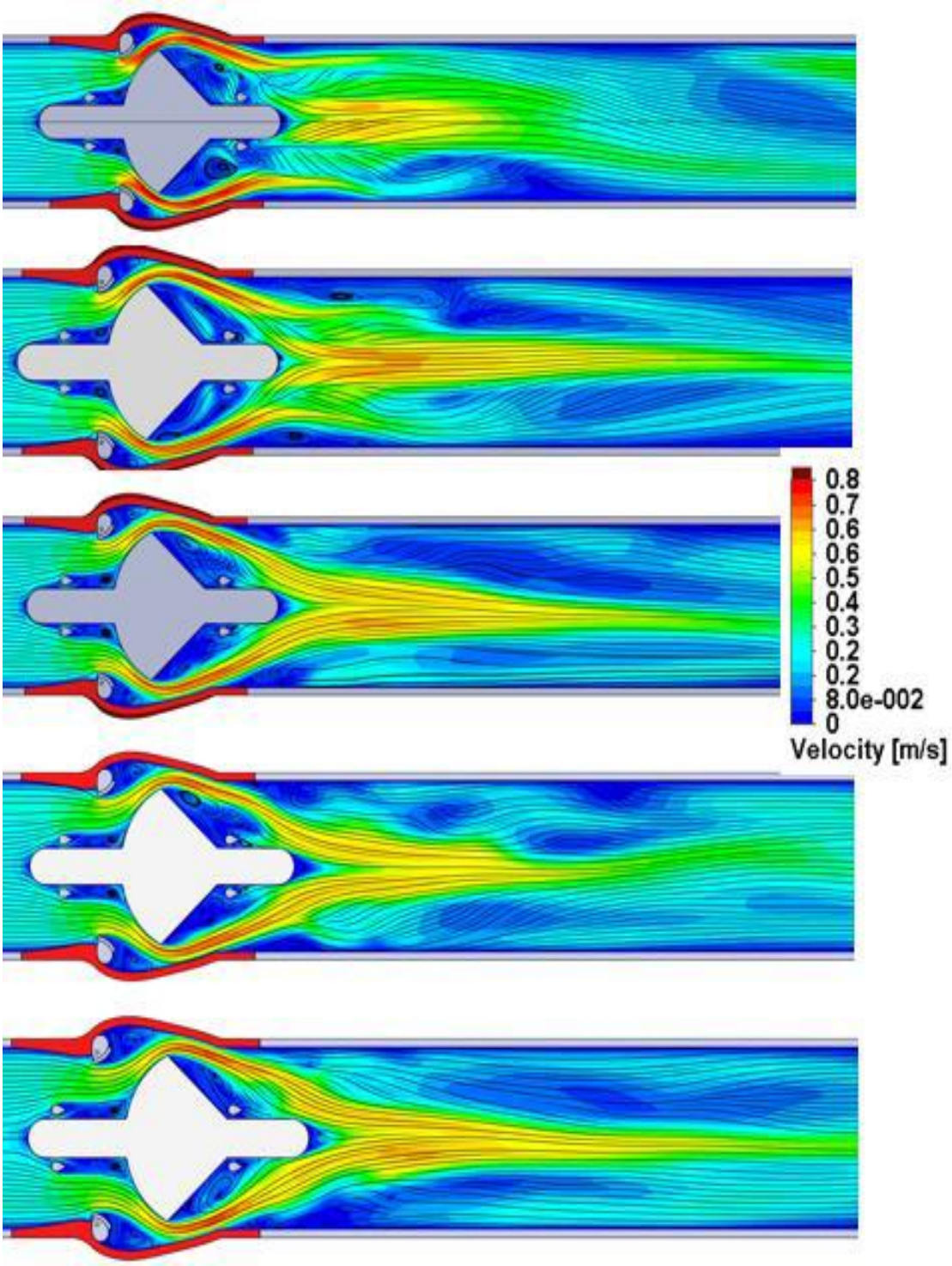

FIGURE 4.15: **Velocity cut plots during the entire systolic phase with the poppet in different valve positions.**

4.2 Phase II: Pulse duplication results

i. Introduction

The pulse duplication tests were performed at the Department of Cardiothoracic Surgery, University of the Free State, Bloemfontein, South Africa. Five different valves were tested:

1. 21mm Glycar valve
2. 21 mm Carbomedics bi-leaflet valve
3. 21 mm Perimount tissue valve
4. 19 mm Medtronic-Hall tilting disc valve
5. 21 mm ViVitro non tilting disc valve

A 21 mm Medtronic-Hall valve could not be procured for this study as they are no longer being manufactured and thus not commercially available, therefore a 19 mm valve was used. The ViVitro Labs. Inc. control valve (non-tilting disk valve) was used during the calibration of the pulse duplication system and as a reference valve for the different CO simulations.

As outlined in table 4.5, five conditions were analysed for each of the five valves; differing by the stroke volume, the beats per minute and the cardiac output. The mean pressure was maintained at 80 mmHg throughout the data acquisition phase.

Table 4.5: **Testing conditions for the pulse duplication**

Measurement point	Mean aortic pressure (mmHg)	Beats per minute	Stroke volume (ml)	Cardiac output (L/min)
1. Resting state	80	60	60	3.6
2. Minimal effort	80	70	70	4.9
3. Moderate effort	80	80	80	6.4
4. Exercise	80	100	80	8.0
5. High intensity sustained effort	80	120	80	9.6

mmHg = millimeter mercury; ml = milliliter; L/min = liter per minute.

The results from the pulse duplication were analysed in accordance with ISO 5840:2015. Using the collected data, the following parameters were analysed to assess each of the valves:

1. Transvalvular pressure drop
2. Q_{rms}
3. EOA
4. Regurgitant fraction
5. Transvalvular energy losses

ii. Validation of the pulse duplicator data

a. The ViVitro reference valve

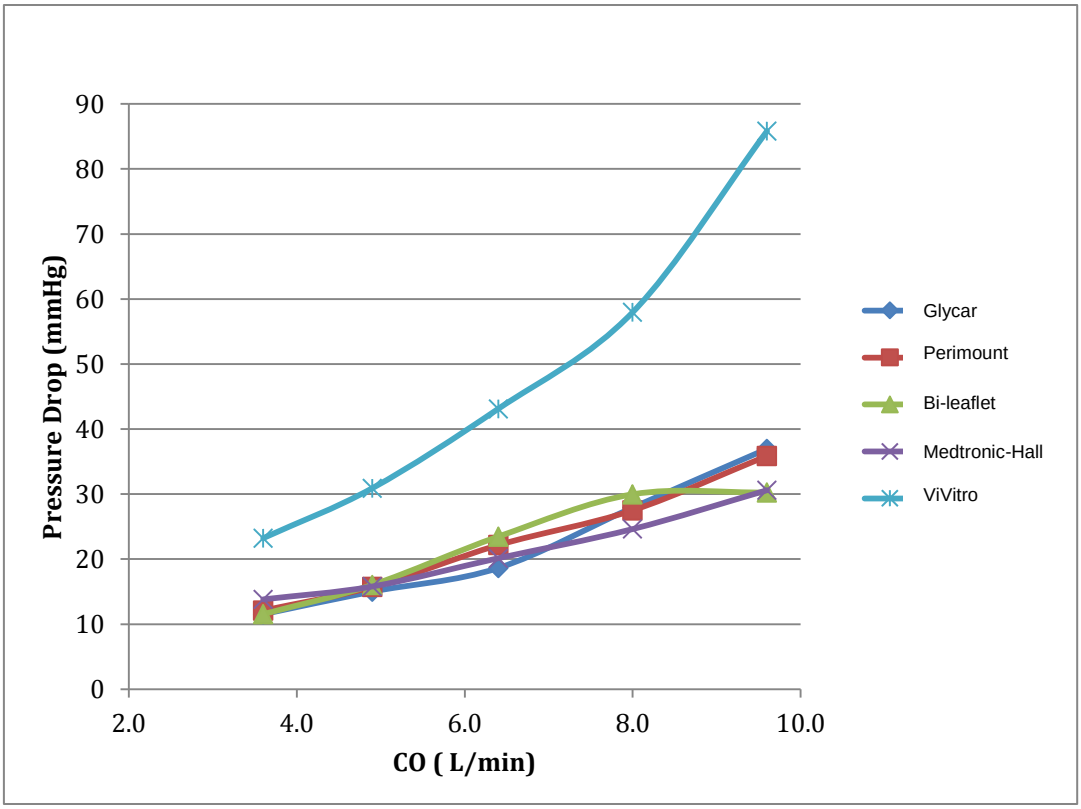

FIGURE 4.16: **Pressure drop in mmHg for the different valves at increasing cardiac output.** CO = cardiac output; mmHg = millimeter mercury; L/min = liter per minute (Adapted from Mrs L Thompson-Jooste).

The transvalvular pressure drop is shown in figure 4.16. The pressure drop was calculated over the period where the ventricular pressure was higher than the aortic pressure during forward flow denoting the Q_{rms} phase. The ViVitro valve was used as a reference valve to validate the data acquisition. In figure 4.16 the ViVitro valve had a much higher pressure drop in comparison to all of the other valves, but it was well within the reference parameters as provided by ViVitro labs Inc.

b. Literature comparison

The SJM bi-leaflet valve was tested with a cardiac output of 4.5 L/min at 72 bpm, SV 62.5 ml and a mean arterial pressure of 100 mmHg. The pressure drop across the valve obtained from Nobili *et al.* (2008) is shown in figure 4.17, with the pressure drop across the 21 mm Carbomedics Bi-leaflet valve from own data derived being shown in figure 4.18. As the two valves were tested under different conditions, two tests conditions for the Carbomedics valve are shown in figure 4.18: one at 60 BPM with an SV of 60 ml (CO 3,6 L/min) and the other at 70 bpm with an SV of 70 ml (CO 4,9 L/min).

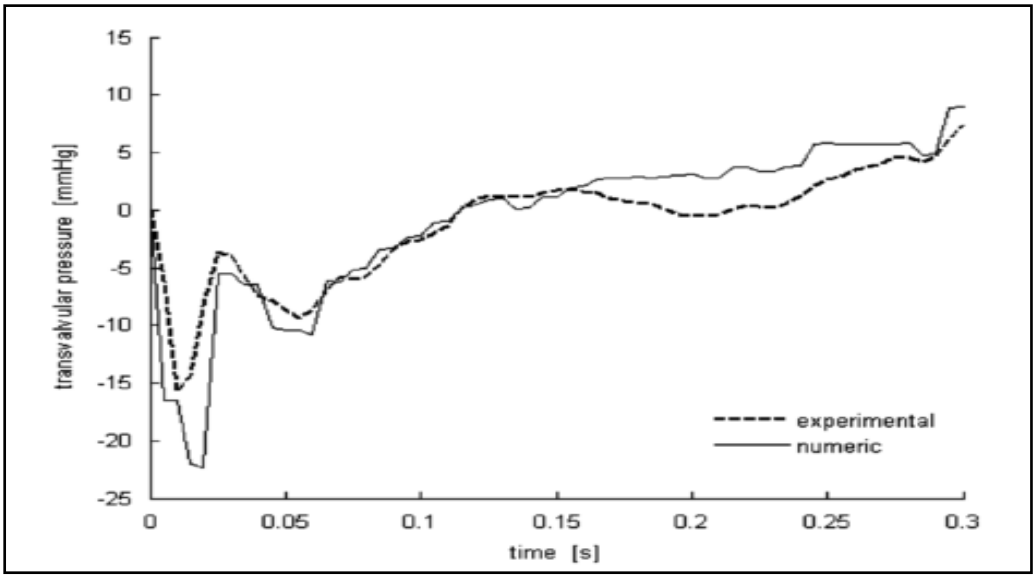

FIGURE 4.17: **Comparison between the transvalvular pressures generated over time between the 27 mm SJM bi-leaflet and a numerical simulation** (Adapted from Nobili *et al.,* 2008).

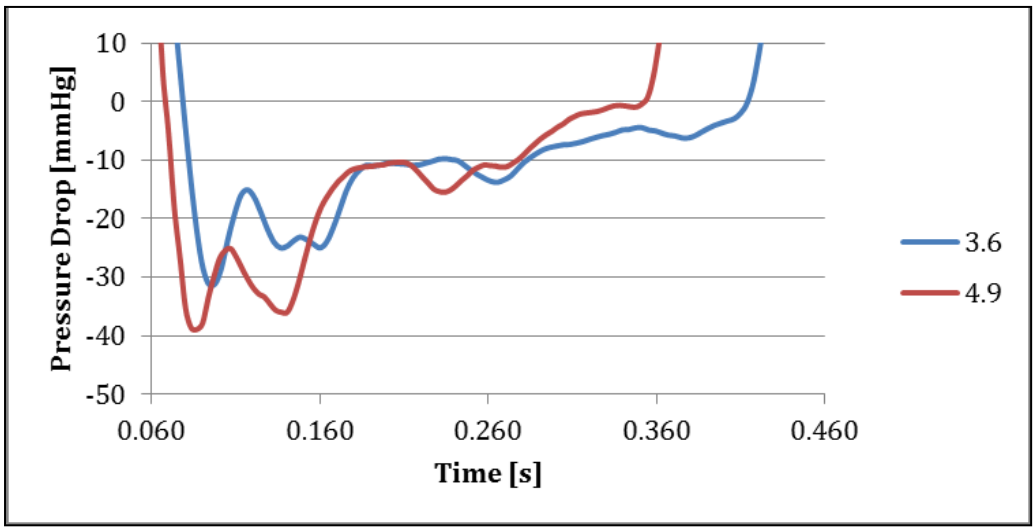

FIGURE 4.18: **The pressure drop generated across the 21 mm Carbomedics bi-leaflet valve.** The red graph represents the pressure drop at 70 bpm (CO 4.9) and the blue graph 60 bpm (CO 3.6). S= seconds; mmHg= millimeter mercury.

Piatti *et al.* (2015) determined that a 19 mm tri-leaflet polymeric heart valve at 70 bpm and CO 5.6 L/min generated an EOA of 1.47 cm^2 (Figure 4.17). The EOA of the Perimount tissue valve

at a CO of 4.9 L/min was 1.28 cm^2, whilst the EOA at a cardiac output of 6.4 L/min was 1.45 cm^2. The EOA vs CO of the tissue valve is shown in figure 4.19. Using the polynomial at a cardiac output of 5.6 L/min, an EOA of 1.37 cm^2 is determined.

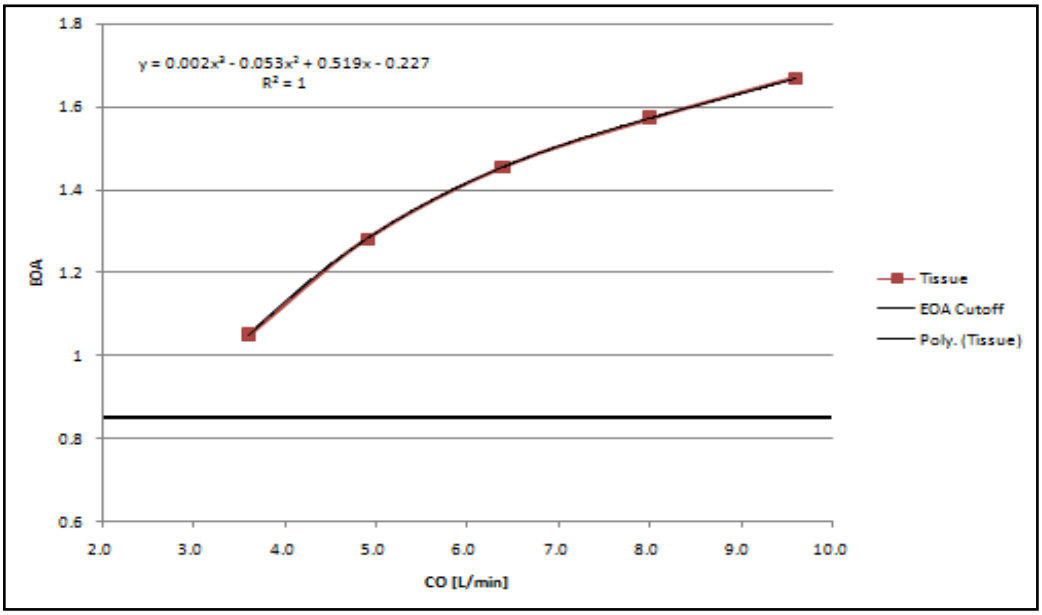

Figure 4.19**: The EOA plotted against the CO for the tri-leaflet valve (red graph) and the Perimount tissue valve** (black graph). The horizontal black line represents the minimal EOA for the valves according to ISO 5840:2015. EOA = effective orifice area; CO = cardiac output; L/min = liters per minute.

iii. The total forward flow volume (Q_{rms})

The Q_{rms} as calculated for each of the five valves at the different cardiac outputs is represented in table 4.6 and figure 4.20. To ensure accuracy in the data acquisition, ten measurements of each of the test valves for each of the test conditions or configurations were performed during the evaluation. An average was calculated and the standard deviation of the measurements determined. The data for the Q_{rms} (average) were plotted for each of the valves for each of the test conditions and is seen in figure 4.20.

Table 4.6: **The Q_{rms}, pressure drop and EOA data collected during the five tests conditions.**

Cycle	Glycar valve					Perimount tissue valve					Carbomedics bi-leaflet					Medtronic-Hall					Vivitro				
	R: 60	R: 70	R: 80	R: 100	R: 120	R: 60	R: 70	R: 80	R: 100	R: 120	R: 60	R: 70	R: 80	R: 100	R: 120	R: 60	R: 70	R: 80	R: 100	R: 120	R: 60	R: 70	R: 80	R: 100	R: 120
	Qrms [ml/s]																								
1	183.24	183.24	183.24	183.24	183.24	183.24	183.24	183.24	183.24	183.24	183.24	183.24	183.24	183.24	183.24	183.24	183.24	183.24	183.24	183.24	183.24	183.24	183.24	183.24	183.24
2	184.47	252.93	309.99	421.49	581.58	189.06	262.63	358.50	427.09	608.71	184.13	265.74	349.95	418.11	430.88	186.71	252.44	346.79	415.57	601.16	189.09	259.43	339.84	415.88	527.42
3	183.68	251.21	311.28	421.60	504.68	190.10	261.00	357.97	427.09	599.06	185.85	255.39	351.47	418.78	419.88	187.02	251.20	341.63	419.34	600.00	188.91	258.02	338.22	416.15	525.01
4	184.23	250.78	310.14	421.05	501.71	189.02	267.81	358.91	428.27	607.93	186.31	267.69	349.10	425.85	419.45	184.72	255.08	344.15	420.65	595.12	191.41	259.69	338.21	415.17	524.81
5	183.32	252.34	312.89	423.23	582.09	190.93	269.28	361.04	430.57	602.42	183.22	256.85	351.82	417.03	423.53	186.29	252.32	337.48	418.07	594.88	189.21	258.51	339.91	419.65	521.56
6	184.42	250.09	310.76	423.50	581.29	188.87	266.98	355.95	431.54	604.09	185.10	264.08	349.69	423.71	420.31	186.22	251.37	338.72	418.53	601.19	190.03	258.27	340.36	417.50	524.29
7	184.11	252.51	309.84	424.38	505.57	189.45	261.28	356.66	429.25	607.12	183.56	257.52	349.88	420.65	419.52	185.28	251.82	341.15	420.23	601.68	188.01	258.61	339.55	416.53	523.21
8	183.63	251.30	314.14	422.33	582.35	190.15	268.29	357.94	425.23	604.69	183.64	255.39	349.93	422.87	420.52	186.69	249.32	343.57	416.02	595.28	189.22	259.17	340.69	416.74	526.13
9	183.56	252.39	314.85	422.43	584.10	190.19	261.44	356.62	425.36	608.03	186.39	264.27	347.93	420.93	422.82	186.39	250.04	340.90	419.52	597.61	188.91	258.44	338.23	416.03	520.97
10	183.23	252.60	310.99	419.52	583.74	188.45	263.53	357.60	426.72	608.20	182.94	262.59	347.17	419.56	418.23	185.90	253.53	342.55	419.05	596.98	190.79	258.79	337.44	417.00	525.49
Ave	183.79	251.66	311.60	422.27	558.94	189.54	264.18	357.87	427.95	605.75	184.73	261.27	349.75	420.54	421.45	186.03	251.95	341.81	418.59	597.97	189.36	258.88	339.20	416.26	524.31
SD	0.48	1.01	1.76	1.41	37.94	0.77	3.56	1.43	2.08	3.14	1.38	4.55	1.43	2.85	3.68	0.77	1.64	2.67	1.66	2.77	1.10	0.62	1.09	1.93	1.98
	Pressure Drop (mmHg)																								
1	11.70	15.33	19.49	29.02	54.24	12.28	15.69	23.08	28.07	56.68	11.93	16.84	24.95	30.27	30.49	14.02	16.19	20.96	25.09	48.42	23.90	31.70	44.57	58.33	88.44
2	11.78	15.22	19.23	28.39	54.71	12.45	16.13	22.89	28.09	57.23	11.75	16.93	24.08	30.54	32.00	14.23	16.16	21.45	25.34	49.61	23.76	31.61	44.08	59.29	88.32
3	11.86	15.35	19.62	28.48	38.43	12.38	15.93	23.14	28.12	53.32	11.91	15.75	24.10	31.35	30.64	14.25	16.03	20.57	24.99	48.90	23.82	31.73	44.12	59.31	88.23
4	11.81	15.26	19.21	28.39	37.48	12.38	16.50	22.95	27.99	55.76	11.96	17.39	23.92	31.49	31.06	14.16	16.42	20.63	25.34	46.75	23.97	31.62	44.36	58.89	88.10
5	11.86	15.26	19.61	29.04	53.57	12.43	16.72	23.17	28.44	55.18	11.73	15.95	24.58	30.00	31.24	14.14	16.17	20.11	25.55	47.86	23.86	31.61	44.28	59.12	87.95
6	11.92	15.38	19.43	28.58	53.58	12.28	16.50	22.90	28.04	55.04	11.83	16.83	24.18	31.28	30.97	14.12	16.08	20.40	25.06	49.43	24.00	31.61	44.54	59.34	88.48
7	11.97	15.31	19.50	28.82	38.67	12.51	15.82	22.94	28.22	56.77	11.78	15.93	24.11	31.17	31.06	14.13	16.22	20.57	25.18	49.24	23.82	31.63	44.33	59.36	88.33
8	11.88	15.33	19.55	28.45	53.59	12.40	16.43	23.10	28.26	55.49	11.85	15.81	24.69	31.62	30.86	14.24	15.87	20.99	25.26	47.92	23.90	31.62	44.09	59.14	88.45
9	11.86	15.42	19.81	28.78	54.82	12.44	15.95	22.75	28.42	55.67	11.96	16.86	23.72	30.78	31.34	14.13	16.11	20.57	24.91	47.92	23.68	31.62	43.62	59.38	86.57
10	11.87	15.51	19.27	28.61	54.82	12.35	16.02	22.98	27.98	55.63	11.70	16.58	23.53	30.31	30.32	14.18	16.46	20.99	25.32	48.09	23.87	31.81	43.69	58.95	87.75
Ave	11.85	15.34	19.47	28.66	49.39	12.39	16.17	22.99	28.16	55.68	11.84	16.49	24.19	30.88	31.00	14.16	16.17	20.73	25.20	48.41	23.86	31.66	44.17	59.11	88.06
SD	0.08	0.08	0.19	0.25	7.75	0.07	0.34	0.13	0.17	1.10	0.10	0.58	0.44	0.58	0.48	0.07	0.17	0.38	0.19	0.88	0.10	0.07	0.32	0.32	0.58
	EOA (cm2)																								
1	1.04	1.25	1.37	1.53	1.54	1.05	1.28	1.45	1.57	1.57	1.05	1.25	1.37	1.48	1.48	0.96	1.22	1.45	1.63	1.67	0.75	0.90	0.99	1.05	1.09
2	1.05	1.26	1.38	1.54	1.53	1.04	1.27	1.46	1.57	1.57	1.05	1.26	1.39	1.47	1.48	0.96	1.22	1.46	1.61	1.66	0.76	0.90	1.00	1.05	1.09
3	1.04	1.25	1.37	1.54	1.59	1.05	1.27	1.45	1.57	1.60	1.05	1.25	1.39	1.46	1.48	0.96	1.22	1.47	1.63	1.67	0.75	0.89	0.99	1.05	1.09
4	1.04	1.25	1.38	1.54	1.60	1.05	1.28	1.46	1.58	1.59	1.05	1.25	1.39	1.48	1.47	0.96	1.23	1.48	1.63	1.70	0.76	0.90	0.99	1.05	1.09
5	1.04	1.26	1.38	1.53	1.55	1.05	1.28	1.46	1.57	1.58	1.04	1.25	1.38	1.48	1.48	0.97	1.22	1.47	1.61	1.67	0.75	0.90	0.99	1.06	1.08
6	1.04	1.24	1.37	1.54	1.55	1.05	1.28	1.45	1.59	1.59	1.05	1.25	1.39	1.48	1.47	0.97	1.22	1.46	1.63	1.67	0.76	0.89	0.99	1.06	1.09
7	1.04	1.26	1.37	1.54	1.58	1.04	1.28	1.45	1.57	1.57	1.04	1.26	1.39	1.47	1.47	0.96	1.22	1.46	1.63	1.67	0.75	0.90	0.99	1.05	1.08
8	1.04	1.25	1.38	1.54	1.55	1.05	1.29	1.45	1.56	1.58	1.04	1.25	1.37	1.46	1.47	0.96	1.22	1.46	1.61	1.67	0.75	0.90	1.00	1.06	1.09
9	1.04	1.25	1.38	1.53	1.54	1.05	1.28	1.46	1.55	1.59	1.05	1.25	1.39	1.48	1.47	0.97	1.21	1.46	1.64	1.68	0.76	0.90	1.00	1.05	1.09
10	1.04	1.25	1.38	1.53	1.54	1.04	1.28	1.45	1.57	1.59	1.04	1.26	1.39	1.48	1.48	0.96	1.22	1.46	1.62	1.68	0.76	0.89	0.99	1.06	1.09
Ave	1.04	1.25	1.38	1.54	1.55	1.05	1.28	1.45	1.57	1.58	1.05	1.25	1.39	1.47	1.47	0.96	1.22	1.46	1.62	1.67	0.76	0.90	0.99	1.05	1.09
SD	0.00	0.01	0.01	0.01	0.02	0.00	0.01	0.00	0.01	0.01	0.00	0.00	0.01	0.01	0.01	0.00	0.00	0.01	0.01	0.01	0.00	0.00	0.00	0.00	0.00

R= rate; Ave= average; SD= standard deviation; Q_{rms}= total forward flow volume; mmHg= millimeter mercury; EOA= effective orifice area; ml/s= milliliter per second

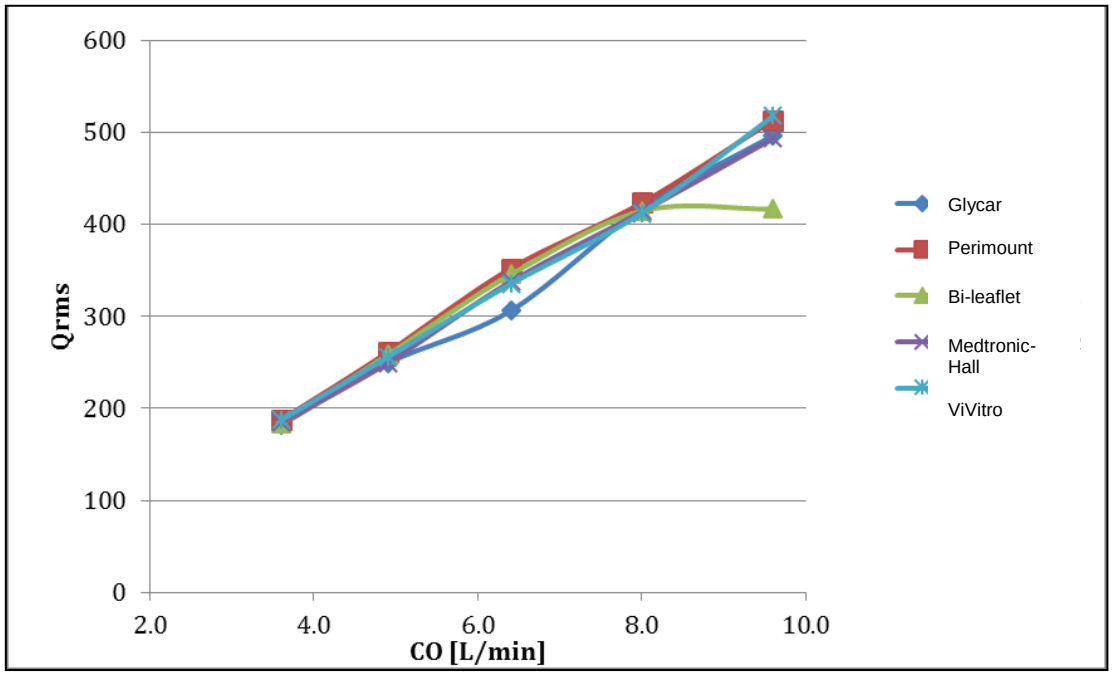

FIGURE 4.20: **The Q_{rms} for each of the valves at different cardiac outputs**. CO = cardiac output; Q_{rms}= total forward flow; L/min=liters per minute (Adapted from Mrs L Thompson-Jooste).

iv. The effective orifice area (EOA)

The EOA was calculated for each valve at increasing CO (Figure 4.21). The EOA cut-off (black line on the graph) is the minimum EOA required to meet ISO 5840:2015 and FDA approval for 21mm heart valves. The data set for the measurements are presented in table 4.6. Ten measurements were taken for each valve during each of the test conditions. The result is presented in figure 4.20.

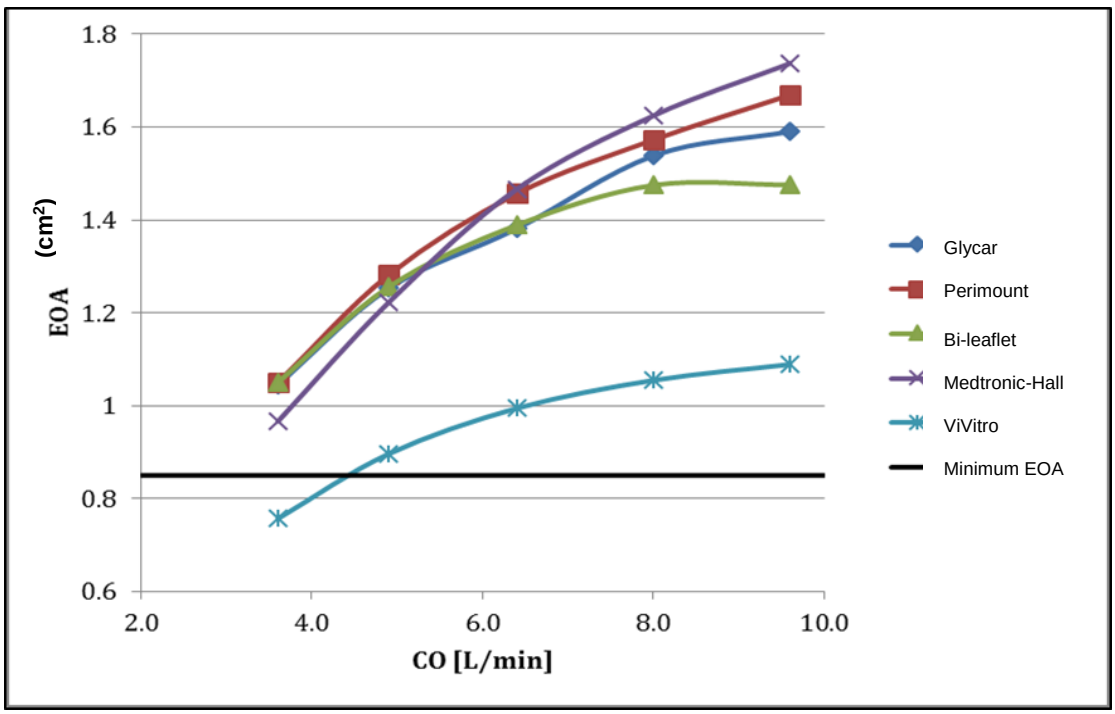

FIGURE 4.21: **Comparison between the EOA and CO.** EOA= effective orifice area; CO= cardiac output; L/min= liter per minute; cm^2= centimeter square (Adapted from Mrs L Thompson-Jooste).

v. Pressure drop (Δp)

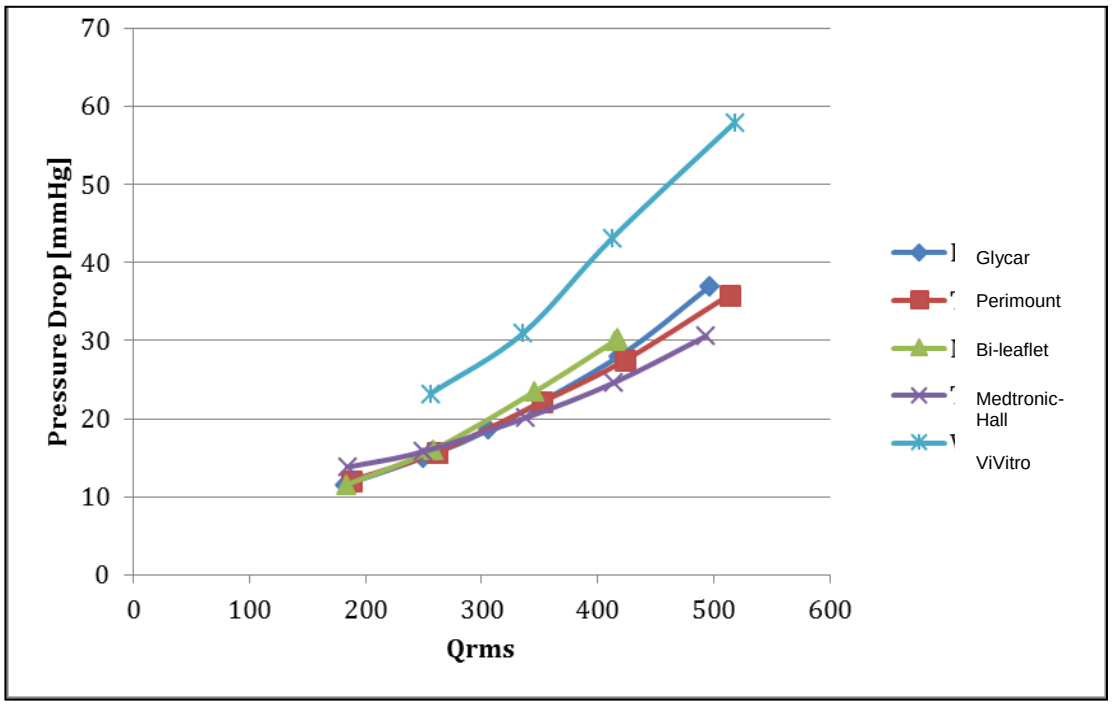

FIGURE 4.22. **Q_{RMS}= total forward flow volume**; mmHg= millimeter mercury (Adapted from Mrs L Thompson-Jooste).

Table 4.6 represents the measured pressure drop across each valve for each of the test conditions. The pressure drop was compared to the Q_{rms} for each of the valves and the results can be examined in figure 4.22. Refer to Figure 4.16 for the pressure drop comparison to the CO for the different testing conditions.

vi. The regurgitant fraction (RF)

The data for the RF during the different testing conditions for each of the valves can be seen in table 4.7 and in figure 4.23. The RF was determined by calculating the closing volume and the stroke volume. By subtracting the closing volume from the stroke volume the RF is determined and this value is represented as a percentage of the stroke volume. Figure 4.23 compares the RF of the different valves during each of the testing conditions.

All the valves performed similarly up to a CO of 8.0 L/min. The RF for the Glycar valve was 10% higher than the maximum value determined by the ISO standard.

Table 4.7: **Regurgitation data during the five test configurations for the different valves.**

Cycle	Glycar valve					Perimount tissue valve					Carbomedics bi-leaflet					Medtronic-Hall					Vivitro				
	R: 60	R: 70	R: 80	R: 100	R: 120	R: 60	R: 70	R: 80	R: 100	R: 120	R: 60	R: 70	R: 80	R: 100	R: 120	R: 60	R: 70	R: 80	R: 100	R: 120	R: 60	R: 70	R: 80	R: 100	R: 120
	Stoke Volume																								
	60	70	80	80	80	60	70	80	80	80	60	70	80	80	80	60	70	80	80	80	60	70	80	80	80
	Closing Volume Percentage Stroke Volume																								
1	5.45%	4.05%	3.20%	8.94%	8.12%	1.28%	0.96%	0.86%	1.00%	0.89%	1.94%	1.17%	1.76%	1.28%	1.05%	4.69%	3.05%	2.64%	2.87%	2.09%	0.02%	0.04%	0.14%	0.64%	0.72%
2	5.49%	4.10%	3.31%	8.76%	7.44%	1.33%	1.03%	0.75%	0.84%	0.67%	2.36%	1.53%	1.01%	2.79%	0.79%	3.25%	3.08%	2.83%	3.74%	2.43%	0.04%	0.10%	0.18%	0.40%	0.75%
3	4.84%	3.63%	3.04%	9.13%	7.92%	1.31%	1.05%	0.82%	1.00%	1.16%	1.59%	1.60%	2.02%	1.15%	1.48%	3.60%	3.97%	2.91%	2.56%	3.26%	0.08%	0.11%	0.15%	0.45%	0.81%
4	5.55%	4.14%	3.59%	8.91%	8.75%	1.07%	0.81%	0.71%	1.04%	0.90%	1.89%	1.64%	0.88%	1.07%	1.78%	3.79%	1.97%	2.84%	2.99%	3.84%	0.04%	0.12%	0.34%	0.51%	0.76%
5	5.06%	4.09%	3.22%	9.50%	7.93%	1.14%	0.82%	0.77%	0.83%	0.62%	2.98%	1.72%	0.95%	1.57%	1.40%	4.10%	3.20%	3.53%	3.88%	2.40%	0.03%	0.04%	0.28%	0.39%	0.90%
6	4.66%	3.90%	3.05%	9.99%	8.15%	1.11%	0.94%	0.97%	1.05%	0.98%	1.91%	2.36%	1.30%	1.37%	1.79%	3.83%	3.36%	2.74%	2.93%	2.22%	0.08%	0.11%	0.23%	0.52%	0.99%
7	4.48%	3.92%	3.37%	9.15%	7.46%	0.94%	1.13%	0.97%	0.89%	0.97%	2.54%	1.40%	1.33%	0.63%	2.69%	4.78%	3.20%	3.85%	2.58%	1.62%	0.04%	0.10%	0.25%	0.69%	0.97%
8	5.00%	4.29%	2.88%	9.45%	7.54%	1.02%	1.12%	0.94%	0.34%	0.97%	2.19%	1.86%	1.41%	1.79%	1.59%	3.18%	4.14%	2.52%	2.84%	1.97%	0.03%	0.14%	0.22%	0.48%	0.75%
9	5.13%	4.00%	3.55%	9.70%	8.14%	1.24%	1.12%	0.74%	0.98%	1.02%	1.87%	1.70%	2.05%	2.20%	1.70%	3.64%	4.09%	3.65%	2.51%	2.32%	0.06%	0.12%	0.23%	0.47%	0.71%
10	4.69%	3.61%	2.80%	9.00%	9.55%	1.31%	1.07%	0.85%	0.70%	0.80%	1.49%	1.07%	0.90%	2.12%	1.81%	4.01%	2.10%	2.68%	3.16%	3.03%	0.10%	0.16%	0.31%	0.41%	0.91%
Ave	5.03%	3.97%	3.20%	9.25%	8.10%	1.17%	1.01%	0.84%	0.87%	0.90%	2.07%	1.61%	1.36%	1.60%	1.61%	3.89%	3.22%	3.02%	3.01%	2.52%	0.05%	0.11%	0.23%	0.49%	0.83%
SD	0.00374	0.00216	0.00263	0.00392	0.00646	0.00137	0.0012	0.00096	0.00216	0.00165	0.00452	0.00362	0.0045	0.00637	0.00509	0.00532	0.00748	0.00474	0.00473	0.00669	0.00026	0.0004	0.00064	0.00101	0.00106
	Leakage Volume Percentage Stroke Volume																								
1	3.44%	2.25%	2.08%	1.81%	1.32%	2.23%	1.81%	1.72%	1.49%	1.54%	5.08%	3.75%	2.42%	2.58%	1.85%	4.58%	3.69%	2.42%	1.73%	1.63%	0.18%	0.23%	0.64%	0.43%	0.47%
2	2.30%	2.14%	1.00%	1.78%	2.17%	2.93%	1.51%	1.59%	1.96%	1.62%	4.85%	4.05%	3.02%	3.05%	2.43%	4.96%	2.41%	3.02%	3.29%	2.73%	0.94%	0.68%	0.45%	0.72%	0.45%
3	2.95%	1.61%	1.72%	1.29%	1.13%	1.75%	1.76%	2.02%	1.14%	2.40%	5.04%	3.43%	2.81%	2.74%	2.58%	3.66%	1.86%	2.19%	1.37%	2.75%	1.55%	0.73%	0.33%	0.33%	0.57%
4	2.67%	1.74%	1.72%	1.70%	1.56%	2.25%	1.42%	2.61%	1.36%	2.02%	5.86%	3.89%	2.08%	2.68%	2.11%	3.23%	2.24%	2.39%	2.21%	2.26%	1.03%	1.16%	0.58%	0.45%	0.44%
5	1.93%	2.12%	1.47%	1.58%	1.60%	2.56%	1.56%	1.94%	1.64%	1.79%	3.12%	4.15%	2.61%	2.82%	2.68%	5.61%	2.32%	3.20%	2.81%	2.03%	0.54%	0.94%	0.67%	0.57%	1.05%
6	2.43%	1.28%	1.30%	0.99%	1.56%	2.95%	1.55%	1.28%	1.19%	1.79%	4.29%	3.42%	2.55%	2.19%	2.01%	5.05%	2.48%	1.88%	1.42%	1.79%	0.88%	1.11%	0.87%	0.46%	0.67%
7	2.30%	1.83%	1.53%	0.95%	1.13%	1.59%	2.59%	1.99%	2.20%	2.54%	4.51%	3.73%	2.25%	2.04%	1.75%	4.18%	1.71%	1.81%	2.48%	4.91%	0.23%	0.43%	0.47%	0.66%	0.76%
8	2.22%	2.12%	1.24%	1.19%	1.40%	2.08%	2.10%	1.81%	2.39%	3.31%	4.66%	5.12%	3.22%	1.62%	2.07%	4.07%	2.34%	2.68%	1.72%	2.15%	1.04%	1.02%	0.73%	0.80%	0.51%
9	2.58%	2.12%	1.97%	0.80%	1.45%	1.79%	1.76%	1.50%	1.31%	1.94%	4.13%	3.23%	2.72%	1.56%	2.01%	4.72%	2.19%	1.69%	2.51%	2.38%	0.76%	0.36%	1.33%	0.65%	0.98%
10	2.78%	0.99%	1.74%	3.10%	1.26%	3.51%	1.75%	1.47%	2.57%	1.67%	5.00%	4.88%	2.48%	4.13%	3.12%	5.28%	2.39%	2.00%	2.37%	3.30%	1.35%	1.13%	0.56%	0.57%	0.59%
Ave	2.56%	1.82%	1.58%	1.52%	1.46%	2.37%	1.78%	1.79%	1.72%	2.06%	4.65%	3.96%	2.62%	2.54%	2.26%	4.53%	2.36%	2.33%	2.19%	2.59%	0.85%	0.78%	0.66%	0.56%	0.65%
SD	0.00427	0.0042	0.00334	0.00664	0.00302	0.00619	0.00344	0.00377	0.0052	0.00545	0.00725	0.00617	0.00343	0.00754	0.00429	0.00745	0.00527	0.00514	0.00623	0.00952	0.00442	0.00345	0.0028	0.00145	0.00217
	Regurgitation as Percentage of Stroke Volume																								
1	8.89%	6.30%	5.28%	10.75%	9.44%	3.51%	2.77%	2.58%	2.49%	2.43%	7.02%	4.92%	4.18%	3.86%	2.91%	9.27%	6.73%	5.06%	4.60%	3.71%	0.20%	0.27%	0.79%	1.07%	1.20%
2	7.79%	6.24%	4.31%	10.54%	9.61%	4.26%	2.54%	2.34%	2.81%	2.29%	7.22%	5.57%	4.03%	5.84%	3.21%	8.21%	5.49%	5.85%	7.03%	5.16%	0.98%	0.78%	0.63%	1.11%	1.19%
3	7.79%	5.25%	4.76%	10.41%	9.05%	3.05%	2.81%	2.83%	2.13%	3.57%	6.63%	5.02%	4.84%	3.89%	4.06%	7.26%	5.83%	5.10%	3.93%	6.01%	1.63%	0.84%	0.48%	0.78%	1.37%
4	8.22%	5.88%	5.31%	10.61%	10.31%	3.32%	2.23%	3.33%	2.40%	2.92%	7.75%	5.53%	2.96%	3.74%	3.88%	7.02%	4.21%	5.23%	5.20%	6.10%	1.08%	1.28%	0.91%	0.96%	1.20%
5	7.00%	6.21%	4.69%	11.08%	9.52%	3.70%	2.38%	2.72%	2.47%	2.41%	6.09%	5.87%	3.56%	4.39%	4.08%	9.71%	5.52%	6.73%	6.69%	4.43%	0.57%	0.98%	0.95%	0.96%	1.95%
6	7.09%	5.18%	4.35%	10.98%	9.71%	4.06%	2.50%	2.25%	2.23%	2.77%	6.19%	5.78%	3.85%	3.56%	3.80%	8.88%	5.83%	4.62%	4.35%	4.01%	0.96%	1.23%	1.10%	0.97%	1.66%
7	6.78%	5.75%	4.90%	10.10%	8.60%	2.53%	3.73%	2.96%	3.09%	3.51%	7.06%	5.13%	3.59%	2.67%	4.44%	8.96%	4.91%	5.66%	5.06%	6.53%	0.27%	0.54%	0.72%	1.35%	1.73%
8	7.22%	6.40%	4.12%	10.64%	8.95%	3.10%	3.22%	2.75%	2.72%	4.28%	6.85%	6.98%	4.63%	3.41%	3.66%	7.26%	6.48%	5.20%	4.56%	4.12%	1.07%	1.16%	0.95%	1.28%	1.26%
9	7.71%	6.12%	5.52%	10.50%	9.60%	3.04%	2.88%	2.24%	2.28%	2.96%	6.00%	4.93%	4.78%	3.75%	3.71%	8.37%	6.28%	5.34%	5.02%	4.70%	0.82%	0.48%	1.57%	1.12%	1.69%
10	7.47%	4.59%	4.54%	12.10%	10.81%	4.82%	2.82%	2.32%	3.27%	2.47%	6.49%	5.95%	3.38%	6.25%	4.92%	9.29%	4.50%	4.67%	5.53%	6.33%	1.44%	1.29%	0.87%	0.98%	1.50%
Ave	7.60%	5.79%	4.78%	10.77%	9.56%	3.54%	2.79%	2.63%	2.59%	2.96%	6.73%	5.57%	3.98%	4.14%	3.87%	8.42%	5.58%	5.35%	5.20%	5.11%	0.90%	0.88%	0.90%	1.06%	1.47%
SD	0.0063	0.00599	0.00471	0.00542	0.00645	0.00685	0.00435	0.00355	0.00375	0.00644	0.00554	0.00631	0.00632	0.01098	0.00572	0.00963	0.00834	0.00616	0.00991	0.01058	0.0046	0.00365	0.00295	0.00167	0.0027

R= rate; Ave= average; SD= standard deviation

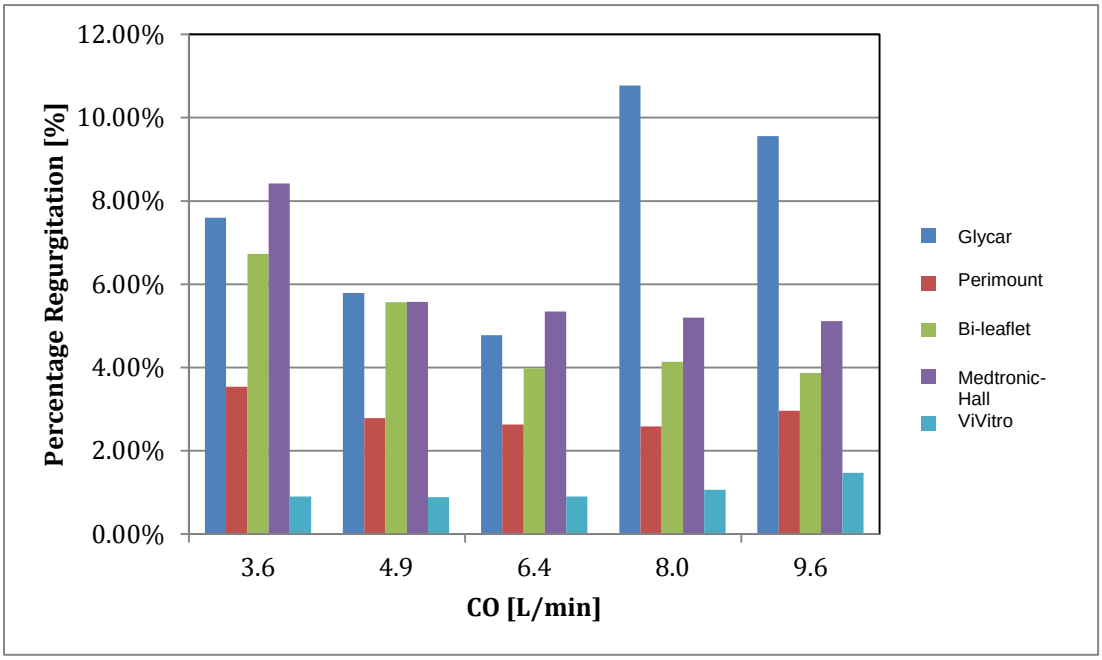

FIGURE 4.23: **The percentage regurgitation for the different valves with increasing CO**. CO= cardiac output; L/min= liter per minute (Adapted from Mrs L Thompson-Jooste).

vii. Transvalvular energy losses

The forward energy loss, the closing energy and the leakage energy for each cycle are shown in table 4.8 below.

Figure 4.25 compares the closing energy valves under the testing conditions. Figure 4.26 reflects the energy loss due to regurgitant back flow of each of the valves.

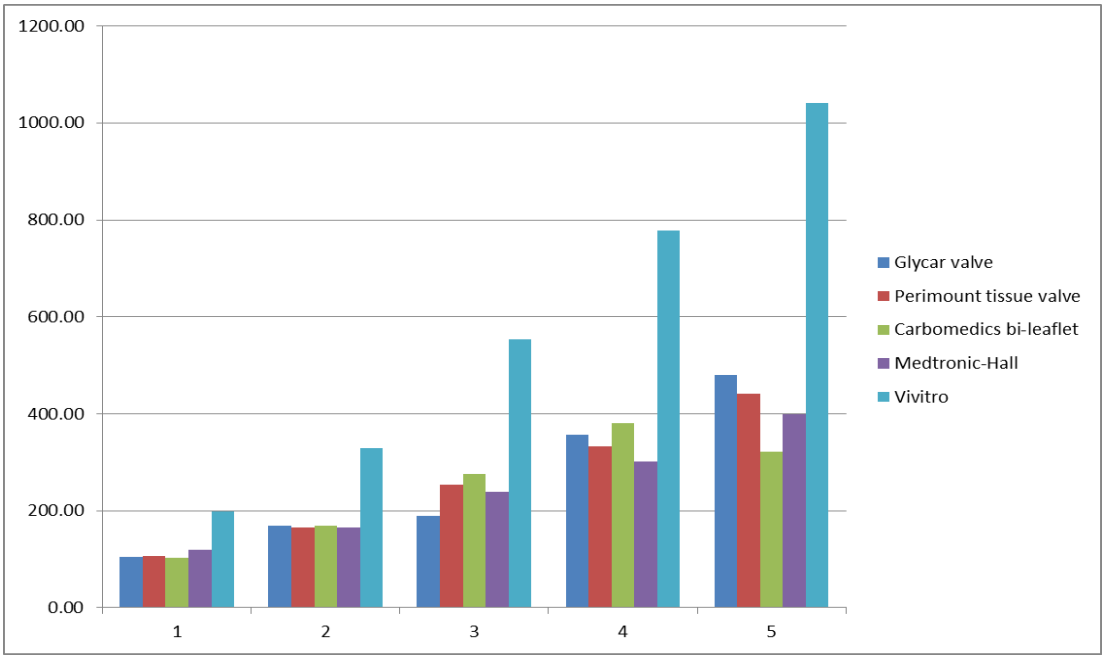

FIGURE 4.24: **The forward energy losses for each of the test valves during each of the testing conditions in milli Joule.** 1 = 3.6 L/min, 2 = 4.9 L/min, 3= 6.4 L/min, 4 = 8.0 L/min, 5= 9.6 L/min (Adapted from Mrs L Thompson-Jooste).

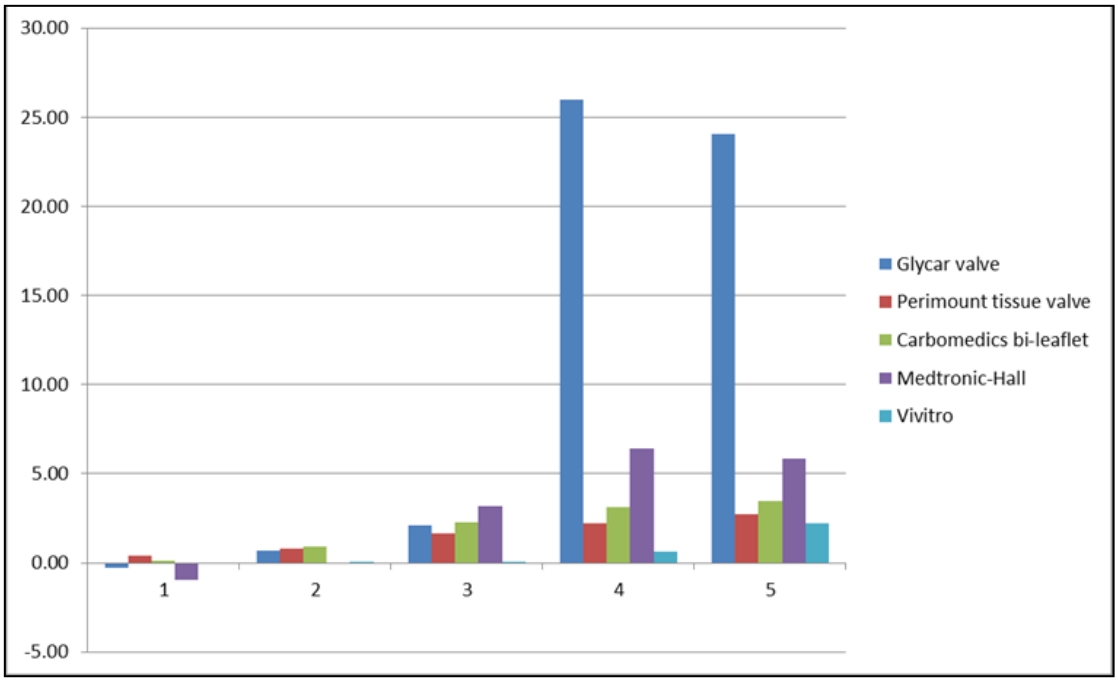

FGURE 4.25: **The closing energy needed for each of the valves during the test conditions**. mJ= millijoule, 1 = 3.6 L/min, 2 = 4.9 L/min, 3= 6.4 L/min, 4 = 8.0 L/min, 5= 9.6 L/min (Adapted from Mrs L Thompson-Jooste).

TABLE 4.8: **The energy losses for each of the valves during the test conditions.**

Cycle	Glycar valve					Perimount tissue valve					Carbomedics bi-leaflet					Medtronic-Hall					Vivitro				
	R: 60	R: 70	R: 80	R: 100	R: 120	R: 60	R: 70	R: 80	R: 100	R: 120	R: 60	R: 70	R: 80	R: 100	R: 120	R: 60	R: 70	R: 80	R: 100	R: 120	R: 60	R: 70	R: 80	R: 100	R: 120
Forward Energy [mj]																									
1	103.93	168.62	191.03	360.61	482.86	106.48	165.44	253.30	338.64	442.39	103.57	168.66	279.22	379.26	321.06	118.81	168.01	242.70	301.48	407.17	205.11	339.14	568.41	778.65	1054.13
2	105.27	169.27	191.15	355.99	487.76	105.60	166.00	254.03	326.85	431.53	102.71	170.23	275.82	380.23	321.98	119.33	164.57	238.31	309.81	393.15	193.81	322.87	560.53	778.81	1033.04
3	105.25	169.16	191.14	357.93	486.74	105.88	165.59	256.36	330.14	449.54	103.16	168.87	271.97	383.07	322.82	119.78	160.90	234.35	301.43	385.37	193.80	329.39	552.35	778.08	1030.34
4	105.24	167.81	190.60	354.61	482.47	106.69	166.52	252.61	331.09	440.98	104.01	168.99	268.41	381.45	324.06	115.87	168.75	233.95	294.24	398.34	200.93	329.65	553.55	778.01	1050.85
5	104.79	168.67	189.22	360.42	485.60	103.96	166.57	252.00	323.74	450.11	103.25	169.12	277.51	375.37	321.31	117.85	157.68	240.18	307.10	397.37	197.33	325.24	560.15	774.51	1041.20
6	105.14	167.95	189.39	355.93	476.67	106.21	166.81	256.38	337.43	447.45	103.30	168.45	277.19	382.23	324.45	119.23	156.25	237.62	302.29	405.48	200.41	320.98	556.36	768.79	1055.80
7	105.60	169.64	189.58	356.20	477.69	106.27	164.59	241.41	330.54	439.81	103.45	170.52	276.13	382.16	324.02	118.61	168.23	241.21	293.75	395.62	191.10	327.88	543.12	780.58	1032.51
8	104.90	169.52	183.22	351.38	483.17	106.31	164.07	255.52	336.34	439.84	102.79	169.24	282.11	383.32	321.22	119.64	165.84	240.78	306.53	401.44	192.50	331.21	547.60	781.05	1038.82
9	104.18	164.37	192.33	358.50	471.96	106.58	165.86	254.62	339.74	441.78	103.58	169.34	271.54	381.55	323.78	120.17	168.66	240.10	304.98	397.63	203.80	334.68	550.05	774.37	1025.51
10	103.88	169.53	190.82	358.29	471.24	105.85	166.51	254.65	326.01	434.89	102.60	167.61	272.04	380.71	317.33	118.06	170.92	240.98	298.12	401.66	203.42	326.93	548.95	782.28	1049.03
Ave	104.82	168.45	189.85	356.99	480.62	105.98	165.80	253.09	332.05	441.83	103.24	169.10	275.20	380.94	322.20	118.74	164.98	239.02	301.97	398.32	198.22	328.80	554.11	777.51	1041.12
SD	0.61	1.57	2.52	2.78	5.92	0.79	0.90	4.36	5.67	5.99	0.44	0.84	4.14	2.32	2.15	1.25	5.05	2.94	5.38	6.27	5.17	5.39	7.43	3.99	10.78
Closing Energy [mj]																									
1	-0.46	0.66	2.22	25.14	23.89	0.35	0.58	1.69	2.64	2.82	0.15	0.67	2.76	1.99	2.20	-1.31	-0.05	2.94	6.26	4.50	0.11	0.02	0.04	0.79	1.85
2	-0.13	0.58	2.01	24.79	21.48	0.41	0.77	1.45	2.06	1.47	0.17	1.10	1.72	6.02	1.78	-0.83	0.18	3.24	8.08	5.53	-0.03	-0.05	0.06	0.48	2.02
3	-0.31	0.75	2.07	24.85	23.24	0.48	0.81	1.57	2.72	4.40	0.20	0.82	3.04	2.38	2.69	-0.67	-0.20	3.15	5.19	7.58	-0.05	-0.03	0.04	0.61	2.20
4	-0.09	0.61	2.30	25.51	26.36	0.35	0.69	1.43	2.73	2.40	0.01	0.96	1.63	1.96	4.19	-0.84	0.35	2.95	6.72	9.77	-0.03	-0.05	0.11	0.57	2.00
5	-0.44	0.48	2.15	26.83	22.98	0.34	0.56	1.48	2.05	1.52	0.20	1.09	1.60	2.77	2.82	-1.19	-0.05	3.42	8.18	5.41	0.17	0.53	0.12	0.43	2.28
6	-0.20	0.61	2.04	28.28	25.63	0.44	0.82	1.92	2.84	3.09	0.19	0.98	2.31	2.98	3.73	-0.94	0.04	2.88	6.28	5.04	-0.06	-0.06	0.05	0.67	2.73
7	-0.20	0.70	2.14	25.94	21.75	0.36	0.96	1.97	2.52	3.06	0.23	0.95	2.25	1.10	6.10	-1.45	0.01	3.61	5.61	3.42	-0.03	-0.06	0.04	0.90	2.73
8	-0.28	0.79	1.90	26.62	21.53	0.37	0.90	1.90	0.41	3.25	0.18	0.88	2.42	3.88	3.66	-0.72	-0.43	2.79	5.94	4.68	-0.03	-0.03	0.05	0.60	1.93
9	-0.33	0.97	2.20	27.00	23.47	0.47	0.98	1.43	2.41	3.19	0.22	0.94	3.14	4.73	3.71	-0.87	-0.13	3.89	5.41	5.47	-0.02	-0.06	0.10	0.65	2.12
10	-0.31	0.77	1.73	25.02	30.03	0.42	0.88	1.63	1.96	2.20	-0.35	0.68	1.65	3.61	3.55	-1.02	0.21	3.01	6.44	7.05	-0.06	-0.07	0.08	0.49	2.46
Ave	-0.28	0.69	2.08	26.00	24.04	0.40	0.79	1.65	2.23	2.74	0.12	0.91	2.25	3.14	3.44	-0.98	-0.01	3.19	6.41	5.84	0.00	0.01	0.07	0.62	2.23
SD	0.12	0.14	0.17	1.15	2.67	0.05	0.15	0.21	0.71	0.88	0.18	0.15	0.59	1.46	1.21	0.26	0.22	0.36	1.02	1.83	0.08	0.18	0.03	0.14	0.32
Leakage Energy [mj]																									
1	18.82	11.78	15.86	14.19	4.81	7.16	4.97	7.57	2.82	-0.48	28.47	25.35	19.90	24.52	15.31	24.35	21.79	16.44	15.71	19.78	-14.57	-18.02	1.54	-5.87	-21.09
2	9.10	10.68	-0.84	9.62	14.26	14.88	3.59	8.46	11.18	10.14	27.50	28.21	23.89	27.27	25.54	26.18	11.60	19.44	26.72	20.18	-7.14	-4.44	-8.36	-4.84	-20.15
3	14.39	4.61	8.98	5.86	0.12	0.84	4.97	13.22	-0.50	18.21	28.00	22.04	21.34	25.74	23.79	18.92	7.86	15.02	1.93	31.91	0.37	-5.90	-11.10	-3.40	-2.49
4	13.67	5.15	11.77	11.25	8.36	8.48	-0.57	18.67	-2.13	12.85	32.09	28.02	12.45	28.11	20.53	17.31	6.97	17.91	17.28	21.27	-3.06	-3.87	-3.20	-12.83	-4.59
5	6.79	9.97	4.07	9.17	4.20	11.26	-0.94	9.74	10.51	16.11	16.38	27.72	20.21	26.02	27.11	29.22	6.61	23.82	22.64	20.82	-6.15	-9.87	-8.76	-14.15	5.37
6	11.69	0.09	3.34	0.33	6.14	12.44	-4.25	-3.56	-1.34	9.50	24.74	21.21	18.22	13.76	19.92	27.07	15.01	4.27	5.82	14.00	-10.21	-2.31	-15.59	-3.45	-14.01
7	7.50	9.66	8.49	-1.61	3.29	-2.87	16.21	9.23	13.68	24.72	25.48	26.96	18.53	17.33	15.38	22.80	7.51	12.18	22.67	50.48	-16.64	-8.10	-13.01	-2.81	-9.14
8	11.01	8.32	-1.36	6.20	-1.93	9.01	8.60	10.31	16.44	27.12	26.73	36.68	26.55	13.13	18.97	21.66	9.40	20.92	15.20	24.71	-2.72	-0.76	-7.13	-8.33	-11.93
9	11.04	12.91	16.46	-3.52	-7.47	3.14	1.00	5.14	-5.41	7.98	24.65	19.31	17.26	7.69	21.49	24.82	7.81	14.37	18.29	27.17	-5.25	-16.45	-2.06	-5.00	0.38
10	13.83	-5.78	10.71	20.08	1.61	16.67	1.07	8.59	19.85	9.99	28.49	35.61	16.50	35.51	27.15	27.26	10.13	12.49	21.77	39.93	-4.88	-2.26	-16.47	-7.35	-13.12
Average	11.78	6.74	7.75	7.16	3.34	8.10	3.47	8.74	6.51	13.61	26.25	27.11	19.49	21.91	21.52	23.96	10.47	15.69	16.80	27.03	-7.02	-7.20	-8.41	-6.80	-9.08
Standard I	3.59	5.86	6.31	7.33	5.90	6.22	5.78	5.66	8.86	8.21	4.11	5.68	3.94	8.54	4.35	3.81	4.73	5.46	7.74	10.99	5.34	5.97	5.90	3.94	8.68

R= rate; Ave= average; SD= standard deviation; mJ= millijoule.

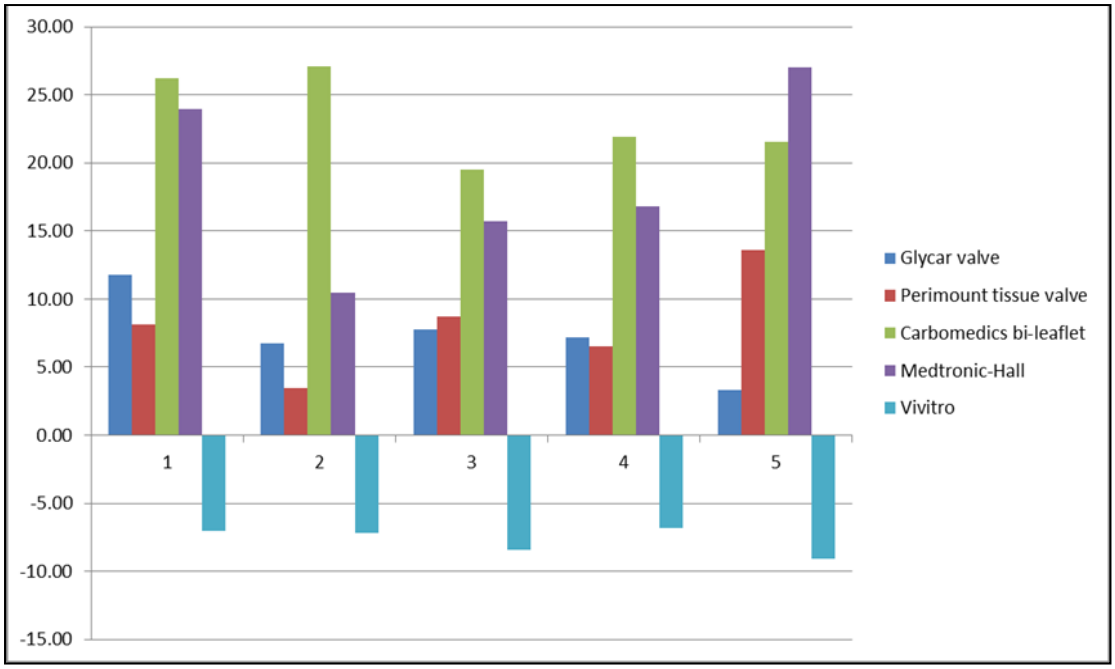

FIGURE 4.26: **The total energy loss for each of the valves because of regurgitation during the test conditions.** 1 = 3.6 L/min, 2 = 4.9 L/min, 3= 6.4 L/min, 4 = 8.0 L/min, 5= 9.6 L/min, mJ= millijoule (Adapted from Mrs L Thompson-Jooste).

viii. Comparative analysis between the Carbomedics bi-leaflet valve and the Glycar valve

Figure 4.27 represents a comparison of the pressure drop (gradient) across the Glycar valve and the Carbomedics bi-leaflet valve in the aortic position. At a CO of 3.6 L/min the gradient for both valves was 12 mmHg. At a CO of 4.9 L/min the gradient was 15 mmHg for the Glycar valve and 16 mmHg for the Carbomedics valve, at 8.0 L/min the gradient was 28 mmHg and 30 mmHg respectively. At a CO of 9.6 L/min the gradient of the Glycar valve was 37 mmHg compared to 30 mmHg of the Carbomedics valve.

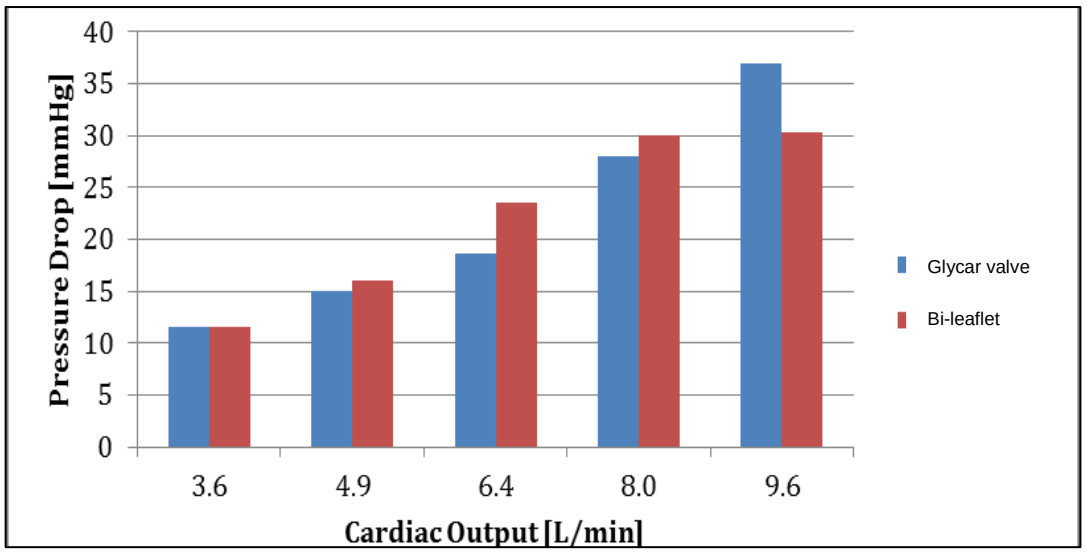

FIGURE 4.27: **Mean pressure difference plotted against the CO for the Glycar and Carbomedics valve**. mmHg = millimeter mercury; L/min = liter per minute.

The Q_{rms} for the different stroke rates (CO) was calculated for the Glycar and Carbomedics valves and the comparison is represented in figure 4.28. Throughout the cardiac cycle the Q_{rms} for both the valves was comparative up to 8.0 L/min.

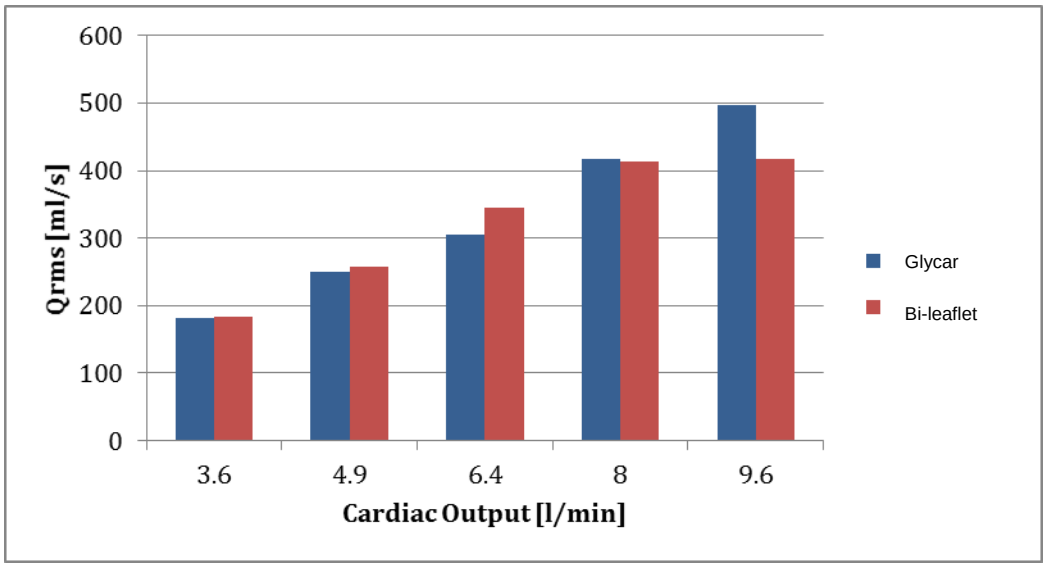

FIGURE 4.28: **Calculated Q_{rms} flow rate for each type of valve plotted against CO for the Glycar and Carbomedics valve.** Q_{rms}= total forward flow volume, L/min= liter per minute, ml/s= milliliter per second.

A closing volume comparison was made between the poppet and the bi-leaflet and the data are summarised in figure 2.29. The Glycar valve had a higher closing volume (regurgitant flow) than the bi-leaflet valve design at a CO greater than 8.0 L/min.

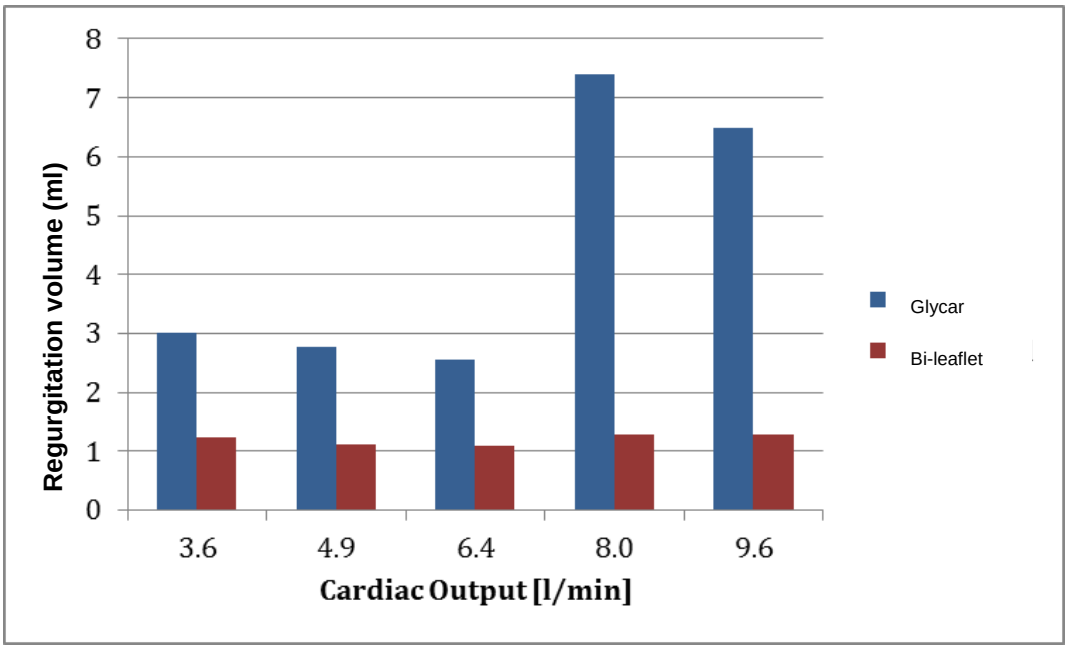

FIGURE 4.29: **Calculated closing volume for the Glycar and the bi-leaflet valve plotted against CO for the Glycar and Carbomedics valve.** ml= milliliter; L/min= liter per minute.

The regurgitant volume is seen in figure 4.30 which represents the volume loss once the valve is in the closed position for each of the testing conditions. Note the extremely low leakage volume for the Glycar valve of 1.25 to 1.55 ml.

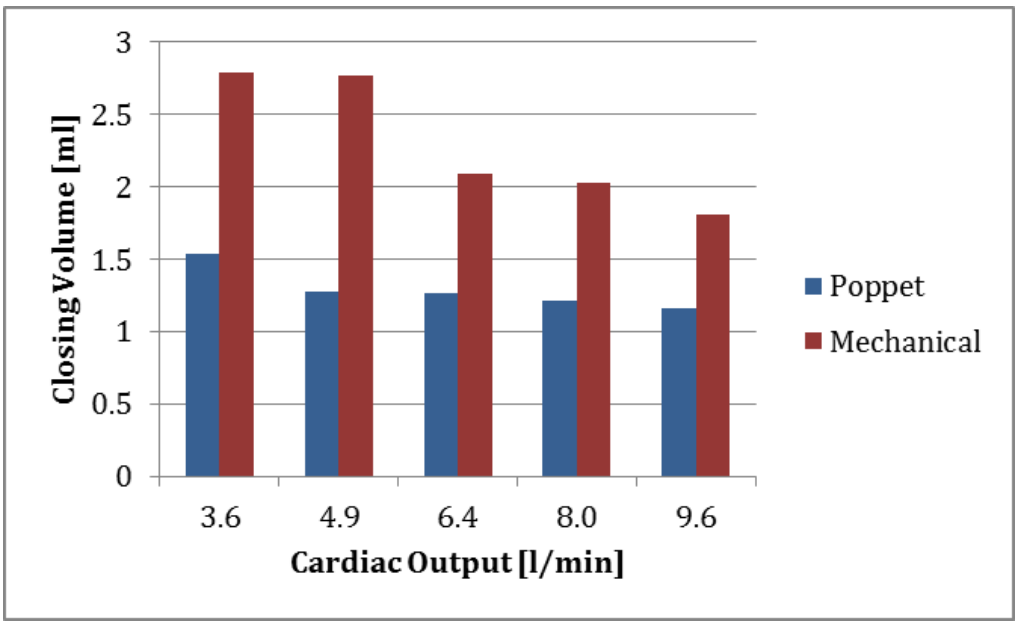

FIGURE 4.30: **Calculated leakage volume for each type of valve plotted against CO.** ml= milliliter; L/min= liter per minute.

4.3 Phase III: The *in* vivo evaluation of the Glycar valve

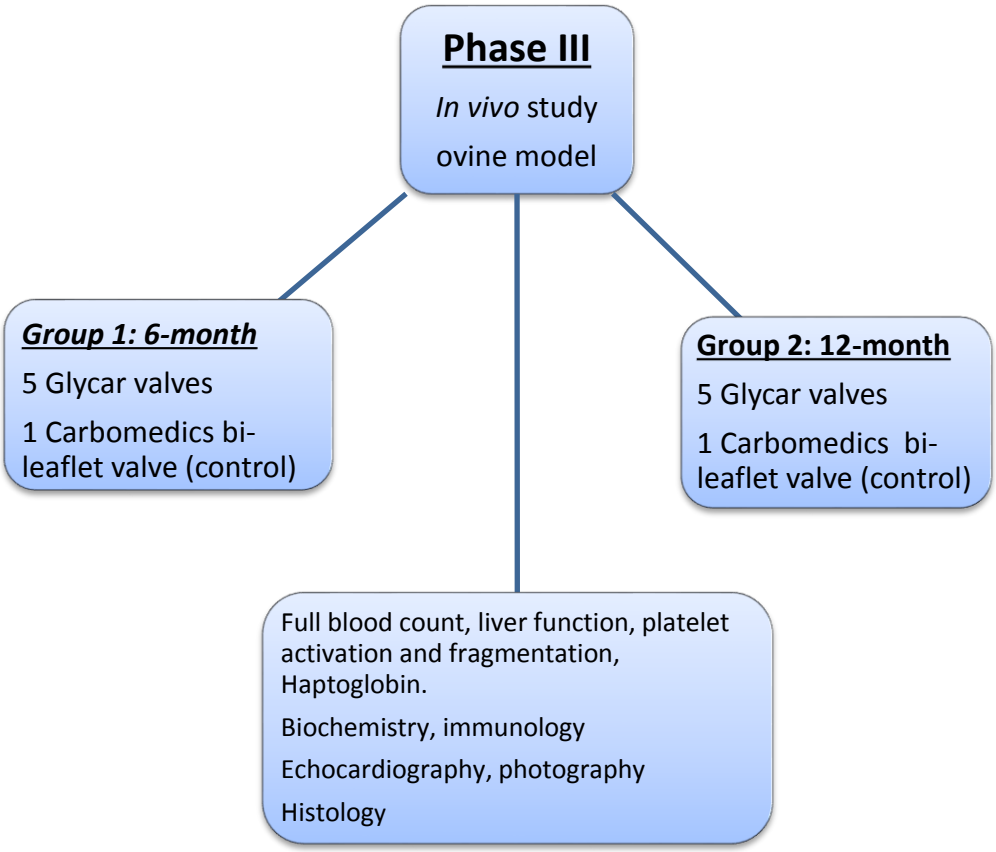

Results are presented chronologically, that is in the order that samples were obtained or tests performed during the study cycle. In the first group, which was the short term follow-up group, the sheep were sacrificed at six months. This group consisted of six sheep with five sheep receiving the 21 mm Glycar valve and one sheep receiving a 21 mm Carbomedics bi-leaflet valve as the control. The second group duplicated the first group but was sacrificed at one year after implantation.

In both groups there was one mortality (17%), both of which were Glycar valves. In both of the cases death occurred secondary to infective endocarditis. A post mortem was performed in each case and the results are portrayed in the respective groups in the results section. Haemodynamic and serology were not obtained from these animals at post mortem as it were futile during necropsy.

4.3.1 Results: Short term follow-up (six months)

i. Valve photography

a. Carbomedics valve

During pre-anaesthesia the sheep was evaluated and found to be clinically in perfect health with no pulmonary or cardiac pathology. During dissection there were small bilateral pleural effusions, a small pericardial effusion and no ascites. On cut sections the lungs were normal with no signs of macroscopic emboli.

Proximal: Viewing the valve from the RVOT

The valve was normal with clean leaflets and unimpeded motion as well as no visible macroscopic clots. The sewing cuff was normal with no thrombi adhered to the material. There were areas where incomplete covering of the sewing cuff was noted but it did not lead to thrombus formation. There was no pannus either. Viewing the valve from the RVOT (figures 4.31 and 4.32) no visible clots were observed and the hinge mechanism was clear. The housing was free of pannus. The following photos demonstrate the Carbomedics valve during explantation.

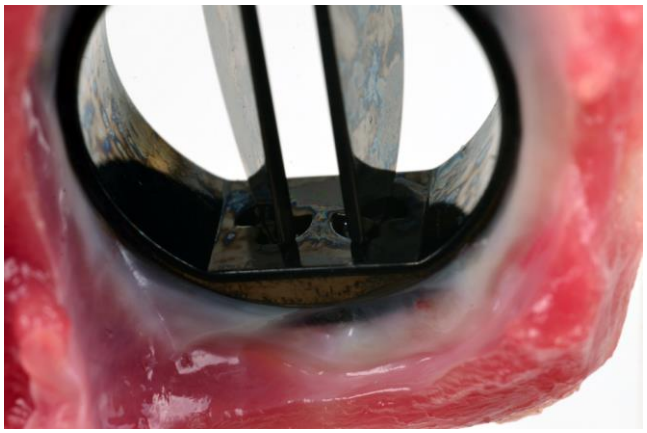

FIGURE 4.31: **The Carbomedics valve viewed from the RVOT**

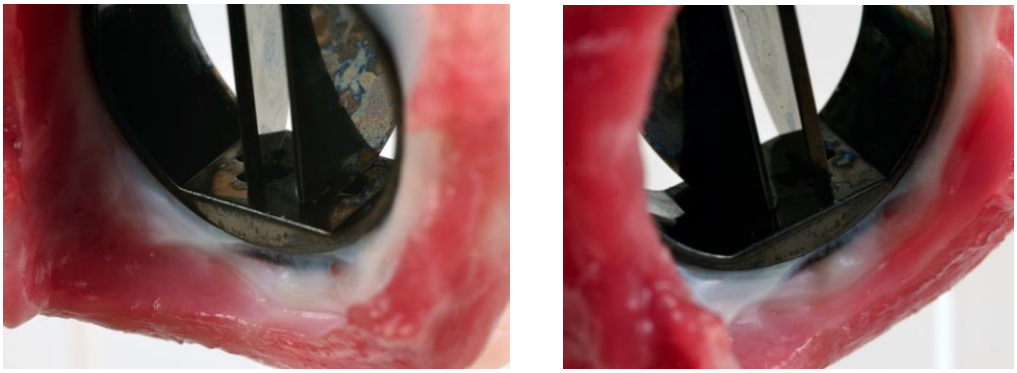

FIGURE 4.32: **The hinge mechanism viewed from different angles from the RVOT.**

Distal: Viewing the valve from the pulmonary artery.

FIGURE 4.33: **The Carbomedics valve seen from the PA.** The valve in the closed position (left) and in the open position (right). The valve is obscured in the right upper border by native pulmonary artery captured in the photo (the valve in this area was clear of any tissue).

The valve viewed from the pulmonary artery side can be seen in figures 4.33 and 4.34. As with the proximal RVOT view no pannus can be seen. There is incomplete healing along the sewing cuff but there were no visible thrombi. The leaflet motion was unimpeded and clear of any pathology. The hinge mechanism was pristine even though the sheep had no anti-coagulation during the test interval of six months.

FIGURE 4.34: **The hinge mechanism of the Carbomedics valve from different angles viewed from the PA.**

b. Glycar valves

Except for the sheep that developed infective endocarditis, all of the other sheep were in perfect health. None of the sheep were in clinical cardiac failure or in respiratory distress. There were no incidents during the six-month follow-up period, even though none of the sheep had received anti-coagulation. Each one of the valves in this study group is shown below in order of sacrifice. As can be seen from the photographs the poppet, the housing, the struts and restraining ring and all of the surfaces are free of thrombus. Potential problem areas will be highlighted at the end of this section. (FCTV referes to the sheep number in the study, refer to Table 4.11 and 4.15)

Viewing the valves in order of sacrifice:

As can be appreciated from the following photographs (figure 4.35 to 4.38) of explanted Glycar valves at six months, there was no major pathology. All of the valves were clean of any clot or thrombi. The poppets functioned perfectly normal and there was no problematic pannus overgrowth. Healing between the sewing cuff in most of the cases was very good. Where the sewing cuff was not fully covered, there were no thrombi visible.

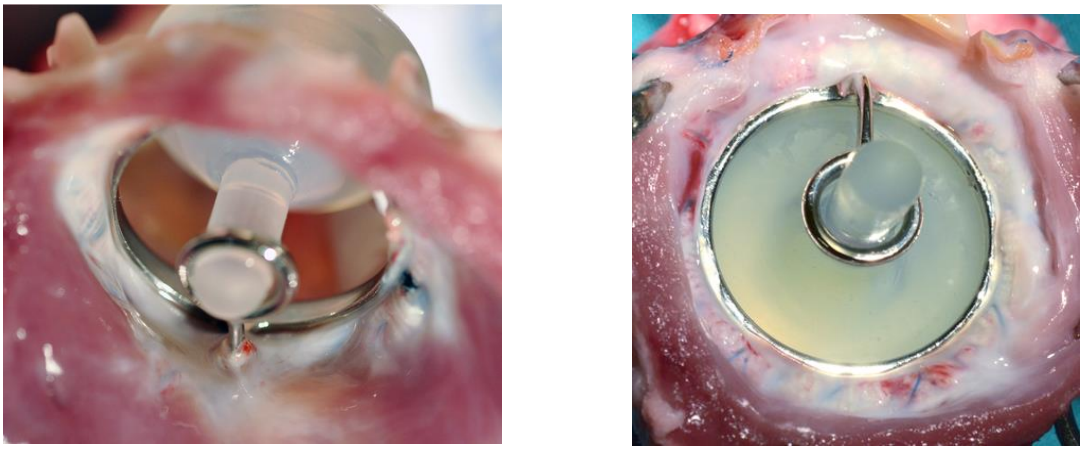

FIGURE 4.35: **Explanted Glycar valve FCTV 6 viewed from the RVOT**. The silicone poppet had no visible cracks or signs of frictional wear. There was no impact damage to the proximal poppet near the housing or the restraing ring. Notice the pannus on the housing on the RVOT side of the valve (left photo).

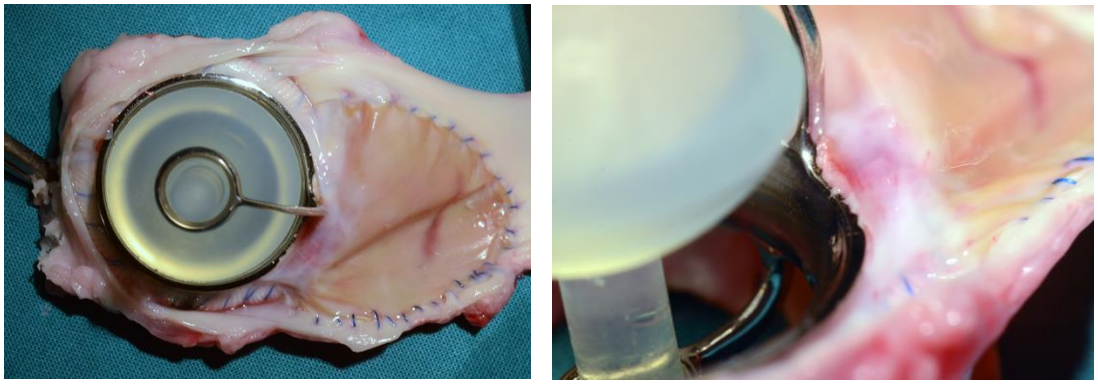

FIGURE 4.36: **The Glycar valve, FCTV 10 seen from the PA**. Note the pericardial patch on the side of the guiding strut. The photo on the right concentrates on the healing between the pericardial patch, the sewing cuff and the native PA. No contact damage was visible on the pericardial patch.

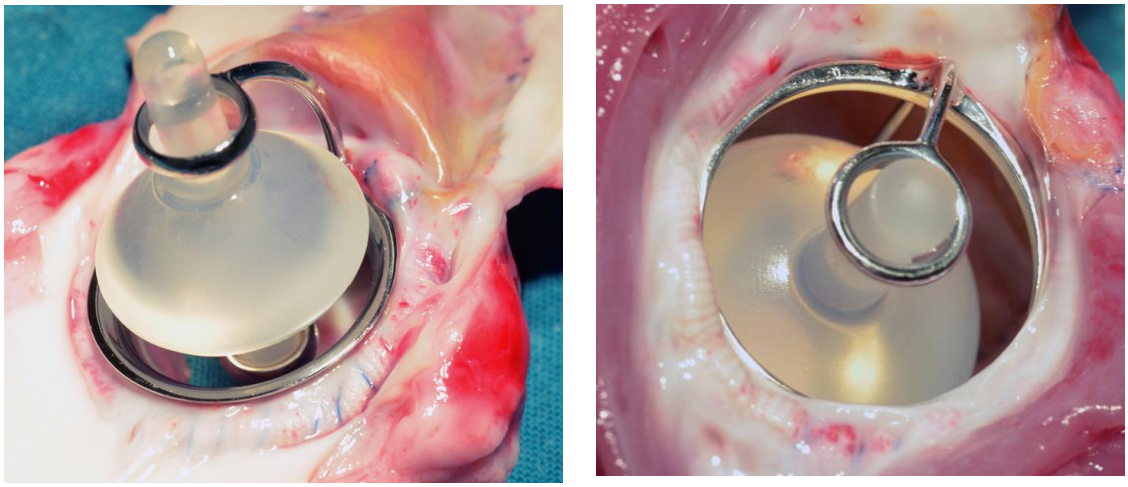

FIGURE 4.37: **The Glycar valve from FCTV 8.** The valve viewed from the PA on the left and the RVOT on the right. Notice the area of cicatrition at the sewing cuff on the RVOT side at the three to six o'clock positions.

Although there was no evidence of thrombus on the valve explanted from FCVT 8 (figure 4.37) there were cicatrition and pannus overgrowth on the RVOT side of the housing. Due to the redundancy of the sewing cuff, it was pulled into the RVOT, pulling the Dacron onto the housing and initiating tissue overgrowth.

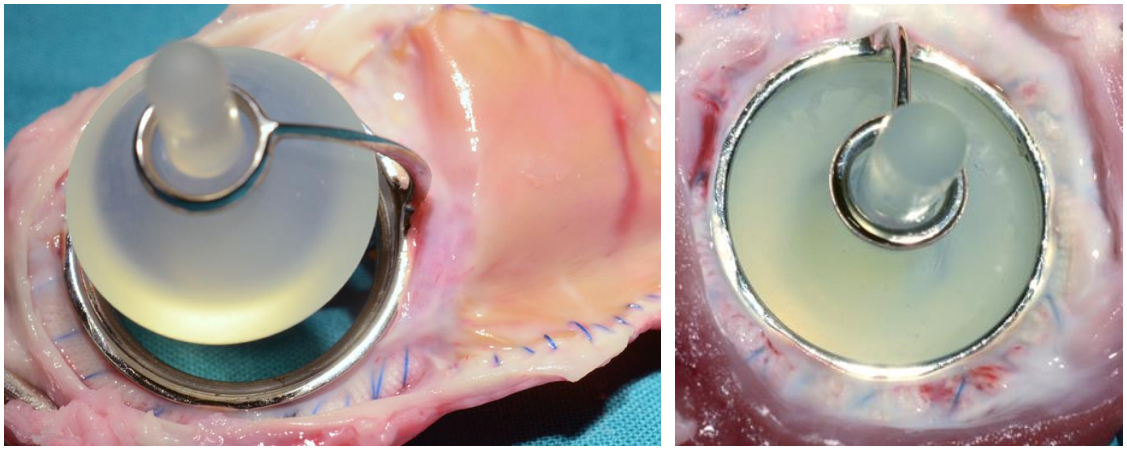

FIGURE 4.38: **The valve explanted from FCTV 9 viewed from the PA on the left and the RVOT on the right**.

ii. Serology results

Blood samples from the six sheep were obtained and sent for analysis to the department of Haematology and cell biology at the Faculty of Health Sciences and to the NHLS. Statistically, due to the small number of samples a meaningful statistical analysis was not feasible, therefore a mean value was used in the reporting of the data and any outlier values will be referenced to. No clear pattern could be inferred from the results obtained from the haematology, liver functions or immunology in any of the groups. No biochemical or haematological evidence indicating possible haemolysis or activation of platelets was observed. As advised by the statistician, no attempt was made to perform a statistical analysis on the serology obtained before euthanasia

due to the low sample numbers. However, in the frequency tables no obvious trend could that would identify a marked haematological or immune process could be observed in any specific group.

Table 4.9: **Blood results (mean values) for the Glycar group during the six-month follow-up.**

Days post-operative		0	1	7	15	30	90	180
Biochemistry								
Urea	(mmol/l)	7.2	4.8	7.6	7.9	4.8	3.7	5.0
Creatinine	(µmol/l)	54	48	57	57	55	61	79
Sodium	(mmol/l)	141	153	150	143	147	143	143
Potassium	(mmol/l)	3.9	3.9	5.4	4.9	4.4	4.7	4.0
Liver functions								
Albumin	(g/l)	13	12	14	15	16	16	12
AST	(U/l)	121	215	102	97	96	90	89
ALT	(U/l)	19	31	20	18	20	22	24
ALP	(U/l)	221	200	212	221	241	236	140
GGT	(U/l)	47	46	55	55	52	47	54
LD	(U/l)	683	728	591	548	447	511	514
Bili	(µmol/l)	2	1	1	<1	1	1	2
Immunology profile								
CRP	(mg/l)	<1.0	<1.0	<1.0	<1.0	<1.0	<1.0	<1.0
IgG	(g/l)	<0.30	<0.30	<0.30	<0.30	<0.30	<0.30	<0.30
IgA	(g/l)	<0.04	<0.04	<0.04	<0.04	<0.04	<0.04	<0.04
IgM	(g/l)	0.03	0.01	<0.01	<0.01	<0.01	0.16	0.15
Coagulation profile								
PT	(sec)	10	10	12	10	11	10	11
PTT	(sec)	27	26	54	50	42	30	31
INR		0.9	1.0	0.9	0.9	1.1	1.1	1.1
Haematology								
White cells	(x 10^9/l)	7.15	6.36	8.55	8.95	8.54	11.02	6.48
Hb	(g/dl)	10.8	10.4	11.4	12.9	10.9	11.7	9.5
Platelets	(x10^9/l)	368	523	981	527	554	610	279
Neutrophil	(x 10^9/l)	3.43	3.01	3.25	3.76	4.79	6.1	3.66
ESR	(mm/h)	1	1	1	2	1	1	2
RPI		0	0	0,3	0	0	0	0
Haptoglobin	(g/l)	<0.20	<0.20	<0.20	<0.20	<0.20	<0.20	<0.20

AST= Aspartate aminotransferase ; ALT= Alanine transaminase ; ALP= Alkaline phosphatase; GGT= Gamma glutamyl transferase; LD= Lactate dehydrogenase; Bili= Bilirubin; CRP= C reactive protein; IgG= Immunoglobulin G; IGA= Immunoglobulin A; IGM= Immunoglobulin M; PT= Prothrombin time; PTT= Partial thromboplastin time; INR= International normalised ratio; HB= Haemoglobin; ESR= Erythrocyte sedimentation rate; RPI= Red cell production index; sec= seconds; mm/h= millimeter per hour; mmol/l= millmole per liter; g/l= gram per liter; U/l= units per liter; g/dl= gram per deciliter; mg/l= milligram per liter.

Table 4.10: **Blood results for the Carbomedics bi-leaflet valve during the six-month follow-up.**

Days post-operative		0	1	5	14	28	88	183
Biochemistry								
Urea	(mmol/l)	1.1	4.2	4.1	3.4	6.1	5.8	9.3
Creatinine	(µmol/l)	69	62	54	75	89	63	60
Sodium	(mmol/l)	-	150	144	-	147	144	142
Potassium	(mmol/l)	4	3.9	4.6	5.1	-	4.6	4.6
Liver functions								
Albumin	(g/l)	14	11	13	16	16	16	17
AST	(U/l)	89	170	124	89	115	137	160
ALT	(U/l)	13	22	19	12	14	23	20
ALP	(U/l)	114	77	162	-	139	243	298
GGT	(U/l)	-	-	-	-	-	-	44
LD	(U/l)	379	600	490	480	-	-	626
Bili	(µmol/l)	2	1	1	2	1	1	1
Immunology profile								
CRP	(mg/l)	<1.0	<1.0	<1.0	<1.0	<1.0	<1.0	<1.0
IgG	(g/l)	<0.30	<0.30	<0.30	<0.30	<0.30	<0.30	<0.30
IgA	(g/l)	<0.04	<0.04	<0.04	<0.04	<0.04	<0.04	<0.04
IgM	(g/l)	0.03	0.01	<0.01	<0.03	<0.01	0.16	0.15
Coagulation profile								
PT	(sec)	-	-	-	11	-	10	10
PTT	(sec)	61	69	49	57	69	48	-
INR		1	1	0.9	1	1	0.9	0.9
Haematology								
White cells	(x 10^9/l)	6.85	12.74	7.52	9.27	11.65	10.45	12.9
Hb	(g/dl)	10.3	10.1	9.0	12.1	12.0	10.8	13.1
Platelets	(x10^9/l)	313	331	763	353	365	253	243
Neutrophil	(x 10^9/l)	2.44	9.81	3.16	2.6	-	3.97	3.61
ESR	(mm/h)	2	1	2	2	2	2	2
RPI		0	0	0	0	0	0	0

AST= Aspartate aminotransferase ; ALT= Alanine transaminase ; ALP= Alkaline phosphatase; GGT= Gamma glutamyl transferase; LD= Lactate dehydrogenase; Bili= Bilirubin; CRP= C Reactive protein; IgG= Immunoglobulin G; IGA= Immunoglobulin A; IGM= Immunoglobulin M; PT= Prothrombin time; PTT= Partial thromboplastin time; INR= International normalised ratio; HB= Haemoglobin; ESR= Erythrocyte sedimentation Rate; RPI= Red cell production index; sec= seconds; mm/h= millimeter per hour; mmol/l= millmole per liter; g/l= gram per liter; U/l= units per liter; g/dl= gram per deciliter; mg/l= milligram per liter.

iii. Echocardiography results

At sacrifice all of the test animals had a normal right ventricular function with no pericardial effusions or pulmonary effusions. The pericardial patches showed no calcification with no abnormal dilatation of the ascending pulmonary artery. The valves functioned well and the poppet motion was unimpeded. The gradients across the valves were never in excess of 20 mmHg. None of the valves had any regurgitation. No thrombi, pannus or valvular pathology was found in any of the valves. Statistical analysis could not find any difference between the Glycar valves and compared well with the Carbomedics valve. FCTV 3 died prior to planed explantation, therefore no echographic data is available.

Table: 4.11: **The echographic data captured at sacrifice for the six-month follow-up group.**

Echocardiographic data: Glycar study – six-month sacrifice group																				
						CFD over the valve							PWD in RVOT							
Time interval	Sheep no	Valve type	Occluder motion	LV function	RV function	Regurgitation	Vena contracta	V max	V mean	P max	P mean	VTI	V max	V mean	P max	P mean	VTI	EOA	Pannus	Thrombus	Paravalvular leak
6 months	FCTV 3	P	X	X	X	X	X	X	X	X	X	X	X	X	X	X	X	X	X	X	X
	FCTV 6	P	N	N	N	None	None	1.5	1.07	8.95	5.21	34.4	1.82	1.51	13.2	9.12	14.1	1.53	No	No	No
	FCTV 8	P	N	N	N	None	None	1.34	0.97	7.18	3.76	-	1.71	1.34	11.6	7.24	-	-	No	No	No
	FCTV 9	P	N	N	N	None	None	1.91	1.22	14.6	5.95	-	-	-	-	-	-	-	No	No	No
	FCTV 10	P	N	N	N	None	None	1.64	1.45	10.7	8.4	-	-	-	-	-	-	-	No	No	No
	Control 2	B	N	N	N	None	None	1.36	0.86	7.40	2.96	31,8	0.65	0.44	1.69	0.77	15.2	1.29	No	No	No

FCT = The number; LV = Left ventricle; RV = Right ventricle; CFD = Colour flow doppler; PWD = Pulse wave doppler; RVOT = Right ventricle outflow tract; P = Poppet; B = Bi-leaflet; N = Normal; V max = Maximum velocity in ms^{-1}; V mean = Mean velocity in ms^{-1}; P max = maximum pressure drop; P mean = Mean pressure drop; VTI = Velocity time integral; EOA= effective orifice area in centimeter square; **X** = Values not obtained sheep died; - = Values not available.

iv. Haemodynamic data

Table 4.12: Haemodynamic data: six-month follow-up group.

OPERATIVE DATA	Short term outcome	6 month sacrifice										
Carbomedics control												
Pressure Measurements	**Ao_Sys**	**Ao_Diast**	**Ao_Mean**	**CVP_Sys**	**CVP_Diast**	**CVP_Mean**	**RVOT_Sys**	**RVOT_Diast**	**RVOT_Mean**	**MPA_Sys**	**MPA_Diast**	**MPA_Mean**
Pre-bypass	86	69	75	10	3	7	23	1	11	18	9	13
Post-bypass	106	63	77	8	2	6	26	3	15	16	11	15
Pre-sacrifice	81	56	67	10	1	5	45	0	15	19	8	12
FCTV 03 -2014												
Pressure Measurements	**Ao_Sys**	**Ao_Diast**	**Ao_Mean**	**CVP_Sys**	**CVP_Diast**	**CVP_Mean**	**RVOT_Sys**	**RVOT_Diast**	**RVOT_Mean**	**MPA_Sys**	**MPA_Diast**	**MPA_Mean**
Pre-bypass	81	48	65	13	5	8	22	7	14	22	16	19
Post-bypass	72	52	58	13	9	11	29	6	18	19	12	16
Pre-sacrifice	X	X	X	X	X	X	X	X	X	X	X	X
FCTV 06 - 2014												
Pressure Measurements	**Ao_Sys**	**Ao_Diast**	**Ao_Mean**	**CVP_Sys**	**CVP_Diast**	**CVP_Mean**	**RVOT_Sys**	**RVOT_Diast**	**RVOT_Mean**	**MPA_Sys**	**MPA_Diast**	**MPA_Mean**
Pre-bypass	79	60	68	8	0	3	6	0	3	12	9	10
Post-bypass	105	78	88	14	7	10	29	2	18	20	12	17
Pre-sacrifice	77	61	68	8	1	5	20	7	13	22	5	14
FCTV 08 - 2014												
Pressure Measurements	**Ao_Sys**	**Ao_Diast**	**Ao_Mean**	**CVP_Sys**	**CVP_Diast**	**CVP_Mean**	**RVOT_Sys**	**RVOT_Diast**	**RVOT_Mean**	**MPA_Sys**	**MPA_Diast**	**MPA_Mean**
Pre-bypass	121	95	104	10	1	6	28	0	12	30	7	17
Post-bypass	75	33	54	7	1	4	27	2	15	26	14	9
Pre-sacrifice	125	95	103	12	0	4	31	2	14	27	10	17
FCTV 09 - 2014												
Pressure Measurements	**Ao_Sys**	**Ao_Diast**	**Ao_Mean**	**CVP_Sys**	**CVP_Diast**	**CVP_Mean**	**RVOT_Sys**	**RVOT_Diast**	**RVOT_Mean**	**MPA_Sys**	**MPA_Diast**	**MPA_Mean**
Pre-bypass	59	39	46	7	1	5	23	1	13	22	17	19
Post-bypass	101	76	86	5	0	2	33	0	16	25	10	15
Pre-sacrifice	104	87	93	8	5	6	43	0	16	29	17	21
FCTV 10 - 2014												
Pressure Measurements	**Ao_Sys**	**Ao_Diast**	**Ao_Mean**	**CVP_Sys**	**CVP_Diast**	**CVP_Mean**	**RVOT_Sys**	**RVOT_Diast**	**RVOT_Mean**	**MPA_Sys**	**MPA_Diast**	**MPA_Mean**
Pre-bypass	114	85	97	2	0	1	13	3	8	14	10	12
Post-bypass	90	45	74	9	5	7	22	7	16	20	6	15
Pre-sacrifice	105	88	97	7	0	3	27	1	10	15	10	12

Ao= aorta, Sys= systole; Diast= diastole; CVP= central venous pressure; RVOT= right ventricular outflow tract; MPA= main pulmonary artery; FCTV= the animal number assigned during the study. All values were measured in mmHg, **X**=values were not obtained as the sheep died.

v. Histological examination

Histology was performed according to the histology protocol (appendix C). Microscopic examination of the sewing cuff shows the presence of suture material, ventricular muscle and pericardial patch (figure 4.39). There is a foreign body giant cell reaction to the suture material as well as focal involvement of the pericardial patch. There was no acute inflammation, calcification, platelet deposition or thrombus formation noted on either the patch or the sewing cuff.

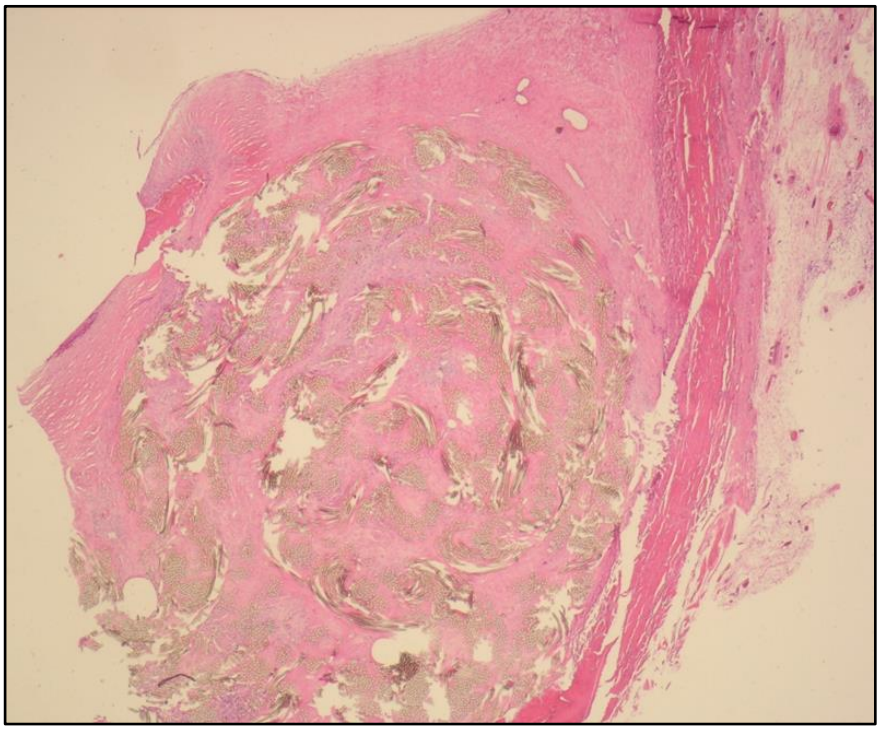

FIGURE 4.39: **Histology of the sewing cuff junction with the pericardium** (40 X magnification, H&E). No platelet deposits can be seen on the sewing cuff and there is good healing between the patch and the cuff.

vi. Post mortem results

a. Necropsy results

The third sheep to receive the Glycar valve developed infective endocarditis. It was doing extremely well and showed no signs of complications when it suddenly presented with lethargy and a loss of appetite. Clinically, it was sick and it was treated for a possible airway infection. There was no improvement and the sheep eventually developed cardiac failure clinically. The poppet opening and closing sounds were not audible and subsequently a planned sacrifice was performed. Due to the limited timeframe no haemodynamic studies were performed and no echocardiography was obtained.

During the explantation the following findings were made. There was a small clear pleural effusion in the right hemithorax, no pleural effusion on the left and no pericardial effusion. Bulky mediastinal lymphadenopathy was clustered mainly around the trachea. Multiple large infective areas which drained puss upon incision, were observed in both lungs (figure 4.40). External examination of the heart found it to be normal.

.

FIGURE 4.40: **Cut section of the left upper lobe of the lung.** Consolidation can be seen with puss draining from the incision.

b. Photography of the explanted valve

Once the pulmonary artery had been transected, the cause of death was apparent (figures 4.41 to 4.43). The entire prosthetic valve was clotted with old organised and new soft thrombus surrounding the poppet and the struts on the arterial side. A massive vegetation, originating from the suture line at the junction between the sewing cuff, poppet guide struts and the pericardial patch was found under the new thrombus. The vegetation encapsulated the poppet guide, was

bulky and it impeded poppet motion. Areas in and around the vegetation contained puss and a clinical diagnosis of infective endocarditis was made.

FIGURE 4.41: **The Glycar valve during post mortem**. Note the vegetation on the guiding strut with thrombus. The thrombus started at the sewing cuff at the junction with the pericardial patch.

FIGURE 4.42**: The Poppet in the open position viewed from the PA**. It clearly demonstrates the vegetation and thrombus originating at the sewing cuff at the pericardial patch junction, extending up the guide strut to end and surround the distal guide ring.

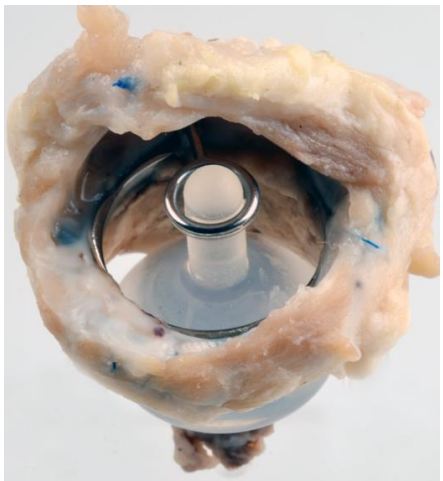

FIGURE 4.43: **The valve viewed from the RVOT**. The poppet motion was impaired due to the disruption at the guide ring on the PA side. The rest of the annulus is healthy.

c. Histology of the explanted valve

Microscopic examination shows suture material and pericardial patch with focal foreign body giant cell infiltration (figure 4.44 and 4.45). A fibrinopurulent exudate is noted on the surface of the tissue with infiltration of large colonies neutrophils as well as scattered bacterial colonies into the underlying patch. The features are indicative of infective endocarditis. A mild lymphocyte infiltrate is noted in the surrounding adventitia.

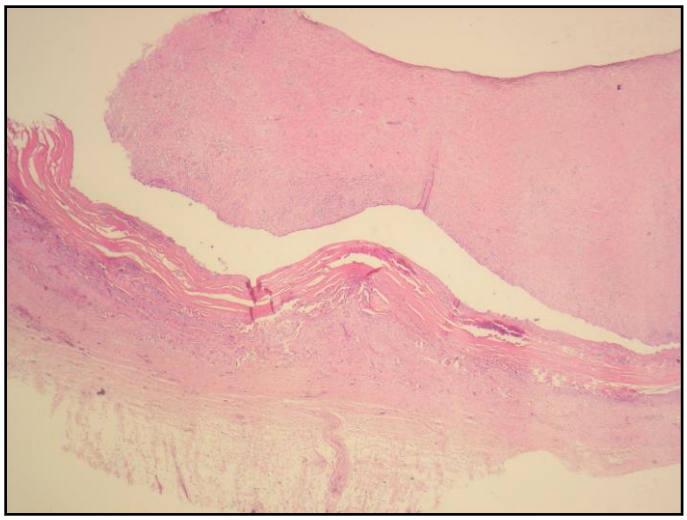

FIGURE 4.44 **Histology of the pericardial patch** (40 X magnification, H&E).

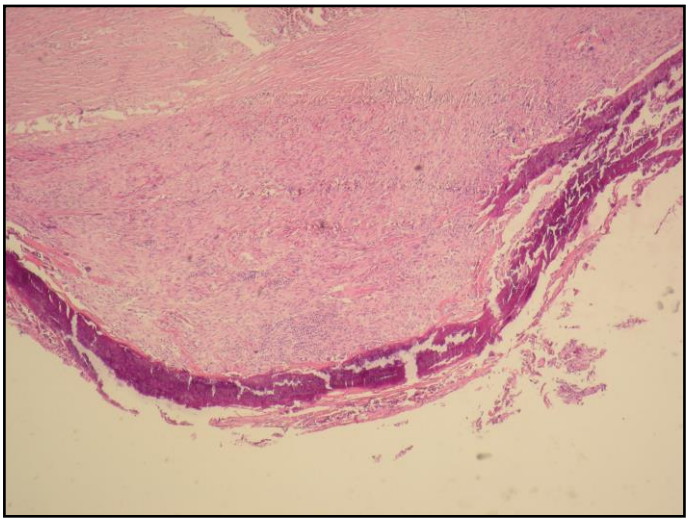

FIGURE 4.45: **Histology of the pericardial patch** (40 X magnification, H&E). Large colonies of Neutrophil infiltration as well as scattered bacterial colonies invading the pericardial patch can be seen.

4.3.2 Results: Long term follow-up (twelve months)

i. Valve photography

a. Carbomedics valve

Decent healing was observed around the pulmonary artery with minimal adhesions between the pericardium, pulmonary artery and lung. There was no sign of pleural effusion or infection. The pulmonary valve was removed *en bloc* and the pulmonary artery opened up posteriorly to expose the valve, according to protocol.

Proximal: Viewing the valve from the RVOT

There was good healing on the sewing cuff with complete circumferential covering. However, there was a lot of pannus overgrowth between the six to nine o'clock positions, encroaching on the leaflets (figure 4.46). The sewing cuff was completely covered with tissue but the hinge mechanism of the valve was clean. There was an area between the pannus and the sewing cuff at the twelve o'clock position suggestive of a small clot. However, it did not cause any gross clinical manifestations and upon macroscopic examination the lungs were found to be within normal parameters. Even though the valve was *in situ* for twelve months without any anti-coagulation, the valve looked exceptionally well.

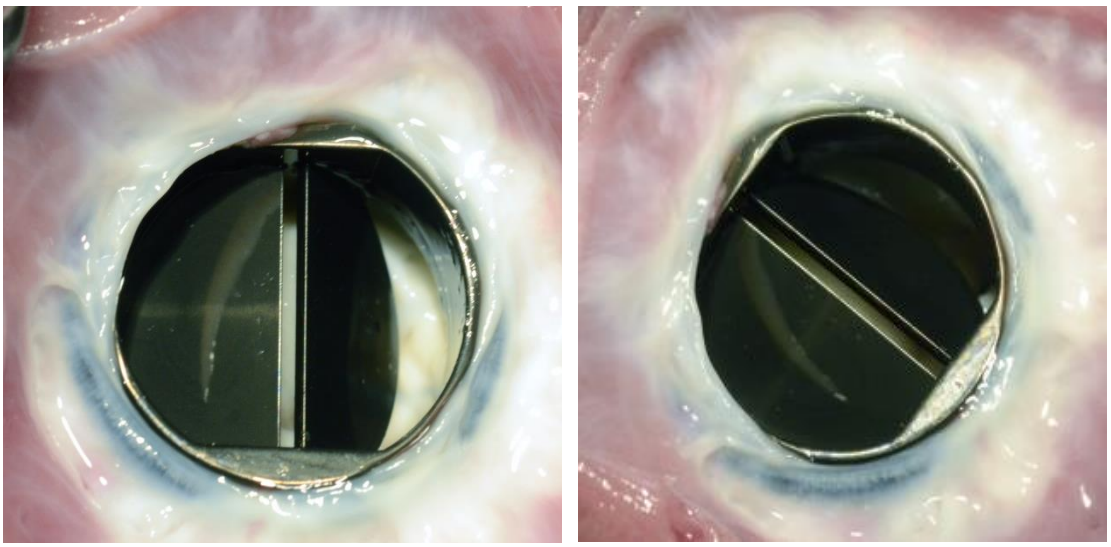

FIGURE 4.46: **Explanted Carbomedics valve viewed from the RVOT**. Note the pannus overgrowth between the nine and twelve o'clock positions. A possible clot can be seen at the upper hinge area.

The valves were clear of any macroscopic thrombi on the leafllets, hinge mechanism and housing. The b-datum line was clear and no obvious pitting was observed on the leaflets. There was free movement of the leaflets (figure 4.47).

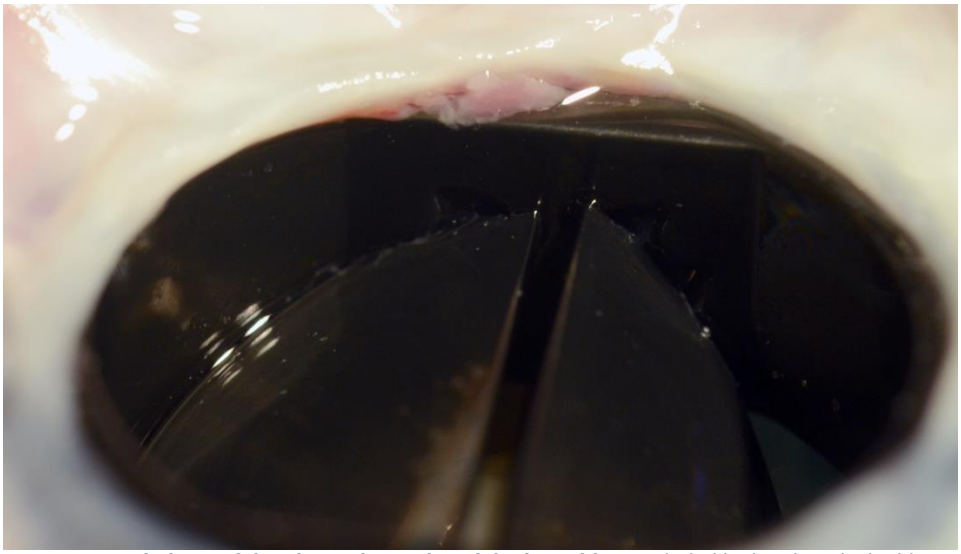

FIGURE 4.47: **A zoomed photo of the clot at the twelve o'clock position**. Included in the photo is the hinge mechanism of the bi-leaflet showing no thrombi.

Distal: Viewing the valve from the PA.

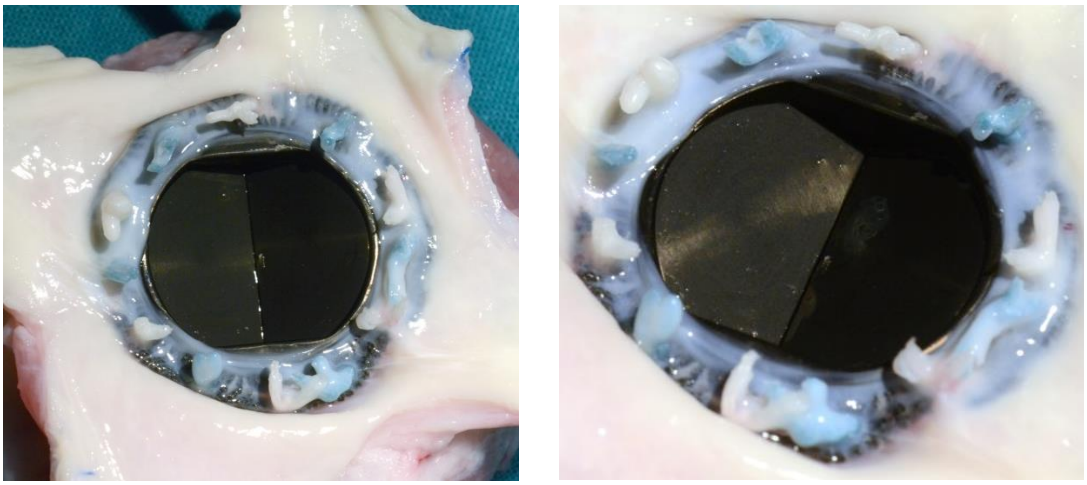

Figure 4.48: **The Carbomedics bi-leaflet valve seen from the PA.**

There was good quality healing on the sewing cuff with no pannus overgrowth as well as complete covering of the entire cuff. The hinge mechanism was clean and the valve leaflets were normal. No clots in or around the valve or focus for clot formation were noticed. Healing between the sewing cuff and the native pulmonary artery tissue was complete and no recesses were observed.

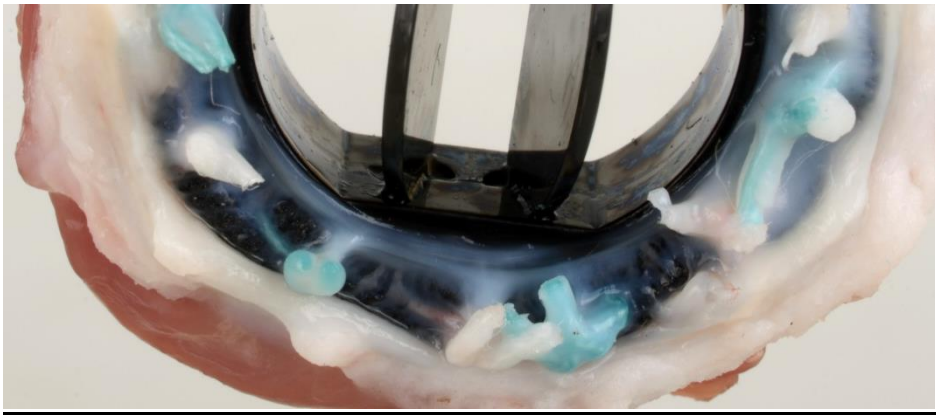

FIGURE 4.49: **The bi-leaflet valve seen from the PA**. The leaflets are in the open position revealing normal valve leaflets, devoid of macroscopic pathology.

b. Glycar valves

All the Glycar valves, except for the valve with infective endocarditis, were completely clean at explantation and showed no signs of clots on the sewing cuff, the housing, the poppet or guiding struts (figure 4.50 to 4.54). There was normal healing between the pericardial patch and the native PA as well as between the patch and the sewing cuff. The lungs were completely normal and no macroscopic evidence of emboli could be detected on cut sections of the lung. The following series of photographs depicts the Glycar valves from the different sheep at explantation. Two views of each valve are shown: the view from the RVOT and a view from the PA.

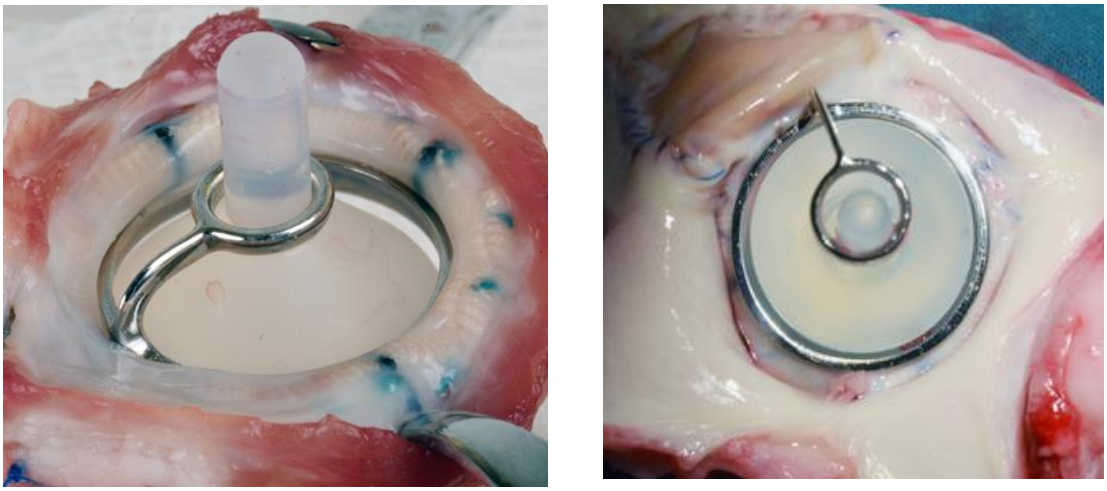

FIGURE 4.50: **The Glycar valve from FCTV 1. The RVOT view on the left and the PA view on the right.**

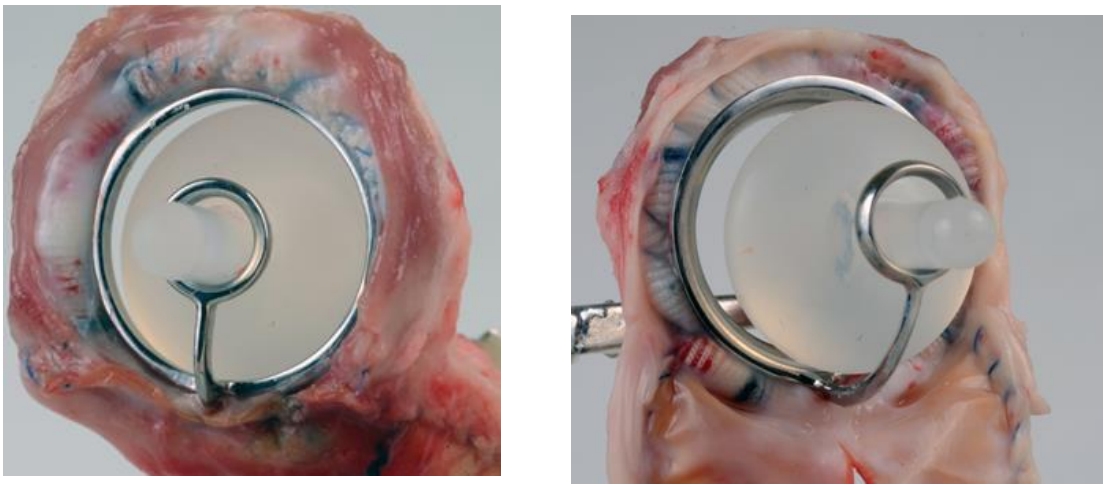

Figure 4.51: **The Glycar valve from FCTV 2.** Viewed from the RVOT on the left and the PA on the right.

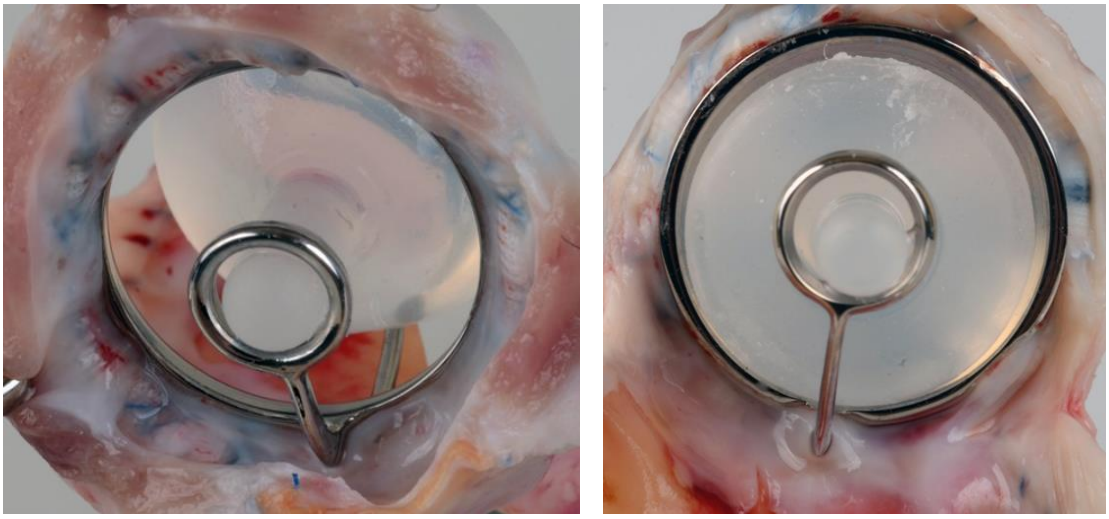

Figure 4.52: **The Glycar valve from FCTV 4**. A clean valve with no thrombi with normal poppet motion can be seen.

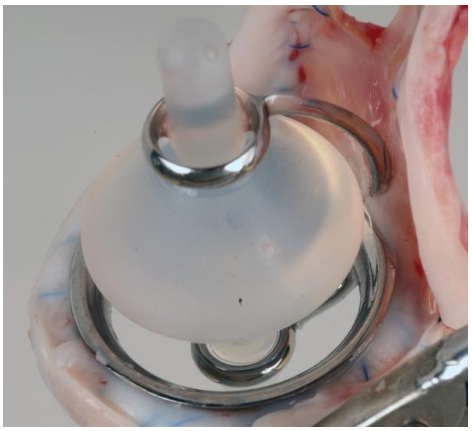

FIGURE 4.53: **The Glycar valve from FCTV 7 viewed from the PA.** Notice the contact point and the reaction between the pericardial patch and the base of the guide strut.

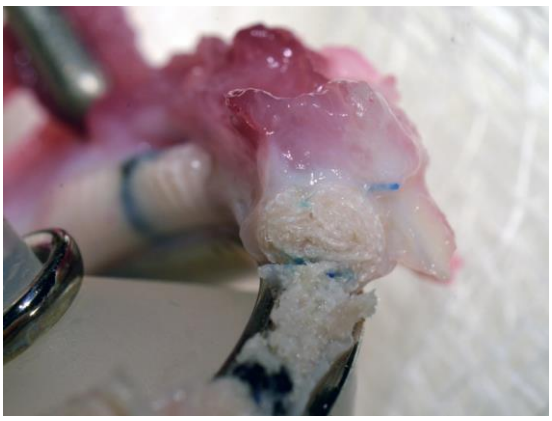

FIGURE 4.54: **The cut section of the sewing cuff of the Glycar valve. The cut is at the junction with the PA and the pericardial patch viewed from the RVOT**. Note the healing across the material with complete covering on both the low pressure and the high pressure sides.

c. Problem areas observed in the 12 month group

FIGURE 4.55: **A small area on the sewing cuff that may be a focus of microthrombi**. It is very small though and no other abnormalities were seen (explanted from FCTV 1).

In figure 4.55 a small area that contain possible ulceration on the sewing cuff can be seen. Although it did not lead to clinical thrombi the possibility does exist that this may produce microemboli. The lung would accommodate these microthrombi without clinical consequence. The lung was normal on cut sections though.

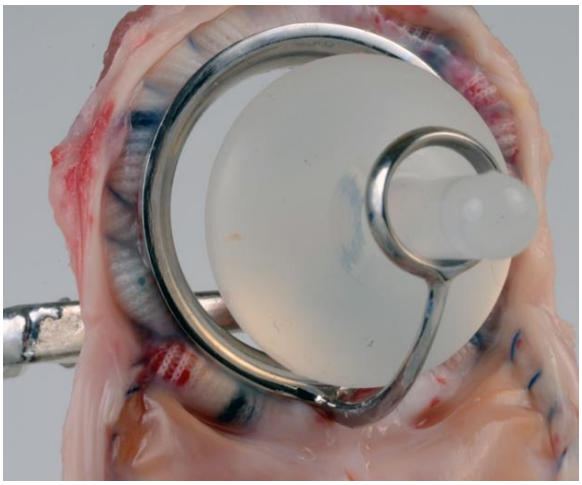

FIGURE 4.56: **Incomplete sewing cuff covering with pitting between the pericardial patch and the sewing cuff** (explanted from FCTV 02).

Figure 4.56 demonstrates an area where incomplete tissue covering of the sewing cuff was evident. Closer to the pericardial patch junction with the sewing cuff at the base of the guiding strut, pannus overgrowth can be seen. On the RVOT side this was not a concern.

The continuous suture technique used to implant the Glycar valves in the pulmonary annulus caused the sewing in cuff in FCTV 4 to prolapse into the RVOT (figure 4. 57), causing subvalvular obstruction and flow changes. It also caused pannus overgrowth on the housing from the ten to twelve o' clock positions. At twelve months it did not pose a problem and did not influence the flow across the valve clinically and echocardiographically.

A tissue reaction was seen where the pericardial patch and the sewing ring made contact. This can be appreciated in figure 4.53, 4.56 and 4.58. The poppet motion was not impeded in either of these valves.

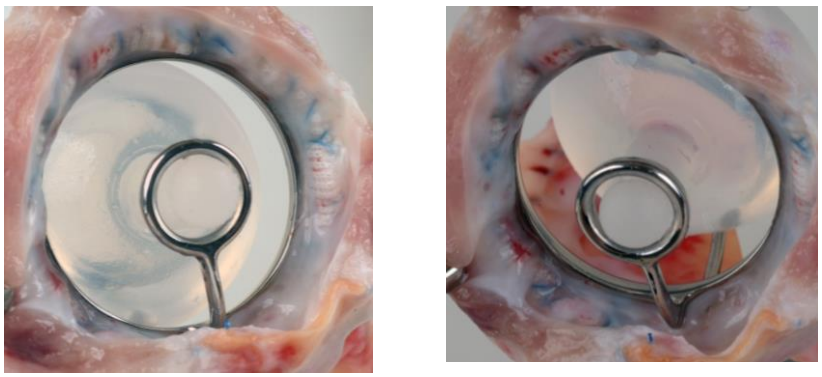

FIGURE 4.57: **The sewing cuff from FCTV 4 viewed from the RVOT.** The sewing cuff was somewhat redundant at implantation and this caused the cuff to fold into the RVOT.

FIGURE 4.58: **Pannus overgrowth can be seen at the junction between the proximal strut, valve housing and the pericardial patch.**

ii. Serology results

Except for the one sheep that died of infective endocarditis the blood results for the remainder of the sheep (the Glycar group and the Carbomedics valve) showed no pathology. There were no signs of infection, haemolysis or immune reactions. However, there was an increase in the LDH but it recovered and there were no other biochemical signs of possible haemolysis. Liver and kidney functions remained normal throughout the study interval. On advice from the statistician, no attempt was made to perform statistical analysis on the serology obtained before

euthanasia due to the low sample numbers. However, in the frequency tables no obvious trend could be observed that would identify a marked haematological or immune process in any specific group.

Table 4.13: **Blood results for the Glycar valve group during the twelve-month post-operative follow-up.**

Post-operative days	0	1	7	14	30	90	180	360
Biochemistry								
Urea (mmol/l)	1.9	7.1	8.4	2.1	3.7	7.9	5.1	1.8
Creatinine (µmol/l)	79	84	91	68	87	85	79	88
Sodium (mmol/l)	143	147	147	144	145	139	143	142
Potassium (mmol/l)	4.0	4.2	4.3	4.5	4.7	5.2	4.4	4.1
Liver functions								
Albumin (g/l)	11	8	10	11	12	14	14	12
AST (U/l)	84	179	101	99	96	96	89	87
ALT (U/l)	8	16	6	7	9	10	8	9
ALP (U/l)	289	108	100	107	217	116	133	93
GGT (U/l)	40	47	72	64	50	54	40	50
LD (U/l)	447	573	584	784	623	524	562	473
Bili (µmol/l)	2	1	1	<1	1	1	2	1
Immunology profile								
CRP (mg/l)	<1.0	<1.0	<1.0	<1.0	<1.0	<1.0	<1.0	<1.0
IgG (g/l)	<0.30	<0.30	<0.30	<0.30	<0.30	<0.30	<0.30	<30
IgA (g/l)	<0.04	<0.04	<0.04	<0,04	<0,04	<0.04	<0,04	<0.04
IgM (g/l)	0.03	0.01	<0.01	<0.01	<0.01	<0.01	<0.01	<0.01
Coagulation profile								
PT (sec)	10	10	12	10	11	10	11	10
PTT (sec)	31	40	36	30	33	38	29	32
INR	0.9	1.2	1.0	0.9	1.0	1.1	0.9	0.9
Haematology								
White cells (x 10^9/l)	7.15	20.86	14.92	11.0	13.64	12.4	6.98	7.21
Hb (g/dl)	12.5	8.9	6.6	10.3	11.7	9.2	10.9	11.0
Haematocrit (l/l)	0.298	0.214	0.168	0.321	0.317	0.307	0.316	0.352
Platelets (x10^9/l)	242	64	1175	352	293	511	312	298
Neutrophil (x 10^9/l)	2.76	13.35	8.5	3.3	4.64	1.58	2.21	2.64
ESR (mm/h)	1	1	1	1	1	1	2	1
RPI	0	0	0	0	0	0	0	0
Haptoglobin (g/l)	<0.20	<0.20	<0.20	<0.20	<0.20	<0.20	<2.0	<0.20

AST= Aspartate aminotransferase ; ALT= Alanine transaminase ; ALP= Alkaline phosphatase; GGT= Gamma glutamyl transferase; LD= Lactate dehydrogenase; Bili= Bilirubin; CRP= C-reactive protein; IgG= Immunoglobulin G; IGA= Immunoglobulin A; IGM= Immunoglobulin M; PT= Prothrombin time; PTT= Partial thromboplastin time; INR= International normalised ratio; HB= Haemoglobin; ESR= Erythrocyte sedimentation rate; RPI= Red cell production index; sec= seconds; mm/h= millimeter per hour; mmol/l= millmole per liter; g/l= gram per liter; U/l= units per liter; g/dl= gram per deciliter; mg/l= milligram per liter.

Table 4.14: **Blood results for the Carbomedics valve during the twelve-month post-operative follow-up.**

Post-operative days	0	1	5	14	60	90	177	378
Biochemistry								
Urea (mmol/l)	4.4	6.6	4.6	3.5	4.3	1.3	4.4	3.6
Creatinine (µmol/l)	79.0	98.0	54.0	99.0	108.0	104.0	102.0	77.0
Sodium (mmol/l)	144.0	146.0	149.0	147.0	147.0	143.0	143.0	150.0
Potassium (mmol/l)	4.6	4.6	5.1	4.5	4.9	5.7	5.0	3.5
Liver functions								
Albumin (g/l)	15	12	12	15	15	13	14	14
AST (U/l)	114	-	125	99	103	108	132	108
ALT (U/l)	9	10	6	8	8	9	8	9
ALP (U/l)	163	-	112	254	251	242	244	154
GGT (U/l)	-	-	-	59	40	-	-	-
LD (U/l)	980	-	-	-	-	-	-	508
Bili (µmol/l)	3	1	2	2	3	1	1	1
Immunology profile								
CRP (mg/l)	<1.0	<1.0	<1.0	<1.0	<1.0	<1.0	<1.0	<1.0
IgG (g/l)	<0.30	<0.30	<0.30	<0.30	<0.30	<0.30	<0.30	<0.30
IgA (g/l)	<0.04	<0.04	<0.04	<0,04	<0,04	<0.04	<0,04	<0.04
IgM (g/l)	0.03	0.01	<0.01	<0.01	<0.01	<0.01	<0.01	<0.01
Coagulation profile								
PT (sec)	11	10	11	10	11	11	11	10
PTT (sec)	37	39	35	33	34	38	32	31
INR	1.1	1.2	1.0	0.9	1.0	1,1	0.9	0.9
Haematology								
White cells (x 10^9/l)	8.9	-	11.2	14.8	-	11.6	9.11	8.04
Hb (g/dl)	10.4	-	9.8	11.5	-	10.5	10.9	8.55
Haematocrit (l/l)	0.298	-	0.260	0.321	-	0.307	0.316	0.240
Platelets (x10^9/l)	521	-	436	292	-	489	373	314
Neutrophil (x 10^9/l)	1.7	-	5.33	5.48	-	3.16	3.46	4.5
ESR (mm/h)	2	2	2	1	1	1	2	1
RPI	0	0	0	0	0	0	0	0
Haptoglobin (g/l)	<0.20	<0.20	<0.20	<0.20	<0.20	<0.20	<0.20	<0.20

AST= Aspartate aminotransferase ; ALT= Alanine transaminase ; ALP= Alkaline phosphatase; GGT= Gamma glutamyl transferase; LD= Lactate dehydrogenase; Bili= Bilirubin; CRP= C-reactive protein; IgG= Immunoglobulin G; IGA= Immunoglobulin A; IGM= Immunoglobulin M; PT= Prothrombin time; PTT= Partial thromboplastin time; INR= International normalised ratio; HB= Haemoglobin; ESR= Erythrocyte sedimentation rate; RPI= Red cell production index; sec= seconds; mm/h= millimeter per hour; mmol/l= millmole per liter; g/l= gram per liter; U/l= units per liter; g/dl= gram per deciliter; mg/l= milligram per liter.

iii. Echocardiography results

All the animals had normal left and right ventricular function and there were no pericardial effusions or pulmonary effusions. The pericardial patches showed no calcification or any abnormal dilatation of the ascending pulmonary artery. The valves functioned well and the poppet motion was unimpeded. The gradients across the valves were never in excess of 15 mmHg. None of the valves had any regurgitation. No thrombi, pannus or valvular pathology was found in any of the valves. Statistically there is no difference between the Glycar valves and the Carbomedics valve and it compared well.

Table 4.15: **Echocardiographic data at sacrifice, twelve-month follow-up group.**

Echocardiographic data																				
						CFD over the valve							PWD in RVOT							
Time interval	Sheep no	Valve type	Occluder motion	LV function	RV function	Regurgitation	Vena contracta	V max	V mean	P max	P mean	VTI	V max	V mean	P max	P mean	VTI	EOA	Pannus	Thrombus	Paravalvular leak
12 months	FCT-1	P	N	N	N	None	None	1.98	1.12	13.3	6.36	41.1	1.98	1.75	15.7	12.25	-	-	No	No	No
	FCT-2	P	N	N	N	None	None	1.73	1.08	11.9	5.62	38.3	0.52	0.35	1.08	0.57	12.8	2.25	No	No	No
	FCT-4	P	X	X	X	X	X	X	X	X	X	X	X	X	X	X	X	X	X	X	X
	FCT-5	P	N	N	N	None	None	1.45	0.88	8.47	3.1	20.8	-	-	-	-	-	-	No	No	No
	FCT-7	P	N	N	N	None	None	1.67	1.21	11.6	5.84	-	-	-	-	-	-	-	No	No	No
	Control 1	B	N	N	N	None	None	1.49	0.86	8.88	2.97	94.9	0.7	0.49	1.96	1.07	15.2	1.28	No	No	No

FCT= The designated sheep number; LV= left ventricle; RV= right ventricle; CFD= colour flow doppler; PWD= pulse wave doppler; RVOT= right ventricle outflow tract; P= poppet; B= bi-leaflet; N= normal; V max= maximum velocity in ms^{-1}; V mean= mean velocity in ms^{-1}; P max= maximum pressure drop; P mean= mean pressure drop; VTI= velocity time integral; EOA= effective orifice area; **X**= Values not obtained (sheep died); - = values not available

iv. Haemodynamic data

Table 4.16: **Haemodynamic data: twelve-month follow-up group**

OPERATIVE DATA	Long term outcome 12 month sacrifice											
Carbomedics Control												
Pressure Measurements	**Ao_Sys**	**Ao_Diast**	**Ao_Mean**	**CVP_Sys**	**CVP_Diast**	**CVP_Mean**	**RVOT_Sys**	**RVOT_Diast**	**RVOT_Mean**	**MPA_Sys**	**MPA_Diast**	**MPA_Mean**
Pre-bypass	122	96	106	17	X	17	35	6	14	22	14	17
Post-bypass	115	78	103	17	17	19	49	5	23	33	14	19
Pre-sacrifice	118	99	107	16	3	9	66	1	30	31	14	23
GLYCAR valve												
FCTV 01 - 2014												
Pressure Measurements	**Ao_Sys**	**Ao_Diast**	**Ao_Mean**	**CVP_Sys**	**CVP_Diast**	**CVP_Mean**	**RVOT_Sys**	**RVOT_Diast**	**RVOT_Mean**	**MPA_Sys**	**MPA_Diast**	**MPA_Mean**
Pre-bypass	106	71	85	8	4	5	36	10	20	30	11	19
Post-bypass	97	58	71	9	3	6	45	4	22	33	0	14
Pre-sacrifice	92	78	83	13	6	9	34	0	15	26	12	18
FCTV 02- 2014												
Pressure Measurements	**Ao_Sys**	**Ao_Diast**	**Ao_Mean**	**CVP_Sys**	**CVP_Diast**	**CVP_Mean**	**RVOT_Sys**	**RVOT_Diast**	**RVOT_Mean**	**MPA_Sys**	**MPA_Diast**	**MPA_Mean**
Pre-bypass	99	50	71	20	12	15	28	10	18	32	20	25
Post-bypass	104	41	61	18	10	13	38	8	22	34	9	21
Pre-sacrifice	72	60	64	0	X	X	27	0	9	15	5	9
FCTV 04 -2014												
Pressure Measurements	**Ao_Sys**	**Ao_Diast**	**Ao_Mean**	**CVP_Sys**	**CVP_Diast**	**CVP_Mean**	**RVOT_Sys**	**RVOT_Diast**	**RVOT_Mean**	**MPA_Sys**	**MPA_Diast**	**MPA_Mean**
Pre-bypass	X	X	X	X	X	X	X	X	X	X	X	X
Post-bypass	X	X	X	X	X	X	X	X	X	X	X	X
Pre-sacrifice	X	X	X	X	X	X	X	X	X	X	X	X
FCTV 05 - 2014												
Pressure Measurements	**Ao_Sys**	**Ao_Diast**	**Ao_Mean**	**CVP_Sys**	**CVP_Diast**	**CVP_Mean**	**RVOT_Sys**	**RVOT_Diast**	**RVOT_Mean**	**MPA_Sys**	**MPA_Diast**	**MPA_Mean**
Pre-bypass	94	53	67	19	7	12	21	0	9	19	8	11
Post-bypass	109	66	53	25	9	16	49	28	35	42	11	21
Pre-sacrifice	X	X	X	X	X	X	X	X	X	X	X	X
OPERATIVE DATA												
Pressure Measurements	**Ao_Sys**	**Ao_Diast**	**Ao_Mean**	**CVP_Sys**	**CVP_Dias**	**CVP_Mean**	**RVOT_Sy**	**RVOT_Diast**	**RVOT_Mean**	**MPA_Sys**	**MPA_Diast**	**MPA_Mean**
Pre-bypass	100	80	89	25	15	20	34	17	27	37	27	32
Post-bypass	102	48	66	22	8	18	37	17	26	37	23	30
Pre-sacrifice	99	80	90	4	0	1	25	0	7	18	2	10

Ao= aorta, Sys= systole; Diast= diastole; CVP= central venous pressure; RVOT= right ventricular outflow tract; MPA= main pulmonary artery; FCTV= the animal number assigned during the study. All values were measured in mmHg, **X**= values were not obtained as the sheep died.

v. Histological examination

Microscopic evaluation of sections of the sewing cuff shows the presence of cardiac muscle, artery wall and suture material with a prominent foreign body giant cell reaction. Focal calcification and metaplastic ossification surrounding the suture material are observed (figure 4.59). No inflammation, platelet deposition or thrombus is evident.

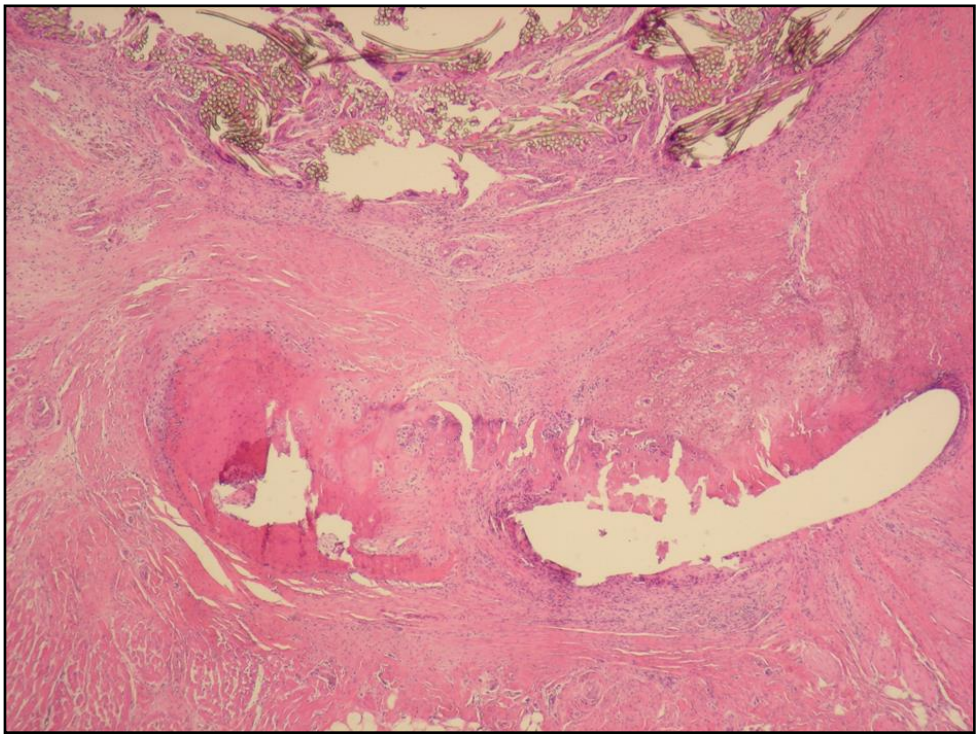

FIGURE 4.59: **Histology of the pericardial patch and sewing cuff junction (100 X magnification,** H&E**).**

vi. Post mortem results

a. Necropsy results

This was the first sheep that had received a Glycar valve. The sheep was booked for scheduled sacrifice twelve months after implantation. Two days prior to scheduled sacrifice the research team was alerted to the sudden poor health status of the sheep. It was doing well before it stopped feeding and presented with lethargy. The sheep had poor mobility and was in respiratory distress. Clinically, the sheep was in cardiac failure. The heart sounds were faint and no opening or closing sounds from the poppet could be detected. The sheep was pre-terminal and a planned sacrifice was not possible, therefore no haemodynamic investigations or echo data could be obtained and no bloods were drawn for evaluation.

During the autopsy small bilateral pleural effusions and a small pericardial effusion were found. The abdomen was distended due to ascites and the liver was engorged.

Although the Glycar pericardium was tightly adhered to the surrounding tissue there were no signs of infection, inflammation or calcification. The pulmonary artery and pulmonary valve were excised and the pulmonary artery opened posteriorly, opposite from the pericardial patch. The valve had a large clot on its pulmonary arterial side (figure 4.60). It was a large, fresh clot with its origin at the sewing cuff at the junction with the guiding strut, reaching up across the strut towards the distal guide ring, as can appreciated in the photos below.

b. Photography of the explanted valve

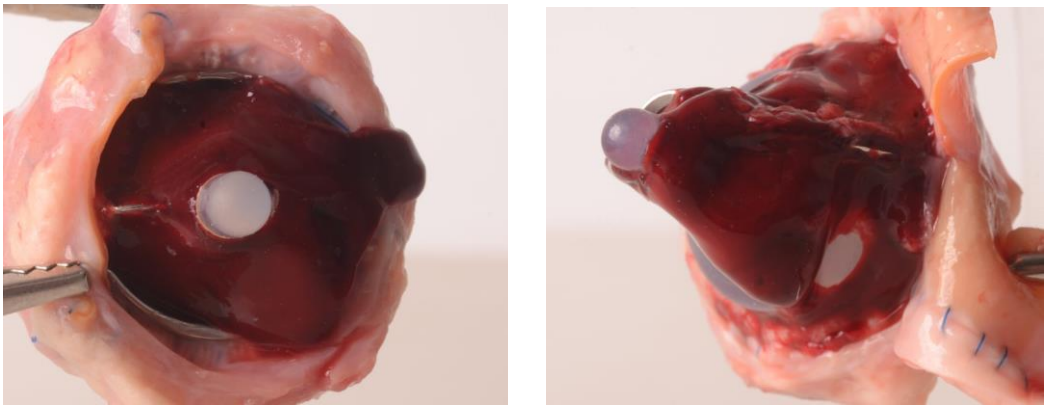

FIGURE 4.60: **The thrombosed Glycar valve**. Notice the large fresh clot on the poppet and the guide strut of the Glycar valve, starting at the base of the sewing cuff. The sewing cuff shows signs of infective endocarditis and can be seen on the photo on the right.

The thrombus was removed, thereby revealing the cause of the thrombus. At the junction between the pericardial patch and the strut was a mass of tissue on the arterial side of the sewing cuff. This tissue extended around the annulus of the valve for approximately 1.5 cm. There were

more tissue overgrowth and vegetations at three points on the RVOT side, at positions four, six and seven o'clock (figure 4.61).

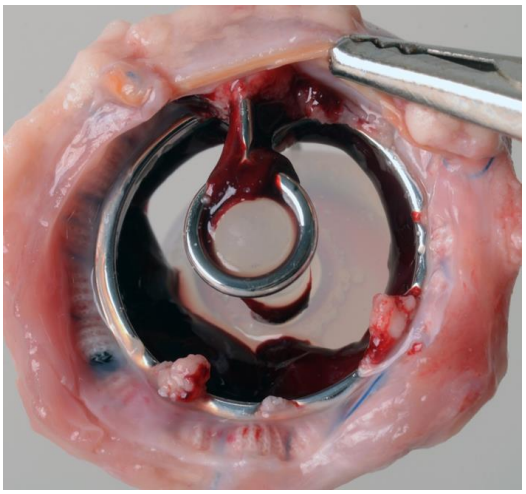

FIGURE 4.61: **The thrombosed Glycar valve viewed from the RVOT.** Notice the multiple vegetations on the valve originating from the sewing cuff, resulting in acute valvular thrombosis.

FIGURE 4.62: **The thrombosed Glycar valve viewed from the PA.** A zoomed view of the inner surface of the housing is shown. Vegetations on both sides of the valve can be seen.

The PA side of the sewing cuff had several areas of tissue overgrowth and vegetations. Almost the entire circumference of the sewing cuff had vegetations. This picture fits in with the clinical suspicion of prosthetic valve infective endocarditis with acute valvular thrombosis. However, healing between the Glycar pericardium patch and the native pulmonary artery was normal and the patch had no signs of calcification or infection. No vegetations were adhered to the patch.

c. Histology of the explanted valve

Microscopic examination shows suture material and pericardial patch with focal foreign body giant cell infiltration (figure 4.63). A fibrinopurulent exudate is noted on the surface of the tissue with infiltration of neutrophils as well as scattered bacterial colonies into the underlying patch. The features are compatible with infective endocarditis. A mild lymphocyte infiltrate is noticed in the surrounding adventitia.

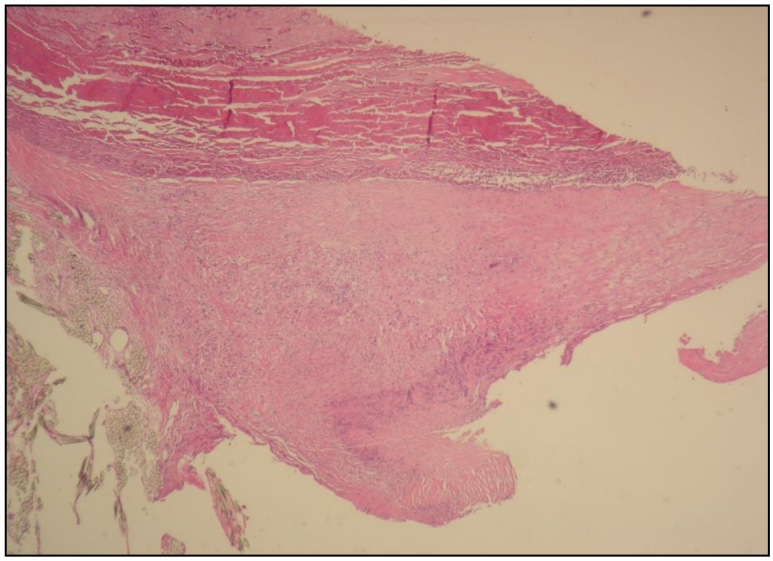

FIGURE 4.63: **Microscopy of the pericardial patch and the sewing cuff**. Colonies of bacteria and neutrophils can be seen in the tissue (40 X magnification, H&E).

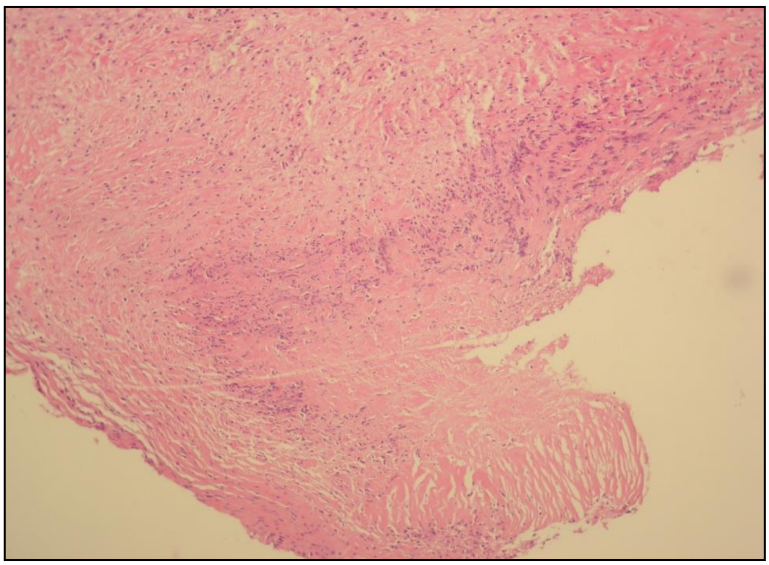

FIGURE 4.64: **Microscopy of the infected sewing cuff.** The extent of the infection can be appreciated in this photo of the patch seen in figure 4.61 (100 X magnification, H&E).

Liver

Microscopic evaluation of the sections of the liver shows the presence of macroscopic steatosis (figure 4.65). No inflammation, necrosis or fibrosis was evident.

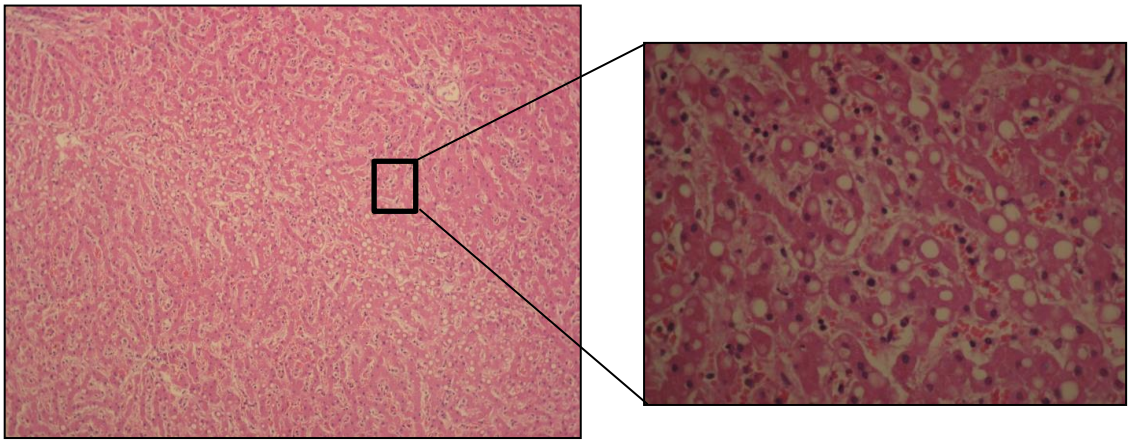

FIGURE 4.65: **Histology of the liver showing hepatic steatosis secondary to the infective endocarditis**. (40 X magnification on the left and 100 X magnification on the right, H&E).

Pulmonary artery wall with pericardial patch:

Microscopic evaluation of the native pulmonary artery shows the presence of small foci of calcification. In some areas an endothelial lining is evident. No thrombus formation is seen. A focal neutrophil infiltrate surrounding the pericardial patch with scattered bacterial colonies is evident (figure 4.66).

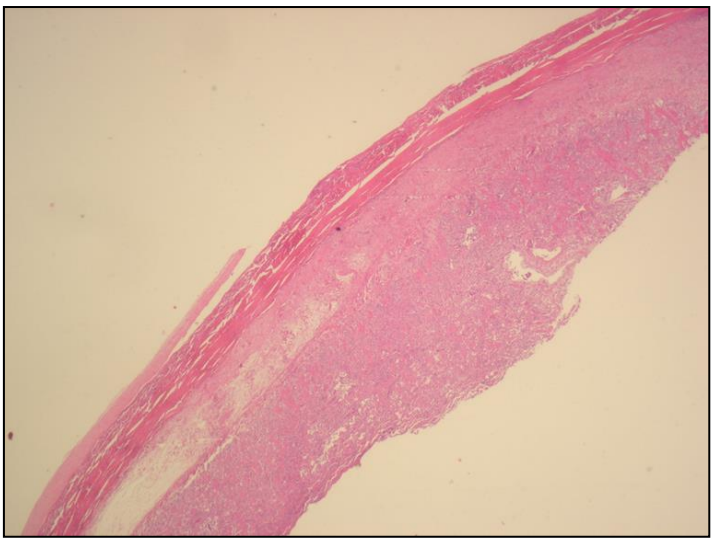

FIGURE 4.66: **Microscopic evaluation of the PA wall showing focal neutrophil infiltrates surrounding the pericardial patch** (40 X magnification, H&E).

CHAPTER 5

Discussion

5.1 Introduction

During the planning phase of this study three main objectives were considered:

1. Firstly, to understand the principles of heart valve functioning and the resulting influence on thrombosis in an in-depth literature review focussing on valve design, fluid-structure interaction within the different valve designs and the subsequent activation of the coagulation cascade. These principles were then applied during the re-designing of a poppet valve prototype that will be cost-effective and easy to produce, whilst at the same time being safe to utilise without any anti-coagulation.
2. Secondly, to investigate the hydrodynamic principles of both CFD and pulse duplication and to apply the principles in the *in vitro* evaluation of the prototype Glycar valve in comparison to a commercially available bi-leaflet heart valve.
3. Lastly, to study the Glycar valve *in vivo* in the ovine model; to evaluate the consequence of the changes made to the valve design and to assess the thrombogenetic potential of the Glycar valve.

5.2 Phase I: Re-engineering of the Glycar valve and CFD

5.2.1 Re-engineering of the Glycar valve

The UCT poppet valve has been around for the past fifty years. From our own experience we know that after being in a patient for thirty years, explanted valves have been shown to be clear of thrombosis in the absence of Warfarin therapy. A historical series published in the 1960s is supportive and it is unfortunate that this valve design did not receive more attention. Comparative and long term studies might have changed the landscape as we know today.

Based on our experience of the UCT valve, we deemed it important to re-evaluate the poppet design. Based on an extensive literature review on the concepts of valve design and flow interaction, validated concepts were incorporated into the Glycar valve prototype.

The systolic/forward flow across the poppet valve was improved by:

- increasing the rounding of the leading and trailing edges of the poppet, reducing stagnation distal to the poppet rod and allowing for laminar flow over the poppet,
- increasing the angle of the distal conal tapering of the poppet to improve laminar flow across the poppet and to reduce flow separation during forward flow,
- removing the sharp edges at the periphery of the poppet at the junction between the cone and the belly and rounded to reduce flow acceleration across the edges of the poppet, reducing viscous shear stress,
- configuring the proximal and distal restraining arms into a teardrop shape as well as the proximal and distal guiding rings to improve fluid dynamic interaction,
- increasing the guiding ring diameters to 5.6 mm proximal and 6.5 mm distal, allowing for a circular motion of the distal poppet rod during valve excursion to dissipate vortex shedding downstream from the poppet,
- increasing the valve housing height by 1.5 mm, simulating the height-to-diameter ratio of a native valve (as in the On-X valve) reducing turbulence and improving laminar forward flow,
- adding a rounded configuration to the inner surface of the housing to simulate aerofoil principals. The aerofoil housing profile optimises the organisation of flow across the valve, turbulent flow is decreased, pressure recovery is favoured and surface continuity with the suture ring is improved. It also provides poppet protection from tissue encroachment from the sewing cuff,
- increasing the distal diameter of the housing by 2 mm, resulting in a flared housing design. Blood flow is directed laterally around the poppet promoting laminar blood flow. The flare produces an increased volume of flow, comparable to that of a larger orifice valve due to smooth, organised flow and a reduction in turbulence.

The diastolic profile was improved by:

- allowing the poppet to seat flush against the housing. The conical shape of the occluder creates a smooth slope down towards the valve housing, directing laminar retrograde blood flow across the conical shape of the conus, over the valve housing and the sewing cuff, into the sinuses of the aorta. Points of stasis around the junction between the poppet and the sewing cuff as well as between the sewing cuff and native tissue interface are eliminated,
- forming a tight seal between the poppet and the housing dispelling retrograde flow and eliminating the so called ‘washing jets’. No blood cells are subjected to the shear stresses experienced in the hinge areas of bi-leaflets and therefore no platelet activation should occur,
- reducing the sewing cuff profile to allow for healing across the sewing cuff and the increased housing hight preventing overgrowth over the housing protecting the poppet against encroachment of cicatricial tissue or pannus,
- the soft landing of the poppet during valve closure due to the compliant silicone poppet striking the housing, thereby reducing impact trauma,

- machining the entire housing and guiding struts from a solid block of stainless steel, circumventing the problems associated with welding of the struts to the housing, Possible areas of metal weakness at these joints, prone to metal fatigue and fracturing, are eliminated.

5.2.2 Computational fluid dynamics of the Glycar valve

The objective of the CFD analysis was first of all to understand the flow patterns generated over the Glycar prototype valve and its components. Secondly, to determine the pressure drop created across the valve and finally, to identify areas of possible stagnation, flow recirculation and regions of high shear stress, which could contribute to haemolysis and platelet activation, prior to *in vivo* evaluation.

During the static evaluation emphasis was placed on the pressure drop across the valve and the flow patterns generated as the CO was increased. The calculated pressure drop across the Glycar valve at a CO of 4.9 L/min was 1.5 mmHg and at a CO of 8.2 L/min 3.5 mmHg. This corresponded to a minimum transvalvular velocity across the valve of 0.242 ms^{-1} at a CO of 1.65 L/min and a maximum velocity of 1.443 ms^{-1} at 8.25 L/min. The low transvalvular velocities are directly proportional to the laminar flow patterns generated by the housing design and the shape of the poppet and therefore, the low gradient. It thus supports the design modifications made to the Glycar valve as a whole and clearly illustrates the impact of streamlined laminar flow through an elongated housing governed by aerofoil principles on the resistance placed during the forward flow phase.

The flow path across the valve was largely laminar with small areas of recirculation in regions where convergence of flow occurred, around the poppet and directly after the retaining rings. Small eddies were seen at the junction of the poppet belly and the guide rod and at the contact point between the distal retaining ring and the poppet. The arms to which the guide rings are attached had no influence on the flow velocity contours and therefore had no impact on cellular interaction. The teardrop shape of the struts and guide rings had a negligible FSI with minimal viscous shear stresses.

The flared housing seems to have encouraged laminar flow through the valve and around the poppet belly and has reduced the incidence and magnitude of eddies and turbulence distal to the housing in the sinuses. However, there were areas where the velocity flow profiles, at the highest flow rate, showed numerous vortices and regions of recirculation, which may lead to turbulent flow around the valve as shown in figure 5.1.

As the CO increased, flow accelerated between the poppet and the aortic wall, which may be responsible for increased viscous shear stress on the surface of the poppet. When the viscous shear stress and the velocity distribution were combined it became apparent that the outer most

edge of the poppet was a major contributor to high viscous shear stress and was responsible for the maximum velocity experienced. A maximum peak viscous shear stress of 20 Pa (at maximal flow of CO 8.2 L/min) was calculated on the surface of the proximal retaining ring facing the flow of blood and at the outermost edge of the poppet during peak forward flow. However, these areas are small and the platelet transit time minimal with hardly any platelet interaction. The viscous shear stress is also well below the platelet activation threshold and therefore the coagulation cascade should not be initiated.

The highest pressure on the Glycar valve at peak forward flow occurred at the front end of the poppet due to stagnation and maximal structural-fluid interaction. The lowest pressure was recorded distal to the poppet guide rod, which was secondary to flow divergence and flow separation around the poppet and therefore the cause of recirculation. This distal area may result in stagnation but as the poppet is in constant motion, stasis will be at a minimal. When the flow velocity contours across the valve areas were mapped, there were regions where the velocity approached zero distal to the retaining rings and the poppet, which was secondary to the shape of the poppet causing recirculation. These areas may lead to stagnation with possible sites for thrombosis. In the wake of the poppet during peak flow, an intricate pattern of large interacting shed vortices can be seen and is responsible for the constant motion of the distal rod of the poppet, preventing platelet adhesion.

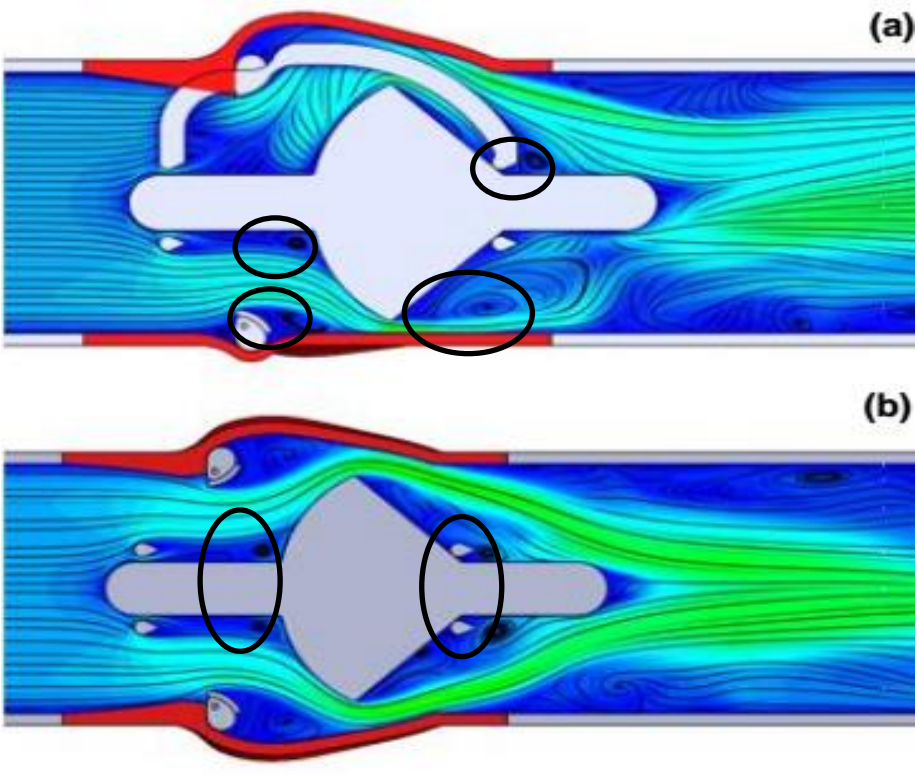

FIGURE 5.1: **Areas of vorticity around the Glycar valve.** (a) front and (b) top plane.

The dynamic simulation at a CO of 4.9 L/min, showed that, as the position of the poppet increased, the pressure gradient on the converging flow side decreased but it increased on the diverging side, which was related to the respective flow areas. The lowest pressure drop was

measured at the 7 mm position, measuring 1.55 mmHg, somewhat lower than in the fully open position at 8 mm with a pressure of 1.56 mmHg. As can be expected, the velocity was in relation to the pressure drop with the lowest peak velocity measured at the 7 mm position at 0.75 ms^{-1}.

The CFD analysis of the Glycar design proved to be excellent. The modifications in the overall design prototype had clearly improved the flow dynamics across the valve and contributed to the laminar flow resulting in a low calculated pressure drop. The areas of turbulence and flow separation were very small and not significant and the viscous shear stress on the poppet and the guides was negligible, well below the platelet activation threshold. The design allowed for streamlined blood flow across the valve without the detrimental fluid structure interaction that causes an increase in platelet activation and the initiation of the coagulation cascade.

5.3 Phase II: Pulse duplication

i. Validation of the pulse duplicator data:

The validation of the pulse duplicator data was succsessfull and was supported by both the tests as outlined in the methodology.

With reference to the literature comparison the pulse duplication setup and data acquisition accuracy were supported. Although the maximum pressure drop for the Carbomedics valve was higher than the SJM in the study, the graph waveform for both the valves was comparable and similar, confirming the accuracy of the testing arrangement. When the data were compared to the data from the study performed by Piatti *et al.* (2015), an excellent correlation was found supporting the validity and accuracy of the data.

The ViVitro reference valve findings in our pulse duplication model (Q_{rms}, pressure drop, EOA and RF) correlated with the data as provided by ViVirtro, supporting the measuring and simulation setup.

ii. The total forward flow volume (Q_{rms})

As most of the measurements and calculations are based on the accuracy of the Q_{rms}, measurements were taken at ten different intervals for each of the valves during the different testing conditions to ensure consistency (the standard deviation was determined and was very low throughout). ISO 5840:2015 and FDA requires that all MHV tested up to 5.0 L/ min. During this simulation the valves were exposed to testing conditions greater than is required as the performance of all the valves was very similar. Therefore the valves were tested until a point was found where discernible differences were seen, which occurred at 9.6 L/min (equal to strenuous exercise).

When the Q_{rms} was charted against the pressure drop the Glycar valve and the Carbomedics valve were similar in performance, even at a CO of 8.0 L/min; the Glycar valve outperformed the requirements as determined by ISO 5840:2015 and the FDA for 21 mm mechanical heart valves for licencing purposes comfortably. The performance of the Glycar valve in relation to the other commercial valves was on par with no significant difference.

iii. The effective orifice area

When comparing the EOA of each of the valves a similar picture emerges. Each of the valves outperformed the minimum EOA as required by ISO 5840-1:2015 and FDA approval for 21mm

MHV (>0.85 cm^2). The ViVitro poppet valve was the only valve that failed when the CO dropped below 4 L/min however, this valve was not designed to have advanced haemodynamics. The Glycar valve performance was comparable to all of the commercially available valves with a similar EOA. As the CO increased the performance of the Glycar valve improved, outperforming the bi-leaflet valve. The EOA for the 21 mm Glycar valve at a CO 6.0 L/min was 1.39 cm^2.

iv. Pressure drop

The pressure drop determined for the Glycar valve during pulse duplication was higher than the CFD generated gradient however, the Carbomedics bi-leaflet valve and the Glycar valve had similar gradients as the CO increased up to 6.0 L/min, well within the ISO 5840:2015 and FDA requirements. Only when high level testing was conducted, was the gradient for the Glycar valve greater than the bi-leaflet's gradient (38 mmHg vs. 30 mmHg at CO 9.6 L/min). It is uncertain if the higher gradient will have any clinical relevance. Although the Glycar valve had a higher gradient during high level testing, the Perimount tissue valve had the same pressure drop and was therefore equal in performance.

v. The regurgitant fraction

The RF and closing volumes were similar for all the valves in the simulation. The performance of the ViVitro valve was outstanding and had the lowest RF at less than 1%. This was due to the spring loaded closing mechanism of the leaflet aiding early valve closure, artificially reducing regurgitation. The valve also had no valve leakage once the disc occluder was in the closed position as the valve had no 'washing jets' in the design.

The closing volumes for the bi-leaflet and the Perimount tissue valves were lower than the closing volumes for the Glycar and the Medtronic-Hall valves, all of them well within the ISO 5840:2015 and FDA requirements. As the CO increased the Glycar valve maintained its regurgitant fraction, however above 8.0 L/min the closing volume increased, still within the 10% limit as required by ISO 5840:2015 for a 21 mm valve.

During the simulation the poppet was unable to move back into position on top of the housing once the CO was beyond 8.0 L/min, resulting in an increased closing volume. This could possibly be attributed to the mass of the poppet, where the forward inertia of the poppet is greater than the forces acting on the poppet during diastole to propel the poppet back onto the housing in order to allow for valvular closure before systole begins. The weighted inertia of the poppet might therefore limit the excursion distance at higher frequencies (heart rate). However, once the poppet was fully seated, the Glycar valve had the lowest leakage volume of all the commercially available valves.

vi. Transvalvular energy losses

In comparison, all of the valves performed well except for the ViVitro valve, due to the obstructive nature of the disk. In comparison the Glycar valve and the Carbomedics valves had similar energy losses at a low CO (CO 3.6 L/min: 104 mJ vs. 102 mJ). As the CO increased, the systolic energy losses increased. At a CO of 9.6 L/min the total systolic energy loss for the Glycar valve was 471 mJ compared to 317mJ for the Carbomedics valve. This discrepancy might be attributed to the inertial weight of the poppet requiring more energy to displace the poppet during retrograde flow and due to the initial increased RF (closing volume).
The energy loss for the Glycar valve is however within the ISO 5840:2015 requirements.

vii. Summary of bench testing and conclusion

Considering the ISO 5480:2015 and the FDA requirements for bench testing for MHV licensing purposes, the Glycar valve performance exceeded in each of the requirements. In comparison to different commercially available valves and designs, the Glycar valve had an outstanding performance with properties equating it's bi-lealfet valve counterpart (regarded as the gold standard for comparative testing). Overall, the Glycar valve appeared to more closely emulate the haemodynamic properties of the native tissue valve than the traditional bi-leaflet design.

Although CFD is not part of the standard ISO bench testing and is not required for licensing purposes, the Glycar valve was subjected to a detailed CFD evaluation. The influence of the alterations made to the Glycar design on flow dynamics/FSI was studied and the performance of the valve exceeded expectations and reinforced the phase II evaluation. With a high EOA and a low pressere drop, the modifications in the overall design prototype had clearly improved the flow dynamics across the valve and contributed to laminar flow.

The areas of turbulence and flow separation were not significant and the viscous shear stress on the poppet and the guides was negligible, well below the platelet activation threshold. The design allows for streamlined flow across the valve without the detrimental FSI that causes an increase in platelet activation and the initiation of the coagulation cascade.

Pulse duplication demonstrated that the Glycar valve performance was on par with all current MHV designs, including the bi-leaflet valve. The Glycar valve exceeded in all of the criteria as required by ISO 5840:2015 and FDA, up to a CO of 8 L/min. Above a CO of 8.0 L/min the valve performance was compromised with a higher RF however, the clinical significance thereof is questionable. Following on the success of the pulse duplication, animal studies proceeded.

5.4 Phase III: The *in vivo* evaluation of the Glycar valve

The aim of phase III was to evaluate the modified Glycar prototype in the animal model to determine the haemodynamic performance of the valve in comparison to a commercially available bi-leaflet valve. The valve was also evaluated in the absence of anti-coagulation to determine the thrombogenic potential of the Glycar valve. Cellular interaction such as haemolysis was determined throughout the follow-up interval and at explantation the valves were evaluated macroscopically and microscopically for evidence of thrombosis.

During the study interval both study groups of the Glycar valves performed well in the absence of anti-coagulation and none of the test animals showed signs of valvular dysfunction, such as cardiac failure, pleural effusions or emboli. Haematology, immunology, biochemistry and liver functions were unremarkable throughout the study interval. Although most of the sheep had a higher LDH level immediately post-operatively, it recovered soon after surgery and was normal at explantation. None of the sheep had serology suggestive of haemolysis.

All of the valves functioned well on echocardiography during implantation and at explantation in both the short term and long term follow-up groups. The poppet motion of the Glycar valve was normal and unimpeded by the pericardial patch or the RVOT. There were no signs of right ventricular failure, pleural effusions or pericardial effusions. The average EOA on echo was 1.53 cm^2 for the Glycar valve, 19.53% greater than the Carbomedics EOA at 1.28 cm^2. The average gradient for the Glycar valve was 10.84 mmHg with a mean gradient of 10.70 mmHg. The low gradients were in line with the performance predicted by CFD and pulse duplication and therefore the modifications made to the Glycar valve was substantiated. In comparison to the bi-lealfet, the echocardiographic performance of the Glycar valve was excellent.

At explantation the Glycar valves functioned well and there was no evidence of pannus overgrowth over the sewing cuff and there were no para valvular leaks. In both groups none of the valves showed any form of dysfunction with normal excursion of the poppets. Haemodynamically all of the valves performed well however, the bi-leaflet valves had the highest peak-to-peak gradients measured in the pulmonary position after implantation and at sacrifice. The Glycar valves had more favourable gradients. The peak-to-peak gradients for the Glycar valve at implantation was on average 3.50 mmHg and at explantation 3.29 mmHg.

Visually and photographically all of the valves, except for the Glycar valves that had had infective endocarditis, were clear of thrombi and functioned normally, including the control valves. The poppets were clean and clear of thrombus and none of the silicone poppets showed signs of wear, surface defects or cracks. The struts and the guiding rings were equally devoid of thrombi as was the valve housing. From our findings is was apparent that the sewing cuff design was not optimal and will be addressed in the updated prototype, with a complete redesign.

Histology was unremarkable in all of the sheep showing normal healing. The sewing cuff showed a prominent giant cell reaction with small areas of metaplastic ossification and no signs of inflammation, platelet deposition or thrombus.

Both of the sheep that died prior to scheduled explantation presented with late, acute valvular dysfunction secondary to acute prosthetic valve thrombosis. The cause in both was evident at explantation as the valves presented with infective endocarditis with large vegetations on the sewing cuff at the junction between the sewing cuff and the valve housing. In this area incomplete covering of the sewing cuff material was evident, presumably acting as a nidus or site for bacterial adhesion with secondary prosthetic valve infective endocarditis. Both of the sheep did well, far into the follow-up interval (five months and twelve months respectively) suggesting late onset infection, ruling out intra-operative contamination.

It was evident that the Glycar valve performed as predicted in the animal model and in comparison to the control valve it did extremely well. The low pressure environment the valves were exposed to in the pulmonary position, may have contributed to the success of the study, especially with regard to the bi-leaflet valves. When exposed to the higher pressures in the aortic position the bi-leaflet valves should fare poorly as the velocity of the regurgitation jets will be accentuated, increasing viscous shear, creating a pro-coagulant environment around the valve.

Overall, the Glycar valve performed satisfactory in comparison to the Carbomedics valve when the flow-dynamics in the *in vivo* environment were evaluated. The Glycar valve had a lower transvalvular flow velocity and therefore a lower gradient across the valve in all of the cases. The valve also had a greater EOA. However, the bulky nature of the valve precludes the use of the valve in the small aorta and in the small ventricle. The valve is not intended for mitral valve replacement and therefore no attempt was made to simulate the mitral position.

5.5 Conclusion

During the last four decades, significant advances in the development of bio-compatible materials used in blood interfacing implants have been observed. In the case of MHV replacements, pyrolyte carbon has become the material of choice in the manufacturing of valve leaflets and housings. Pyrolytic carbon is chemically inert and exhibits very little wear, even after more than twenty years of use in situ. However, thrombo-embolic complications still remain significant. The complex dynamics of valve function and the resulting mechanical stresses on the formed elements of blood appear to be the main cause for initiation of thrombosis. However, by changing the carbon composition of a valve, or covering the carbon with layers such as heparin or removing the silicone from the pyrolyte had no added benefit in lowering the thrombogenicity of heart valves.

Based on the premise that the material used in the manufacturing of the valve should not have an effect on coagulation, as long as it is biocompatible and that the exclusion of the washing jets in the design should reduce the thrombogenicity of the valve, the Glycar valve was designed. Due to the availability, the low cost of the materials and the relative ease of manufacturing the Glycar valve was constructed from biocompatible stainless steel (316L alloy) and the poppet from medical grade cured silicone.

During the diastolic phase the aortic valve has a blood contact time of 0.5 seconds (at a heart rate of 60 bpm), therefore the stagnant blood contact time during this phase is very long. Much has been written about stagnation in the hinge mechanism and the prevention thereof but the entire valve is in contact with stagnant blood during diastole. Therefore, if the material were an issue, the entire valve would thrombose, but this is not what happens in reality.

The forward flow across a mechanical heart valve might theoretically lead to an increase in coagulation due to enhanced platelet activation and adhesion and the activation of the clotting cascade due to the increased viscous shear stress secondary to increased flow velocities across valve surfaces. However, the opposite is true when evaluating native aortic valve stenosis. The stenotic valve causes an increase in flow velocity and the turbulence created is greater than that experienced by any MHV.

The viscous shear stress experienced in severe aortic valve stenosis is greater than the platelet threshold, which should theoretically increase thrombogenesis. The surface of the valve is also irregular due to calcification and in some patients this can be extreme and quite easily also increase thrombosis. Counter-intuitive to the principles governing thrombosis in an MHV during forward flow, thrombosis in AS is not enhanced. As a matter of fact, thrombosis occurs at a lower rate secondary to vWF degradation. The proposal therefore is that coagulation should not be influenced by the forward flow phase during systole in the aortic valve position by the Glycar poppet, as long as the flow is laminar across the valve.

Of greater importance to valvular thrombosis though, is the flow patterns across MHV during the regurgitant flow seen during the back flow phase. The principles of shear induced platelet activation experienced in the valve hinge during the closed phase is vital. It is during this phase that a valve in the aortic position, exposed to high pressure differences between the aorta and the left ventricle allows high velocity 'washing jets' to flow over the hinge mechanism, between the leaflets and the housing and in the b-datum line.

The shear stresses experienced in these areas are above the threshold for platelet activation and each platelet will be exposed to the valve between 9 600 to 29 000 times during its life-span of ten days. Many attempts have been made to improve on the hinge mechanism, some with great success (On-X valve), other with dismal results (Medtronic Parallel valve). Structural failure of implanted mechanical valves as well as pitting and erosion observed on the pyrolytic carbon surfaces have been attributed to cavitation during valve closure, supporting the theory that the 'washing jets' cause an increase in thrombosis.

By eliminating the 'washing jets' in the Glycar valve several associated complications are avoided or attenuated:

- Cavitation cannot take place, reducing the incidence of material wear and erosion and the activation of coagulation.
- The absence of shear induced platelet activation
- The activation of vWF and factor 12

As the viscous shear stress experienced during the forward flow phase across the Glycar valve is lower than the threshold for the activation for platelets, thrombosis is not initiated or influenced. The poppet of the Glycar valve seats snugly against the housing, eliminating regurgitant jets that would have formed during the back flow phase. The regurgitant flow from the Glycar valve is negligible, eliminating the shear stresses experienced in the hinge areas of bi-leaflet valves.

The nature of the silicone poppet allows for a certain amount of pliability of the poppet. The poppet seats snugly and softly against the housing of the valve during diastole and is not plagued by the water hammer effect as experienced by the tilting disk and bi-leaflet valves. The poppet does not slam into the housing because the closing energy is absorbed by the poppet and results in a non-traumatic closure of the valve with little to no harm to the cellular component of blood.

This modified Glycar valve was evaluated and the functionality of the valve was compared with commercially available heart valves in a non-inferiority study; evaluating the flow characteristics with CFD and then comparing the hydrodynamic interaction using pulse duplication. CFD exhibited a streamlined laminar flow pattern both during systole and diastole with a greater than expected EOA and transvalvular gradient. Flow separation, shear stress, turbulence induced shear stress and vortex formation revealed favourable patterns in this design. The valve proved

to be a suitable alternative to a bi-leaflet valve due to the valve's excellent hydrodynamic properties and characteristics in the simulated pulsatile environment conforming to the requirements as stipulated by ISO 5840:2015 and FDA.

The current Glycar valve design in the pulmonary position in the ovine model proved to be reliable and thrombo-resistant in the absence of anti-coagulation in the short term as well as in the long term follow-up. The biocompatibility of both stainless steel and cured silicone has been proven when exposed to blood flow under stressed conditions in many previous studies. This study reiterated the safety of both materials as well as their thrombo-resistance. There were some aspects that will need attention in further evaluation of the valve, which were highlighted in the discussion of the valve design. The next step will be to test the valve in a high pressure environment such as in the aortic position before human trials can be considered.

5.6 Future recommendations and limitations

5.6.1 Valve design

1. In front of the poppet rod, a stagnation region forms which contributes to the overall pressure drop. Although this pressure drop is probably small relative to the other regions that also contribute to the overall pressure drop, a more streamlined leading edge could reduce the size of the stagnation region. Figure 5.2 illustrates the current design and one that is more streamlined.

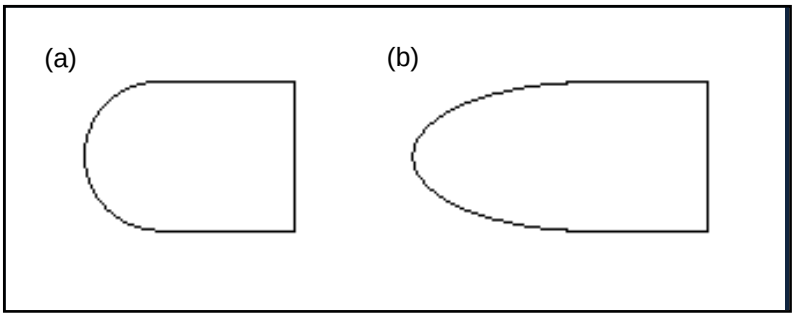

Figure 5.2: **Poppet leading edge design**. (a) the current design, (b) the proposed modification.

2. Downstream of the guiding ring, a large recirculation region forms. The flow breaks away, resulting in a low pressure area. Here again the cross-section shape of the entire ring can be investigated to assess its influence on the overall pressure drop. Figure 5.3 illustrates the current design and a design which may be considered. The design to be considered takes on a more elliptical shape. An elliptical shape may also reduce the pressure drop across the valve, as the drag coefficient would be less. Figure 5.4 below shows the drag coefficient of an ellipse as a function of the length divided by the height. It can be seen that for a longer ellipse to height ratio, the drag coefficient decreases.

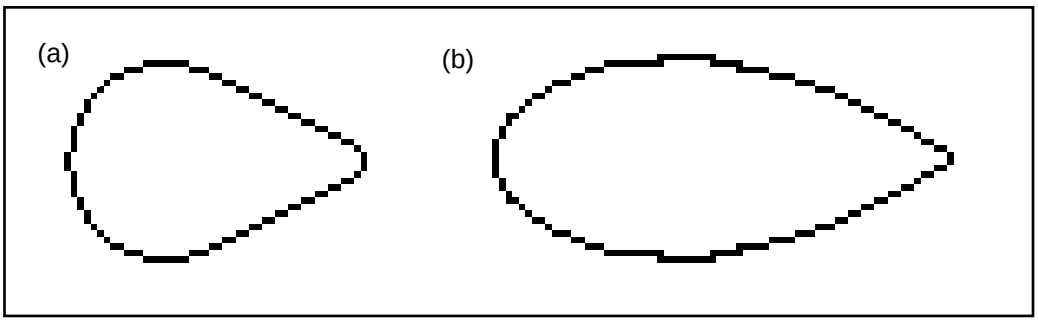

FIGURE 5.3: **Design changes suggested to the cross sectional area of the struts**. (a) the current design and (b) the modification

.

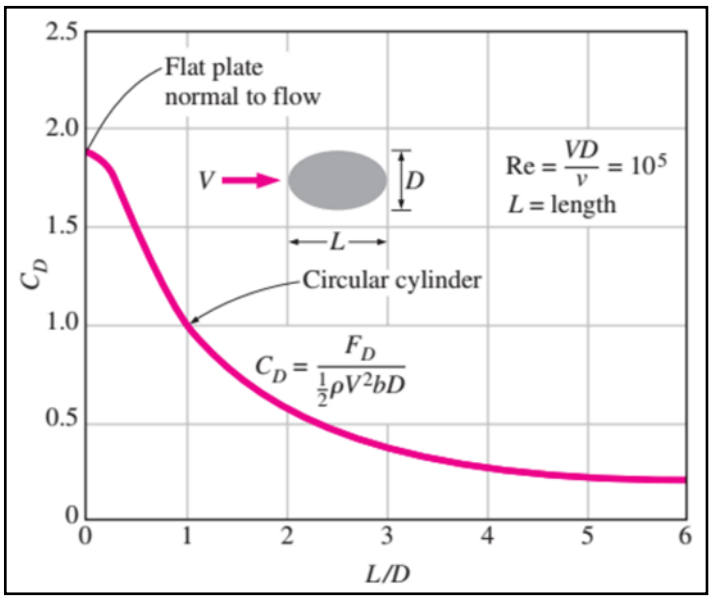

Figure 5.4: **Front guiding ring design: drag coefficient of an ellipse as a function of the length divided by the height.** V= velocity; L= length; D= diameter; C_D= drag coefficient; L/D= length to diameter ratio.

3. Another static region occurs when the poppet starts to increase in diameter. This is due to a combination of the front guide ring and the poppet itself. The poppet contribution is as a result of the sharp corner caused by a rapid increase of area. Here a rounded edge, as shown in figure 5.5 could aid in improving the flow patterns. By eliminating the sharp corner, the possibility for fatigue crack growth becomes less. Not only can cracks cause the poppet to break and fail, but it may also serve as a point where small clots can accumulate.

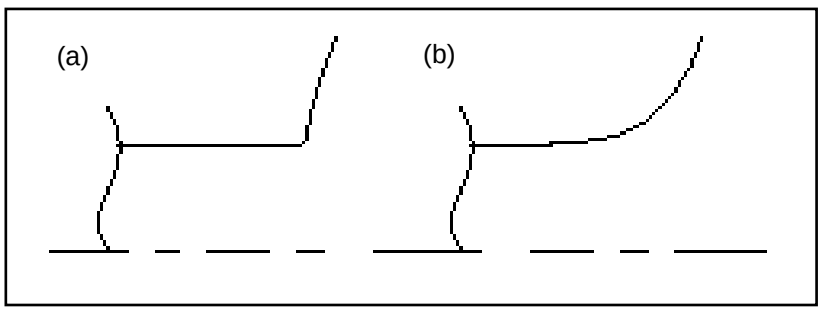

Figure 5.5: **Improved poppet free edge.** (a) current poppet edge, (b) proposed poppet **edge.**

4. The poppet shape after the sharp edge and before its area starts to reduce and does not have a noticeable effect on the flow. However, this shape could be investigated to assess its influence on the pressure drop and the valve response. A general rule of thumb for this kind of shape, which causes flow to converge, is that it should represent a hemisphere or the front end of an ellipse, in that the length should be equal or larger than the radius. The contributions to the pressure drop are those of converging flow and those due to friction (friction losses are generally very small). If the length increases, the

pressure drop caused by the accelerating flow decreases and the pressure drop due to friction increases.

5. The trailing edge of the poppet or the region where the area of the poppet reduces is causing significant areas of static flow and recirculation. This is due to the flow detaching from the poppet's surface. Typically, the reduction angle should be gradual enough to ensure that flow does not separate and cause vortices and circulation. The limitations to this would be the response or reaction time of the poppet.

6. The sewing cuff will have to be redesigned as the redundancy of the cuff caused prolapse of the Dacron into the RVOT, influencing the blood flow across the valve. Fortunately, this is easily remedied and the new cuff design will be included into the new prototype.

7. Finally, the solid silicone poppet had a high inertial weight, which proved to be problematic at a high CO due to the inability of the poppet to close properly resulting in an unacceptable high regurgitation. A reduction in the poppet mass might make the poppet more responsive to sudden directional changes, leading to earlier valve closure.

5.6.2 CFD

1. The CFD report did include a mesh refined around the valve, but did not include a grid independence study. A grid independence study is performed by running simulations with a coarse mesh and increasing the fineness of the mesh until the results do not change with a finer mesh. This eliminates the potential changes in results induced from the mesh alone.

2. A problem with the simulation model is the lack of a turbulence model. The study's CFD analysis used a laminar model to simulate the flow, with the result that there was no turbulence. However, a laminar model would not pick up turbulence in the flow even if turbulence was present. No experimental data are linked to the simulation as to what the flow profile is, so it is unclear if turbulence would be present. An indication that turbulence could be present in the valve is the various vortices apparent in the velocity profiles. These recirculation regions could induce high shear stress, once again causing thrombosis or platelet activation. Steady state analysis is not indicative of normal valve operation. An attempt was made to account for the transient (non-steady state) nature of heart valve operation by fixing the volumetric flow rate and changing the position of the poppet.

References

ACC/AHA 2006 Guidelines for the Management of Patients With Valvular Heart Disease: Executive Summary: A Report of the American College of Cardiology/American Heart Association Task Force on Practice Guidelines (Writing Committee to Revise the 1998 Guidelines for the Management of Patients With Valvular Heart Disease): Developed in Collaboration With the Cardiovascular Angiography and Interventions and the Society of Thoracic Society of Cardiovascular Anaesthesiologists: Endorsed by the Society Cardiovascular Angiography and Interventions and the Society of Thoracic Surgeons. *Circulation*. 2006; 114: 450–537

Akhthar RP, Abid AR, Zafar H, Khahn JS. Anticoagualation in patients following heart valve replacements. *Ann Thoracic Cardiovasc Surg.* 2009; 15:10-17

Akins CW. Mechanical cardiac valvular prosthesis. *Ann Thorac Surg.* 1991; 52:161-172

Akutsu T and Higuchi D. Effect of mechanical prosthetic heart valve orientation on the flow field inside the simulated ventricle: comparison between St. Jude Medical Valve and Medtronic-Hall *Valve. J Artif Organs.* 1999; 2:39-45

Alemu Y and Bluestein D. Flow induced platelet activation and damage accumulation in a mechanical heart valve: Numerical studies. *Artificial organs.* 2007; 31(9):677-688

Aluri S and Chandran KB. Numerical simulation of mechanical mitral heart valve closure. *Ann Biomed Eng*. 2001; 29:665–676

Andersen TS, Johansen P, Christensen BO, Paulsen PK, Nygaard H, Hasenkam M. Intraoperative and Post-operative Evaluation of Cavitation in Mechanical Heart Valve Patients. *Ann Thorac Surg.* 2006; 81:34-41

Annerel S, Claessens T, Van Ransbeeck P, Segers P, Verdonck P, Vierendeels J. State-of-the-art methods for the numerical simulation of aortic BMHVs. *Aortic Valve.* 2011; 1:1-50

Ansell J, Hirsh J, Hylek E. Pharmacology and management of the vitamin K antagonists: American college of chest physicians evidence-based clinical practice guidelines (8th Edition). *Chest.* 2008; 133:160S–198S

Antunes MJ, Wessels A, Sadowski RG, Schutz JG, Vanderdonck KM, Oliveira JM, et al. Medtronic Hall valve replacement in a third-world population group. A review of the performance of 1000 prosthesis. *J Thorac Cardiovasc Surg*. 1988; 95(6):980–93

Aoyagi N, Tanaka I, Nishi Y, Yamashita M, Oryouji A, Hara T, Kosuga K, Ooishi K. Long-term result of MRV by SJM valve (in Japanese). *J Jpn Thorac Cardiovasc Surg.* 1991; 39:1126-1130

Aramendi JI, Mestres CA, Martinez-León J, Campos V, Muñoz G, Carlos Navas. Triflusal versus oral anticoagulation for primary prevention of thromboembolism after bioprosthetic valve replacement (trac): prospective, randomized, co-operative trial. *Eur J Cardiothorac Surg* 2005; 27 (5): 854-860

Arefin MS and Morsi YS. Fluid structure interaction simulation of the left ventricle during the early filling wave (E-wave), diastasis and atrial contraction wave (A-wave). *Australas. Phys. Eng. Sci. Med.* 2014; 37:413–42

Arom KV, Nicoloff DM, Kersten TE, Northrup WF, Lindsay WG, Emery RW. Ten years' experience with the SJM valve prosthesis. *Ann Thorac Surg.* 1989; 47:831–7

Arfken, G. *Mathematical Methods for Physicists*, 3rd ed. Orlando, FL: Academic Press, 1985

ATS Medical, Inc. Pre-market Approval Application – Summary of Safety and Effectiveness: 2000. Washington D.C.: U.S. Food and Drug Administration; 2000

Babuška I, Banerjee U, Osborn E. Generalized Finite Element Methods: Main Ideas, Results, and Perspective. *Int J Computational Methods.* 2004; 1(1): 67–103

Badduke ER, Jamieson ER, Miyagishima RT. Pregnancy and childbearing in a population with biologic valvular prosthesis. *J Thorac Cardiovasc Surg*. 1991; 102:179–186

Baldwin JT, Tarbell JM, Deutsch S, Geselowitz DB. Mean velocities and Reynolds stresses within regurgitant jets produced by tilting disk valves. *ASAIO Trans.* 1991; 37:348-349

Barbetseas J, Nagueh SF, Pitsavos C, Toutouzas PK, Quiñones MA, Zoghbi WA. Differentiating thrombus from pannus formation in obstructed mechanical prosthetic valves: an evaluation of clinical, transthoracic and transoesophageal echocardiographic parameters. *J Am Coll Cardiol.* 1998; 32(5):1410-7

Barnard C, Shrire V, Goosen C. Total aortic valve replacement. *Lancet.* 1963; 2:856-859

Barreto-Filho JA, Wang Y, Dodson JA, Desai MM, Sugeng L, Geirsson A. Trends in aortic valve replacement for elderly patients in the United States, 1999–2011. *J Am Med Assoc.* 2013; 310(19):2078–2085

Bates SM, Greer IA, Middeldorp S. VTE, thrombophilia, antithrombotic therapy, and pregnancy: antithrombotic therapy and prevention of thrombosis, 9th ed: American College of Chest Physicians Evidence-Based Clinical Practice Guidelines. *Chest.* 2012; 141:691-736

Baudet EM, Oca CC, Roques XF, Laborde MN, Hafez AS, Collot MA, Ghidoni IM. A 5 1/2 year experience with the St. Jude Medical cardiac valve prosthesis. Early and late results of 737 valve replacements in 67~ patients. *J Thorac Cardiovasc Surg.* 1985; 90:137-144

Beckmann A, Hamm C, Figulla HR, Cremer J, Kuck KH, Lange R, Zahn R, Sack S, Schuler GC, Walther T, Beyersdorf F, Böhm M, Heusch G, Funkat AK, Meinertz T, Neumann T, Papoutsis, Schneider S, Welz A, Mohr FW. The German Aortic Valve Registry (GARY): A Nationwide Registry for Patients Undergoing Invasive Therapy for Severe Aortic Valve Stenosis. *Thorac cardiovasc Surg.* 2012; 60(05): 319-325

Bhatt DL. Platelets in cardiovascular disease.1 st edition. London: Imperial College Press, 2008

Birkmeyer NJO, Birkmeyer JD, Tosteson ANA, Grunkemeier GL, Marrin CAS, O'Connor GT. Prosthetic valve type for patients undergoing aortic valve replacement: a decision analysis. *Ann Thorac Surg.* 2000; 70:1946–52

Bjork VO. Advantages and long-term results of the Bjork-Shiley valve. J.H.K. Vogel (Ed.). Cardiovascular medicine, Raven Press, New York. 1982; 293–294

Blot WJ, Ibrahim MA, Ivey TD, Acheson DE, Brookmeyer R, Weyman A, Defauw J, Smith JK, Harrison D. Twenty-Five–Year Experience With the Björk-Shiley Convexo-concave Heart Valve. A Continuing Clinical Concern. *Circulation.* 2005; 111:2850-2857

Bluestein D. Research approaches for studying flow induced thrombo-embolic complications in blood recirculating devices. *Expert Rev. Med. Devices.* 2004; 1:65-80

Bluestein D, Niu L, Schoephoerster RT, Dewanjee MK. Steady flow in an aneurysm model: Correlation between fluid dynamics and blood platelet deposition. J Biomech Engin Trans ASME. 1996; 118:280–286

Bluestein D, Rambod E, Gharib M. Vortex shedding as a mechanism for free emboli formation in mechanical heart valves. *J Biomech Eng*. 2000; 122(2):125-34

Bokros JC, Ely JL, Emken MR. Prosthetic Heart valve with improved blood flow. US Patent No. 5,772,694: Issued June 30, 1998

Bokros JC, Ely JL, Emken MR. Prosthetic heart valve. US Patent No. 5,641,324: Issued June 24, 1997

Bokros JC, Emken MR, Haubold AD. Prosthetic heart valve. US Patent No. 5,308,361: Issued May 3, 1994 and US Patent No. 5,137,532: Issued Aug. 11, 1992

Bokros JC, Gott VL, La Grange LD, Fadall AM, Vos KD, Ramos MD. Correlations between blood compatibility and heparin adsorptivity for an impermeable isotropic pyrolytic carbon. *J Biomed Mater Res*. 1969; 1(3):497–528

Bokros JC, Stupka JC, More RB. Prosthetic heart valve. US Patent No. 6,096,075: Issued Aug., 1, 2003

Bonow RO, Carabello BA, Kanu C, de Leon AC Jr, Faxon DP, Freed MD, Gaasch WH, Lytle BW, Nishimura RA, O'Gara PT, O'Rourke RA, Otto CM, Shah PM, Shanewise JS, Smith SC Jr, Jacobs AK, Adams CD, Anderson JL, Antman EM, Faxon DP, Fuster V, Halperin JL, Hiratzka LF, Hunt SA, Lytle BW, Nishimura R, Page RL, Riegel B. ACC/AHA 2006 guidelines for the management of patients with valvular heart disease: a report of the American College of Cardiology/American Heart Association Task Force on Practice Guidelines. *Circulation,* 2006; 114: 84-231

Boloori-Zadeh P, Corbett SC, Nayeb-Hashemi H. Effects of fluid flow shear rate and surface roughness on the calcification of polymeric heart valve leaflet. *Materials Science and Engineering*. 2013; 33(5):2770-2775

Boloori-Zadeh P, Corbett SC, Nayeb-Hashemi H. In-vitro calcification study of polyurethane heart valves. *Materials science and eng.* 2014; 35:335-340

Bor J, Herbst AJ, Newell ML and Bärnighausen T. Increases in adult life expectancy in rural South Africa: valuing the scale-up of HIV treatment. *Science.* 2013; 339:961–965

Borazjani I, Ge L, Le T, Sotiropoulos F. A parallel overset-curvilinear-immersed boundary framework for simulating complex 3D incompressible flows. *Comput. Fluids.* 2013; 77:76–96

Brown CH, Leveret LB, Lewis CW, Alfrey CP, Hellums JD. Morphological, biochemical and functional changes in human platelets subjected to shear stress. *J. Lab. Clin. Med.* 1975; 86:462-471

Brucker C. Duel camera DPIV for flow studies past artificial heart valves. *Exp. Fluids.* 1997; 22:496-506

Butchart EG, Gohlke-Bärwolf C, Antunes MJ, Tornos P, De Caterina R, Cormier B, Prendergast B, Lung B, Bjornstad H, Leport C, Hall RJC, Vahanian A. Recommendations for the management of patients after heart valve surgery. *European Heart Journal.* 2005; 26 (22): 2463-2471

Butchart EG, Li HH, Payne N, Buchan K, Grunkemeier GL. Twenty-year experience with the Medtronic-Hall valve. J Thorac Cardiovasc Surg. 2001; 121:1090-100

Budnitz DS, Lovegrove MC, Shehab N, Richards CL. Emergency hospitalizations for adverse drug events in older Americans. *N Engl J Med*. 2011; 365:2002–2012

Butany J, Collins MJ. Analysis of prosthetic cardiac devices: a guide for the practicing pathologist. *J Clin Pathol.* 2005;58(2): 113-24

Cannegieter SC, Rosendaal FR, Wintzen AR. Optimal oral anti-coagulant therapy in patients with mechanical heart valve prosthesis: the Leiden artificial valve and anti-coagulation study. *N Engl J Med.* 1995; 333:11–17

Cáceres-Lóriga FM, Morais H. Thrombotic obstruction in left-side prosthetic valves: Role of thrombolytic therapy. *Indian Heart Journal*. 2015; 67:10-12

Cáceres-Lóriga FM, Pérez-López H, Santos-Gracia J, Morlans-Hernandez K. Prosthetic heart valve thrombosis: Pathogenesis, diagnosis and management. *Int J Cardiol*. 2006; 7:1-6

Castellano JM, Narayan RL, Vaishnava P, Fuster V. Anti-coagulation during pregnancy in patients with a prosthetic heart valve. *Nature Reviews Cardiology*. 2012; 9:415–424

Cieślik M, Kot M, Reczyński W, Engvall K, Rakowski W, Kotarba A, Parylene coatings on stainless steel 316L surface for medical applications. Mechanical and protective properties. *Materials Science and Engineering*. 2012; 32(1):31-35

Chambers JB, Pomar JL, Mestres CA and Palatianos GM. Clinical event rates with the On-X bi-leaflet mechanical heart valve: a multicenter experience with follow-up to 12 years, *J Thorac and Cardiovasc Surg.* 2013; 145:420–424

Chan V, Jamieson WR, Lam BK, Reul M, Ling H, Fradet G. Influence of the On-X mechanical prosthesis on intermediate-term major thrombo-embolism and haemorrhage: a prospective multicentre study. *J Thorac Cardiovasc Surg.* 2010; 140(5):1053–1058

Chanderan KB, Cheng R, Lai Y. Three dimensional fluid structure interactions simulation of Bi-leaflet mechanical heart valve flow-dynamics. *Ann Biomed Eng.* 2004; 32:1471-1483

Chandran KB, Cabell GN, Khalighi B, Chen CJ. Laser anemometry measurements of pulsatile flow past aortic-valve prosthesis. *J Biomechanics*. 1983; 16:865–73

Chandran KB, Khalighi B, Chen CJ. Experimental-study of physiological pulsatile flow past valve prosthesis in a model of human aorta*. J Biomech.* 1985; 18:763–5

Chandran KB, Rittgers SE, Yoganathan AP. Bio fluid Mechanics: The Human Circulation. CRC Press; Boca Raton: 2006

Chandran KB, Dexter EU, Aluri S, Richenbacher WE. Negative pressure transients with mechanical heart valve closure: correlation between *in vitro* and *in vivo* results. *Ann Biomed Eng.* 1998; 26:546–556

Cheng R, Lai YG, Chandran KB. Three-dimensional fluid-structure interaction simulation of bi-leaflet mechanical heart valve flow-dynamics. *Ann Biomed Eng*. 2004; 32(11):1471-83

Christensen K, Doblhammer G, Rau R, Vaupel JW. Ageing populations: the challenges ahead. *Lancet.* 2009:374:1196–1208

Choi YJ, Vedula V, Mittal R. Computational study of the dynamics of a bi-leaflet mechanical heart valve in the mitral position. *Ann. Biomed. Eng.* 2014; 42:1668–1680

Christensen TD, Skjoth F, Nielsen PB, Maegaard M, Grove EL, Larsen TB. Self-management of anti-coagulant therapy in mechanical heart valve patients: a matched cohort study. *Ann Thorac Surg.* 2016;101:1494-1499

Claibone TE, Xenos M, Sherrif J, Chiu WC, Soares J, Alemu Y, Gupa S, Judex S, Slepian MJ, Bluestein D. Towards Optimization of a Novel Trileaflet Polymeric Prosthetic Heart Valve Via Device Thrombogenicity Emulation (DTE). *ASAIO J.* 2013; 59:275-283

Cohn LH, Allred EN, DeSesa VJ, Sawtelle K, Shemin RJ, Collins JJ. Early and late risk of aortic valve replacement. *J Thorac Cardiovasc Surg.* 1984; 88:695–705

Colli A, Verhoye JP, Heijmen R, Strauch JT, Hyde JA, Pagano D, Antunes M, Koertke H, Ohri SK, Bail DH, Leprince P, Van Straten BH, Gherli T. Antithrombotic therapy after bio prosthetic aortic valve replacement: ACTION Registry survey results. *Eur J Cardiothorac Surg*. 2008; 33:531–536

Colli A, Verhoye JP, Leguerrier A, Gherli T. Anti-coagulation or antiplatelet therapy of bio prosthetic heart valves recipients: an unresolved issue. *Eur J of Cardio-Thorac Surg.* 2007; 31:573-577

Colman RW, Clowes AW, George JN, et al. Overview of hemostasis. *Hemostasis and Thrombosis*, 5th ed. Philadelphia: Lippincott Williams and Wilkins; 2006:3–16

Cooley DA, Okies JE, Wukasch DC, Sandiford FM, Hallman GL. Ten year experience with cardiac replacement: results with a new prosthesis. *Ann Surg.* 1973;177:818-26.

Daebritz SH, Fausten B, Hermanns B, Schroeder J, Groetzner J, Autschbach R, Messmer BJ, Sachweh JS. Introduction of a flexible polymeric heart valve prosthesis with special design for aortic position. *Eur J Cardiothorac Surg*. 2004; 25(6):946-52

Dagum P, Green GR, Timek TA, Daughters GT, Foppiano LE, Tye TL, Bolger AF, Ingels NB Jr, Miller DC. Functional evaluation of the Medtronic stentless porcine xenograft mitral valve in sheep. *Circulation*. 1999; 100(19):1170-1177

Dahl SK, Vierendeels J, Degroote J, Annerel S, Hellevik LR, Skallerud B. FSI simulation of asymmetric mitral valve dynamics during diastolic filling. *Comput. Methods Biomech. Biomed. Eng.* 2012; 15:121–130

Dalby AJ, Wessels P, Opie LH. Warfarin use in atrial fibrillation. *South African Medical Journal*. 2013; 103:901-904

Dasi LP, Ge L, Simon HA, Sotiropoulos F, Yoganathan AP. Vorticity dynamics of a bi-leaflet mechanical heart valve in an axisymmetric aorta. *Physics Fluids.* 2007; 17:19-25

Dasi LP, Simon HA, Sucosky P, Yoganathan AP. Fluid mechanics of artificial heart valves. Clin Exp Pharmacol Physiol. 2009; 36(2): 225–237

Deviri E, Sareli P, Wisenbaugh T, Cronje SL. Obstruction of mechanical heart valve prosthesis: clinical aspects and surgical management. *J Am Coll Cardiol*. 1991; 17(3):646-50

DeWall RA, Qasim N, Carr L. Evolution of mechanical heart valves. *Ann Thorac Surg.* 2000; 69:1612–1621

Ding EJ and Aidun CK. Cluster size distribution and scaling for spherical particles and red blood cells in pressure-driven flows at small Reynolds number. *Phys Rev Lett.* 2006:96; 502-506

Dumont K, Vierendeels J, Kaminsky R, van Nooten G, Verdonck P, Bluestein D. Comparison of the hemodynamic and thrombogenic performance of two bi-leaflet mechanical heart valves using a CFD/FSI model. *J Biomech Eng*. 2007 Aug; 129(4):558-565

Durrleman N, Pellerin M, Bouchard D. Prosthetic valve thrombosis: twenty-year experience at the Montreal Heart Institute. *J Thorac Cardiovasc Surg* 2004; 127:1388–1392

Duveau D, Michaud JL, Despins P, Patra P, Train M, Dupon H, Rozo L, Carlier R. Mitral valve replacement with St. Jude Medical prosthesis: 242 cases with clinical results and an evaluation of pros- 135 thesis positioning. In: De Bakey IME, edition. Advances in cardiac valves: clinical perspectives (Proceedings of the Third International Symposium on the St. Jude Valve, November, 1982, Scottsdale, Arizona). *New York: Yorke Medical Books*, 1983:183- 90

Eichler MJ and Reul HM. Mechanical heart valve cavitation: valve specific parameters. *Int J Artif Organs*. 2004; 27(10):855-67

Eikelboom JW, Connolly SJ, Brueckmannetal M. Dabigatran versus Warfarin in patients with mechanical heart valves. *The New England Journal of Medicine*. 2013; 369:1206–1214

Elkayam U and Bitar F. Valvular heart disease and pregnancy, part II: prosthetic valves. *J Am Coll Cardiol.* 2005; 46:403–410

Elkayam U and Khan S. Pregnancy in the patient with artificial heart valve. *Cardiac Problems in Pregnancy*, Wiley-Liss, New York, NY; 1998:61–78

Ellis JT, Healy TM, Fontaine AA, Saxena R, Yoganathan AP. Velocity measurements and flow patterns within the hinge region of a Medtronic Parallel™ bi-leaflet mechanical valve with clear housing. *J Heart Valve Dis.* 1996; 5:591–9

Ellis JT, Travis BR, Yoganathan AP. An *in vitro* study of the hinge and near-field forward flow-dynamics of the St. Jude MedicalI Regent™ bi-leaflet mechanical heart valve. *Ann Biomed Eng.* 2000; 28:524–32

Ellis JT and Yoganathan AP. A comparison of the hinge and near-hinge flow fields of the St. Jude Medical Hemodynamic Plus and Regent bi-leaflet mechanical heart valves. *J Thorac Cardiovasc Surg.* 2014; 119:83–93

Emery RW, Van Nooten GJ, Tesar PJ. The initial experience with the ATS Medical mechanical cardiac valve prosthesis. *Ann Thorac surg.* 2003; 75(2):444-452

Esterly JS, Darin KM, Gerzenshtein L, Othman F, Postrlnick MJ, Scarsi KK. Clinical implications of antiretroviral drug interactions with Warfarin: a case-control study. *J Antimicrob Chemother.* 2013; (6)68:1360-1363

Falkovich, G. *Fluid Mechanics, a short course for physicists*. Cambridge University Press. 2011:11-17

Falahatpisheh A, Pedrizetti G, Kheradvar A. 3D reconstruction of cardiac flows based on multiplanar velocity fields. *Exp. Fluids.* 2014; 55:1-15

Fallon AM, Dasi LP, Marzec UM, Hanson SR, Yoganathan AP. Procoagulant properties of flow fields in stenotic and expansive orifices. *Ann Biomed Eng.* 2008; 36:1–13

Fallon AM, Shah N, Marzec UM, Warnock JN, Yoganathan AP, Hanson SR. Flow and Thrombosis at Orifices Simulating Mechanical Heart Valve Leakage Regions. ASME. *J Biomech Eng.* 2005; 128(1):30-39

Fanikos J, Grasso-Correnti N, Shah R. Major bleeding complications in a specialized anti-coagulation service. *Am J Cardiol.* 2005; 96:595–598

FDA, Safety Labelling Changes Approved by the FDA Centre for Drug Evaluation and Research (CDER). www.fda.gov/Safety/MedWatch/SafetyInformation/ucm250657.htm [Accessed 2 March 2015]

Figliola RS and Mueller TJ. Fluid stresses in vicinity of disk, ball, and tilting disk prosthetic heart-valves from *in vitro* measurements. *J Biomech Eng Trans ASME*. 1977; 99:173–7

Fillon M, Liang H, Liu WM. Tribology International. http://www.journals.elsevier.com/tribology-international. Accessed May 2015

Fisher J, Jack GR, Wheatley DJ. Design of a functional test apparatus for prosthetic heart valves. Initial results in the mitral position. *Clin. Phys. Physiol. Meas.* 1986; 7:63-73

Forsberg P and DeSancho. Role of novel anti-coagulants for patients with mechanical heart valves. Clinical trials and their interpretations. *Current Atherosclerosis Rep.* 2014; 16:448-552

Frater RWM. The UCT aortic valve used without anti-coagulants. *New York Surgical Clinics*, 1969

Freed D, Walker WF, Dube CM. Effects of vaporous cavitation near prosthetic surfaces. *Trans Am Soc Arti Int Org.* 1981; 27:105–109

Furie B and Furie BC. *In vivo* thrombus formation. *J Thromb Haemost* 2007; 5:12–17

Gallegos RP, Rivard AL, Suwan PT, Black S, Bertog S, Steinseifer U, Armien A, Lahti M, Bianco RW. *In-vivo* experience with the Triflo trileaflet mechanical heart valve. *J Heart Valve Dis.* 2006; 15(6):791-9.

Garcia D, Regan S, Crowther. Warfarin maintenance dosing patterns in clinical practice. *Chest.* 2005; 127:2049-2056

Ge L, Jones SC, Sotiropoulos F, Healy TM, Yoganathan AP. Numerical simulation of flow in mechanical heart valves: grid resolution and flow symmetry. *J Biomech. Eng.* 2003; 125:708-718

Gherli T, Colli A, Fragnito C, Nicolini F, Borrello B, Saccani S, D'Amico R, Beghi C. Comparing Warfarin with aspirin after biological aortic valve replacement: a prospective study. *Circulation*. 2004; 110:496–500

Golomb G, Wagner D. Development of a new *in vitro* model for studying implantable polyurethane calcification. *Biomater.* 1991; 12:397–405

Godje OL, Fishlein T, Adelhart K, Nollert G, Klinner W, Reichard B. The thirty year results of Starr-Edwards prosthesis in the aortic and mitral positions. *Ann Thorac surg.* 1997; 63(3):613-619

Gohlke-Barwolf C, Acar J, Oakley C, Butchart E, Burckhart D, Bodnar E, Hall R, Delahaye JP, Horstkotte D, Kremer R, Krayenbuh HP, Krzeminska-Pakula M, Samama M. Guidelines for prevention of thrombo-embolic events in valvular heart disease: Study Group of the Working Group on Valvular Heart Disease of the European Society of Cardiology. *Eur Heart J.* 1995; 16: 1320–1330

Goldhaber SZ. ‘‘Bridging’’ and mechanical heart valves: perils, promises, and predictions. *Circulation.* 2006; 113:470–472

Gonzalez B, Benitez H, Rufino K, Echevarria W. Biomechanics of mechanical heart valve. *App Eng Mech Medicine.* 2003; 1-39

Gott VL, Daggett RL, Whiffen JD, et al. A hinged-leaflet valve for total replacement of the human aortic valve. *J Thorac Cardiovasc Surg.* 1964; 48:713–25

Gott VL, Daggett RL. Serendipity and the development of heparin and carbon surfaces. *Ann Thorac Surg.* 1999; 68:19–22

Gott VL, Whiffen JD, Dutton RC. Heparin bonding on colloidal graphite surfaces. *Science*. 1963; 142:1297–1298

Graf T, Fischer H, Reul H, Rau G. Cavitation potential of mechanical heart valve prosthesis. *Int J Artificial Organs*.1991; 14:169–174

Graf T, Reul H, Detlefs C, Wilmes R, Rau G. Causes and formation of cavitation in mechanical heart valves. *J Heart Valve Dis*. 1994; 3 Suppl 1:49-64

Grigioni M, Daniele C, D'Avenio G, Morbiducci C, Di Meo D. Innovative technologies for the assessment of cardiovascular devices. *Expert Rev. Med. Devices.* 2004; 1:81-93

Gross JM, Shermer CD, Hwang NH. Vortex shedding in bi-leaflet heart valve prosthesis. *ASAIO Trans*. 1988; 34(3):845-50

Gross JM, Shu MCS, Dai FF, Ellis J, Yoganathan AP. Microstructural flow analysis within a bi-leaflet mechanical heart valve hinge. *J Heart Valve Dis*. 1996; 5:581–90

Grunkemeier GL, Li H, Naftel DC, Starr A, Rahimtoola SH. Long-term performance of heart valve prosthesis. *Curr Probl Cardiol.* 2000; 25:78–154

Hakki A, Iskandrian A, Bemis C, Kimbiris D, Segal B, Brice C. A simplified valve formula for the calculation of stenotic cardiac valve areas. *Circulation.* 1981; 63(5): 1050–5

Harken DE, Soroff HS, Taylor WJ. Partial and complete prosthesis in aortic insufficiency. *J Thorac Cardiovasc Surg.* 1960; 40:744–53

Harker L and Slichter S. Studies of Platelet and Fibrinogen Kinetics in Patients with Prosthetic Heart Valves. *The New England Journal of Medicine*. 1970; 283:1302-1305

Harrison DC, Ibrahim MA, Weyman AE, Kuller LH, Blot WJ, Miller DE. The Bjork-Shiley convexo-concave heart valve experience from the perspective of the supervisory panel. *Am J Cardiol.* 2013; 112:1921–1931

Hasler D, Landolt A, Obrist D. Tomographic PIV behind a prosthetic heart valve. *Exp Fluids* 2016; 57:80-86.

Healy TM, Fontaine AA, Ellis JT, Walton SP, Yoganathan AP. Visualization of the hinge flow in a 5: 1 scaled model of the Medtronic parallel bi-leaflet heart valve prosthesis. *Experiments Fluids*. 1998; 25:512–18

Hellums JD. Whitaker lecture – Bio rheology in thrombosis research. *Ann. Biomed. Eng.* 1994; 22:445-455

Heras M, Chesebro JH, Fuster V, Penny WJ, Grill DE, Bailey KR, Danielson GK, Orszulak TA, Pluth JR, Puga FJ, Schaff HV, Larsonkeller JJ. High risk of thromboembolic early after bio prosthetic cardiac valve replacement. *J Am Coll Cardiol*. 1995; 25:1111–1119

Herbertson LH, Deutsch SS, Manning KB. Near valve flows and potential blood damage during closure of a bi-leaflet mechanical heart valve. ASME. *J Biomech Eng.* 2011; 133(9):094507-094507

Holdeman JT, Kim JW. Computation of incompressible thermal flows using Hermite finite elements. *Comput. Methods Appl. Mech*. *Eng*. 2010; 199 (49–52): 3297–3304

Horstkotte D, Piper C, Schulte HD. Thrombosis of prosthetic heart valves: diagnosis and management. *Z Kardiol,* 1998; 87(suppl 4): 20–32

Horstkotte D and Burckhardt D. Review Prosthetic valve thrombosis. *J Heart Valve Dis*. 1995; 4:141-53

Huang ZJ, Merkle CL, Abdallah S, Tarbell JM. Numerical simulation of unsteady laminar flow through a tilting disk heart valve: prediction of vortex shedding. *J. Biomech*. 1994; 27:391–402

Huang G, Schaff HV, Sundt TM, Rahimtoola SH. Treatment of obstructive thrombosed prosthetic heart valve**.** *J Am Coll Cardiol*. 2013; 62:1731–1736

Huth C, Friedl A and Rost A, for the GELIA Study Investigator Group. Intensity of oral anti-coagulation after implantation of St. Jude Medical aortic prosthesis: analysis of the GELIA Database (GELIA 4). *Eur Heart J Suppl*. 2001; 3: (Supplement Q), Q33–Q38

Hwang NHC, Reul H, Reinhard P. *In vitro* evaluation of the long-body On-X bi-leaflet heart valve, *Journal of Heart Valve Disease*. 1998; 7:561–568

Idelsohn SR, Costa LE, and Ponso R. A comparative computational study of blood flow through prosthetic heart valves using the finite element method*. J. Biomech*. 1995; 18: 97–115

Ikeda Y, Handa M, Kawano K, et al. The role of von Willebrand factor and fibrinogen in platelet aggregation under varying shear stress. *Journal of Clinical Investigation.* 1991; 87(4):1234-1240

Ikeda, Y., M. Murata, Y. Araki, K. Watanabe, Y. Ando, I. Itagaki, Y. Mori, M. Ichitani, and K. Sakai. Importance of fibrinogen and platelet membrane glycoprotein Ilb-IIIa in shear-induced platelet aggregation. *Thromb*. 1988; 51:157-163

Jamieson WR, Cartier PC, Allard M, Boutin C, Burwash IG, Butany J, de Varennes B, Del Rizzo D, Dumesnil JG, Honos G, Houde C, Munt BI, Poirier N, Rebeyka IM, Ross DB, Siu SC, Williams WG, Rebeyka IM, David TE, Dyck JD, Feindel CM, Fradet GJ, Human DG, Lemieux MD, Menkis AH, Scully HE, Turpie AG, Adams DH, Berrebi A, Chambers J, Chang KL, Cohn LH, Duran CM, Elkins RC, Freedman R, Huysman HA, Jue J, Perier P, Rakowski H, Schaff HV, Schoen FA, Shah P, Thompson CR, Warnes C, Westaby S, Yacoub MH. Surgical management of valvular heart disease 2004. *Can J Cardiol*. 2004; 20 (suppl E): 7E–120E

Jamieson WR, Moffatt-Bruce SD, Skarsgard P, Hadi MA, Ye J, Fradet GJ, Abel JG, Janusz MT, Cheung A, Germann E. Early antithrombotic therapy for aortic valve bio prosthesis: is there an indication for routine use? *Ann Thorac Surg.* 2007; 83:549–556

Jamieson WRE, Rosado LJ, Munro AI. Carpentier-Edwards standard porcine bio prosthesis: primary tissue failure (structure valve deterioration) by age groups. *Ann Thorac Surg.* 1998; 46:155–162

Jasak H and Tukovic Z. Dynamic mesh handling in open foam applied to fluid structure interaction simulations. *V European conference Comp Fluid Dynamics,* ECCOMAS CFD 2010

Jilma-Stohlawetz P, Peter Quehenberger P, Schima H, Stoiber M, Paul Knöbl P, Steinlechner B, Felli A, Jilma B. Acquired von Willebrand factor deficiency caused by LVAD isADAMTS-13 and platelet dependent. *Thromb research.* 2016; 137:196-201

Jin XY, Gibson DG, Pepper JR. The effects of cardioplegia on coronary pressure-flow velocity relationships during aortic valve replacement. *Eur J Cardiothorac Surg*. 1999; 16:324–330

Jones M and Eidbo EE. Doppler Colour Flow Evaluation of Prosthetic Mitral Valves: Experimental Epicardial Studies. *JACC*. 1989; 13:234-240

Jun BH, Saikrishnan N, Arjunon S, Min Yun BB, Yoganathan AP. Effect of Hinge Gap Width of a St. Jude Medical Bi-leaflet Mechanical Heart Valve on Blood Damage Potential—An *In Vitro* Micro Particle Image Velocimetry Study. ASME. *J Biomech Eng.* 2014; 136(9):8-11

Kae J., Ely Jl, Schwartz AS. Microstructural observations of pure pyrolytic carbons for heart valves. Twenty-second Biennial Conference on Carbon*. J Transaction.* 1995:742-43

Kalmar P, Irrgang E. Cardiac surgery in Germany during 1999. A report by the German Society for Thoracic and Cardiovascular Surgery. *Thorac Cardiovasc Surg.* 2000; 48:27-30

Kamensky D, Hsu M, Schillinger D, Evans JA, Aggarwal A, Bazilevs Y, Sacks MS, Hughes TJR. An immersogeometric variational framework for fluid–structure interaction: Application to bio prosthetic heart valves. *Comp Methods in Applied Mech Eng.* 2015:284(1):1005-1053

Kaneko T, Aranki SF. Anti-coagulation for prosthetic valves. *Thrombosis,* 2013; 346-752

Kang J, Zhang DM, Restle DJ, Kallel F, Acker MA, Atluri P, Bartoli CR. Reduced continuous-flow left ventricular assist device speed does not decrease von Willebrand factor degradation. *J Thorac Cardiovasc Surg.* 2016; 151(6):1747-1754

Kheradvar A, Groves EM, Goergen GJ, Alavi H, Tranquillo R, Simmons CA, Dasi LP, Grande-Allen J, Canic S. Emerging Trends in Heart Valve Engineering: Part II. Novel and Standard Technologies for Aortic Valve Replacement. *Ann Biomed Eng*. 2014; 43:1-8

Kheradvar A, Groves EM, Falahatpisheh A, Mofrad MK, Alavi SH, Tranquillo R, Simmons CA, Dasi LP, Grande-Allen J, Griffith B. Emerging Trends in Heart Valve Engineering: Part IV. Computational modelling and experimental studies. *Ann Biomed Eng.* 2015; 43:2314-2333

King MJ, Corden J, David, T. and Fisher J. Three Dimensional Time-Dependent Analysis of Flow Through a Bi-leaflet Mechanical Heart Valve: Comparison of Experimental and Numerical Results. *J. Biomech*.1996; 29:609–618

King MJ, David T, and Fisher J. An Initial Parametric Study on Fluid Flow Through Bi-leaflet Mechanical Heart Valves Using Computational Fluid Dynamics. *J. Eng. Med.* 1994; 208: 63–71

Kini V, Bachman C, Fontaine A, Deutsch S, Tarbell JM. Flow visualization in mechanical heart valves: occluder rebound and cavitation potential. *Ann of Biomed Eng.* 2000; 28:431–441

Kinsley RH, Antunes MJ, Colsen PR. St. Jude Medical valve replacement. An evaluation of valve performance. *J Thorac Cardiovasc Surg.* 1986; 92(3):349–60

Kiris CD, Kwak D, Rodgers S, Chang I. Computational approach for probing the flow through artificial heart devices. *J Biomech Eng.* 1997; 119:452-460

Kleine P, Hasenkam JM, Nygaard H, Perthel M, Wesemeyer D, Laas J. Tilting disc versus bi-leaflet aortic valve substitutes: intraoperative and post-operative hemodynamic performance in humans. *J Heart Valve Dis*. 2000; 9:308–312

Kleine P, Scherer M, Abdel-Rahman UAE, Klesius A, Ackermann H, Moritz A. Effect of mechanical aortic valve orientation on coronary artery flow: Comparison of tilting disc versus bi-leaflet prosthesis in pigs. *J Thorac Cardiovasc Surg.* 2002; 5:925-932

Klepetko W, Moritz A, Mlczoch J, Domaning E, Wolner E. Leaflet fracture in Edwards-Duromedics Bi-leaflet valves. *J Thorac Cardiovasc Surg.* 1989; 97:90-94

Klusak E, Bellofiore A, Loughnane S, Quinlan NJ. High-Resolution Measurements of Velocity and Shear Stress in Leakage Jets from Bi-leaflet Mechanical Heart Valve Hinge Models. ASME. *J Biomech Eng.* 2015; 137(11):111008-11

Koertke H, Zittermann A, Minami K, Tenderich G, Wagner O, El-Arousy M, Krian A, Ennker J, Taborski U, Klovekorn WP, Moosdorf R, Saggau W, Morshuis M, Koerfer J, Seifert D, Koerfer R. Low dose INR-self-management—a promising tool to achieve low complication rates after mechanical heart valve replacement. *Ann Thorac Surg.* 2005; 79:1909–1914

Koertke H, Zittermann A, Wagner O, Koerfer R. Self-management of oral anti-coagulation therapy improves long-term survival in patients with mechanical heart valve replacement. *Ann Thorac Surg*. 2007; 83:24–29

Kornberg A, Wildhirt, Schulze C, Kreuzer E. Leaflet escape in Omnicarbon mono-leaflet valve. *Eur J Cardiothorac Surg*. 1999; 15(6):867-869

Krishnan S, Udaykumar HS, Marshall JS, Chandran KB. Two-dimensional dynamic simulation of platelet activation during mechanical heart valve closure. *Ann Biomed Eng. 2006;* 34(10):1519-34

Kuettinga M, Sedaghatb A, Utzenratha M, Sinningb JM , Schmitza C, Roggenkampa J, Wernerb N, Schmitz-Rodea T, Steinseifer U. *In vitro* assessment of the influence of aortic annulus ovality on the hydrodynamic performance of self-expanding trans-catheter heart valve prosthesis. *Journal of Biomechanics.* 2014; 47:957-965

Lai YG, Chandran KB, Lemmon J. A numerical simulation of mechanical heart valve closure fluid dynamics. *Journal of Biomechanics.* 2002; 35:881–892

Lee CS and Chandran KB. Numerical simulation of instantaneous back flow through central clearance of bi-leaflet mechanical heart valves at the moment of closure: shear stress and pressure fields within clearance. *Med Biolog Eng and Computing.* 1995; 33:257–263

Lee CS, Aluri S, Chandran KB. Effect of valve holder flexibility on cavitation initiation with mechanical heart valve prosthesis: an *in vitro* study. *J Heart Valve Disease.* 1996; 5:104–113

Lee H, Homma A, Taenaka Y. Hydrodynamic characteristics of bi-leaflet mechanical heart valves in an artificial heart: cavitation and closing velocity. *Artificial Organs.* 2007; 31 (7):532–537

Lee H, Tatsumi E, Homma A, Tsukiya T, Taenaka Y. Mechanism for cavitation of mono-leaflet and bi-leaflet valves in an artificial heart. *J Artif Organs.* 2006; 9:154-160

Lei M, Van Steenhoven AA, and Van Campen DH. Experimental and numerical analyses of the steady flow field around an aortic Bjork-Shiley standard valve prosthesis. *J. Biomech*.1992; 3:213–222

Lengyel M. Diagnosis and treatment of left-sided prosthetic valve thrombosis. *Expert Rev Cardiovasc Ther*. 2008; 6(1):85-93

Leo HL, He ZM, Ellis JT, Yoganathan AP. Micro flow fields in the hinge region of the Carbomedics bi-leaflet mechanical heart valve design. *J Thorac Cardiovasc Surg.* 2002; 124:561–74

Leo HL, Simon H, Carberry J, Lee SC, Yoganathan A. A comparison of flow field structures of two tri-leaflet polymeric heart valves. *Ann Biomed Eng*. 2005; 33:429–43

Levi M, ten Cate H, van der Poll T. Endothelium: interface between coagulation and inflammation. *Crit Care Med.* 2002; 30(suppl 5):S220–S224

Lillehei CW, Nakib A, Kaster RL. The origin and development of three new mechanical valve designs: toroidal disc, pivoting disc and rigid bi-leaflet cardiac prosthesis. *Ann Thorac Surg.* 1989; 48:S35–36

Lim WL, Chew YT, Low HT, Foo WL. Cavitation phenomena in mechanical heart valves: the role of squeeze flow velocity and contact area on cavitation initiation between two impinging rods. *J Biomechanics*. 2003; 36:1269-1280

Lindblum D, Rodriguez L, Bjork VO. Mechanical failure of the Bjork-Shiley valve: updated follow-up and considerations on prophylactic replacement. *J Thorac Cardiovasc Surg.* 1989; 97:95–97

Rosenfeld M, Avrahami I, Einav S. Unsteady effects on the flow across tilting disk valves. *Journal of Biomechanical Engineering*. 2002; 124:21–29

Ma WG, Hou B, Abdurusul A, Gong DX, Tang Y, Chang Q, Xu JP, Sun HS. Dysfunction of mechanical heart valve prosthesis: experience with surgical management in 48 patients. *J Thorac Dis*. 2015; 7(12):2321-2329

Machler H, Reiter G, Perthel M, Reiter U, Bergmann P, Zink M, Rienmuller R, Laas J. Influence of a tilting prosthetic mitral valve orientation on the left ventricular flow — an experimental *in vivo* magnetic resonance imaging study. *Eur J Cardio-Thorac surg.* 2007; 32:102-107

Mackman N, Tilley RE, Key NS. Role of the extrinsic pathway of blood coagulation in hemostasis and thrombosis. *Arterioscler Thromb Vasc Biol.* 2007; 27(8):1687–1693

Magovern GJ, Lieber GA, Park SB. Twenty-five-year review of the Magovern-Cromie sutureless aortic valve. *Ann Thorac Surg.* 1989; 48:S33–4

Manning KB, Herbertson LH, Fontaine AA, Deutsch S. A Detailed Fluid Mechanics Study of Tilting Disk Mechanical Heart Valve Closure and the Implications to Blood Damage. ASME. *J Biomech Eng.* 2008; 130(4):041001-8

Massel DR and Little SH. Antiplatelet and anti-coagulation for patients with prosthetic heart valves. *Cochrane Database Syst Rev*. 2013; 9(7): doi: 10.1002/14651858. CD003464.pub2

McAnulty JH, Rahimtoola SH. Antithrombotic therapy for valvular heart disease. In: Fuster V, O'Rourke RA, Walsh RA, Poole-Wilson P, eds. *Hurst's The Heart*. New York, NY: McGraw-Hill; 2008: 1800–1807

McKellar SH, Abel S, Camp CL, Suri RM, Ereth MH, and Schaff HV. Effectiveness of dabigatran etexilate for thrombo prophylaxis of mechanical heart valves. *Journal of Thoracic and Cardiovascular Surgery*. 2011; 141:1410– 1416

McLaren MJ, Hawkins DM, Koornhof HJ, Bloom KR, Bramwell-Jones DM, Cohen E, et al. Epidemiology of rheumatic heart disease in black school children of Soweto, Johannesburg. *Br Med J*. 1975; 3(5981):474–478

Meuris B, Verbeken E, Flameng W. Mechanical valve thrombosis in a chronic animal model: Differences between monoleaflet and bi-leaflet valves. *J Heart Valve Dis.* 2005:14:96–104

Mihalef V, Ionasec RI, Sharma P, Georgescu B, Voigt I, Suehling M, Comaniciu D. Patient-specific modelling of whole heart anatomy, dynamics and hemodynamics from four-dimensional cardiac CT images. *Interface Focus*. 2011; 1: 286–296

Mohammadi H and Mequanint C. Prosthetic aortic heart valves: Modeling and design. J *Med Eng & Phys.* 2011; 33(2):131–147

Mohammadi H, Ahmadian MT, Wan WK. Time-dependent analysis of leaflets in mechanical aortic bi-leaflet valve in closing phase using the finite strip method. *J Med Eng and Phys*. 2006; 28:122–133

Mohammadi H, Boughner D, Millon LE, Wan WK. Design and simulation of a poly (Vinyl Alcohol) bacterial cellulose nanocomposite mechanical aortic heart valve prosthesis. Proceedings of the Institution of Mechanical Engineers, Part H, *Journal of Engineering in Medicine.* 2009; 223(6):697–711

Mohammadi H. Design and simulation of prosthetic heart valves. PhD thesis. Ontario: Biomedical Engineering. The University of Western Ontario; 2009

Mohr F, Holzhey D, Möllmann H, Beckmann A, Veit C, Reiner H, Jochen F, Karl-Heinz F, Rüdiger K, Zahn R. The German Aortic Valve Registry: 1-year results from 13 680 patients with aortic valve disease. *Eur J Cardiothorac Surg* (2014) 46 (5): 808-816

Murphy DA, Levine FH, Buckley MJ. Mechanical valves: A comparative-analysis of the Starr-Edwards and Bjork-Shiley prosthesis. *J Thorac Cardiovasc Surg.* 1983; 86:746–52

Murphy DW, Dasi LP, Vukasinovic J, Glezer A, Yoganathan AP. Reduction of Procoagulant Potential of b-Datum Leakage Jet Flow in Bi-leaflet Mechanical Heart Valves via Application of Vortex Generator Arrays. ASME. *J Biomech Eng.* 2010; 132(7):071011-10

Nair K, Muraleedharan CV, Bhuvaneshwar GS. Developments in mechanical valve prosthesis. *Sadhana.* 2003; 28:575-587

Nicosia MA, Cochan RP, Rutland CJ, Kunzelman KS. A coupled fluid structure finite element method of the aortic valve and root. *J Heart Valve Dis.* 2003; 12(6):781–789

Nishimura RA, Otto CM, Bonow RO, Carabello BA, Erwin JP 3rd, Guyton RA et al. 2014 AHA/ACC guideline for the management of patients with valvular heart disease: executive summary: a report of the American College of Cardiology/American Heart Association Task Force on Practice Guidelines. *Circulation*. 2014; 129(23):2440–2492

Nobili M, Morbiducci U, Ponzini R, Del C, Balducci A, Grigioni M, Maria F, Redaelli A. Numerical simulation of the dynamics of a bi-leaflet prosthetic heart valve using a fluid – structure interaction approach. *J Biomech.* 2008; 41:2539-2550

North RA, Sadler L, Stewart AW, McCowan LME, Kerr AR, White HD. Long-term survival and valve-related complications in young women with cardiac valve replacement. *Circulation.* 1999; 99:2669–2676

Nygaard H, Paulsen PK, Hasenkam JM, Kromann-Hansen O, Pedersen EM, Rovsing PE. Quantitation of the turbulent shear stress distribution of normal, diseased and artificial valve prosthesis in human beings. J Thorac Cardiovasc Surg. 1992; 6:609-17

O'Brien JR. Shear-induced platelet aggregation. *The Lancet*. 1990; 335(8691):711-713

Oden A, Fahlen M. Oral anti-coagulation and risk of death: a medical record linkage study. *Br Med J.* 2002; 325:1073–1075

On-X valve. Available from: www.onxlti.com. [Accessed 17 March 2015]

Otto C: Echocardiographic evaluation of prosthetic valve dysfunction. In: Otto C, ed. Textbook of Clinical Echocardiography. Philadelphia, PA, WB Saunders, 2000

Ozaki S, Herrigers P, Flameng W. A new model to test the calcification characteristics of bio prosthetic heart valves. *Ann Thorac surg.* 2004; 10:23-28

Palatianos GM, Laczkovics AM, Simon P. Multicentre European study on safety and effectiveness of the On-X prosthetic heart valve: intermediate follow-up. *Annals of Thoracic Surgery*. 2007; 83:40–46

Pareira F, Gharib D, Dabiri D, Modarress D. Defocusing digital particle image velocimetry: a 3D 3 component DPIV measurement technique. *Exp Fluids.* 2000; 29:S078-S084

Paulsen PK, Jensen BK, Hasenkam JM, Nygaard H. High-frequency pressure fluctuations measured in heart valve patients. *J Heart Valve Dis.* 1999; 8(5):482-6

Pelagalli A, Belisario MA, Tafuri S, et al: Adhesive properties of platelets from different animal species. *J Comp Pathol.* 2003; 128:127–131

Perera MA, Cavallari LA, Limdi NA, Gamazon ER, Konkashbaev E, Daneshjou R, Pluzhnikov A, Crawford DC, Wang J, Liu N, Tatonetti N, Bourgeois S, Takahashi H, Bradford Y, Burkley BM, Johnsonk JA. Genetic variants associated with Warfarin dose in African-American individuals: a genome-wide association study. *Lancet.* 2013; 382:790-796

Piatti F, Sturla F, Marom G, Sheriff J, Claiborne TE, Slepian MJ, Redaelli A, Bluestein D. Hemodynamic and thrombogenic analysis of a trileaflet polymeric valve using a fluid-structure interaction approach. *J Biomech.* 2015; 48:3641-49

Pibarot P, Dumesnil JG. Prosthetic heart valves. Selection of the optimal prosthesis and long term management. *Circ*. 2009; 119:1034-1048

Piccin A, Murphy WG, Smith OP. Circulating microparticles: pathophysiology and clinical implications. *Blood Rev*. 2007; 21(3):157–171

Pinney DH. The Modelling of Mechanical Heart Valve Closure Dynamics. *M Sc. thesis,* University of Sheffield. 2004

Pipilis AG, Efstratiadis T, Kyrtatos P, Mallios K. Thirty-seven-year follow-up of a ‘less known’ aortic valve prosthesis. *Eur Heart J.* 2007; 15:1813

Pruefer D, Dahm M, Dohmen G, Horstkotte D, Bergemann R and Oelert H. Intensity of oral anti-coagulation after implantation of St. Jude Medical mitral or multiple valve replacement: lessons learned from GELIA (GELIA 5). *Eur Heart J Suppl.* 2001; 3:Q39–Q43

Puskas J, Gerdisch M, Nichols D, Quinn R, Anderson C, Rhenman B. Reduced anti-coagulation after mechanical aortic valve replacement: interim results from the prospective randomized On-X valve anti-coagulation clinical trial randomized Food and Drug Administration investigational device exemption trial. *J Thorac Cardiovasc Surg.* 2014; 147(4):1202–1210

Puskas JD, Nichols D, Gerdisch M. Reduced Anti-coagulation after Mechanical Aortic Valve Replacement: Interim Results from the PROACT randomized FDA IDE Trial. American Association of Thoracic Surgery. Minneapolis, Minn, USA, 2012

Rayner J, Coffey S, Newton J, Prendergast BD. Aortic valve disease. *Int J Clin Pract*. 2014; 68(10):1209–1215

Reul H, Van Son JAM, Steinseifer U, Schmitz B, Schmidt A, Schmitz C. *In vitro* comparison of bi-leaflet aortic valve prosthesis. *J Thorac Cardiovasc Surg*. 1993; 9:412–420

Rosenberger M., Amerio O., Schvezov C. Optimizing of the design of a prosthetic heart valve with three leaves. www.fac.org.ar/ccvc/llave/tl211/tl211.php

Rosenfeld M, Avrahami I, Einav S. Unsteady effects on the flow across tilting disk valves. *ASME J Biomech Eng.* 2002; 124:21–29

Ross DN. Homograft replacement of the aortic valve. *Lancet.* 1962; 2: 487

Roudaut R, Serri K, Lafitte S. Thrombosis of prosthetic heart valves: diagnosis and therapeutic considerations. *Heart*. 2007; 93(1):137-142

Rudolph TK, and Baldus S. Jena valve trans-femoral technology. Euro Intervention: Journal of Euro PCR in collaboration with the Working Group on Interventional Cardiology of the European Society of Cardiology. 2013; 9:101-106

Ruggeri ZM. The role of von Willebrand factor in thrombus formation. *Thromb.* Res. 2007; 120:S5-S9

Sacks M. The biomechanical effects of fatigue on the porcine bio prosthetic heart valve. *J Clin Pathol*. 2001; 11:231-47

Saddoughi SA, Steinberg DH, Ikonomidis JS. Functioning Cooley-Cutter aortic valve prosthesis 40 years after implantation. *Cardio vasc surg.* 2014; 147(3):e21-e22

Sagripanti A, Carpi A. Antithrombotic and prothrombotic activities of the vascular endothelium. *Biomed Pharmacother.* 2000; 54(2):107–111

Schimmelpfennig S and Glaser B. One Step Forward toward Characterization: Some Important Material Properties to Distinguish Bio-characteristics. *J. Environ. Qual.* 2012; 41:1001-1013

Schouten M, Wiersinga WJ, Levi M. Inflammation, endothelium, and coagulation in sepsis. *J Leukoc Biol.* 2008; 83(3):536–545

Schrire V, Beck W, Hewetson RP, Barnard CN. Immediate and long term results of aortic valve replacement with the University of Cape Town aortic valve prosthesis. *B Heart J*. 1970; 32:255-263

Seo JH, Mittal R. Effect of diastolic flow patterns on the function of the left ventricle. *Phys. Fluids*. 2013; 25:1–21

Seo JH, Shoele K. Mittal R. Computational modelling of the effect of mitral-valve leaflet dynamics on intraventricular flow. Presentation at 11th. World Congress on Computational Mechanics (WCCM XI), Barcelona, Spain, July 2014:1–2

Shi Y, Ahzo Y, Yeo TJ, Hwang NH. Numerical simulation of opening process in a process in a bi-leaflet mechanical heart valve under pulsatile flow condition. *Journal of Heart Valve Disease*. 2003; 12(2):245–255

Shim E and Chang K. Three dimensional vortex flow past a tilting disk valve using a segregated finite element scheme. *Compu. Dyne.* 1994; 3:205-211

Shu MCS, Gross JM, O'Rouke KK, Yoganathan AP. An integrated macro/micro approach to evaluating pivot flow within the Medtronic ADVANTAGE bi-leaflet mechanical heart valve. *J Heart valve disease.* 2003; 12:503-512

Shu MCS, Leuer LH, Armitage TL, Schneider TE, Christiansen DR. Cavitation threshold ranking and erosion characteristics of bi-leaflet heart valve prosthesis. *J Heart Valve Disease.* 1994; 3:S83–S93

Simon HA, Dasi LP, Leo HL, Yoganathan AP. Spatial-temporal flow analysis in bi-leaflet heart valve hinge regions: Potential analysis for blood element damage. *Ann Biomed Eng.* 2007; 35:1333–46

Simon HA, Ge L, Sotiropoulos F, Yoganathan AP. Simulation of the three-dimensional hinge flow fields of a bi-leaflet mechanical heart valve under aortic conditions. *Ann Biomed Eng*. 2010; 38(3): 841–853.

Simon HA, Leo HL, Carberry J, Yoganathan AP. Comparison of the hinge flow fields of two bi-leaflet mechanical heart valves under aortic and mitral conditions. *Ann Biomed Eng.* 2004; 32:1607–1615

Smadi O, Hassan I, Pibarot P, Kadem L. 17 Numerical and experimental investigations of pulsatile blood flow pattern through a dysfunctional mechanical heart valve. *J Biomech.* 2010; 10:1565-1572

Smith SA. The cell-based model of coagulation. *J Vet Emerg Crit Care.* 2009; 19(1):3-10

Sotiropoulos F, Bao Le T, Gilmanov A. Fluid Mechanics of Heart Valves and Their Replacements. *Annual Review of Fluid Mechanics*. 2016; 48:259-283

South African national HIV prevalence, incidence and behavior survey, 2012. www.hsrc.ac.za. [Accessed 17 March 2015].

Ståhle E, Kvidal P, Nyström SO, Bergström R. Long-term relative survival after primary heart valve replacement. *Eur J Cardiothorac Surg*. 1997; 11(1):81-91.

Star Edwards Model 6100. Available from: https://www.flickr.com/photos/sacdrbob/7430185090. [Accessed on 15 March 2015]

Starr A, R. Herr, Wood JA. Accumulated experience with the Starr-Edwards prosthesis 1960-1968. L.A. Brewer III (Ed.), Prosthetic heart valves, Charles C. Thomas, Springfield, IL. 1969:148–163

Stefanidis C, Nana AM, De Canniere D. 10-year experience with the ATS mechanical valve in the mitral position. *Ann Thorac Surg.* 2005; 79:1934–1938

Stoney WS. Evolution of Cardiopulmonary Bypass. *Circulation*. 2009; 119:2844-2853

Subramanian A, Mu H, Kadambi JR, Wernet MP, Brendze AM, Harasaki H. Particle image velocimetry investigation of intravalvular flow fields of a bi-leaflet mechanical heart valve in a pulsatile flow. *Journal of Heart Valve Disease*. 2000; 9(5):721–725

Taljaard JJ and Doubell AF. Prosthetic valve obstruction at Tygerberg Hospital between January 1991 and February 2001. *Cardiovasc J South Afr*. 2003; 14:182–188

Tansley GD, Edwards RJ, and Gentle CR. Role of Computational Fluid Mechanics in the Analysis of Prosthetic Heart Valve Flow. *Med. Biol. Eng. Comput*. 1988; 26:175–185

Thaden JJ, Nkomo VT, Enriquez-Sarano M. The global burden of aortic stenosis. *Prog Cardiovasc Dis*. 2014; 56(6):565–571

The components of a bi-leaflet, mechanical heart valve available from www.ctsnet.org/products/sorin-group/carbomedics-top-hat%C2%AE-supra-annular-aortic-valve. [Accessed 20 March 2015]

Tillman P, Carson SN, Talken L: Platelet function and coagulation parameters in sheep during experimental vascular surgery. *Lab Anim Sci.* 1981; 31:263–267

Tran HS, Chrzanowski FA, Puc MM. A sheep model for thoracic aortic surgery in the presence of systemic coagulopathy. *J Invest Surg*. 2000; 13:111–116

Tropea, Cameron; Yarin, Alexander L. Foss, John F. Springer handbook of experimental fluid mechanics. Springer. 2007; 661-676

UCT valve, mark 1. Available from: www.flickr.com/photos/68899531@N02/sets/72157630259843560. [Accessed 10 March 2015]

Unger F and Ghosh P. International cardiac surgery. *Semin Thorac Cardiovasc Surg,* 2002; 14(4):321-3

Vahanian A, Baumgartner H, Bax J, Butchart E, Dion R, Filippatos G, Flachskampf F, Hall R, Lung B, Kasprzak J, Nataf P, Tornos P, Torracca L, Wenink A. Guidelines on the management of valvular heart disease: the Task Force on the Management of Valvular Heart Disease of the European Society of Cardiology. *Eur Heart J*. 2007; 28:230–268

Van Ryn J, Stangier J, Haertter S, Liesenfeld KH, Wienen W, Feuring M, Clemens A. Dabigatran etexilate--a novel, reversible, oral direct thrombin inhibitor: interpretation of coagulation assays and reversal of anti-coagulant activity. *Thrombosis and Haemostasis*. 2010; 103:1116–27

Versteeg HH, Heemskerk JWM, Levi M, Reitsma PH. New Fundamentals in Haemostasis. *Physiol Rev*. 2013; 93:327-358

Vincent, Gott L , Dian E, Alejo E, Cameron E. Mechanical Heart Valves: 50 Years of Evolution. *Ann Thorac Surg*. 2003; 76:2230-2239

Wheatley DJ, Raco L, Bernacca GM. Polyurethane: material for the next generation of heart valve prosthesis? *Eur J Cardiothorac Surg,* 2000; 17:440–448.

Williams MA and Van Riet S, The On-X heart valve: mid- term results in a poorly anticoagulated population. *J Heart Valve Dis*. 2006; 15:80–86

Wong Y and Bronzino JD. *Biomaterials.* CRC Press. 2007; 12–13

Woo YR, Yoganathan AP. *In vitro* pulsatile flow velocity and shear stress measurements in the vicinity of mechanical heart valve prosthesis. *J Biomech.* 1986; 19:33–51

Wu ZJ, Shu MCS, Scott DR, Hwang NHC. The closing behaviour of Medtronic Hall mechanical heart valve. *American Soc Artif Int Org*. 1994; 40(3):702–708

Wurzinger LJ, Opitz R, Wolf M, Schmidschonbein H. Shear induced platelet activation: A critical reappraisal. *Biorheology.* 1985; 22:399–413

Xenos M, Girdhar G, Alemu Y, Jesty J, Slepian M, Bluestein D. Device Thrombogenicity Emulator (DTE) − Design optimization methodology for cardiovascular devices: A study in two bi-leaflet MHV designs. *J Biomech.* 2010; 43(12):2400-2409

Xiaogang SUN, Shengshou HU, Guoqi Qi, Yuyan ZHOU. Low standard oral anti-coagulation therapy for Chinese patients with St. Jude mechanical heart valves. *Chinese Med Journ*. 2003; 116(8):1175-1178

Yacoub MH and Takkenberg JJ. Will heart valve tissue engineering change the world? *Nat Clin Pract Cardiovasc Med*. 2005; 2:60–61

Yamaji-Hasegawa A, Tsujimoto M. Asymmetric distribution of phospholipids in bio membranes. *Biol Pharm Bull* 2006; 29(8):1547–1553

Yamak B, Iscan Z, Mavita B, Ulus AT, Katircioglu SF, Tasdemir O, Bayazit K. Low-dose Oral Anti-coagulation and Antiplatelet Therapy with St. Jude Medical Heart Valve Prosthesis. *J Heart Valve Dis.* 1999; 8:1-15

Yezbick AB, Ho JK, Crowley R, Sanchez E, Mahajan A. Echocardiographic signature of the On-X valve. *Echocardiography.* 2008; 25(9):1016–1018

Yin W, Krukenkamp B, Saltman A, Gaudette G, Suresh K, Bernal O, Jesty J, Bluestein D. Thrombogenic performance of a St. Jude bi-leaflet mechanical heart valve in a sheep model. *ASAIO Journal*. 2006; 52:28-33

Yoganathan AP, Chandran KB, Rittgers SE. Bio fluid Mechanics: The Human Circulation. CRC Press; Boca Raton: 2006

Yoganathan AP, Chandran KB, Sotiropoulos F. Flow in prosthetic heart valves: State of the art and future directions. *Ann Biomed Eng.* 2005; 12:1689-1694

Yoganathan AP, He Z, Jones CS. Fluid mechanics of heart valve. *Ann Rev Biomed Eng*. 2004; 6:331–362

Yoganathan AP. Cardiac valve prosthesis. Handbook of biomedical engineering, 123, CRC Press, New York. 1995:1847–1870 Jones M, Eidbo EE. Doppler colour flow evaluation of prosthetic mitral valves: Experimental epicardial studies. *JACC.* 1989; 13:234-240

Yoganathan AP, Woo YR, Sung HJ. Turbulent shear stress measurements in the vicinity of aortic heart valve prosthesis. *J Biomech*. 1986; 19:433–442

Yuan Q, Xu L, Ngoi BKA, Yeo TJH, Hwang NHC. Dynamic impact analysis of a bi-leaflet mechanical heart valve. *J Heart Valve Dis*. 2003; 12:102–109

Yun BM. Simulations of pulsatile flow through bi-leaflet mechanical heart valves using a suspension flow model: to assess blood damage. *Mechanical Engineering.* Georgia Institute of Technology. Doctor of Philosophy, Atlanta. 2014; 464

Yun BM, McElhinney DB, Arjunonc S, Mirabellac L, Aiduna CK, Yoganathan AP. Computational simulations of flow-dynamics and blood damage through a bi-leaflet mechanical heart valve scaled to pediatric size and flow. *J Biomechanics*. 2014; 47:3169-3177

Yurdakök M. Foetal and neonatal effects of anti-coagulants used in pregnancy: a review. *Turk J Pediatr*. 2012; 54(3):207-15

Zeng H, Yin W, Catausan G, Moldovan N, Carlisle J. Ultrananocrystaline diamond integration with pyrolytic carbon components of mechanical heart valves. *Diamond and Related Materials*. 2016; 63:227-231

Zheng X, Seo JH, Vedula V, Abraham T, Mittal R. Computational modelling and analysis of intra cardiac flows in simple models of the left ventricle. *Eur. J. Mech. B Fluids*. 2012; 35:31–39

Zhang H, Deng X, Cianciulli TF, Zhang Z, Chappard D, Lax JA, Saccheri MC, Redruello HJ, Jordana JL, Prezioso HA, King M, Guidoin R. Clinical device-related article pivoting system fracture in a bi-leaflet mechanical valve: a case report. *J. Biomed. Mater. Res. B Appl. Biomater.* 2009; 90:952-960

Zilla P, Brink J, Human P, Bezuidenhout D. Prosthetic heart valves: Catering for the few. *Biomaterials*. 2008; 29:385–406

Zoghbi WA, Chambers JB, Dumesnil JG, Foster E, Gottdiener JS, Grayburn PA, Khandheria BK, Levine RA, Marx GR, Miller FA Jr, Nakatani S, Quiñones MA, Rakowski H, Rodriguez LL, Swaminathan M, Waggoner AD, Weissman NJ, Zabalgoitia M. Recommendations for evaluation of prosthetic valves with echocardiography and doppler ultrasound: a report From the American Society of Echocardiography's Guidelines and Standards Committee and the Task Force on Prosthetic Valves, developed in conjunction with the American College of Cardiology Cardiovascular Imaging Committee, Cardiac Imaging Committee of the American Heart Association, the European Association of Echocardiography, a registered branch of the European Society of Cardiology, the Japanese Society of Echocardiography and the Canadian Society of Echocardiography, endorsed by the American College of Cardiology Foundation, American Heart Association, European Association of Echocardiography, a registered branch of the European Society of Cardiology, the Japanese Society of Echocardiography, and Canadian Society of Echocardiography. *J Am Soc Echocardiogr*. 2009; 22(9):975-1014

Zwaal RF, Comfurius P, Bevers EM. Surface exposure of phosphatidylserine in pathological cells. *Cell Mol Life Sci.* 2005; 62(9):971–988

Appendices

APPENDIX A	**Echocardiography Report Form**
APPENDIX B	**Animal Sacrifice Protocol**
APPENDIX C	**Histology Protocol**
APPENDIX D	**Tensile strength testing of the Titanium**
APPENDIX F	**Research Outcomes**
APPENDIX G	**Research Team**
APPENDIX H	**Ethical Clearance**

APPENDIX A

Echocardiography Report Form

The dynamic and coagulation characteristics of a re-engineered mechanical heart valve in an Ovine model

Echocardiography report form

Dr. C J Jordaan
Dept Cardiothoracic surgery
University of the Free State
Bloemfontein

Glycar study *in vivo* echocardiographic data	
Sheep number:	
Date:	
Valve type:	
Time period:	☐1 Pre operation ☐2 Intra operative valve surgery ☐3 Pre sacrifice
Left ventricle function:	☐1 Normal ☐2 Mild impairment ☐3 Moderate impairment ☐4 Severe impairment
Right ventricle function:	☐1 Normal ☐2 Mild impairment ☐3 Moderate impairment ☐4 Severe impairment
Pulmonary valve:	
Regurgitation: - Central/ Eccentric:	
VC:	
Regurgitation Doppler signal density:	
Velocities over valve – V max (ms^{-1}): VTI	
Velocities over valve – V mean (ms^{-1}): VTI	
Gradients over valve – P max (mmHg):	
Gradients over valve – mean (mmHg):	
Velocities in RVOT – V max (ms^{-1}): VTI	
Velocities in RVOT – V mean (ms^{-1}): VTI	
Gradients in RVOT – P max (mmHg):	
Gradients in RVOT – P mean (mmHg):	
EOA:	
Poppet valve: excursion of poppet:	☐1 Normal ☐2 Abnormal
Pannus:	☐1 Absent ☐2 Present ☐3 Impending on valve
Thrombus:	☐1 Absent ☐2 Present ☐3 Impending on valve

ms^{-1}= meter per second; VC= vena contracta; VTI= velocity time integral; mmHg= millimeter mercury; RVOT= right ventricle outflow tract

APPENDIX B

Animal Sacrifice Protocol

The dynamic and coagulation characteristics of a re-engineered mechanical heart valve in an Ovine model

Sacrifice protocol

Dr C J Jordaan
Dept. Cardiothoracic surgery
University of the Free State
Bloemfontein

Introduction

The sheep for sacrifice is divided into two main groups. The first group consists of 5 sheep with the GLYCAR valve implanted and two sheep with bi-leaflet mechanical heart valve prosthesis. This first group will be sacrificed at 6 months after implantation. The second group is identical to the first in terms of valve implantation but this group will be sacrificed at one year after implantation.

Prior to sacrifice all the sheep will be assessed clinically. Any signs of cardiac failure or gross neurological deficits will be noted. They will be examined and the valves assessed clinically. Should any of the sheep die prior to scheduled sacrifice it will be noted as such and necropsy will be performed to determine the cause of death. Haemodynamic studies and trans-oesophageal echocardiography will therefore not be performed and the data not collected. The heart and organs will be removed and examined as per protocol and the valve examined in detail.

1. Anaesthesia:

All of the sheep will be fasted for 48 hours; however they will have free access to water. This is to facilitate trans-oesophageal echocardiography and to reduce the risk of aspiration.
The sheep will be managed in the right decubitus position.
The neck and the left thorax will be shaved to clear wool from the surgical sites.

A 14 F CVP catheter will be placed in the left external jugular vein, the relevant bloods will be taken (see blood tests) prior to induction.

The sheep will be anaesthetized using Thiopentone induction; standard intra operative monitoring will be connected and will be intubated using a no. 9 endotracheal tube.

Heparin is administered until an ACT (activated clotting time) of 480 sec. is reached
Surgery will then commence (see surgery) and after all the relevant hemodynamic tests and echocardiography have been performed a lethal dose of Potassium-chloride will be administered intravenously, thereby ending anaesthesia.

2. Surgery:

Perform a left lateral thoracotomy over the previous incision wound. Resect the second to fourth ribs and remove the sternal rib adhesions. The sternum must also be resected to allow for unobstructed epicardial echocardiography of the heart.

Proceed to obtain hemodynamic data: After zeroing the transducer at the height of the right atrium, a needle is placed into the following chambers and the pressures recorded:

- Right atrium
- Right ventricle outflow tract
- Main pulmonary artery
- Aorta

The diastolic, systolic and mean pressures will be measured, as well as the heart rate.

The inferior vena cava is transected after a lethal dose of potassium chloride is administered and the subject is exsanguinated. The pulmonary valve is dissected en bloc from the heart, taking care not to disturb any clots that may have formed on the valve or sewing cuff.

The pulmonary artery is opened on the posterior aspect opposite the pericardial patch. The struts and the valve is inspected for any macroscopic clots in the following areas:

- Pericardial patch, proximal and distal to the valve/sewing cuff
- Sewing cuff/annulus junction
- Sewing cuff, proximal and distal to the valve
- The housing and the struts
- The guide openings in the struts
- The poppet

The pericardial patch is then inspected. Look for any signs of strut contact with the patch or the pulmonary artery. Inspect the sewing cuff for any pannus overgrowth.

The specimen is now prepared for photography:

- Remove any excess tissue around the annulus and the pulmonary artery taking care not to disturb any clots or artefacts that may have formed in and around the valve.
- Gently rinse the valve in saline, not water as this will injure and remove platelets from the valve and sewing cuff.
- Place the valve on the photography table.
- Photos taken should include the following areas of interest:

- Pericardial patch, proximal and distal to the valve/sewing cuff
- The sewing cuff/annulus junction
- Sewing cuff, proximal and distal to the valve
- The housing and the struts
- The guide openings in the struts
- The poppet

The valve is now placed in formalin for further processing.

Both lungs are removed and inspected for any macroscopic abnormalities. Sections are then cut into the lung to inspect it for any infarctions at 1 cm intervals. Any suspicious lung is the sampled and placed into formalin for further histological examination.

At the completion of the evaluation the sheep is sent for incineration.

3. Blood tests:

Blood must be taken from the sheep before any surgery is performed, any anaesthesia is given or heparin is administered. The following blood tests must be performed:

Glycar Study
Blood results.

Sheep no: Surgery Date:
Ear tag no:

Date:									
Days post op	0	1	7	14	30	60	120	180	360
Coagulation evaluation									
Thrombin Time									
INR									
PTT									
Prothrombin time									
Biochemistry									
Na									
K									
Urea									
Creatinine									
Albumin									
Haematology									
White blood count									
Neutrophyl count									
Eosinophils									
Haemoglobin									
Haptoglobin									
Platelets									
RPI									
ESR									
CRP									
Liver functions									
Bilirubin total									
Bilirubin conj.									
AST									
ALP									
GGT									
LD									
Immunology									
IgE									
IgG									

AST= Aspartate aminotransferase; ALT= Alanine transaminase; ALP= Alkaline phosphatase; GGT= Gamma glutamyl transferase; LD= Lactate dehydrogenase; Bili= Bilirubin; CRP= C Reactive Protein; IgG= Immunoglobulin G; IGA= Immunoglobulin A; IGM= Immunoglobulin M; PT= Prothrombin time; PTT= Partial thromboplastin time; INR= International normalised ratio; HB= Haemoglobin; ESR= Erythrocyte sedimentation rate; RPI= Red cell production index; sec= seconds; mm/h= millimeter per hour; mmol/l= mill mole per liter; g/l= gram per liter; sec= seconds; U/l= units per liter; g/dl= gram per deciliter; mg/l= milligram per liter.

4. Echocardiography:

The following measurements must be made during the epicardial and/or trans-oesophageal echocardiographic evaluation during the evaluation of the valve:

- Right and left ventricular function and contraction
- RV volume
- Right ventricle outflow tract velocity time integral (RVOT - VTI)
- Peak systolic velocity across the prosthetic valve
- Doppler velocity index (DVI): Peak velocity RVOT to the peak velocity across the valve
- Acceleration time
- Systolic contour tracing
- Effective orifice area (EOA)
- Gradient across the valve
- Poppet excursion
- Regurgitation evaluation
- Any signs of clot/ pannus impeding poppet motion

5. Photography:

The specimen has to be prepared for photography:

- Remove any excess tissue around the annulus and the pulmonary artery taking care not to disturb any clots or artefacts that may have formed in and around the valve.
- Gently rinse the valve in 0.9% saline, not water as this will injure and remove platelets from the valve and sewing cuff.
- Place the valve on the photography table.
- Macro photos taken of the valve should include the following areas of interest, focusing on areas with pathology:
    - Pericardial patch, proximal and distal to the valve/sewing cuff
    - The sewing cuff/annulus junction
    - Sewing cuff, proximal and distal to the valve
    - The housing and the struts
    - The guide openings in the struts
    - The poppet

The valve is now placed in formalin for further processing.

APPENDIX C

Histology Protocol

The dynamic and coagulation characteristics of a re-engineered mechanical heart valve in an Ovine model

Histology protocol.

Explantation of mechanical heart valve prosthesis:

Dr. C J Jordaan
Dept Cardiothoracic surgery
University of the Free State
Bloemfontein

Valve Explantation	
Sheep no	
Date of sacrifice	
Date of implantation	
Days on study	
Scheduled sacrifice	
Valve type	
Complications	

The National Health Laboratory Service (NHLS) evaluated the Haematoxylin and eosin stains (H&E) according to their Standard operating procedures (SOP's). H & E were performed after surgical excision of the valve.

Specimens for histology:

- Removed the pulmonary valve en-bloc from the heart and remove the tissue from the right ventricular outflow tract up to the sewing cuff with care, taking care not to dislodge any clot or thrombus that may have formed on or around the valve.
- Rinse the valve carefully with 0.9 % Saline solution.
- Note any abnormalities on the proximal side of the valve and take photographs of this area.
- Dissect the pulmonary artery and remove a sliver of the native pulmonary artery and the Glycar patch for analysis.
- Remove a part of the sewing cuff of the Glycar valve bordering the pericardial patch and place the specimen in formalin.
- Removed any clot or thrombus from the struts after the valve is photographed according to protocol, and place the valve in formalin.
- A sliver of tissue containing the junction between the pericardial patch and the sewing cuff and a sliver of tissue containing native pulmonary artery and sewing cuff is taken and placed in formalin.
- Cut sections are made through the lungs at 1 cm intervals evaluating the lung for possible pulmonary emboli. Specimens of any suspicious lesions are taken and placed in formalin for histology.

The following questions has to be answered by the Pathologist:

- Sewing cuff:
  - Is there cellular infiltration of the sewing cuff? Which cells are they?
  - Is the sewing cuff covered with pannus or epithelium?
  - Are there platelets adhered to the cuff?
  - Are there signs of thrombus on the cuff?
  - Is there signs of infective endocarditis (SBE)?
- Thrombus:
  - Is this only organised clot or are there signs of SBE?
- Pulmonary artery wall:
  - Look at the healing between the pericardial patch and the pulmonary artery. Is the pericardial patch covered with endothelium? Any signs of calcification of the pericardial patch?
- Lung**:** Any signs of pulmonary embolism?

- **Pulmonary artery:**

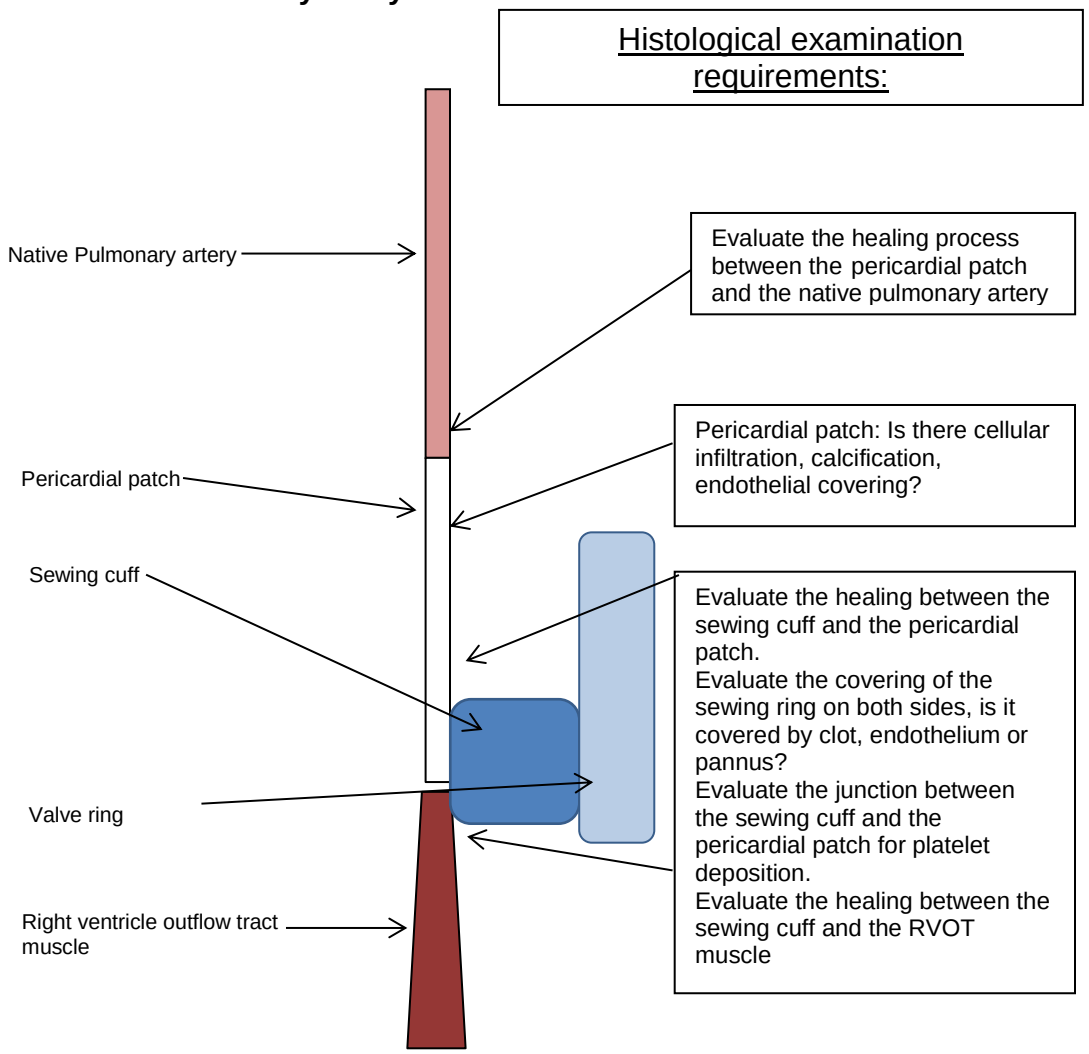

A cross sectional view of the pulmonary artery up to the sewing cuff, showing the junction between the pericardial patch, the valve sewing cuff and the right ventricle muscle.

APPENDIX D

Tensile strength testing of the titanium Glycar housing prototype

Introduction

Six Glycar titanium valve assembly prototypes (designated: Ti6Al4V) were produced using direct metal laser sintering (DMLS) ('3D printing') on the EOSINT M280 system (Electro Optical Systems, Munich, Germany) at the centre for rapid prototyping and manufacturing, Central University of Technology, Bloemfontein, South Africa.

Direct metal laser sintering (DMLS) is an additive manufacturing technique that uses an Ytterbium fibre laser fired into a bed of powdered metal (e.g. titanium). The laser is automatically aimed at points in space defined by a 3D model, melting or rather, welding the material together to create a solid structure. Inside the working chamber, there is a material dispensing platform and a building platform or base, along with a recoater blade used to apply a new layer of powder over the platform once the laser have finalised the layer. Parts are therefore built up additively layer by layer, typically applying layers 20 micrometers thick. During the production process supportive material is added to the construction to ensure stability of the strut positions. The supportive material is removed from the frame and the annealing process started to strengthen the metal frame. Manufacturing is completed by laser polishing the frame.

Mr Gerrie Booysen, the chief engineer involved in the manufacturing of the valve housings, produced the titanium housing assemblies in two orientations in order to evaluate the influence that manufacturing positioning may have on the tensile strength of the assembly.

All six assemblies were 'printed' at the same time in a single batch on the same baseplate to ensure uniformity during the manufacturing process. CAD renderings of the Glycar valve housing was supplied by Southern Medical, Pretoria, South-Africa. The two different orientations is referred to as Back and Flat (Figure 1) orientations. The Back orientation has the guiding struts face inferiorly, downwards towards the base plate. The supportive material (in red) in this position is minimised as no material is needed to support the guiding rings. Handling of the housing after production will therefore be less with reduced post production altering to remove the supporting material from the frame. The Flat orientation has the guiding struts face parallel to the base plate. In this position however, more supportive material is needed during the

production process with material having to support the guiding rings. It is uncertain if this extra material and the post process tooling may have an influence on the strength of the struts.

The assemblies were cleaned and all of the supportive material removed. The assemblies were then tested in their 'raw', unprocessed state. To avoid any interference in the titanium molecular integrity the frames were not polished, shot peened or annealed, thereby excluding any external factors that may influence the tensile strength of the frame. The struts and the guide rings were measured to ensure uniformity between the housings, the rings and the guide struts.

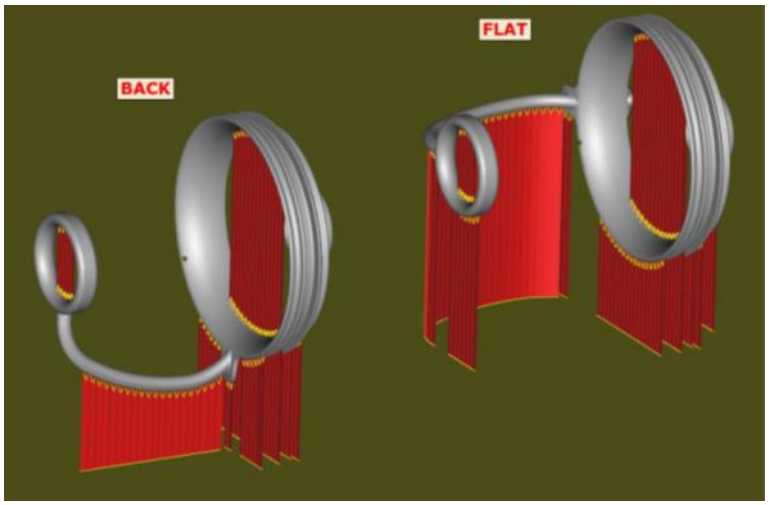

FIGURE 1: **CAD renderings of the 'printing' orientation of the titanium Glycar housing assembly**. Back orientation on the left and Flat on the right. The supporting material is shown in red.

Summary of methodology

1. After the samples were received (Figure 3), three in the flat configuration and three in the back configuration, they were scrutinized for any visible defects and all excess support material was removed.
2. No post processing of the housing assembly was performed as this may influence the metal tensile strength.
3. The guide strut was measured for a base dimension to ensure that the valve assemblies complied with the minimal and maximal dimensions and to ensure uniformity of the specimens.
4. The quality of the assemblies were assessed by evaluating the porosity of the assemblies with Computed Tomography (CT) at the University of Stellenbosch.
5. Tensile strength testing was performed by Mr. Johan Els on the prototype Glycar titanium housing at the Centre for rapid prototyping and manufacturing, Central

University of Technology, Bloemfontein, South Africa. Failure of the housing assembly were induced for quality and feasibility purposes.

a. The machine grips were prepped to accept the valve geometry.
b. The sample was mounted (Figure 2).
c. Slight pretension was applied.
d. An extension rate of 3mm/min was selected.
e. The load was increased at 3mm/min extension until failure of the assembly was induced.
f. The broken housing assembly was removed.
g. Final observations and inspections were performed of the assembly.
h. The report was exported and the data captured.

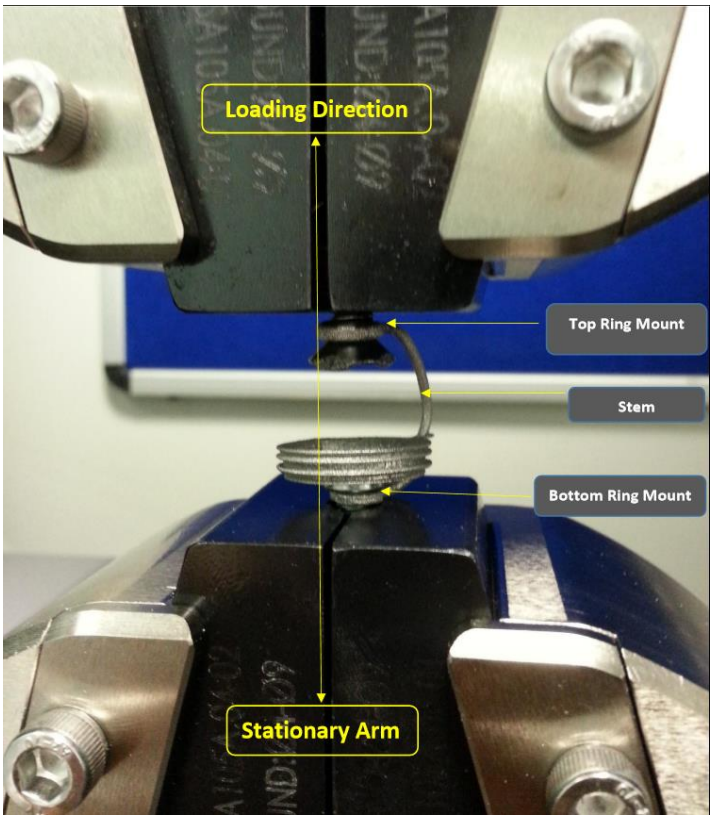

FIGURE 2: **Mounting of the housing assembly in the machine grips.**

FIGURE 3: **Samples of the titanium housing in the two orientations Flat and Back.** The assemblies have been cleaned and the supportive material removed.

Results

Result of the computed tomography scan

Only two of the six samples showed porosity on the CT scan as can be appreciated in Figure 4 and 5. These pores were 120 microns in diameter in both assemblies and occurred on the housing in Flat 2 and on the retaining ring of Flat 3. The porosity may be due to powder bed disturbances during DMLS because of the recoater.

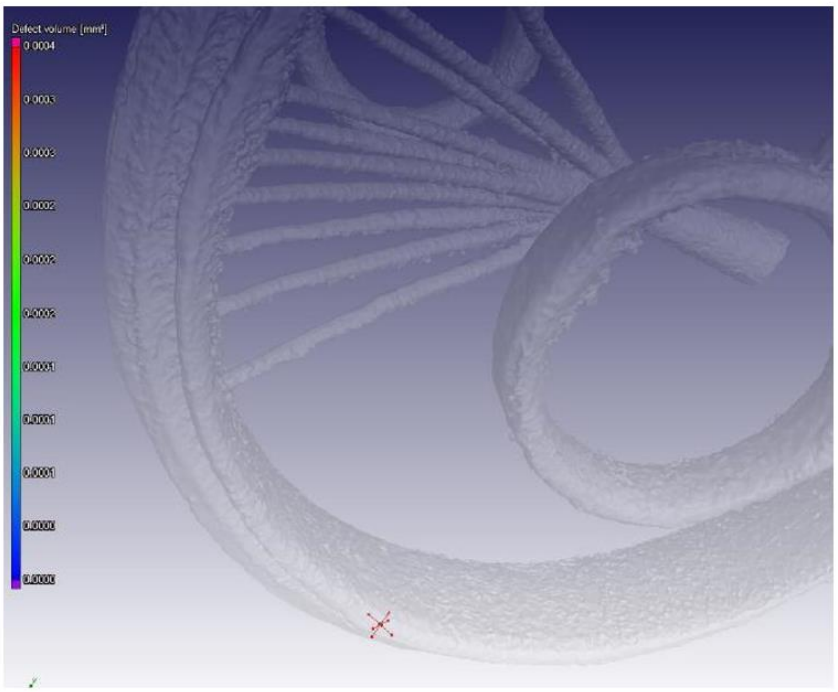

FIGURE 4: **Computed tomography of Flat 2 with a 120 micron pore indicated by the red cross on the housing.**

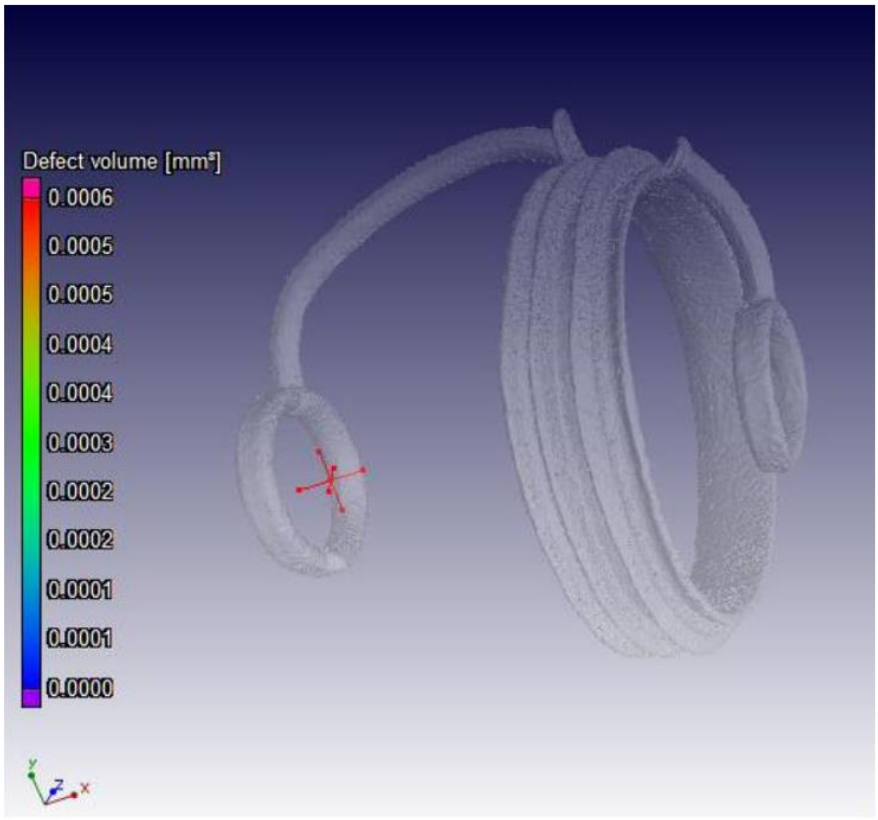

FIGURE 5: **Computed tomography of Flat 3 with a 120 micron pore indicated by the red cross on the retaining ring**

Results of the tensile strength test

66% (4/6) of samples failed at the top ring, where the strut separated from the top-ring at the joint. 16% of the sample showed a ductile break in the mid stem and 16% of samples had bottom stem separation from the main outer ring. In two independent tensile tests one sample separated at the top ring and the other mid stem. Table 1 summarizes the breaking points of the different assemblies. The mean failure load was 162 N, the maximum failure load 216 N (Flat 3) and the minimum failure load 116 N (Flat 2).

TABLE 1: Breaking point for the different assemblies

Sample	Peak Load
Back 1	152 N
Back 2	166 N
Back 3	158 N
Flat 1	163 N
Flat 2	116 N
Flat 3	217 N

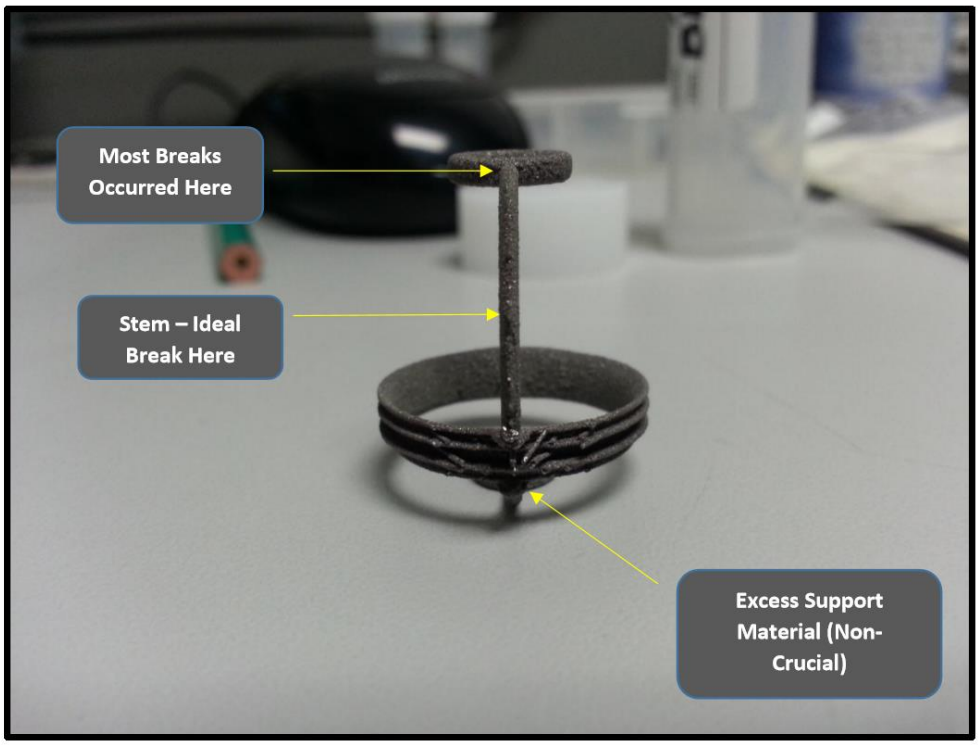

FIGURE 6: **The titanium Glycar housing showing the most common sites of assembly failure.**

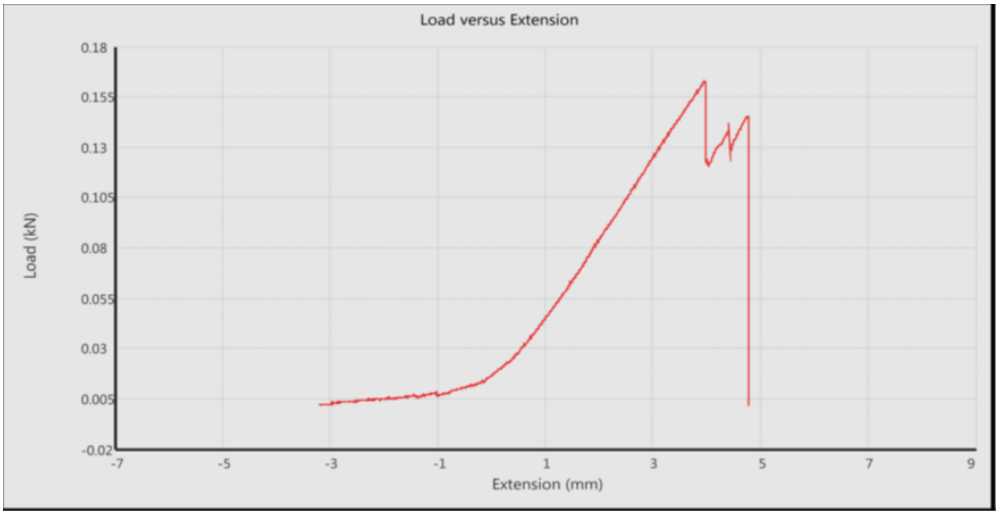

FIGURE 7: **Tensile graph for Flat 1.**

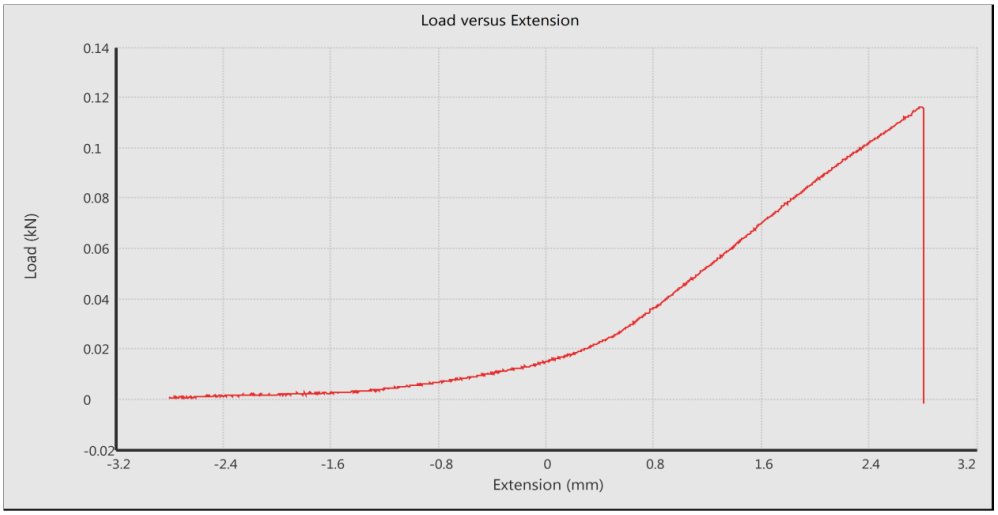

FIGURE 8: **Tensile graph for Flat 2**. Premature failure due to porosity is present in this sample (as identified previously by CT-Scan). Porosity may be due to some powder bed disturbance during DMLS because of the recoater.

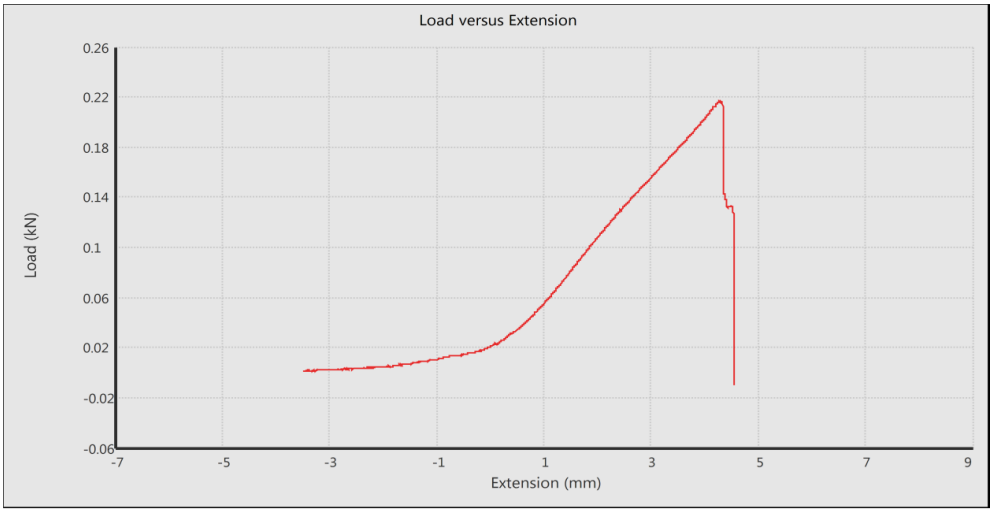

FIGURE 9: **Tensile graph for Flat 3**.

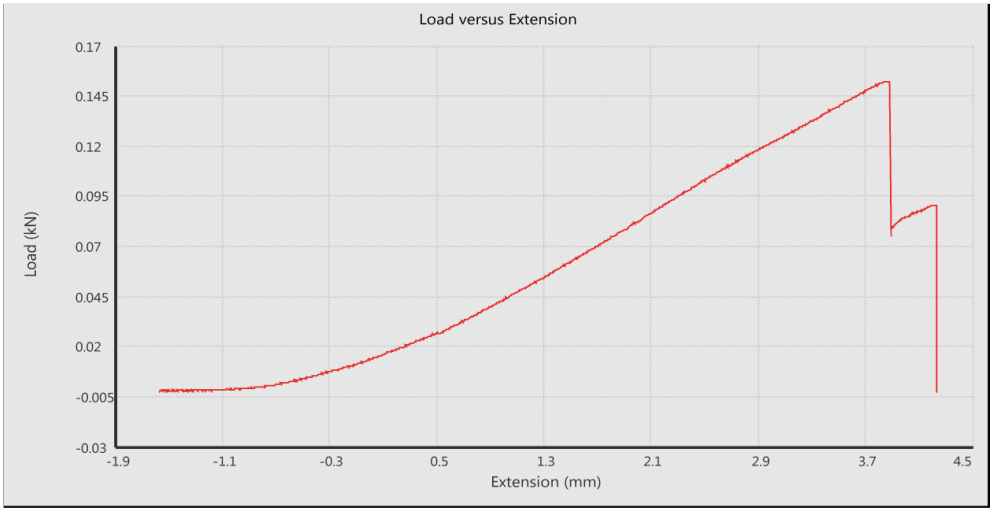

FIGURE 10: **Tensile graph for Back 1**.

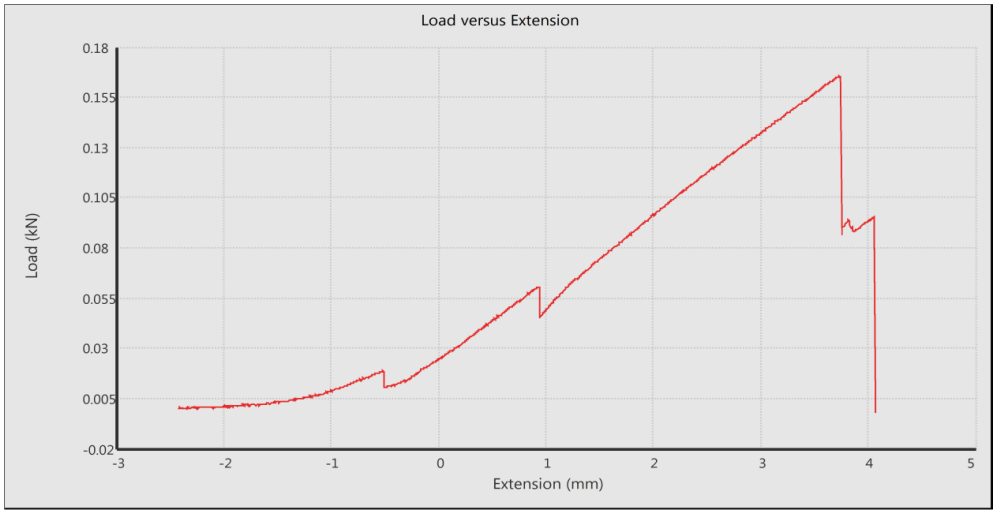

FIGURE 11: **Tensile graph for Back 2.** Two incremental yielding dips are seen due to surface roughness of the specimen.

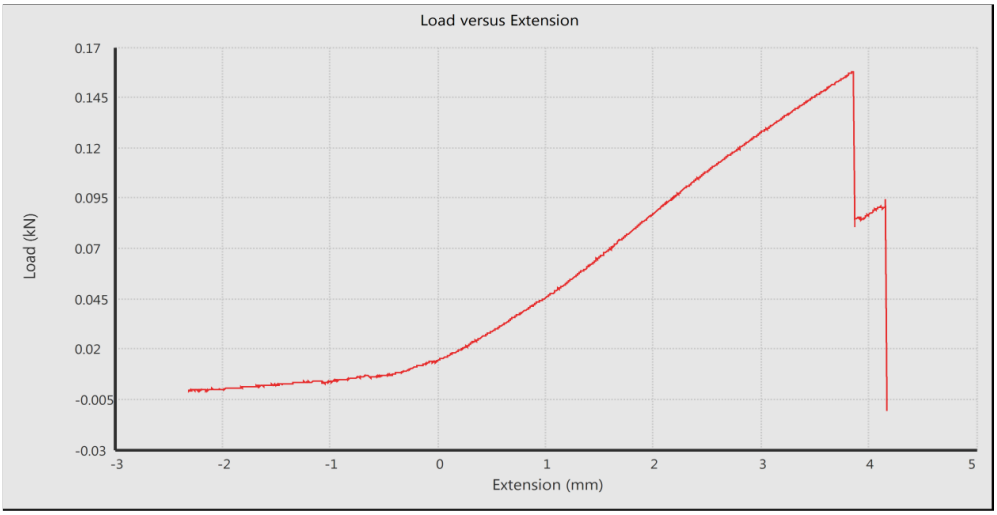

FIGURE 12: **Tensile graph for Back 3.**

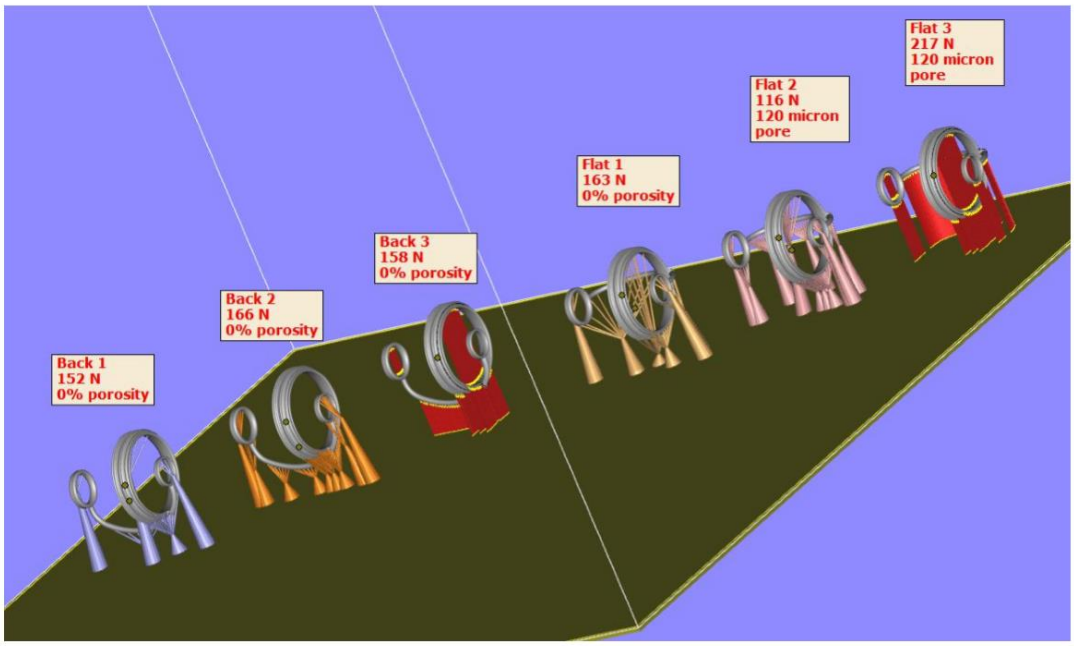

FIGURE 13: **The assembly orientation is combined with the tensile strength**

Discussion

Due to the geometry of the valve housing assembly the tensile testing is relatively complex, be that as it may. The valve housing assembly showed good tensile strength with a mean failure at 163 N, average of 162 N. There were slight inconsistencies in one sample because of porosity (Flat 2), which could have contributed to its premature failure of the housing at a failure point of 116 N. This however is an anomaly that occurred during manufacturing and can be controlled via CT and visual inspection. Failure due to crack initiation which in turn is due to surface roughness can be improved by polishing the samples. Smooth surface finishing will invariably lead to higher load capacities. There were no differences between the different printing orientations. The highest tensile strength was measured in sample Flat 3. In this orientation the guiding strut faced parallel to the base plate. Flat 2 fractured prematurely because of the porosity of the housing. If this specimen is disregarded the average tensile strength in this Flat group performed better than the Back group. The result however is not powered to prove superiority of the production orientation but it was interesting to note the increased strength of the Flat housings. Further investigation is however needed.

Shot peening, annealing and hand polishing are possible avenues that will increase the tensile strength of the titanium. Utilizing the brush recoater on the EOSINT M280 system may also contribute to less inconsistencies of the samples which would promote strength.

APPENDIX E

ISO 5840:2015 Guideline (Condensed)

ISO 5840:2015 Guidelines

Foreword

ISO (the International Organization for Standardization) is a worldwide federation of national standards bodies (ISO member bodies). The work of preparing International Standards is normally carried out through ISO technical committees. Each member body interested in a subject for which a technical committee has been established has the right to be represented on that committee. International organizations, governmental and non-governmental, in liaison with ISO, also take part in the work. ISO collaborates closely with the International Electro technical Commission (IEC) on all matters of electro technical standardization.

The procedures used to develop this document and those intended for its further maintenance are described in the ISO/IEC Directives, Part 1. In particular the different approval criteria needed for the different types of ISO documents should be noted. This document was drafted in accordance with the editorial rules of the ISO/IEC Directives, Part 2 (see www.iso.org/directives).

Attention is drawn to the possibility that some of the elements of this document may be the subject of patent rights. ISO shall not be held responsible for identifying any or all such patent rights. Details of any patent rights identified during the development of the document will be in the Introduction and/or on the ISO list of patent declarations received (see www.iso.org/patents).

Any trade name used in this document is information given for the convenience of users and does not constitute an endorsement. For an explanation on the meaning of ISO specific terms and expressions related to conformity assessment, as well as information about ISO's adherence to the WTO principles in the Technical Barriers to Trade (TBT) see the following URL: Foreword - Supplementary Information

The committee responsible for this document is ISO/TC 150, *Implants for surgery*, Subcommittee SC 2, *Cardiovascular implants and extracorporeal systems.*
This first edition of ISO 5840-1, together with ISO 5840-2 and ISO 5840-3, cancels and replaces ISO 5840:2005, which has been technically revised.
ISO 5840 consists of the following parts, under the general title *Cardiovascular implants — Cardiac valve prostheses:*

- *Part 1: General requirements*
- *Part 2: Surgically implanted heart valve substitutes*
- *Part 3: Heart valve substitutes implanted by transcatheter techniques*

1. Introduction

There is, as yet, no heart valve substitute which can be regarded as ideal. The ISO 5840–series has been prepared by a group well aware of the issues associated with heart valve substitutes and their development. In several areas, the provisions of the ISO 5840–series deliberately have not been specified to encourage development and innovation. It does specify the types of tests, test methods, and/or requirements for test apparatus and requires documentation of test methods and results. The areas with which the ISO 5840–series are concerned are those which will ensure that associated risks to the patient and other users of the device have been adequately mitigated, facilitate quality assurance, aid the clinician in choosing a heart valve substitute, and ensure that the device will be presented at the operating table in convenient form. Emphasis has been placed on specifying types of *in vitro* testing, on preclinical *in vivo* and clinical evaluations, on reporting of all *in vitro*, preclinical *in vivo*, and clinical evaluations, and on the labelling and packaging of the device. Such a process involving *in vitro*, preclinical *in vivo*, and clinical evaluations is intended to clarify the required procedures prior to market release and to enable prompt identification and management of any subsequent problems.

With regard to *in vitro* testing and reporting, apart from basic material testing for mechanical, physical, chemical, and biocompatibility characteristics, the ISO 5840–series also covers important hydrodynamic and durability characteristics of heart valve substitutes. The ISO 5840–series does not specify exact test methods for hydrodynamic and durability testing, but it offers guidelines for the test apparatus.

The ISO 5840–series is incomplete in several areas. It is intended to be revised, updated, and/or amended as knowledge and techniques in heart valve substitute technology improve.

2. Scope

This part of ISO 5840 is applicable to heart valve substitutes intended for human implantation and provides general requirements. Subsequent parts of the ISO 5840–series provide specific requirements.

This part of ISO 5840 is applicable to both newly developed and modified heart valve substitutes and to the accessories, packaging, and labelling required for their implantation and for determining the appropriate size of the heart valve substitute to be implanted.

This part of ISO 5840 outlines an approach for qualifying the design and manufacture of a heart valve substitute through risk management. The selection of appropriate qualification tests and methods are derived from the risk assessment. The tests may include those to assess the physical, chemical, biological, and mechanical properties of heart valve substitutes and of their materials and components. The tests may also include those for preclinical *in vivo* evaluation and clinical evaluation of the finished heart valve substitute.

This part of ISO 5840 defines operational conditions for heart valve substitutes.

This part of ISO 5840 excludes homografts.

3. Normative references

The following documents, in whole or in part, are normatively referenced in this document and are indispensable for its application. For dated references, only the edition cited applies. For undated references, the latest edition of the referenced document (including any amendments) applies.

- ISO 5840-2, *Cardiovascular implants — Cardiac valve prostheses —Part 2: Surgically implanted heart valve substitutes*
- ISO 5840-3, *Cardiovascular implants — Cardiac valve prostheses —Part 3: Heart valve substitutes implanted by transcatheter techniques*
- ISO 11135, *Sterilization of health-care products — Ethylene oxide — Requirements for the development, validation and routine control of a sterilization process for medical devices*
- ISO 11137 (all parts), *Sterilization of health care products — Radiation*
- ISO 11607 (all parts), *Packaging for terminally sterilized medical devices*
- ISO 14155, *Clinical investigation of medical devices for human subjects — Good clinical practice*
- ISO 14160, *Sterilization of health care products — Liquid chemical sterilizing agents for single-use medical devices utilizing animal tissues and their derivatives — Requirements for characterization, development, validation and routine control of a sterilization process for medical devices*
- ISO 14630:2012, *Non-active surgical implants — General requirements*
- ISO 14937, *Sterilization of health care products — General requirements for characterization of a sterilizing agent and the development, validation and routine control of a sterilization process for medical devices*
- ISO 14971, *Medical devices — Application of risk management to medical devices*
- ISO 17665 (all parts), *Sterilization of health care products — Moist heat*

4. Terms and definitions

For the purposes of this document, the following terms and definitions apply.

1. **Accessories:** device-specific tools that are required to assist in the implantation of the heart valve substitute
2. **Adverse event (AE):** untoward medical occurrence in a study subject which does not necessarily have to have a causal relationship with study treatment. Note 1 to entry: An AE can be an unfavourable and unintended sign (including an abnormal laboratory finding), symptom, or disease, temporary or permanent, whether or not related to the prosthetic valve implantation or procedure.
3. **Actuarial methods:** Statistical technique for calculating event rates over time. Note 1 to entry: Standard actuarial methods calculate the probability of freedom from events within pre-specified intervals of time. When the intervals approach zero width, the methods are called Kaplan-Meier methods.
4. **Arterial end diastolic pressure:** minimum value of the arterial pressure during diastole
5. **Arterial peak systolic pressure:** maximum value of the arterial pressure during systole
6. **Back pressure: D**ifferential pressure applied across the valve during the closed phase
7. **Body surface area (BSA):** total surface area (m^2) of the human body. Note 1 to entry: This can be calculated (Mosteller's formula) as the square root of the product of the weight in kg times the height in cm divided by 3 600 (see Reference [31]).
8. **Cardiac index:** cardiac output (3.9) (CO, L/min) divided by the body surface area (3.7) (BSA, m^2) with units L/min/m^2
9. **cardiac output (CO):** stroke volume (3.59) times heart rate
10. **closing volume:** portion of the regurgitant volume that is associated with the dynamics of valve closure during a single cycle. Note 1 to entry: See Figure 1.
11. **Coating: T**hin-film material that is applied to an element of a heart valve system to modify its physical or chemical properties
12. **Compliance:** relationship between change in diameter and change in pressure of a deformable tubular structure (e.g. valve annulus, aorta, conduit) defined in this part of ISO 5840 as

$$C = 100\% \times \frac{(r_2 - r_1) \times 100}{r_1 \times (p_2 - p_1)}$$

where

C is the compliance in units of % radial change/100 mmHg;

p_1 is the diastolic pressure, in mmHg;

p_2 is the systolic pressure, in mmHg;

r_1 is the inner radius at p_1, in millimeters;

r_2 is the inner radius at p_2, in millimeters.

Note 1 to entry: Reference ISO 25539-1.

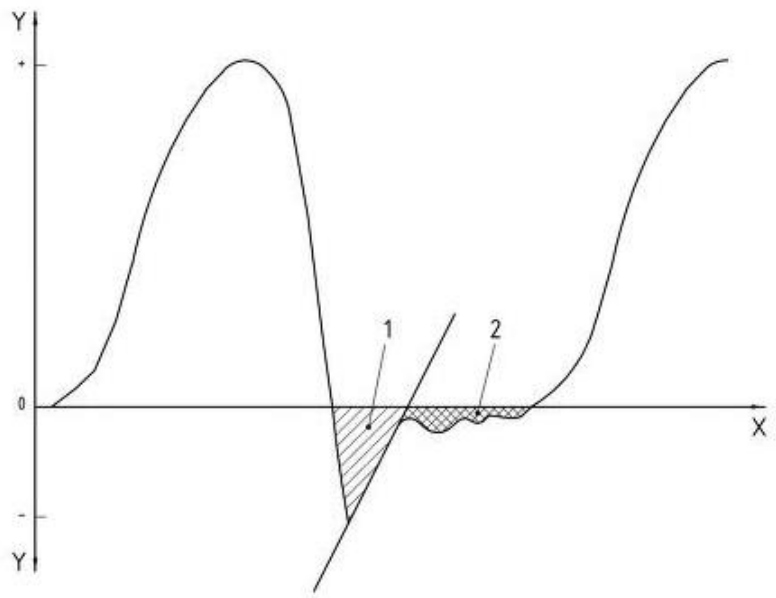

FIGURE 1: **Schematic representation of flow waveform and regurgitant volumes for one cycle.** X = time; Y = flowrate; 1 = closing volume; 2 = leakage volume

13. **Component-joining material:** material such as a suture, adhesive, or welding compound used to assemble the components of a heart valve system
14. **Cumulative incidence:** statistical technique where events other than death can be described by the occurrence of the event over time without including death of the subjects. Note 1 to entry: Cumulative incidence is also known as “actual” analysis.
15. **Cycle:** one complete sequence in the action of a heart valve substitute under pulsatile-flow conditions
16. **Cycle rate:** number of complete cycles per unit of time usually expressed as cycles per minute (cycles/min)
17. **Design verification:** establishment by objective evidence that the design output meets the design input requirements
18. **Design validation:** establishment by objective evidence that device specifications conform with user needs and intended use(s)
19. **Device embolization:** dislodgement from the intended and documented original position to an unintended and non-therapeutic location
20. **Device failure;** inability of a device to perform its intended function sufficient to cause a hazard
21. **Device migration:** detectable movement or displacement of the heart valve substitute from its original position within the implant position and without device embolization
22. **Effective orifice area (EOA):** orifice area that has been derived from flow and

$$EOA = \frac{q_{V_{RMS}}}{51{,}6 \times \sqrt{\frac{\Delta p}{\rho}}}$$

pressure or velocity data for *in vitro* testing, EOA is defined as: where

EOA	is the Effective Orifice Area (cm^2);
$q_{V_{RMS}}$	is the root mean square forward flow (ml/s) during the positive differential pressure period;
Δp	is the mean pressure difference (measured during the positive differential pressure period) (mmHg);
ρ	is the density of the test fluid (g/cm^3).

27. **Failure mode:** mechanism of device failure. Note 1 to entry: Support structure fracture, calcification, and prolapse are examples of failure modes.
28. **Flexible surgical heart valve substitute**: surgical heart valve substitute wherein the occluder is flexible under physiological conditions. Note 1 to entry: The orifice ring may or may not be flexible.
29. **Follow-up:** continued assessment of patients who have received the heart valve substitute
30. **Forward flow volume:** volume of flow ejected through the heart valve substitute in the forward direction during one cycle
31. **Fracture:** complete separation of any structural component of the heart valve substitute that was previously intact
32. **Heart valve substitute:** device used to replace the function of a natural valve of the heart
33. **Heart valve system:** implantable device
34. **Implant site/implant position:** intended location of heart valve substitute implantation or deployment
35. **Intended use:** use of a product or process in accordance with the specifications, instructions, and information provided by the manufacturer
36. **Kaplan-Meier methods:** statistical approaches for calculating event rates over time when the actual dates of events for each person in the population are known
37. **Leakage volume:** portion of the regurgitant volume which is associated with leakage during the closed phase of a valve in a single cycle and is the sum of the transvalvular leakage volume and paravalvular leakage volume. Note 1 to entry: The point of separation between the closing and leakage volumes is obtained according to a defined and stated criterion (the linear extrapolation shown in Figure 1 is just an example).
38. **Linearized rate:** total number of events divided by the total time under evaluation. Note 1 to entry: Generally, the rate is expressed in terms of percent per patient year.
39. **Major bleeding:** any episode of major internal or external bleeding that causes death, hospitalization, or permanent injury (e.g. vision loss) or necessitates transfusion
40. **Major paravalvular leak:** paravalvular leakage leading to death or reintervention, or causing heart failure requiring additional medication, or causing moderate or severe regurgitation or prosthesis “rocking” on investigation even in the apparent absence of symptoms, or causing hemolytic anemia
41. **Mean arterial pressure:** time-averaged arithmetic mean value of the arterial pressure during one cycle
42. **Mean pressure difference/mean pressure gradient:** averaged arithmetic mean value of the pressure difference across a heart valve substitute during the positive differential pressure period of the cycle
43. **Nonstructural valve dysfunction:** abnormality extrinsic to the heart valve substitute that results in stenosis, regurgitation, and/or hemolytic anemia
44. **Occluder/leaflet:** component that inhibits back flow

45. **Outflow tract profile height:** maximum distance that the heart valve substitute extends axially into the outflow tract in the open or closed position, whichever is greater, measured from the valve structure intended to mate with the top (atrial or aortic/pulmonic side) of the patient's annulus
46. **Pannus:** ingrowth of tissue onto the heart valve substitute which can interfere with normal functioning
47. **Paravalvular leakage volume:** portion of the leakage volume that is associated with leakage around the closed heart valve substitute during a single cycle
48. **Profile height:** maximal axial dimension of a heart valve substitute in the open or closed position, whichever is greater
49. **Prosthetic valve endocarditis:** any infection involving a prosthetic valve based on reoperation, autopsy, or the Duke Criteria for endocarditis
50. **Reference valve:** heart valve substitute with a known clinical experience used for comparative preclinical and clinical evaluations
51. **Regurgitant fraction:** regurgitant volume expressed as a percentage of the forward flow volume
52. **Regurgitant volume:** volume of fluid that flows through a heart valve substitute in the reverse direction during one cycle and is the sum of the closing volume and the leakage volume. Note 1 to entry: See Figure 1.
53. **Rigid surgical heart valve substitute:** surgical heart valve substitute wherein the occluder(s) and orifice ring are non-flexible under physiological conditions
54. **Risk analysis:** systematic use of available information to identify hazards and to estimate the associated risks
55. **Risk assessment:** overall process comprising a risk analysis and a risk evaluation
56. **Root mean square forward flow (RMS forward flow):** square root of the integral of the volume flow rate waveform squared during the positive differential pressure interval of the forward flow phase used to calculate EOA. Note 1 to entry: Defining the time interval for flow and pressure measurement as the positive pressure period of the forward flow interval for EOA computation provides repeatable and consistent results for comparison to the minimum device performance requirements. Note 2 to entry: This is calculated using the following equation:

$$q_{V_{RMS}} = \sqrt{\frac{\int_{t_1}^{t_2} q_V(t)^2 dt}{t_2 - t_1}}$$

where

$q_{V_{RMS}}$ is root mean square forward flow during the positive differential pressure period;

$q_V(t)$ is instantaneous flow at time (t);

t_1 is time at start of positive differential pressure period;

t_2 is time at end of positive differential pressure period.

Note 3 to entry: The rationale for use of Qv_{rms} is that the instantaneous pressure difference is proportional to the square of instantaneous flow rate and it is the mean pressure difference that is required (See Figure 2).

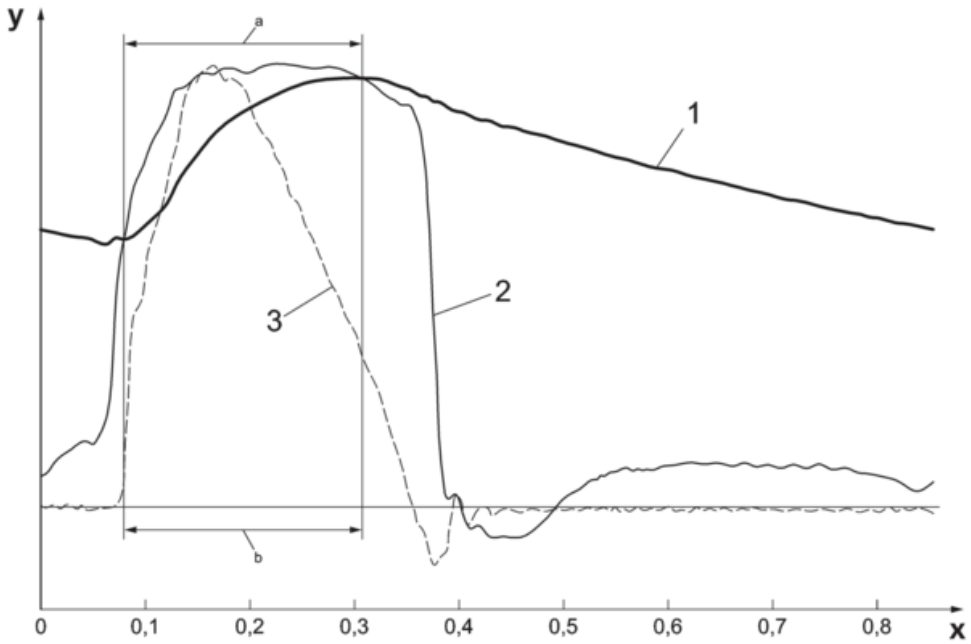

FIGURE 2: **Schematic representation of the positive pressure period of an aortic forward flow interval.** 1 = aortic pressure; 2 = left ventricular pressure; 3 = aortic flow rate; X = time; Y = pressure in mmHg and flow in L/min; a = positive pressure range; b = Qr_{ms} range

57. **Safety:** freedom from unacceptable risk
58. **Severity:** measure of the possible consequences of a hazard
59. **Simulated cardiac output:** forward flow volume times heart rate
60. **Sterility assurance level (SAL):** probability of a single viable microorganism occurring on an item after sterilization. Note 1 to entry: The term SAL takes a quantitative value, generally 10^{-6} or 10^{-3}. When applying this quantitative value to assurance of sterility, an SAL of 10^{-6} has a lower value, but provides a greater assurance of sterility than an SAL of 10^{-3}.
61. **Sterilization:** validated process used to render a product free from viable microorganisms. In a sterilization process, the rate of microbial inactivation is exponential and thus, the survival of a microorganism on an individual item can be expressed in terms of probability. While this probability can be reduced to a very low number, it can never be reduced to zero.
62. **Stroke volume (SV):** volume of blood pumped by a ventricle in one contraction
63. **Structural valve deterioration:** change in the function of a heart valve substitute resulting from an intrinsic abnormality that causes stenosis or regurgitation. This definition excludes infection or thrombosis of the heart valve substitute. It includes intrinsic changes such as wear, fatigue failure, stress fracture, occluder escape, suture line disruption of components of the prosthesis, calcification, cavitation erosion, leaflet tear and stent creep.
64. **Support structure:** component of a heart valve substitute that houses the occluder(s) (e.g. stent, frame, housing)
65. **Surgical heart valve substitute:** heart valve substitute generally requiring direct visualization and cardiopulmonary bypass for implantation
66. **Systolic duration (systole):** portion of cardiac cycle time corresponding to ventricular contraction

67. **Thrombo-embolism:** embolic event involving clot that occurs in the absence of infection. Note 1 to entry: Thrombo-embolism may be manifested by a neurological event or a noncerebral embolic event.
68. **Transcatheter heart valve substitute:** heart valve substitute delivered through a catheter and implanted in a manner generally not involving direct visualization and generally involving a beating heart
69. **Transvalvular leakage volume:** component of the leakage volume that is associated with leakage through the closed valve during a single cycle

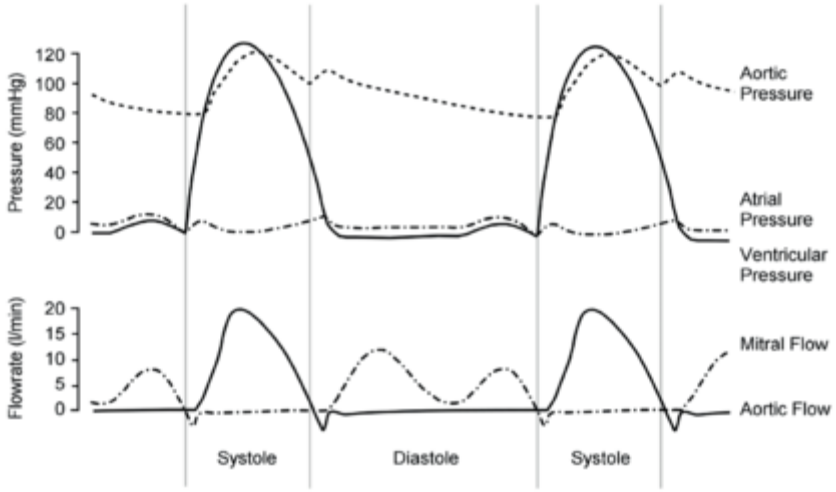

FIGURE 3: **Wiggers Diagram, showing various events of a cardiac cycle**

5. Abbreviations

For the purposes of this document, the following abbreviations apply. .

AEO	Effective Orifice Area
AF	Atrial Fibrillation
ALARP	As Low As Reasonably Practicable
AWT	Accelerated Wear Testing
BSA	Body Surface Area
BSE	Bovine Spongiform Encephalopathy
CFD	Computational Fluid Dynamics
ECG	Electrocardiogram
ESRD	External Sewing Ring Diameter
FEA	Finite Element Analysis
FMEA	Failure Mode and Effect Analysis
FTA	Fault Tree Analysis
IFU	Instructions For Use
INR	International Normalized Ratio
lOA	Internal Orifice Area
OPC	Objective Performance Criteria
PROB	Probability Rating
RIND	Reversible Ischemic Neurological Deficits
RPN	Risk Priority Number = SEV x PROB
SEV	Hazard Severity Rank
SEM	Scanning Electron Microscopy
TAD	Tissue Annulus Diameter

6. Fundemental requirements

The manufacturer shall determine, at all stagesof the product life cycle, the acceptability of the product population, potential adverse advents and intended use.

7. Device description

a. Intended use

The manufacturer shall identify the physiological condition(s) to be treated, the intended patient population, potential adverse events and intended claims.

b. Design inputs

i. Operational specifications

The manufacturer shall define the operational specifications for the device, including the principles of operation, expected device lifetime, shelf life, shipping/storage limits, and the physiological environment in which it is intended to function. Table 1 defines the expected physiological parameters of the intended patient population for heart valve substitutes for both normal and pathological patient conditions.

Table 1 — Heart valve substitute operational environment

Parameter	Description			
Surrounding medium:	Human heart/Human blood			
Temperature:	34 °C to 42 °C			
Heart rate:	30 beats/min to 200 beats/min			
Cardiac output:	3 l/min to 15 l/min			
Stroke volume:	25 ml to 100 ml			
Blood pressures and resultant pressure loads by patient condition:	Arterial peak systolic pressure mm Hg	Arterial diastolic pressure mm Hg	Differential pressure across closed valve	
			Aortic Δp_A mm Hg	Mitral Δp_M mm Hg
Normotensive	100 to 130	65 to 85	95	115
Hypotensive	60	40	50	60
Hypertensive				
Stage 1 (mild)	140 to 159	90 to 99	123	150
Stage 2 (moderate)	160 to 179	100 to 109	138	170
Stage 3 (severe)	180 to 209	110-119	155	195
Stage 4 (very severe)	> 210	> 120	185	210
Extreme (expected maximum pressure for a single cycle)	300	160	230	300

ii. Performance specifications

The manufacturer shall establish (i.e. define, document and implement) the clinical performance requirements of the device and the corresponding device performance specifications. The limits for device performance specifications shall be determined by the manufacturer for the specific heart valve substitute design in light of the intended use and claims to be made for the device. The following list of desired clinical and device-based performance characteristics describe a safe and effective heart valve substitute.

Specifications shall be defined in respect of at least the following performance characteristics:

1. allows forward flow with acceptably small mean pressure difference;
2. prevents retrograde flow with acceptably small regurgitation;
3. resists embolization;
4. resists hemolysis;
5. resists thrombus formation;
6. is biocompatible;
7. is compatible with *in vivo* diagnostic techniques;
8. is deliverable and implantable in the target population;
9. remains fixed once placed;
    a. has an acceptable noise level;
    b. has reproducible function;
    c. maintains its functionality for a reasonable lifetime, consistent with its generic class;
    d. Maintains its functionality and sterility for a reasonable shelf life prior to implantation.

iii. Packaging, labelling, and sterilization

The heart valve substitute shall meet the requirements for packaging, labelling, and sterilization contained within Annexes P, Q, and S, respectively.

c. Design outputs

i. General

The manufacturer shall establish (i.e., define, document and implement) a complete specification of the heart valve substitute, including component and assembly-level specifications, accessories, packaging and labelling. Figure 3 presents a generic block diagram of a heart valve substitute. Annex I contains a listing of terms that should be used in describing various valve models. Sub clause 6.3.2 provides a listing of examples of typical valve components of some heart valve substitutes.

ii. Examples of components of some heart valve substitutes

The following is a listing of examples of typical valve components of some heart valve substitutes. The following listing is not meant to be exhaustive.

1. **Coating**: any thin-film material that is applied to an element of a heart valve substitute in order to modify its physical or chemical properties;
2. **component-joining material**: material, such as a suture, adhesive or welding compound, used to assemble the components of a heart valve substitute, thereby becoming part of the implant device (see Figures J.1, J.3 and J.4);
3. **covering:** any element applied to enclose any other element of the heart valve substitute (see Figures J.1 , J.3, J.4 and J.5);
4. **occluder/leaflet**: component that inhibits back flow (see Figures J.1 , J.2, J.3, J.4 and J. 5);
5. **occluder retention mechanism:** component(s) of a heart valve substitute which support(s) or retain(s) the occluder(s) (see Figures J.1 and J.2);
6. **orifice ring (also housing):** component of a heart valve substitute that houses tine occluder(s) of a rigid heart valve (see Figure J.1);
7. **sewing ring (also sewing cuff):** component of a heart valve substitute by which it can be attached to tine heart (see Figure J.1);
8. **sewing-ring:** any material within the confines of the sewing ring of the heart valve substitute which provides it with build and shape (see Figure J.1);

9. **sewing-ring retaining material**: material used to prevent separation of the sewing ring from the orifice ring or frame (see Figures J.1 and J.2);
10. **stent (also frame, body):** component of a heart valve substitute that houses the occluder(s) of a flexible leaflet device (see Figure J. 5);
11. **stiffening element:** component which reduces deformation of the orifice ring or stent (see Figure J.1).

iii. Design transfer (manufacturing qualification)

The manufacturer shall generate a manufacturing flowchart identifying the manufacturing process operations and inspection steps. The input of all components and important manufacturing materials shall be indicated on the flowchart.

The manufacturer shall document the results of the validation of all special processes and the validation of all process software.

As part of the risk management process, the manufacturer shall establish the control measures and process conditions necessary to ensure that the device is safe and suitable for its intended use. The risk management file shall identify and justify the verification activities necessary to demonstrate the acceptability of the process ranges chosen.

The manufacturer shall establish the adequacy of full-scale manufacturing by validation of the manufacturing process.

d. Risk management

i. Hazard identification

Sub clause 4.3 of 130 14971:2000 shall apply. The testing and analysis necessary to estimate the risk associated with each hazard shall be determined from information on the nature of the hazard and the corresponding failure modes/causes. In identifying known and foreseeable hazards, particular consideration shall be given to hazards associated with failure modes related to design, manufacturing and human factors for each of the four elements identified in Figure 3. Table B.I contains a list of potential hazards specific to heart valve substitutes which may serve as the basis for a risk analysis.

ii. Failure mode identification

The second and third columns of Table B.1 provide a listing of potential failure modes that may result in the identified hazard. A given hazard may result from one or more failure modes; likewise, a given failure mode may result in one or more hazards.

iii. Risk estimation

Sub clause 4.4 of ISO 14971:2000 shall apply. To facilitate risk estimation for identified hazards, verification and validation testing may be used, as defined by the risk management plan. The testing outlined in Clause 7 serves as a basis for verification and validation test requirements. The last column of Table B.1 contains a list of potential evaluation methods which may facilitate risk estimation through failure mode identification and/or failure probability quantification. This list is not intended to be all-inclusive but rather a representative listing of methods that may be applicable to the specified hazard and failure mode. The rationale explaining how the tests performed facilitate risk estimation for each identified hazard shall be documented in the risk management file.

iv. Risk evaluation

Clauses of ISO 14971:2000 shall apply. Since acceptable risk levels may not be specified by applicable standards, the manufacturer shall establish and justify the risk acceptance criteria used. Any identified risk shall be reduced to a level which is "broadly acceptable" or, if that is not feasible, "as low as reasonably practicable" (ALARP).

v. Risk control

Clauses of ISO 14971:2000 shall apply. The device design and quality assurance requirements, including packaging and labelling specifications, necessary to assure the acceptability of risks, shall be documented in the risk management file.

vi. Risk review

This International Standard requires long-term follow-up of a subset of patients included in the clinical evaluation of the heart valve substitute. The review of post-production information for relevance to device safety shall include evaluating information from the long-term follow-up as well as other sources of information, such as literature reports, reports to regulatory authorities and field experience reports.

8. Verification testing and analysis/Design validation

a. General requirements

The manufacturer shall perform verification testing in order to demonstrate that the device specifications result in a heart valve substitute that meets the design specifications (design output meets design input). The test program shall consist of those tests identified from the risk analysis. The manufacturer shall establish those tests relating to hazards identified from the risk analysis. The protocols shall identify the test purpose, goal, set-up, equipment (specifications, calibration, etc.), test conditions (with a justification of appropriateness to anticipate *in vivo* operating conditions for the device), acceptance criteria, and sample quantities tested.
The manufacturer shall validate the design of the heart valve substitute, its packaging/labelling, and accessories.

b. *In vitro* assessment

i. Test conditions, sample selection and reporting requirements

1. Test conditions and sample selection

Test specimens shall emulate, as closely as possible, the condition of the finished product as supplied for clinical use, including exposure to the maximum number of recommended sterilization cycles, where appropriate.

Where emulation of *in vivo* conditions is applicable to the test method, consideration shall be given to those operational specifications given in Table 1. Where applicable, testing shall be performed using a test fluid of isotonic saline, blood, or a blood-equivalent fluid whose physical properties (e.g. specific gravity, viscosity at working temperatures) are appropriate to the test being performed.

The choice of test fluid will depend on the test goals and methods, as well as on the valve class. The risk assessment shall play a role in the choice of the test fluid.

2. Reporting requirements

Each test report shall include:

1. the rationale for the test;
2. identification and description of the sample tested (e.g. batch number);
3. identification and description of the reference valve(s);
4. number of specimens tested, and sample size rationale;
5. detailed description of the test method;
6. verification that appropriate quality assurance standards have been met (e.g. good laboratory practice) and
7. test results and conclusions.

ii. Material property assessment

1. General

Properties of heart valve substitutes and their components shall be evaluated as applicable to the specific design of the valve as determined by the risk assessment.

2. Biological safety

The biocompatibility of the materials and components used in heart valve substitutes shall be determined in accordance with ISO 10993-1. The test plan recorded in the risk management file shall comprise a biological safety evaluation program with a justification for the appropriateness and adequacy of the information obtained. The documentation shall include a rationale for the commission of any biological safety tests carried out to supplement information obtained from other sources, and for the omission of any tests identified by ISO 10993-1 but not carried out. During the hazard identification stage of a biological safety evaluation, sufficient information shall be obtained to allow the identification of toxicological hazards and the potential for effects on relevant hematological characteristics. Where an identified hazard has the potential for significant clinical effects, the toxicological risk shall be characterized through evaluation of data on, e.g., mode of action, dose-response, exposure level, biochemical interactions and toxi-cokinetics. For heart valve substitutes using animal tissue or their derivatives, tine risk< associated within tine use of these materials shall be evaluated in accordance with EN 12442-1, -2 and -3.

3. Material property testing

Material properties of heart valve substitutes and their components shall be evaluated as applicable to the specific design of the valve. Annex D provides potentially relevant physical and chemical properties by material class and components. Annex K provides a list of standards that may be applicable to testing of materials and components.

iii. Hydrodynamic performance assessment

Hydrodynamic testing shall be performed to provide information on the fluid mechanical performance of the heart valve substitute and provide indicators of valve performance in terms of load to the heart and potential for blood stasis and damage.

A guideline for the performing and reporting of hydrodynamic tests is given in Annex L. The detailed protocols shall be based on the findings of the risk assessment.

Tests shall be carried out on at least three heart valve substitutes of each size and on at least one reference valve of each of the small, medium and large sizes. A different sample size or size distribution may be used if it can be shown from the risk analysis that it provides sufficient information.

The *in vitro* test results shall meet or exceed the minimum performance requirements provided in Table 2, which are given as a function of valve size, TAD, and position. The minimum performance requirements correspond to the following pulsatile-flow conditions: beat rate = 70 cycles/min, simulated cardiac output = 5,0 Ld/min, mean aortic pressure = 100 mm Hg, and systolic duration = 35%. The minimum performance requirements are based on values in the published scientific literature.

Table 2 — Minimum performance requirements

Position	Aortic							Mitral			
Valve size (TAD, mm)	19	21	23	25	27	29	31	25	27	29	31
A_{EO} (cm^2)	⩾ 0,70	⩾ 0,85	⩾ 1,00	⩾ 1,20	⩾ 1,40	⩾ 1,60	⩾ 1,80	⩾ 1,20	⩾ 1,40	⩾ 1,60	⩾ 1,80
Regurgitant Fraction (%)	⩽ 10	⩽ 10	⩽ 10	⩽ 15	⩽ 15	⩽ 20	⩽ 20	⩽ 15	⩽ 15	⩽ 20	⩽ 20
NOTE See Yoganathan and Travis [26] and Marquez et al. [16].											

$$A_{EO} = \frac{q_{v\,RMS}}{51{,}6 \times \sqrt{\frac{\Delta p}{\rho}}}$$

where

A_{EO} is the effective orifice area in square centimetres;

$q_{v\,RMS}$ is the root mean square forward flow in millilitres per second;

Δp is the mean pressure difference (measured over the positive pressure period of the forward flow phase) in millimetres of mercury;

ρ is the density of the test fluid in grams per cubic centimetre.

NOTE This equation is derived from the Bernoulli Equation. The constant (51,6) is not dimensionless, thus this equation is only valid with the units shown.

iv. Structural performance assessment

1. General

An assessment of the ability of the heart valve substitute to withstand the loads to which it will be subjected shall be performed in order to evaluate the risks associated with potential structural failure modes.

2. Device durability assessment

An assessment of the durability of the heart valve substitute(s) shall be performed in order to assess continued function over a reasonable lifetime. Unless the labelling for a particular device includes an explicit statement about anticipated *in vivo* device lifetime, testing shall be performed to demonstrate reasonable assurance that rigid heart valve substitutes will remain functional for 400 million cycles and that flexible heart valve substitutes will remain functional for 200 million cycles. If the labelling for a particular device includes an explicit statement about anticipated *in vivo* device lifetime, testing shall be performed to support the labelling claim.

Testing shall be performed on at least three each of the largest, medium and smallest sizes of each type (aortic and mitral) of heart valve substitute. One equivalent size reference valve shall be tested under identical conditions for each valve size tested.

Tests shall be performed at a defined differential pressure consistent with normotensive conditions specified in Table 1. During the durability testing, the defined target peak differential pressure across the closed valve shall be maintained for 95 % or more of all the test cycles. Each test valve shall experience a differential pressure equal to or greater than the defined differential pressure for 5 % or more of the duration of each cycle. If aortic and mitral heart valve substitutes are identical in design except for the sewing cuff, testing need only be performed under the differential pressure conditions defined for the mitral valve. Cycle rates used for accelerated and quasi-real time durability testing should be justified from the results of the risk analysis. Consideration should be given to the behavior of time-dependent materials when selecting and justifying appropriate cycle rates.

Test valves shall experience the full range of occluder motion associated with normotensive conditions (see Table 1) during testing. Valves undergoing cycling in durability testers shall be observed at regular and frequent intervals (e.g. daily or weekly). Valves shall also be evaluated at intervals of 50 million cycles or less for the duration of the test. The durability assessment shall be performed by comparison between test and reference valves in terms of the observed damage and the extent of damage and by imposing pass/fail criteria for identified damage. The failure modes to be considered, and the pass/fail criteria for the test shall be determined by the risk assessment.

3. Component fatigue assessment

An assessment of the fatigue performance of the heart valve substitute structural components shall be conducted. The lifetime of each structural component shall be determined as the minimum duration for which the component can withstand anticipated repeated loadings associated with *in vivo* conditions. The manufacturer shall determine and justify the fatigue assessment approach and associated characterization technique adopted in order to best determine the structural lifetime for the specific material and valve/component design.
Suggested guidelines are provided in Annex O.

4. Design specific testing

In order to assess structural failure modes that may not be related to durability or component fatigue, design specific testing may be necessary. In some cases (such as stent creep), design specific testing may have direct implications as to the overall structural lifetime of a component or valve.

c. Preclinical *in vivo* evaluation

i. Overall requirements

An appropriate preclinical *in vivo* test program shall be formulated in order to address relevant valve characteristics specific to the test heart valve substitute.

The preclinical *in vivo* evaluation shall:

1. reflect the haemodynamic performance of the heart valve substitute as assessed *in vitro*;
2. provide an assessment of the surgical handling characteristics of the test heart valve substitute and its accessories;
3. provide data to assess the biological reaction to the heart valve substitute. Consideration should be given but not limited to the following items, as relevant to the specific heart valve substitute under evaluation:

    3 healing characteristics (pannus formation, tissue overgrowth);
    4 hemolysis;

4. thrombus formation;
5. embolization;
6. foreign body reaction (inflammation, rejection);
7. calcification (flexible valves);
8. acoustic characteristics (rigid valves), if manufacturer claims are made on this issue;
9. structural deterioration and/or non-structural dysfunction;
10. cavitation
11. use a test heart valve substitute of clinical quality;
12. investigate test heart valve substitute in all positions for which it is intended (aortic, mitral, etc.); subject equally sized control heart valve substitutes to identical test conditions as the test heart valve substitute;

13. use the same surgical techniques for the implantation of both the test and the control heart valve substitutes (e.g. suture technique and orientation);
14. be performed by appropriately experienced and knowledgeable test laboratories;
15. Specific, minor design modifications of existing and clinically well documented in heart valve prostheses may justify omission of animal experimentation evaluation if the preclinical outcome can be transferred directly from previous animal experimentation evaluations.

d. Methods

i. General requirements

Guidance on tine conduct of *in vivo* preclinical evaluation and a series of tests which can be used to address the relevant issues are given in Annex G. It is recognized that complications arising after valve implantation can be attributed to the implanted valve as well as the environment into which it is implanted — or the interaction between the two. Therefore, complications arising during or after valve implantation must be carefully analyzed and interpreted in order to attribute the complication to the valve or the animal or combination of the two. Implant animals shall be of the same species, and preferably of the same gender and similar age. The test heart valve substitutes shall be assessed in a long term setting in all anatomical positions for which it is intended to be used clinically. Animals suffering from heart valve substitute endocarditis may be excluded from the group of study animals, but the endocarditis event shall be reported.

The number of animals used for implantation of test and control heart valve substitutes shall be justified fully for each test based on the risk analysis.

For long term studies, the duration of the observation period of the animals must be specified according to the parameter(s) under investigation. The observation period shall be appropriately justified in each study protocol, but be no less than 90 d. In each long term animal test case where a heart valve substitute has been implanted, a macroscopic and histological post-mortem examination shall be performed. Thus, the data shall include information from all animals that have been entered into the study. If serial blood analysis is performed, sampling shall be made pre-operatively then one week post-operatively then at appropriate intervals during the observation period as well as at termination.

The assessment shall provide at least the following:

6. any macroscopically detectable pathological consequences (including but not limited to: thromboembolic phenomena, pannus formation, inflammatory reactions) around the heart valve substitute and/or in the major organs;
7. any macro- or microscopically detectable structural alterations in the heart valve substitute (e.g. cavitation, macroscopic damage, material degeneration, deformation and calcification);
8. histologic assessment of any thromboembolic material, inflammatory reactions and/or degenerative processes.

ii. Test report

The test laboratory shall produce the test report, which shall include a summary assessment of the data generated during tine course of the investigation. The test report shall include the complete study protocol. All data generated from the preclinical *in vivo* evaluation must be incorporated into a comprehensive test report.

The test report shall include:

8. identification of each of the valves used for implantation (product, serial number and other appropriate valve identification);

9. detailed description of the animal model used; the rationale and justification for its use. The pretest health assessment, including any medication given, of each animal shall include documentation of the gender and age of the animal at implantation;
10. description of the operative procedure, including suture technique, test heart valve substitute orientation, valve position and operative complications;
11. description of the preoperative and postoperative course of each animal including, clinical observations, medication and clinical condition leading to prescription of each drug. If anti-coagulation therapy is used, monitoring data for this treatment [that is. international normalised ratio (INR)];
12. any significant deviations from the protocol or amendments to the protocol;
13. names of the investigators and their institutions along with information about the implanting surgeons and the laboratory experience with heart valve implantation and animal handling;
14. interpretation of data and a recommendation relative to the clinical safety and performance of the heart valve substitute under investigation.

Further details of the test report depend on the defined test protocol.
Guidance on the composition of the test report is given in Annex G.

e. Clinical investigation

i. Principle

Data are obtained on the safety and performance of a heart valve substitute under normal conditions of use in humans; the side effects and related risks of heart valve substitute implantation are documented. The clinical investigation shall include pre-operative, peri-operative and follow-up data from a specified number of patients, each with a minimum of one-year follow-up, to provide statistical justification for the market release of the heart valve substitute.

ii. General

For new heart valve designs, a clinical investigation shall be carried out in accordance with this International Standard. For modification of an existing valve, a clinical investigation shall be considered, based on the results of a risk analysis that evaluates the modification. The clinical investigation shall be conducted in accordance with ISO 14155-1.

iii. Number of institutions

The clinical investigation shall be conducted in a minimum of 8 institutions. The study shall be designed such that the anticipated minimum number of heart valves implanted at any institution shall be 15 of each type (e.g. aortic or mitral) being evaluated.

iv. Number of patients

A minimum number of 150 recipients of isolated aortic heart valve substitutes and a minimum number of 150 recipients of isolated mitral heart valve substitutes shall be evaluated. If the heart valve substitute is intended for implantation in only one position, a minimum of 150 heart valve substitutes shall be evaluated in that position. There shall be a minimum of 15 implants of each valve size of each valve type (e.g. aortic or mitral). Exceptions are: 8 implants of aortic size 1 9 or smaller; 8 implants of aortic size 29 or larger; 8 implants of mitral size 23 or smaller; 8 implants of mitral size 33 or larger. The inclusion and exclusion criteria for patient selection shall be clearly established.

NOTE All valve sizes refer to TAD in millimeters.

v. Duration of the study

1. One-year follow-up

The clinical investigation shall continue until the minimum number of recipients of each valve type have each been followed for a minimum of 1 y. There must be at least 400 valve years of follow-up of each valve type (e.g. aortic or mitral). All implants shall be analyzed, including those patients dying within the first year, and including centers with enrollment below the intended minimum.

2. Long term follow-up

In addition to the one year follow-up on each patient, a long term follow-up evaluation shall be conducted according to the following principles:

1. the long term follow-up cohort shall be an initially determined subset of the original patients, and shall include a minimum of 150 patients; the selection of the specific patients shall be statistically justified so as to minimize selection bias;
2. the duration of the long-term study will depend on the risk assessment for the specific device design and/or device modification. Historically, for a rigid heart valve substitute, the follow-up for each patient has extended for a period of five years from the date of implantation. Historically, for flexible heart valve substitutes, the follow-up for each patient has extended for a minimum of 10y from the date of implantation. The exact period will depend on risk assessment.

vi. Clinical data requirements

1. General

Clinical data specified in 7.4.6.2 to 7.4.6.5 shall be reported for all patients receiving the heart valve substitutes at the institutions referred to in 7.4.3. The clinical study protocol shall be identical for all participating institutions, with the exception of differing national regulatory-related protocol requirements.
All valve-related complications shall be reported to the principal investigator. In addition to the clinical data reporting, adverse events shall be reported promptly, in accordance with national regulations and the reporting requirements of the protocol.
The clinical study shall include appropriate controls, including historical or literature controls, involving a similar type of heart valve substitute in the same position. If literature data are used, these should be from a study published in a peer-reviewed journal during the preceding 5 y.

2. Identifying data

The following data shall be collected:

1. patient's gender and date of birth;
2. investigator's name;
3. name of institution.

3. Pre-operative data

The following pre-operative data shall be collected:

1. diagnosis (e.g. valvular lesion and etiology) and co-existing cardiovascular diseases (e.g. congestive heart failure, cardiomyopathy, peripheral vascular disease, coronary artery disease, previous myocardial infarction), peripheral vascular operations and cardiac rhythm;
2. New York Heart Association functional class;
3. previous cardiovascular operations [e.g. coronary artery bypass, coronary artery angioplasty,
4. percutaneous valvuloplasty (position), operative valvuloplasty (position), annuloplasty (position), previous heart valve substitute replacement];
5. other co-existing medical conditions (e.g. liver, kidney and lung disease, substance abuse, diabetes, hypertension and history of endocarditis);
6. echocardiographic information
7. blood studies, including coagulation profile [including prothrombin time, partial thromboplastin time and International Normalized Ratio (INR), as appropriate];
8. weight, height and body surface area.

4. Peri-operative data

The following data shall be collected:

1. diagnosis (see 7.4.6.3);
2. procedure(s), including any concomitant operative procedure(s);
3. date of operation;
4. heart valve substitute type, model, valve size (TAD) and serial number;
5. tissue annulus diameter (TAD) of patient;
6. suture technique;
7. retention of all or part (specify) of native valve structures;
8. implant position (e.g. aortic or mitral), heart valve substitute positioning in relation to tissue annulus (e.g. supra-annular, intra-annular);
9. heart valve substitute disc/leaflet orientation;
10. complications, including operative mortality and subsequent operative procedures;
11. evaluation by echocardiography within 30 d.

5. Follow-up data

Follow-up data shall be collected within 30 d, between 3 and 6 months after implantation of the heart valve substitute, at one year and annually thereafter until the investigation is completed.
Echocardiography shall be performed at all follow-up assessments unless a risk analysis justifies a less frequent interval.
NOTE Additional follow-up intervals may be appropriate to documenting early or long term structural valve deterioration or non-structural dysfunction.
The following data shall be collected:

1. date and method of follow-up (e.g. office, clinic or hospital);
2. New York Heart Association functional class;
3. hemodynamic evaluation by Doppler echocardiography (see Annex H for a method);
4. blood studies, including coagulation profile and tests for hemolysis, red blood count, white blood count, hematocrit, hemoglobin, serum lactate dehydrogenase, Haptoglobin and reticulocyte count;
5. status of anticoagulant and/or antiplatelet therapy at each follow-up visit;
6. complications, to include thromboembolism, thrombosis, anticoagulant-related hemorrhage, prosthetic
7. valve endocarditis, structural deterioration, non-structural dysfunction, Paravalvular leak, hemolysis and reoperation;
8. reports of electrocardiograms, chest X-rays and cardiac catheterization, magnetic resonance imaging, if performed;

9. cardiac rhythm;
10. re-operation reports;
11. explant analysis when available; wherever feasible, the explanted test heart valve substitute shall be subjected to appropriate functional. X-ray and histopathological investigations. The investigation protocol shall include detailed instructions for the return of the explanted valves to the manufacturer or an
12. independent laboratory for assessment;
13. date and cause of death;
14. autopsy report, if autopsy is performed.

vii. Clinical investigation report

1. General

The report shall tabulate the data collected and shall include:

1. names of the investigators and institutions;
2. analysis of patient population by age and gender;
3. comparison of pre-operative and postoperative New York Heart Association functional class;
4. pre-operative diagnosis of valvular and co-existing disease, operative diagnoses, operative procedures including suture technique, heart valve substitute positioning in relation to the tissue annulus, disc/leaflet orientation, operative complications and subsequent operative procedures;
5. implant position, type, model, valve size (TAD), tissue annulus diameter of patient and effective orifice area of the heart valve substitute;
6. number of months since implantation, and method of follow-up (e.g. office, clinic, hospital);
7. results of hemodynamic evaluation
8. results of blood studies and therapy)];
9. analysis of complications
10. re-operation reports, explant investigation results, cause and date of death, and autopsy reports;
11. pooling of data from the aortic and mitral positions, generally justified by tine fact that short-term morbidity rates are not a significant function of implant position, except for possible early valve thrombosis in the mitral position. The data shall be presented for the entire population, and shall also be stratified by implant position and valve size (TAD).

2. Analysis of complications

The method of reporting shall conform to the Guidelines for reporting morbidity and mortality after cardiac valvular operations, 1996 (see Clause 2) and shall include analysis of cause of death and complications using appropriate statistical techniques.

1. Early complication rates expressed as a percent of patients shall be calculated for events occurring in the first 30 d and again for events occurring in the first year.
2. Linearized rates shall be used for late complications, with other statistical models as appropriate. Late events are those occurring on the 31st day post implant or later.
3. Analyses of survival rates and freedom from complication rates using both the actuarial (Kaplan-Meier), and actual (cumulative incidence) methods.

NOTE Standard errors should be reported using Greenwood's algorithm.

Specific analyses shall include:

1. overall survival;
2. survival without valve-related complications;

3. freedom from specific complications, including but not limited to valve thrombosis, systemic embolism, anticoagulant-related hemorrhage, prosthetic valve endocarditis, structural deterioration of the heart valve substitute, non-structural dysfunction of the heart valve substitute, Paravalvular leak, hemolysis and re-operation.

The specific complications and deaths shall be stratified as follows:

1. all complications shall be stratified by valve position and size (TAD);
2. thromboembolism shall be stratified by anti-coagulation therapy and cardiac rhythm;
3. non-structural dysfunction and structural valve deterioration shall be stratified by nature of dysfunction (e.g. thromboembolism, thrombosis, anticoagulant-related hemorrhage, prosthetic valve endocarditis, structural deterioration, non-structural dysfunction, paravalvular leak, hemolysis, and re-operation). Re-operation, explant and any valve-related complication shall be stratified by fatal versus non-fatal events. The data shall be analyzed to determine any effect of valve tissue annulus diameter on complication rates.

3. Performance criteria

Clinical investigation of a heart valve substitute after implantation requires documentation of specified complications (see 7.4.7.2); a new or modified heart valve substitute shall perform as well or better than the complication rates given in Tables R.I and R.2. Suggested methods for formal statistical evaluation of the clinical data are described in Annex R.

Bibliography

[1] ISO 532:1975, *Acoustics — Method for calculating loudness level*

[2] ISO/TS 11139:2006, *Sterilization of health care products — Vocabulary*

[3] ISO/TS 12417:2011, *Cardiovascular implants and extracorporeal systems — Vascular device-drug combination products*

[4] ISO 13485, *Medical devices—Quality management systems—Requirements for regulatory purposes*

[5] ISO 16061, *Instrumentation for use in association with non-active surgical implants — General requirements*

[6] ISO 22442-1, *Medical devices utilizing animal tissues and their derivatives — Part 1: Application of risk management*

[7] ISO 22442-2, *Medical devices utilizing animal tissues and their derivatives — Part 2: Controls on sourcing, collection and handling*

[8] ISO 22442-3, *Medical devices utilizing animal tissues and their derivatives — Part 3: Validation of the elimination and/or inactivation of viruses and transmissible spongiform encephalopathy (TSE) agents*

[9] ISO 25539-1:2003, *Cardiovascular implants — Endovascular devices — Part 1: Endovascular prostheses*

[10] ISO/IEC 17025, *General requirements for the competence of testing and calibration laboratories*

[11] IEC 60651:1973, *Recommendations for impulse sound level meters, publication 179 A*

[12] IEC 62366, *Medical devices — Application of usability engineering to medical devices*

[13] ASTM F2052, *Standard Test Method for Measurement of Magnetically Induced Displacement Force on Medical Devices in the Magnetic Resonance Environment*

[14] ASTM F2119, *Standard Test Method for Evaluation of MR Image Artifacts from Passive Implants*

[15] ASTM F2182, *Standard Test Method for Measurement of Radio Frequency Induced Heating On or Near Passive Implants During Magnetic Resonance Imaging*

[16] ASTM F2213, *Standard Test Method for Measurement of Magnetically Induced Torque on Medical Devices in the Magnetic Resonance Environment*

[17] ASTM F2503, *Standard Practice for Marking Medical Devices and Other Items for Safety in the Magnetic Resonance Environment*

[18] 2014 AHA/ACC Guideline for the Management of Patients with Valvular Heart Disease. Nishimura RA et al. Circulation 2014;129(23):e521-643

[19] AKINS CW et al. Guidelines for reporting mortality and morbidity after cardiac valve interventions. J. Thorac. Cardiovasc. Surg. 2008, (April) pp. 732–738

[20] T.W. Duerig, D.E. Tolomeo An overview of superelastic stent design. Proceedings of the Int'l Conference on Shape Memory and Superelastic Technologies SMST-2000; (eds.) S. Russell, A. Pelton. pp. 585-604)

[21] ERICKSON R et al. An *In vitro* Study on Mechanical Heart Valve Sound Loudness. J. Heart Valve Dis. 1994, 3 pp. 330–334

[22] European Society of Cardiology (ESC)/European Association for Cardio-Thoracic Surgery (EACTS) Guidelines on the management of valvular heart disease (2012)

[23] R.P. Gangloff Environmental Cracking — Corrosion Fatigue", Chapter 18 in "Corrosion Tests and Standards — Application and Interpretation" 2nd edition, R. Baboian (editor) ASTM International (2005)

[24] Harriet Lane Handbook: a Manual for Pediatric House Officers. C.V. Mosby, St. Louis, 2002

[25] R.G. Kelly Pitting", Chapter 18 in *Corrosion Tests and Standards – Application and Interpretation*, 2nd edition, R. Baboian (editor) ASTM International (2005)

[26] W. Knirsch Cardiac Output in Children: Comparison of the Ultrasound Cardiac Output Monitor with Thermo dilution Cardiac Output Measurement. Intensive Care Med. 2008, 34 pp. 1060–1064

[27] M.B. Leon, N. Piazza, E. Nikolsky Standardized endpoint definitions for transcatheter aortic valve implantation clinical trials: A consensus report from the Valve Academic Research Consortium. J. Am. Coll. Cardiol. 2011, 57 pp. 253–269

[28] A.P. Kapetein, S.J. Head, P. Genereaux J. Am. Coll. Cardiol. 2012, 60 (15) pp. 1438–1454 [– Updated standardized endpoint definitions for transcatheter aortic valve implantation]

[29] T. Magning Corrosion Fatigue Mechanisms in Metallic Materials", Chapter 13 in Corrosion Mechanisms in Theory and Practice, 2nd edition, P. Marcus (editor), Marcel Dekker (2002)

[30] S. Marquez, R.T. Hon, A.P. Yoganathan Comparative hydrodynamic evaluation of bioprosthetic heart valves. J. Heart Valve Dis. 2001, 10 pp. 802–811

[31] R.D. Mosteller Simplified calculation of body-surface area. N. Engl. J. Med. 1987, 317 p. 1098

[32] NYGAARD H et al. Assessment of perceived mechanical heart valve sound level in patients. J. Heart Valve Dis. 1999, 8 pp. 655–661

[33] S.R. Shah, N.R. Vyavahare The effect of glycosaminoglycan stabilization on tissue buckling in bioprosthetic heart valves. Biomaterials. 2008, 29 pp. 1645–1653

[34] D.C. Silverman Types of Data", Chapter 2 in *Corrosion Tests and Standards – Application and Interpretation*, 2nd edition, R. Baboian (editor) ASTM International (2005)

[35] S.F.C. Stewart, H.F. Bushar Improved statistical characterization of prosthetic heart valve hydrodynamics using a performance index and regression analysis. J. Heart Valve Dis. 2002, 11 pp. 270–274

[36] A. Vahanian, O.R. Alfieri, N. Al-Attar Transcatheter valve implantation for patients with aortic stenosis: a position statement from the European Association of Cardio-Thoracic Surgery (EACTS) and the European Society of Cardiology (ESC), in collaboration with the European Association of Percutaneous Cardiovascular Interventions (EAPCI). Eur. J. Cardiothorac. Surg. 2008, 34 pp. 1–8

[37] I. Vesely, D. Boughner, T. Song Tissue buckling as a mechanism of bioprosthetic valve failure. Ann. Thorac. Surg. 1988, 46 (3) pp. 302–308

[38] N. Vyavahare, M. Ogle, F.J. Schoen, R. Zand, D.C. Gloeckner, M. Sacks Mechanisms of bioprosthetic heart valve failure: fatigue causes collagen denaturation and glycosaminoglycan loss. J. Biomed. Mater. Res. 1999, 46 pp. 44–50

[39] Y.X. Wu Clinical evaluation of new heart valve prostheses: Update of objective performance criteria. *The Annals of Thoracic Surgery, Volume 98, Issue 5, 1865 – 1874*

[40] A.P. Yoganathan, B. Travis Fluid dynamics of prosthetic valves. In*: The practice of Clinical Echocardiography*, 2nd Edition: Otto. WB Saunders, Philadelphia, PA, 2002

[41] A.P. Yoganathan, M. Fogel, S. Gamble, M. Morton, P. Schmidt, J. Secunda A new paradigm for obtaining marketing approval for pediatric-sized prosthetic heart valves. J. Thorac. Cardiovasc. Surg. 2013 Oct, 146 (4) pp. 879–886

[42] R. Zegdi, V. Ciobotaru, M. Noghin, G. Sleilaty, A. Lafont, C. Latrémouille Is it reasonable to treat all calcified stenotic aortic valves with a valved stent? Results from a human anatomic study in adults. J. Am. Coll. Cardiol. 2008, 51 pp. 579–584

[43] W.A. Zoghbi, J.B. Chambers, J.G. Dumesnil, E. Foster, J.S. Gottdiener, P.A. Grayburn American Society of Echocardiography recommendations for evaluation of prosthetic valves with two-dimensional and Doppler echocardiography. A report from the American Society of Echocardiography's Guidelines and Standards Committee and The Task Force on Prosthetic valves, developed in conjunction with the American College of Cardiology Imaging Committee, the European Association of Echocardiography of the European Society of Cardiology and The Japanese Echocardiography Society. J Am Soc Echo. 2009, 22 pp. 975–1014

APPENDIX F

Research Team

Principal Investigator: Dr CJ Jordaan
MBChB, MMed Cardiothoracic surgery (UFS),
Certificate in Critical care (CMSA)
Department Cardiothoracic Surgery
University of the Free State, Bloemfontein, South Africa
drjjordaan@gmail.com
051–4053861

Supervisor: Prof FE Smit
Ph.D., M Med Cardiothoracic Surgery (UFS), Assoc FCS (CMSA), MB ChB
Department Cardiothoracic Surgery
University of the Free state, Bloemfontein, South Africa
smitfe@ufs.ac.za
051-4053861

Co-Supervisor: Dr L Botes
D Tech Biomedical Technology (CUT)
Department Cardiothoracic surgery
University of the Free state, Bloemfontein, South Africa
lbotes@cut.ac.za

Prof. Pascal M.C.E. Dohmen
M.D., Ph.D.
Herzzentrum Universitaet Leipzig
Struempellstrasse 39
Leipzig, D-04289
Germany
49 341 865 1421

APPENDIX G

Ethical Clearance

UNIVERSITY OF THE FREE STATE
UNIVERSITEIT VAN DIE VRYSTAAT
YUNIVESITHI YA FREISTATA
UFS
UV

Internal Post Box / Interne Posbus G40
☎(051) 4052812
Faks / Fax (051) 4444359

E-mail address: StraussHS@ufs.ac.za

Me / Ms H Strauss

2012-06-15

PROF FE SMIT
DEPT OF CARDIOTHORACIC SURGERY
FACULTY OF HEALTH SCIENCES
UFS

Dear Prof Smit

ANIMAL EXPERIMENT NR 08/2012
PROJECT TITLE: "EVALUATION OF DECELLULARIZATION AND ANTICALCIFICATION TREATMENTS ON THE PERFORMANCE OF HOMOGRAFT IMPLANTS IN THE RIGHT VENTRICULAR OUTFLOW TRACT OF THE SHEEP MODEL."

You are hereby kindly informed that the Interfaculty Animal Ethics Committee approved the above study at the meeting held on 14 June 2012.

ANIMAL	*NUMBER*	*EXPIRY DATE*
Dorper Sheep	40 Wether	June 2014
Dorper Sheep	30 Female	June 2014

Kindly take note of the following:

1. ***Fully completed and signed applications have to be submitted electronically to StraussHS@ufs.ac.za and a hard copy has to be submitted too.***
2. ***A signed progress report with regard to the above study has to be submitted electronically to StraussHS.ufs.ac.za while a hard copy has to be submitted to Ms H Strauss, Room D115, Francois Retief building, Faculty of Health Sciences. A report has to be submitted when animals are physically involved and after completion of the study. Guidelines with regard to progress reports are available from the secretary and on the Faculty intranet.***
3. ***Researchers that plan to make use of the Animal Experimentation Unit must request a quotation from the Head, Mr Sob Lamprecht***
4. ***Contract research: Fifty (50%) of the quoted amount is payable when you receive the letter of approval.***

Regards

.....
CHAIR:
INTERFACULTY ANIMAL ETHICS COMMITTEE

205 Nelson Mandela Drive/Rylaan, Park West/Parkwes, Bloemfontein 9301, South Africa/Suid-Afrika
P.O. Box/Posbus 339, Bloemfontein 9300, South Africa/Suid-Afrika, T: +27(0)51 401 9111, www.ufs.ac.za

Animal Research Ethics

17-Jun-2016

Dear Dr Christiaan Jordaan

Student Project Number: UFS-AED2016/0091

Project Title: DYNAMICS AND COAGULATION CHARACTERISTICS OF A RE-ENGINEERED MECHANICAL HEART VALVE IN AN OVINE MODEL
Department: Cardiothoracic Surgery (Bloemfontein Campus)

You are hereby kindly informed that, at the meeting held on, the Interfaculty Animal Ethics Committee approved the above project. This is a subproject of the approved 08/2012.

Kindly take note of the following:

1.
A signed progress report with regard to the above study has to be submitted electronically to EthicsFHS@ufs.ac.za while a hard copy has to be submitted to the Ethics Office, Room D104, Francois Retief building, Faculty of Health Sciences. A report has to be submitted when animals are physically involved and after completion of the study. Guidelines with regard to progress reports are available from the Ethics Office and on the Faculty Intranet.

2.
Researchers that plan to make use of the Animal Experimentation Unit must ensure to request and receive a quotation from the Head, Mr. Seb Lamprecht. A copy of the quotation has to be submitted with the application before the application will be considered for approval.

3.
Fifty (50%) of the quoted amount is payable when you receive the letter of approval.

Yours Sincerely

Digitally signed by
Derek Litthauer
Date: 2016.06.20
07:58:07 +02'00'

Prof. Derek Litthauer Chair: Animal Research Ethics Committee